T-4269

A FREQUENCY DOMAIN APPROACH TO DRILLSTRING JARRING ANALYSIS

by

Alfred William Eustes III

T-4269

A thesis submitted to the Faculty and Board of Trustees of the Colorado School of Mines in partial fulfillment of the requirements for the degree of Doctorate of Philosophy (Petroleum Engineering).

Golden, Colorado

Date _____

Signed: _____
Alfred William Eustes III

Approved:_____
Dr. Bill J. Mitchell
Thesis Advisor

Golden, Colorado

Date _____

_____
Dr. Craig W. Van Kirk
Professor and Head,
Department of
Petroleum Engineering

ABSTRACT

In drilling, a time and money consuming operation called fishing often occurs. One method to extract a stuck drill string from the hole is to hit the string with a force impulse. This is called jarring. Before this dissertation, the mathematics necessary to predict the magnitude and duration of the forces generated in jarring had not been developed to the point of functional use. This dissertation examines a new mathematical approach to understanding the forces of jarring and presents a jarring model that can be implemented in the field.

Current mathematical models of jarring use either wave tracking or finite element analysis with time and space being the independent variables. These methods require the use of sophisticated computers with significant central processing power and memory and take an extraordinary amount of time to compute. These methods are not suitable for field use.

The jarring model presented in this dissertation is a finite element approach that uses frequency and space as the independent variables. This approach is called spectral analysis. The advantages of this method are that element sizes are not limited nor are time step sizes critical as they are in previous jarring models.

The spectral analysis method developed in this dissertation is computationally faster and more accurate than any jarring model presented to date. This accuracy has shown some interesting effects that could not be seen

in all previous models. For example, wave reflections from damping alone can be seen. This will be called the damping reflection effect. Also, any number of reflections and transmissions can be incorporated into the model. Previous models could not incorporate multiple reflections with their accumulated effects on the hammer and anvil. In addition, some models do not consider the effect of the anvil movement. The spectral analysis method shows that the anvil movement can be a significant factor in determining the primary impact magnitude. Finally, the impact force is assumed to be a square wave. Although this assumption is used for this dissertation, the spectral analysis method is not limited to square waves but can use any wave function.

The program is written using the commercial software package called MathCad©, version 6.0 Plus. The model includes elements for drill pipe, heavy weight drill pipe, and drill collars. An accelerator can be incorporated and modelled into the string. The jar is modeled with a user preset trigger load and a hammer and anvil. The stuck section of the drill string can be modeled as either a long section or a fixed point. Hole deviation effects can be included by varying the element size and associated damping.

TABLE OF CONTENTS

ACKNOWLEDGEMENTS

There are a number of people and organizations I wish to acknowledge and thank. If not for their encouragement and support, this dissertation would not have been possible.

At the Colorado School of Mines:

Prof. Bill Mitchell, advisor

Prof. Craig Van Kirk

Prof. Ramona Graves

Prof. Robert Thompson

Prof. Michael Pavelich

Prof. Vaughn Griffiths

Prof. Hans-Peter Huttlemaier

Mr. Mark Miller

Mr. Michael Stoner

Mr. Kurt Nordlander

With Cougar Tools Company of Canada

Ray LaBonti

With the Yucca Mountain Site Characterization Project

The United States Department of Energy

Mr. Roy Long

Scientific Applications International Corporation

Mr. Eddie Wright

Raytheon Services

Reynolds Electrical and Engineering Company

TRW

With the Hanford Engineering Works

Westinghouse Corporation

Mr. Jim McCormick

Water Development Corporation

With the Eustes Household

Ms. Susan Eustes

DEDICATION

This dissertation is dedicated to my wife, Susan, for her commitment and understanding. She has supported me for my entire eight years of post graduate school at the University of Colorado and at the Colorado School of Mines. It has been a long and winding road. She deserves a Ph. T. (Put Him Through).

INTRODUCTION

Minimizing rig downtime is critical to drilling an economical well. Any tasks auxiliary to the actual drilling process slow rig production time and increase operational costs. Having a tool stuck in a hole is a major contributor to downtime on today's drilling rigs, yet the mathematics necessary to fully understand the jarring process used to "unstick" the tool have not been developed to the point of field implementation. Thus jarring is often a hit or miss operation. A practical mathematical model that accurately predicts the forces of jarring would minimize the time and costs associated with retrieving lost tools. This dissertation presents such a model and its derivation.

Rig Downtime

No engineer plans to part drill strings or lose drilling tools in the hole. This, as with most unscheduled events, results in downtime. As defined by Amoco, "an unscheduled event is any occurrence which causes a time delay in the progression of planned operations" (Kadaster et al. 1993).

All planned operations can be considered progression toward completing a well (e.g. running planned casing strings, well evaluation, actual drilling). After problems strike (e.g. equipment failure, parting of drill string, wellbore collapse, tools stuck in the hole), no progress is being made toward the completion of the well. These problems cause downtime. Fishing—the process used to retrieve a

lost tool or tools (the “fish”) downhole—is a frustrating, expensive and often prolonged downtime.

Fishing Costs

Any type of downtime is expensive. In the Norwegian North Sea, it is not unusual to see costs associated with drilling to be $200,000 per day per rig (Anderson and Lembourn 1994). According to the previous reference, from 1985 to 1991, 18 percent of exploratory rig time was spent in downtime. This includes: equipment repair (4.0 percent), fishing (3.9 percent), waiting (3.2 percent), other problems (3.2 percent), well control (2.8 percent), and lost circulation (0.9 percent). In 1990 and 1991, Amoco (Kadaster et al. 1993) found that 15 percent of the time spent on drilling operations was downtime. Of that downtime, 16 percent of the time can be attributed to stuck drill string (which was their number one problem).

Using the previous paragraph’s example, in the Norwegian North Sea, an average of $7,800 per day is spent on fishing. This is $2.85 million per year per rig. For an average of 11 rigs per year for the six year study period, the total cost for fishing in the Norwegian North Sea must have been approximately $188 million!

In a recent *Oil and Gas Journal* article (Watson and Smith 1994), anecdotal evidence shows that the cost of stuck drill string operations (which can be considered a subset of fishing operations) varied widely. One operator reported $37 million spent in downtime from stuck drill string from 1987 to 1991. Another indicated that his company’s costs approached that number in one year alone. A

third operator said its company's worldwide stuck drill string costs were $100 million, $40 million of which was in the company's Gulf of Mexico operations.

These examples demonstrate the economic necessity to minimize fishing costs. Even minimal savings per each fishing operation can result in significant overall savings in drilling operations.

Jarring

Jarring is the method used to extract the fish from the hole by hitting the string with a force impulse. This involves a transient wave. The physics needed to predict the amplitude and duration of the forces generated during jarring are intricate and not fully refined. Considerable computer resources are required to solve the multiple equations associated with the forces of jarring; resources which until recently have not been readily available to researchers.

Current jarring analysis involves either the wave tracking method or the finite element method. The independent variables in both methods are space and time. This means that both methods are firmly rooted in the time domain. While this is perhaps a more intuitive approach, there are other ways to look at the problem.

One such way is to look at the sinusoidal components of a wave. As shown by the mathematician J. B. Fourier, in his now commonly accepted Fourier transform, all real time functions can be thought of as being made up of an infinite series of sinusoidal components. Each sinusoidal component has an amplitude, a phase, and a frequency associated with it. The Fourier transform, specifically the fast Fourier transform (FFT), is used to find the sinusoidal com-

ponents from time domain functions. The collection of sinusoidal components make up the frequency domain.

The spectral analysis method described in this dissertation combines the best of the current approaches to jarring analysis within the frequency domain.

Organization of Dissertation

This dissertation first presents an overview of fishing operations and moves to an explanation of the model developed to predict the jarring process.

Chapter 1—Fishing Operations

This chapter discusses drill string components, the different methods of sticking a drill string in the borehole, typical fishing operation techniques and the mechanics of jarring. This discussion includes a description of the types of jars and other tools used in jarring strings.

Chapter 2—Literature Review

This review includes three papers on the wave tracking method of analysis. There is also a review of a finite element method jarring analysis, and there are reviews of two papers that describe jarring operational techniques.

Chapter 3—Time and Frequency Domains

The current jarring analysis methods are discussed in this chapter. Then wave theory and relationships are described. The differences between the time

and frequency domains are shown. Finally, the techniques used to convert from the time domain to the frequency domain (such as the fast Fourier transform) and problems inherent in these techniques are explained.

Chapter 4—Deriving the Spectral Element

This chapter sets forth the details of spectral analysis. It starts with a general description of spectral analysis. Then the static and dynamic forces on a drill string during jarring are shown. Using the dynamic forces, an axial equation of motion for a drill string under jarring conditions is derived and solved. From there, the spectral solution is derived using a finite element model composed of an axial two-noded spectral element and an axial one-noded semi-infinite spectral element. The elements are then globally assembled into one structure, the drill string. A linear algebraic solution for the globally assembled structure is made and post-processing is shown. The general procedure and the limitations of spectral analysis are described.

Chapter 5—The Use of Spectral Analysis in Wave Propagation

This chapter presents five models that validate the spectral analysis method.

Chapter 6—The New Jarring Model

This chapter presents the spectral analysis-based model of jarring. A generic drill string model is described and each phase of the jarring process is presented.

Chapter 7—Jarring Analysis Cases

This chapter presents cases of jarring under various conditions. Cases include the use of drill collars and drill pipe with and without heavy weight drill pipe and with and without an accelerator. Finally, a comparison of the frequency-domain model with a time-domain finite element model demonstrates the superior results of the spectral analysis method derived in this dissertation.

Conclusions and Recommendations

This chapter summarizes the impact of the spectral analysis jarring program. A discussion of future research plans and capabilities of the program are included.

CHAPTER 1

FISHING OPERATIONS

This chapter discusses drill string components, the different methods of sticking a drill string in the borehole, typical fishing operation techniques and the mechanics of jarring. This discussion includes a description of the types of jars and other tools used in jarring strings.

In the drilling industry, fishing operations are not pleasant outings by a lake or river. They involve sleepless nights, exhausting days, much time, and a lot of money. It is up to the rig personnel, primarily the drilling engineer involved, to expeditiously remedy the fishing situation as economically as possible, or determine that the best course of action is to abandon the hole.

Fishing is a term coined by the drillers of the cable tool era. After a cable line broke, the drillers would put a hook on the end of the remaining line and try to “catch” the lost line. Being the innovators that these drillers were, they often devised unique and clever methods of recovering items that were lost in the hole. Many of these items, such as wireline spears and wireline jars (now called bumper subs) still exist and are used daily.

There are many techniques and procedures for fishing, and the drilling engineer must determine the appropriate method for retrieving a lost or stuck item, usually referred to as the “fish.” For example, wireline fishing is considerably different from fishing with drill pipe. The fish itself may dictate the proce-

dures. A fish may be free or stuck. If the fish is stuck, jarring or washover operations may be needed. This dissertation covers only fishing with the use of jars. The reader is referred to other references for information on more techniques and procedures (Kemp 1990) (NL McCullough 1978) (Tri-State Oil Tool Industries, Inc. n.d.).

Jarring is simply the process of impacting the fish with a large force impulse. This is not unlike hitting a stuck item with a hammer. For example, if a mechanic finds a cotter pin stuck in its hole, the first thing usually done is to hit the pin with a hammer. The reaction is a longitudinal wave running back and forth in the pin. The longitudinal wave causes the particles of the pin to move as the wave passes through the particles. This, in turn, causes motion along the side of the pin and the hole in which the pin is stuck. If the forces are large enough to overcome the friction loads at the interface of the pin and hole, the pin will move. With enough hammer blows, the pin eventually comes loose.

The same phenomenon is true using jarring to fish for stuck tools. In this case, the hammer is called a jar. The jar is placed in the drill string in a position to apply a hammer blow to the fish. With each hammer blow, the potential energy in the fish is changed from kinetic energy to strain. Eventually the fish will come loose. The bad news is that this may take days or weeks. At some point, it is more economical to abandon the hole and drill a new one.

Although the process of jarring is generally understood, the fine points are not. How much force does the jar impact give a fish? And, how long does this force last? Where is the jar positioned within the drill string to maximize the chance of successfully freeing the fish? How does damping affect the jarring process? The petroleum industry has invested much time and resources search-

ing for answers to these questions. Thus far, the answers have been less than useful: either the answer is reasonably accurate, but takes too much time and computer resources to find; or, the answer is quick, but not very accurate. The new method presented in this dissertation, called spectral analysis, is both quick and accurate. Before getting to the process of spectral analysis, though, there is the question of how drilling tools get stuck in the first place.

Stuck Drill String Problems

There are more ways to get stuck in a hole than there are words to describe the emotions of the driller after this happens. Just about any item that goes in a hole—including drill pipe, drill collars, casing, and tubing—can get stuck. This section reviews the most common methods of getting stuck, in both open hole and cased hole. (Note: not every case described requires the use of a jar.)

Differential Pressure Sticking

Differential pressure sticking, often called differential sticking, is very prevalent in the drilling industry. Most of the fishing operations in the Gulf of Mexico are caused by differential sticking. Basically, the string is stuck against the side of the well because of a large pressure differential between the fluid in the borehole and the formation.

Differential sticking occurs only across a permeable formation. The higher the permeability, the higher the probability of differential sticking. As the mud (made up of insoluble plate-like solids and a fluid phase to carry the solids) moves across the permeable zone, it has a tendency to lose the fluid phase to

the permeable formation. This leaves the solids to plate on the side of the bore-hole. This nearly impermeable filter cake can grow to be thick. Meanwhile, if the hydrostatic pressure of the mud at the permeable zone is much higher than the formation pressure in the permeable zone, there will be a pressure gradient toward the formation across the borehole wall. If, by chance, the drill pipe or collars are laying in the filter cake, a hydraulic seal can form. Now the pressure gradient is across the string. Because filter cake has a high friction coefficient, the force required to pull the string tangentially across the filter cake is high. In many cases, the rig is not powerful enough to pull the string or the string is not strong enough to handle the load.

Differential sticking is usually the case if the drill string cannot be moved up or down or rotated, yet circulation can be maintained. This is after being stationary across a permeable zone.

An equation used in the petroleum industry for differential sticking is as follows

$$F_{TANGENTIAL} = A\mu P_{NORMAL} \tag{1.1}$$

where

A =hydraulically sealed area

μ =coefficient of friction

P_{NORMAL} = pressure differential between wellbore and formation

$F_{TANGENTIAL}$ = drag force needed to move up or down the hole

Unsticking requires the reduction of the normal force, the coefficient of friction of the filter cake, the hydraulically sealed area, or a combination of any of the previous methods. The sooner these methods can be applied, the greater the chance of success.

One method used to unstick the string is to spot a lightweight fluid with a filter cake destroying chemical and then jar on the string. This fluid reduces the pressure differential, the coefficient of friction of the filter cake, and the hydraulic seal area. An example of this would be to spot an oil-based fluid across the stuck point. Another method is to blow nitrogen past the stuck point. This assumes that there are no potential kick zones above and below the stuck point. Well control can be lost in these cases.

Undergauge Hole Sticking

An undergauge hole is any hole that has a smaller diameter than the bit that drilled that section of hole. One potential cause of an undergauge condition is drilling a high clay content plastic shale with a fresh water mud. If an oil-based mud is used, a plastic salt formation can “flow” into the wellbore. If the wellbore fluid has a hydrostatic pressure less than the formation pressure, the shale or salt will slowly ooze into the wellbore. It is a slow process, but one that can stick drilling tools of the unwary.

An undergauge hole can also occur after a drill bit is worn smaller as it drills through an abrasive formation. In this case, the hole is undergauge be-

cause the bit drilled it that way. If a new bit is run, it can jam into the undergauge section of the hole and become stuck. This is often called tapered hole sticking.

The presence of a thick filter cake, described in “Stuck Drill String Problems, Differential Pressure Sticking” above, can also cause an undergauge hole. The filter cake can become so thick that tools can not drag through it. The filter cake shows as a drag load on the weight indicator.

Sloughing Hole Sticking

Sloughing hole sticking occurs after the hole wall sloughs off. For example, a water sensitive shale that has been invaded by water will swell and break. If circulation is stopped, the broken pieces will collect around the drill string and eventually pack the drill string in place.

Shales under high formation pressure can slough as well. In this case, the formation pressure is greater than the wellbore hydrostatic pressure. Because the shale has a very low permeability, no flow is observed. The rock, having a high pressure differential toward the wellbore, shears off the hole wall. This can be seen as large cuttings on the shale shaker screen. Sometimes, the borehole curvature can be seen on the cuttings, a classic sign of entering a high pressure zone. If too much sloughing occurs or the wellbore is not cleaned properly, the drill string can become stuck. More than likely, circulation will cease and no movement will be possible.

Steeply dipping and fractured formations also can slough into the hole. Drilling in overthrust belts are notorious for this problem. Also, if there are cavities in the wellbore, cuttings can collect there. After the circulation stops, the cuttings in the cavities may fall back into the hole.

Key Seat Sticking

In a deviated hole or after ledges are present, the drill pipe can wear a slot into the borehole wall. This slot, called a keyseat, is basically the same diameter of the drill pipe. While the drill string is being pulled, the drill collars or bit will try to run through the keyseat. As the diameter of this keyseat is smaller than the drill collars or bit, these tools become wedged in the keyseat. Circulation can be maintained in this situation. Of course, the usual action of the driller upon seeing the string start to stick is to pull harder. This exasperates the situation, sticking the string even harder. Key-seat sticking usually occurs while moving the drill string up the hole during a trip.

Sand Sticking and Mud Sticking

Sand sticking and mud sticking are similar. The sand particles or the solids in the mud can settle out of suspension. If there is little or no circulation, the rain of particles settles around the string, sticking the string in place.

Sand sticking usually occurs in cased holes although it can occur in open holes. In cased holes, a leak can develop in the casing allowing sand particles to flow into the well. The sand particles will then fall down and eventually either pile up on a packer or some other restriction in the hole.

Mud sticking is similar. For whatever reason, the solids that make up part of the mud can settle out of suspension. Solids can be barite particles or cuttings. In a high temperature well, the mud can lose the fluid phase (filtrate) leaving the solids packed around the string. In addition, sometimes contamination, such as acids or salts, can alter the mud properties. This can lead to the loss of suspension properties of the mud.

Inadequate Hole Cleaning Sticking

Inadequate hole cleaning sticking occurs after the flow rate of the circulation fluid slows to the point that the solids' carrying capacity of circulation fluid has been exceeded by the force of gravity. If the fluid is not viscous enough or flowing fast enough, the drag forces on the solids are less than the gravity forces. This means that the solids flow down the hole, instead of up and out of the hole. The hole fills up with solids that build up around the string, eventually sticking the string.

This flowrate can slow down for a number of reasons, including: (i) the driller may not be running the pumps fast enough; (ii) there could be a hole enlargement in the drill string that slows the flowrate (e.g. a washout); or, (iii) the amount of solids may become overwhelming as a result of sloughing shales, unconsolidated formations, or lost circulation.

Cemented Sticking

Cemented sticking can occur if the cement that is being circulated goes somewhere other than where it was intended. For example, if a cement plug was

being spotted and the cement flowed higher up the string than anticipated, the cement could set before the string could be pulled out of the cement. The string is stuck. If the cement is not too thick, the string could be jarred loose, otherwise, a washover operation is needed.

The cause of cement sticking can be attributed to a number of factors: (i) mechanical failures, i.e. string leaks, (ii) human error; i.e., miscalculating a displacement or losing track of cement being used to remedy a blowout or lost circulation zone, or (iii) oversized holes.

Blowout Sticking

During an uncontrolled flow of fluid from a well, called a blowout, solids and materials such as drill pipe protector rubbers can flow with the fluids and become lodged against the string. The forces of the blowout then wedge the solids and materials against the string. Also, these solids and materials can bridge across the hole.

Mechanical Sticking

This is a “catch all” sticking problem. Any drilling and completion tool can get mechanically stuck.

Packers

Sometimes, the slips on a packer can become wedged so tightly against the casing, that they can not come free. In addition, retrieving failures can happen. In these cases, sometimes a high force-short duration force pulse can knock the packer loose.

Multiple Strings

Multiple strings can jam in a hole. The two, three, or even four strings in the hole can rotate around each other as they are being run into the hole. It is very difficult to retrieve intertwined strings.

Crooked Pipe

If a drill string is dropped in a mud-filled hole, the string can become permanently bent. This bend can wedge the string against the side of the hole, making it difficult to retrieve. If a string is dropped in an air-drilled hole, there is no hope of recovery.

Junk in the Hole

Junk in the hole is a description for small pieces of man-made materials that either are dropped down the hole or fall off a downhole tool. Examples of items dropped down the hole include: drill collar safety clamps, wrenches, and drill string tools being made in the rotary table. Items that can fall off of downhole tools include slips off of packers, rubber drill pipe protectors, and (especially prevalent) cones off of roller cone bits. This debris can either fall to the bottom of the hole or can wedge against the side of the drill string. If the debris wedges the string in the hole, then jarring could possibly knock it loose.

Fishing

This section will cover a typical fishing operation where the string is stuck in an open hole. This operation involves first determining where the string is stuck in the hole, then determining the procedure needed to unstick the string.

Locating Stuck Point

There are a couple of techniques that can be used to determine the location at which the string is stuck (the “stuck point”). They involve either stretching the string with a known load or running a special wireline tool. The best method depends on the time available and the accuracy needed.

Stretch Calculations

A stretch calculation is the quick method of determining the stuck point. This test assumes that the same type of string is connected from the surface to the fish. To run this test, the string is pulled to a given tension on the weight indicator and a mark is made on the string opposite the rotary table top. Then more tension is pulled on the string and another mark is made on the string opposite the rotary table. There should be some distance between the two marks. That distance is proportional to the load pulled and the length of the string that is free if buckles have been removed.

The equation that describes this is as follows

$$L_{FREE} = \frac{E\Delta LW}{F} \tag{1.2}$$

where

E = modulus of elasticity

ΔL = distance between the two marks

W = weight per foot of the string

F = tension force difference at the two marked points

L_{FREE} = free length of string (distance to the stuck point)

While this method is fast, it is not particularly accurate. It can get the answer to within two or three joints. If the string is to be backed-off, the answer must be closer. In addition, if there is more than one type of pipe in the string, the calculations become more complicated. Also, if the hole is deviated or doglegged, the drag from the string rubbing against the hole wall may preclude any stretching of the string below that point.

Freepoint Tool

The freepoint tool is far more accurate than the stretch method; however, it requires that a wireline tool be run inside the drill string. The freepoint tool has a set of strain gages and spring loaded drag blocks or electromagnets that rub against the inside of the string. As the tool is run into the string, the string has torsion or tension applied. The degree of pipe movement that results from the application of the torsion or tension is transmitted to the surface through the wireline. After the tool is below the stuck point, no movement of the string will be detected.

Backoff the String

After the stuck point has been found, the method of recovery must be determined. Often, the string is broken just above the stuck point and a jarring string is run into the hole. The backoff procedure, as this is called, involves unscrewing or cutting the string above the stuck point. Unscrewing the string is the preferred method as it leaves the string intact. Breaking the string involves explosive, chemical, or mechanical cutting of the metal.

To unscrew a string that is stuck, a string shot is run into the hole. A string shot is a small explosive. The tool joint that is to be unscrewed is found using a collar locator. Then the string shot is run into the middle of the inside of the tool joint. The driller then applies torque and tension to the string. The amount of torque should be sufficient to unscrew the string after the shot, but not before. The string shot is exploded. The torque in the string should unscrew the string at the explosion point. It is similar to hammering a reluctant screw. If all goes well, which it often does not, the string should come loose at that point. The string is then pulled out of the hole leaving the fish stuck in the hole.

Run in the Jars

With the drill string out of the hole, the fishing tools are made up. A fishing string with a jar is often called a jarring string. A typical jarring string will consist of an overshot or screw-in sub, drill collars, a jar, more drill collars, maybe an accelerator, more drill collars, maybe a bumper sub, and drill pipe. The makeup of jarring strings varies considerably and depends on the fish and the amount of jarring force needed. There are no hard and fast rules concerning how to make up a jarring string.

The makeup of this jarring string is really the basis for all the various jarring analysis programs in the world. As mentioned in the Introduction, current analysis is either too slow or too inaccurate. This dissertation's goal is to find a faster and more accurate method for the field people to determine how to make up the jarring string. The amount of impulse, force, and energy developed and applied by the jar to the string is highly dependent upon the make up the jarring string.

Jarring

This section covers the downhole tools that are specific to jarring strings.

Types of Jars

The original type of jars used in cable tool drilling consisted of two links of steel attached to the cable. The links would be loose while attached to the fish. Then the driller would pull on the cable causing the two links to crash together. This applied a jolt to the fish.

Today there are two types of jars. They are either fishing jars or drilling jars. Fishing jars are used in fishing strings. They are built somewhat lighter than drilling jars and are more easily adjusted from the surface. In addition, they are designed to generate a larger impact than the typical drilling jar. Drilling jars are part of the drill string. They are placed in the drill string to be ready for immediate use in case the drill string gets stuck. The two types of jars operate on either a hydraulic or mechanical principle. Most jars can operate either down or up but are really designed to impart a larger impact force up rather than down.

The jar is designed to impart a force impulse into the fish. This is accomplished in the following manner. The string is stretched putting strain energy into the string above and below the jar. The amount of tension put into the string greater than the weight of the string above the jar is called the overpull. At some predetermined load value, the jar is triggered. The top and bottom parts of the jar disconnect from each other and are free to travel up for the top part (called the hammer) and down for the bottom part (called the anvil). Both parts of the string contract at what is known as the free contraction velocity and build kinetic energy. Eventually, after the anvil and hammer have traveled a certain distance (called the stroke), the hammer and anvil impact. Most of the kinetic energy is converted back into strain energy which then propagates up and down the string. Some of this energy will propagate to the stuck point and hopefully jar the fish loose. The amount of force, energy, impulse, etc. depends upon the initial strain energy, stroke length, and wave propagation characteristics of the jarring string.

Hydraulic

Hydraulic jars are often called oil jars. This is because a hydraulic fluid or light oil is used in the jar. In the cocked position, the jar has a tight fitting piston (the hammer) inside of a cylinder. There is fluid in a chamber above the piston. As the string is pulled in tension, the piston tries to move up but the fluid above cannot bypass the piston. The fluid increases in pressure and slowly bypasses the piston through a bypass hole or channel. At some point as the piston slowly travels up the cylinder, the tight fitting clearance opens up to a very loose clearance and the fluid can easily bypass the piston. The jar has triggered. The

sudden reduction in pressure above the piston allows the piston to freely travel up the cylinder until it impacts the anvil. After impact and after the strain waves have died, the jar is reset by slowly recompressing the jar in order that the piston is shoved back into the tight fitting cylinder. This can take a few minutes.

The big advantage of an hydraulic jar is that the impact intensity can be varied from the surface by changing the overpull in the string prior to triggering the jar. However, heat and recocking too fast can destroy the seals in the hydraulic jar. If the seals leak, the jar has failed and a trip is necessary. Hydraulic fishing jars are built somewhat lighter than hydraulic drilling jars.

Some jars can be triggered to impact upward and downward. The upward impact is called an “up hit”. This is the usual operational direction of most jars. However, in some cases, such as unsticking a keyseated string, the jar should be fired downward. This is called a “down hit.” Most jars do not work as well downward as they do upward.

Mechanical

Mechanical jars trigger differently from hydraulic jars. The triggering mechanism can be a set of rollers or a spring detent that is set at a given load for triggering. The given load is set at the surface prior to running in the hole. Once in the hole, most mechanical jars cannot be reset to a different triggering load. A few mechanical jars allow for very limited trigger load changes by using torque from the string to reset the trigger load. These kinds of jars can be recocked up to three times per minute as opposed to the two to three minutes for the hydraulic jars. Mechanical jars tend to be more rugged than their hydraulic counterparts and are used more often in drilling strings.

Accelerator

An accelerator is often called a booster jar or an intensifier. It is a device run in the jarring string somewhere above the jar. It is full of a compressible fluid that acts like a spring. The accelerator can act as a shock absorber for the rest of the jarring string under the impact of the jar, but its main purpose is to intensify the impact force.

The force of the jar impact is directly related to the velocities of the hammer and anvil. The accelerator acts to increase the velocity of the hammer by reflecting the free contraction waves sooner than it would have without the accelerator. The position of the accelerator in the jarring string is critical to the success of this intensification. It allows for a shorter duration and higher force impact.

Bumper Sub

A bumper sub is used to impart a downward impact into a jarring string. It is a mechanical slip joint. The impact occurs because the string is allowed to fall over the length of the slip joint. After the string travels the distance of the slip joint, it stops with an impact.

By maintaining the load such that the slip joint is within its stroke, only the load below the bumper sub is the string. Also, if an overshot or a spear is grappled onto a fish, it takes a downward blow to free the grapples.

CHAPTER 2

LITERATURE REVIEW

This chapter is a review of six major petroleum-oriented papers on jarring. This review will include three papers on the wave tracking method of analysis. There is also a review of a finite element method jarring analysis. And there are reviews of two papers that describe jarring operational techniques.

Summary of Past Work

The six papers discussed advance the technology of jarring and the authors are to be commended. The areas which are not totally and comprehensively addressed by these past authors and which are addressed in this dissertation are the following:

1. Calculational speed and computational accuracy
2. Damping effects on wave propagation including wave reflection from damping
3. Multiple wave reflections and transmissions and their effects on jarring
4. Anvil movement
5. Iimpact wave form

Drillstring Dynamics During Jarring Operations

The paper *Drillstring Dynamics During Jarring Operations* was published in the November 1979 edition of the **Journal of Petroleum Technology.** It was written by Marcus Skeem, Morton Friedman, and Bruce Walker and was presented at the 53rd SPE Fall Convention in Houston, Texas in 1978 as SPE paper 7521 (Skeem et al. 1979).

This paper is the first in the United States to apply an analytical approach to determining the dynamic loads on drill strings under jarring operations. (Some work was done in Russia by A. Fershter, B. Bleikh, and S. Sheinbaum in 1977.) The analysis is performed to determine the best location in the drill string for the jar by studying the stress history at the stuck point. This approach uses a closed form stress wave tracking method under which routine analytical techniques (Kolsky 1963) track the stress waves' propagation and reflections and refractions.

The authors model the drill string as a one-dimensional, piecewise constant elastic medium with large length to diameter ratios. The string is broken into three simple sections: the drill pipe, the drill collars above the jar, and the drill collars below the jar. This implies that lateral and bending loads and associated stresses are not considered. No other components, such as heavy weight drill pipe or stabilizers, are considered. In addition, in this analysis, the authors consider only the free contraction of the string above the jar and ignore all forms of damping.

The study is broken into two parts, pre-impact jarring and post-impact jarring. During pre-impact, the jar is assumed to have just triggered. The string

above the jar (the hammer section) is in free contraction while the string below the jar (the anvil section) is stationary. The end in the jar (the hammer) then accelerates with the return of each reflection off of the drill pipe of the original stress wave. This acceleration continues to increase the velocity of the hammer until it impacts the anvil. The equation for the initial free contraction speed (not considering any reflections of the stress wave) of the drill collars is

$$V_C = \frac{F_O C_A}{A_{DC} E_{DC}} \tag{2.1}$$

where

F_O = overpull force
C_A = longitudinal wave propagation velocity
A_{DC} = cross-sectional area of drill collars
E_{DC} = modulus of elasticity of drill collars
V_C = free contraction speed

The initial wave takes time to propagate up to the drill collar/pipe interface, reflect off of the interface, and return to the hammer. The equation to calculate the time for the wave to make one round trip is

$$t_{reflect} = 2 \frac{L_{DC}}{C_A} \tag{2.2}$$

where

L_{DC} = drill collar length
$t_{reflect}$ = time for reflection to return

Considering the number of returns of the stress wave reflections, the equation representing the velocity of the hammer is

$$V_N = V_c\left(1 + 2\sum_{n=1}^{N}\lambda^n\right) \tag{2.3}$$

where

N = number of reflections

V_N = hammer velocity

and where λ is the ratio of the drill collar and pipe cross sectional areas as shown below as

$$\lambda = \frac{A_{DC} - A_{DP}}{A_{DC} + A_{DP}} \tag{2.4}$$

where

A_{DP} = cross-sectional area of drill pipe

Eventually, the hammer strikes the anvil. The value of N is the number of reflections possible prior to the hammer impacting the anvil. The velocity of the hammer at impact determines the impact force.

The post-impact study starts with the actual impact. The authors assume that the post-impact velocity of the hammer is half the pre-impact velocity and that the anvil is accelerated to half of the pre-impact hammer velocity. This assumes that the cross sectional areas of the hammer and anvil sections are equal. The equation for the force generated by the impact that propagates down to the stuck point is

$$F_I = \frac{A_{DC}E_{DC}}{C_A}\frac{V_N}{2} = \frac{1}{2}\frac{V_N}{C_A}F_O \tag{2.5}$$

where

F_I = impact force

The authors also point out that part of this wave also propagates up the drill string, reflects off of the drill collar/pipe interface, and eventually superimposes its force to the stuck point. To describe the stress history at the stuck point, the authors track each separate contribution of each original and reflected wave and use linear superposition at any given point in time. However, as the authors note that after about three reflections, any further contributions by the residual wave reflections are practically nil.

As the authors state, the peak force derived during the impact is not a good measure of the jar's effectiveness. If the stuck point is truly a mathematical point, then a peak force greater than the sticking force would immediately free the pipe. No time would be considered. However, the stuck point is actually an area of some length. As field experience proves, it takes time and repeated jarring to break a string loose.

In addition, the authors state this method only approximates the forces. In the model, the forces are changed discontinuously whereas in reality, the forces are continuous. The impulse function is introduced as

$$I(F,T) = \int_T F(t)dt \qquad (2.6)$$

where

F(t) = impact force function with respect to time

T = duration of impact

I(F,T) = impulse function

Using this equation, an average force is determined as follows

$$F_{AVG} = \frac{I(F, t)}{T} \tag{2.7}$$

where

F_{AVG} = average force over impulse duration

To make the model more valid, the authors assume that the drill pipe did not have any reflections occur inside it. That means the drill pipe is longer than 1,500 feet. Even though there actually are reflections from inside the drill pipe, the reflections do not return to the drill collars until long after the useful part of the jarring wave has decayed. Also, it is assumed that the jar was not placed within a joint of the drill collar/pipe interface.

An important point that the authors make is that the slip force is an assumed value of force needed to initiate and maintain motion at the stuck point. This force has to be greater than the overpull force (otherwise the string would move!). The string at the stuck point moves with a slip velocity of

$$V_S = \frac{(F - F_S)C_A}{A_{DC}E_{DC}} \tag{2.8}$$

where

F = impact force

F_S = force needed to overcome sticking

V_S = slip velocity

The distance traveled by the string at the stuck point is the product of the slip velocity and the time of the impulse. This distance traveled is very small and would not be seen at the surface. A real concern is the fact that the slip force is rarely known.

The results of this analysis show that moving the jar further up the drill collars results in a higher impact force but at a shorter duration than jars lower in the string. However, the impulse increases with the jars set lower in the string. The optimum location of the jar depends upon the nature of the sticking force.

Although this is a valuable paper, there are too many simplifying assumptions for this method to be useful. With so few parts of the drill string actually considered, this method does not work for the complex strings typically used. Friction is totally ignored. In addition, the stuck point is modeled as a fixed point. Finally, it is not correct to assume that the drill string below the jar is stationary.

Transient Dynamic Analysis of the Drillstring Under Jarring Operations by the FEM

The next major paper on jarring analysis, *Transient Dynamic Analysis of the Drillstring Under Jarring Operations by the FEM,* was written by M. Kalsi, J. Wang, and U. Chandra. It was published in the March 1987 **SPE Drilling Engineering** edition and was presented at the SPE/IADC Drilling Conference in New Orleans, Louisiana in 1985 as SPE paper 13466 (Kalsi 1987).

In this paper, the authors approach the problem of drill string jarring analysis from a different viewpoint. Rather than track individual waves, the authors use the finite element method (FEM) which allows the user to include

complex strings and various forms of damping. With this method, the force, displacement, velocity, and acceleration histories anywhere along the string are available.

A nonlinear transient dynamic analysis is performed using the commercially available FEM software package, ANSYS™, to analyze a typical drill string. The authors compare a uniform collar string to a string with drill collars, accelerator, heavy weight drill pipe, and drill pipe.

This analysis requires three types of elements: 1-D spar, gap, and spring-damper. A 1-D spar element, capable of only axial loads, is used for drill collars and pipe. The cross sectional area is constant across this element. The jar is modeled as a gap element with one side of the gap being the hammer and the other, the anvil. The gap size corresponds to the jar stroke length. The spring-damper elements connect the string to the hole wall. The spring values are set to zero to simulate wall friction. Spring damper elements are also used to model the stuck point as they have the characteristic of a linear relationship of force and displacement until a threshold force is reached. At that point, the force stays constant regardless of the displacement.

A total of 174 elements and 188 nodes are used. The time step is 0.0002 seconds for 0.14 seconds duration. The model is run in two steps. The first step applies the overpull. The second part models the free contraction, impact, and post-impact phases.

The model shows many interesting effects not seen in the previous paper. The accelerator acts as an almost free end. This is the main reflection point for the upwardly propagating waves. But there is a slight departure of the wave arrival times for the anvil. The authors attribute this to the fact that the stuck

point is not modeled as a fixed point, but rather as a stiff spring. The velocity of the hammer is somewhat lower than predicted by theory, too. This can be attributed to the *almost* free end of the accelerator. It is not a *true* free end. In addition, the hammer is slightly decelerating between wave reflections. This is attributed to wall damping.

The impact shows that the anvil motion is important. A stationary anvil assumption can lead to a ±30 percent error in the predicted impact force. Therefore, the authors show the need to model a moving anvil.

The authors also find that acceleration values are numerically very sensitive to the time step chosen. Reducing the time step requires a large computational and storage effort. Acceleration loads are important to know for the design of downhole measurement while drilling (MWD) tools. The authors demonstrate that the velocity changes are not as sensitive to time step selection; therefore, design values can be determined using changes in velocity rather than calculated values of accelerations.

While this is a very good model, there are two major drawbacks. The first is that the FEM can be a very powerful technique; but, it is not easy to use. It takes training and good engineering skills. The second problem is that it takes a very long time to run one analysis. Depending upon the computer and the complexity of the drill string, it can take from 15 minutes to six hours for one run. This makes optimization very time consuming. This is unacceptably long for typical field usage.

A Study of How Heavy Weight Drill Pipe Affects Jarring Operations

This paper, *A Study of How Heavy-Weight Drillpipe Affects Jarring Operations,* was written by M. Lerma. It was presented at the 60th SPE Fall Conference in Las Vegas, Nevada in 1985 (Lerma 1985).

The author uses the wave tracking method developed by Markus Skeem (Skeem et al. 1979). He increases the capability of that model by incorporating a more complex drill string and he includes the effect of heavy weight drill pipe. The author considers two examples, one with 356 feet of drill collars above the jar and one with 960 feet of heavy weight drill pipe above the jars. No attempt was made to put drill collars and heavy weight drill pipe together in the same drill string.

The author runs two cases: (1) with drill collars above the jar, and (2) with heavy weight drill pipe above the jar. The weight above the jars is the same in both cases. The author points out that initially the jarring hammer has a higher velocity in heavy weight drill pipe than in drill collars. He states that this is because the heavy weight drill pipe is more elastic than drill collars. The author also notes that drill collars (in his example) are accelerating faster than the heavy weight drill pipe (because of more reflections in the drill collar example). Still, the author adds, the hammer in the heavy weight drill pipe case would have the higher momentum because the hammer would strike the anvil at a higher velocity.

The author points out that friction causes a significant change in the results. According to the author, running jars in heavy weight drill pipe reduces peak force by 50 percent; but increases impulse by 40 percent as compared to

jars in drill collars. However, if friction is incorporated into both cases (by changing the end boundary conditions, which is not an accurate method to take friction into account) at the stuck point, there is a reduction of peak force by 50 percent, reduction in impulse of 50 percent, and a reduction in displacement by 65 percent.

The author includes a description of the model's limitations: damping is not considered; the impact of the hammer and anvil do not consider inelasticities; energy absorption of the drilling mud (a form of damping) is not calculated; stretch in the lower drill collar section is ignored; and, some bottom hole assembly items are not considered. The author concludes that a more complex model is needed.

Computerized Drilling Jar Placement

The paper, *Computerized Drilling Jar Placement*, was written by W.E. Askew. It was presented at the 1986 IADC/SPE Conference in Dallas, Texas as SPE paper 14746 (Askew 1986).

This paper describes a proprietary jarring program written for Anadrill Schlumberger. The program uses the finite element method to determine optimum drilling jar performance. In this case, optimum performance means the largest jarring force at the stuck point. This paper does not go into the details of their model, but rather describes typical results of the model. These results are broken into three parts: jar placement recommendation, trip setting recommendation, and bottom hole assembly design information.

Their jar placement recommendation meets the following five criteria:

1. *The jar location has to be more than 60 feet from a stabilizer or cross sectional area change.*

This recommendation is made because the concentration of bending stresses near a stabilizer or cross sectional area change tend to be high. Since jars tend to be less stiff than other drill string components of the same diameter, the jar flexes. The flexing coupled with rotation while drilling can lead to jar failure as the parts inside of jar wear out from flexing.

2. Depending upon hole inclination, there is a maximum weight that can be slacked off above a jar while drilling.

Current recommendations are that a jar used in a drill string should be run in tension. This is thought to keep bending stresses to a minimum. In some holes, especially directional drilled holes, the jar can not be run in the tension section of the string. In those cases, there is a maximum compression load that can be run in the jar. For holes from 0° to 10° inclination, a maximum compression load of 10,000 lbf can be used. For every 10° more in inclination, another 5,000 lbf can be added.

3. There is a minimum 5,000 lbf needed to trip the jar.

Because of hydrostatic and hydrodynamic pressure loads, a jar has a tendency to be pumped into the cocked position. This is

sometimes called the extension force. If the weight slacked off above the jar is about the same as the extension force, the jar's interior parts are floating in a neutral position. This can cause the jar to cock. Then vibrations from drilling can cause wear to the cocking mechanism. Having a minimum load for the tripping mechanism minimizes this possibility. This problem usually does not arise in typical drilling operations.

4. A maximum stiffness ratio of 3.0 at the jar is required.

The stiffness ratio is the ratio of the section moduli of the two different sections. This is often called the section modulus ratio (SMR). The section modulus is the polar moment of inertia divided by the section outside diameter (Mitchell 1995). If one section has a modulus of 6 and another section has a modulus of 2, the stiffness ratio would be 3. If the ratio were higher, a very stiff section of pipe would be next to a limber section of pipe. This would cause the limber member to flex far more than it would for a smaller ratio. This, in turn, would lead to fatigue failure in the limber pipe section.

Drilling jars are not as stiff as drill collars. For a jar of the same outside diameter as the drill collar, the stiffness ratio is usually 3, which is satisfactory. If a jar is sandwiched between two very stiff sections, the jar is likely to have a higher than 3 stiffness ratio, leading to eventual jar failure.

5. *A minimum of 5,000 lbf weight must be available above the jar.*

This is the authors' recommendation for the "proper" amount of weight (the authors actually meant mass) above the drill collar for a sufficient amount of mass as the jar impacts up and down.

This jarring program can determine the location of the jar within the string using these five recommendations. It starts checking every 30 feet beginning at the bit. Only those locations meeting the recommendations are then considered for the second part of the program, trip setting recommendation.

This first part of the program determines the trip setting load value (the overpull) needed to trigger the jar. This load must not be greater than the strength of the string. Usually the lowest string strength is in the drill pipe section. Operating the jars with a triggering load near but not exceeding the drill pipe strength will give the peak jarring force capable for that particular string. The model in this paper shows that the peak force and impulse increase proportionally with an increase in the jar triggering load.

In addition, the location of the jar within the string dictates the available triggering load. The higher the jar is in the string, the higher the up triggering load can be set. This is because there is more tensile force available higher in the string. The program chooses a "proper" up hit setting as follows

$$F_{UP\_SETTING} = F_{MAXIMUM} - F_{SAFETY\_UP} - F_{STRING\_ABOVE\_JAR} - F_{DRAG} \quad (2.9)$$

where

$F_{MAXIMUM}$ = maximum overpull force (includes string weight)

F_{SAFETY_UP} = a safety factor force

$F_{STRING\_ABOVE\_JAR}$ = bouyed string weight above the jar

F_{DRAG} = drag force

$F_{UP\_SETTING}$ = recommended up hit setting

Drag is usually assigned a value of 10 percent of the string weight above the jars. A safety load, used for operator uncertainty, of 10,000 to 20,000 lbf is usually considered good.

For a down hit, the equation is

$$F_{DOWN\_SETTING} = F_{BHA\_ABOVE\_JAR}(1 + f_{DRAG})f_{BOUYANCY}\cos(\alpha) + F_{SAFETY\_DOWN} \quad (2.10)$$

where

f_{DRAG} = drag factor (fraction of string weight)

$F_{BHA\_ABOVE\_JAR}$ = bottom hole assembly weight above the jar

$f_{BOUYANCY}$ = bouyancy factor

α = inclination angle

F_{SAFETY_DOWN} =a safety factor force

$F_{DOWN\_SETTING}$ = recommended down hit setting

The drag factor is usually assigned a value of 10 percent. The safety load of 20,000 lbf is considered minimal.

With the jar high in the string, there is more tension available for a high up hit load; but, the down hit load is lessened because there is less weight bottom hole assembly above the jar. Conversely, the lower the jar is in the string, the more down-hit load is available at the expense of the up hit load. However, if the up hit load is set low, the weight of the bottom hole assembly below the jar may be enough the trigger the jar.

The third part of the program provides potentially helpful bottom hole assembly information. This part determines if the current bottom hole assembly is adequate given the calculations of the previous two parts of the program. This part also calculates the jar operating loads.

Although this paper does not have any model mathematics, it is useful in determining the operating parameters and characteristics of the jarring process. Other than that, it is an advertisement for Anadrill Schlumberger.

A Practical Approach to Jarring Analysis

The next paper, *A Practical Approach to Jarring Analysis*, was written by Jaw-Kuang Wang, Monmohan S. Kalsi, René A Chapelle, and Thomas R. Beasley. It was published in the March 1990 edition of the **SPE Drilling Engineering**. The paper was originally given in the 1987 IADC/SPE Conference in New Orleans as SPE paper 16155 (Wang et al. 1990).

This paper picks up where Skeem et al. ends. It is a jarring analysis that is based on a closed form stress wave tracking method. The authors took Skeem's work further by incorporating heavy weight drill pipe and including the stretch in the string below the jars (the anvil section).

As the authors point out, the FEM method is a good method for analytical and research engineers. However, for the person on the rig, the FEM method is not a solution. FEM requires large computational resources, long solution times, and engineering expertise to perform and interpret the analysis. It can take a thousand time steps to do one typical analysis. Since each time step requires an iterative solution, an inordinate amount of time is needed. The author's solution is to use the stress wave method and call it "good enough."

The free contraction and hammer velocity equations used in this model are the same as Equations 2.1, 2.2, 2.3 and 2.4 in Skeem's paper (Skeem et al. 1979). The anvil velocity is assumed to be the free contraction velocity of the string below the jar.

The authors' impact force calculation is somewhat different. Rather than assume a post-impact velocity, they calculate the combined post-impact velocity (V_U) (assuming plastic impact). The equation is

$$V_U = \frac{V_{HAMMER} A_{DC\_A} + V_{ANVIL} A_{DC\_B}}{A_{DC\_A} + A_{DC\_B}} \tag{2.11}$$

where

V_{HAMMER} = hammer velocity

A_{DC_A} = drill collar area above jars

V_{ANVIL} = anvil velocity

A_{DC_B} = drill collar area below jars

V_U = post impact velocity

The impact force is then calculated using

$$F_I = \frac{A_{DC\_A} E_{DC\_A}}{C_{A\_A}} \Delta V_{HAMMER} = \frac{A_{DC\_B} E_{DC\_B}}{C_{A\_B}} \Delta V_{ANVIL} \tag{2.12}$$

where

E_{DC_A} = modulus of elasticity in drill collars above jars

C_{A_A} = longitudinal wave velocity above jars

E_{DC_B} = modulus of elasticity in drill collars below jars

C_{A_B} = longitudinal wave velocity below jars

F_I = impact force

and

$$\Delta V_{HAMMER} = V_{HAMMER} - V_U \tag{2.13}$$

and

$$\Delta V_{ANVIL} = V_U - V_{ANVIL} \tag{2.14}$$

The duration of the impact is the time it takes for the primary impact to travel up to the next highest significant interface and back. The refraction (T for transmission) and reflection (R for reflection) of the stress waves is also calculated. It is

$$\sigma_R = \frac{A_O - A_I}{A_O + A_I}\sigma_I \tag{2.15}$$

and

$$\sigma_T = \frac{2A_I}{A_I + A_O}\sigma_I \tag{2.16}$$

where

σ_R = reflected stress

A_O = cross-sectional area with transmitted wave

A_I = cross-sectional area with incident wave

σ_I = incident stress

σ_T = transmitted stress

These equations are used to calculate the amount of stress wave reflection from an interface as well as the amount of stress wave transmitted through the interface. Implicit in these two equations are the assumptions that the modulus of elasticity and density are equal for both sides of the interface.

The available impulse is calculated using

$$I = (F - F_S)T \tag{2.17}$$

where

F = impact force
I = available impulse

The stuck point displacement is determined by

$$S = \frac{IC_A}{A_{DC}E_{DC}} \tag{2.18}$$

where

S = displacement of stuck point

The authors verify these calculations by comparing them to over 25 FEM runs. They claim that the results for both methods are in agreement.

Using the stress wave approach, a typical run requires 15 seconds for 1,000 combinations of jarring variables as opposed to three hours for one FEM answer. The jarring variables include jar placement within the string, overpull, stuck force and location, length of drill collars or heavy weight drill pipe above the jar, and downhole friction.

The authors also demonstrate the effect of friction on the jar performance. They point out that the friction depends on formation type, hole curvature, dogleg severity, bottom hole assembly inclination, and stabilizer locations and numbers. The friction can be determined by comparing some MWD downhole weight on bit values to the weight on bit at the surface or using a friction decay measurement (Daering and Livesay 1968).

The authors take friction into account by slowing the hammer between reflections. The percentage loss in velocity is assumed to be proportional to the ratio of the interface areas, bottom hole assembly length above the jar, and to the square root of the jar stroke as shown in

$$V_N' = V_N\left(1 - K_1 \frac{A_{DC\_A}}{A_{DC\_B}} L_{DC\_A} (J)^{0.5}\right) \tag{2.19}$$

where:

K_1 = experimentally derived drag constant

L_{DC_A} = length of drill collars above jar

J = jar stroke length

V_N' = drag modified hammer velocity

The friction for the anvil section is

$$V_C' = V_C\left(1 - K_2 (t')^{0.5}\right) \tag{2.20}$$

where

K_2 = experimentally derived drag constant

t' = time from trigger to impact

V_C' = drag modified anvil velocity

For a high impact, the hammer should be traveling as fast as possible. For every reflection, the hammer velocity increases; however, the magnitude of the increase in hammer velocity decreases for every reflection. To get many reflections, the section of drill collars above the jar should be relatively short. According to the authors, the jar stroke is not as important under these conditions. In long drill collar sections above the jar, the jar stroke length is more important. The jar stroke must be long enough to allow the hammer to accelerate fully.

The authors compare a straight drill collar bottom hole assembly to a bottom hole assembly with drill collars and heavy weight drill pipe. The results show that for the straight drill collar bottom hole assembly, there is only one maximum impulse location for the jar. In the case of the heavy weight drill pipe bottom hole assembly, there are two maximum impulse locations for the jar. This is because of the complexities of the stress wave propagation with drill collars and heavy weight drill pipe. In this case, it could be that a jar is set in a location that corresponds to the minimum between the two peaks of impulse. If that should happen, the jars will not be working at optimum performance.

Loads on Drillpipe During Jarring Operations

The latest paper on jarring available at the time of this dissertation, *Loads on Drillpipe During Jarring Operations*, was written by Thor V. Aarrestad and Åge Kyllingstad. It was published in **SPE Drilling and Completion** in December 1994. It was originally presented in the 1992 SPE European Petroleum Conference in Cannes, France. This paper uses the closed form stress wave tracking method (Aarrestad and Kyllingstad 1994).

In some wells, especially deviated wells, the drill pipe at the surface is near its rated tensile capacity. There is some concern that the stresses from jarring may exceed the tensile capacity of the drill pipe and cause a failure. In this paper, the authors show that the drill string loads in the drill pipe during jarring operations are not significant.

The jarring process is broken into five phases. The first phase is loading, the storing of strain energy in the string. This can take a few seconds to a

minute for some hydraulic jars. The next phase is acceleration which occurs after the jar triggers but before the hammer and anvil impact. The strain energy stored in the pipe is converted to kinetic energy. The third phase is impact. This phase is short, lasting 10 to 50 milliseconds. The fourth phase is post-impact where the stress waves are propagating. The fifth and final phase is recocking the jar in order to be able to start the jarring cycle over.

The analysis in this paper makes the following five assumptions:

1. The stuck string can be divided into four sections: the fish (the string under the jar), the jarring mass (the bottom hole assembly above the jar), a heavy weight drill pipe section (if needed), and the drill pipe section. Note that accelerators were not considered.
2. The drill pipe section is so long that no reflections from the surface will be seen during the acceleration, impact, and post-impact phases.
3. Jar release is instantaneous. There is no transition time between the loading and acceleration phases. This release from the static pull to zero force represents a negative force wave travelling up the string.
4. Internal and external friction forces are ignored. The authors make this simplifying assumption by regarding friction forces as static and not dynamic.
5. Residual vibrations in the fish section at impact time are ignored.

The equations used by the authors are the same as in Skeem 1979 paper, *Drillstring Dynamics During Jarring Operations* (Skeem et al. 1979). The force ratio of overpull force to impact force transmitted to the drill pipe is

$$\Phi = \eta \frac{1 + r_{CP} - 2r_{CP}^{n+1}}{1 - r_{CP}^{n}} \tag{2.21}$$

where

Φ = ratio of impact force to overpull force

$$\eta = \frac{A_{DC\_B}}{A_{DC\_B} + A_{DC\_A}} \tag{2.22}$$

$$r_{CP} = \frac{A_{DC\_A} - A_{DP}}{A_{DC\_A} + A_{DP}} \tag{2.23}$$

If Φ is less than one, then the force on the drill pipe during jarring operations will be less than the overpull load. Examples in the paper show that if the number of reflections is four or more, Φ will be less than one.

The addition of heavy weight drill pipe complicates the system because of the multitude of reflections that need to be tracked. In this case,

$$\Phi \approx \eta \frac{4A_{HWDP}A_{DC\_A}}{\left(A_{DC\_A} + A_{HWDP}\right)\left(A_{DP} + A_{HWDP}\right)} \tag{2.24}$$

where

A_{HWDP} = cross-sectional area of heavy weight drill pipe

The values of Φ are slightly greater than in the straight drill collar case. The transmission of stress waves into the drill pipe is more efficient with a tapered string. This reduces the magnitude of the wave being reflected back to the hammer. Because of this, the authors state that a heavy weight drill pipe section reduces the effectiveness of the jar.

Because of an accident on a test drilling rig in Norway, a 4,000 foot drill string with a jar was stuck in the hole. The research engineers measured the forces on the kelly while jarring. One important result showed that the assumption that jar release is instantaneous is not valid. (Although in the paper, the authors claim it is assumption 4, further discussion indicates that they really meant assumption 3.) There is aproximately a 100 millisecond time from jar trigger to full release. This implies that the sharp stair step look to the hammer velocity plots are not truly valid. This also indicates that the discontinuity of force inherent in stress wave analysis procedures are not descriptive of reality.

The waves measured on the kelly are much broader than expected. A sharp wave was expected; instead, the wave appears dispersed over time. This may be because stress waves tend to disperse as a result of the many cross sectional area changes inside the jar. The stress wave must propagate through these changes prior to coming out of the jar and propagating through the rest of the string. This weakens the stress wave. In addition, the wave disperses because of friction. The high frequency components of the wave tend to dampen more than the low frequency components. Also, the tool joints on the drill pipe act to dampen the axial component of the stress wave.

CHAPTER 3

TIME AND FREQUENCY DOMAINS

The current jarring analysis methods are discussed in this chapter. Then wave theory and relationships are described. The differences between the time and frequency domains are shown. Finally, the techniques used to convert from the time domain to the frequency domain (such as the fast Fourier transform) and problems inherent in these techniques are explained.

The mathematical analysis of jarring traditionally has been firmly rooted in the time domain with the two independent variables being time and space (a location). Thus, the analysis is performed at a single point in time on a single location within the string.

One form of time domain analysis is stress wave tracking, which is a closed form partial differential method, It has the advantages of being exact and solvable at any location and time without regard to any previous solutions. However, these types of solutions can be difficult (if not impossible) to solve. The analysis is restricted to constant geometric and material properties. For example, there is no single solution for changes in a cross-sectional area. Finally, only linear functions can be considered. As will be seen, dry sliding friction, called Coulomb damping, is nonlinear and cannot be solved in a linear only fashion.

The other time domain method is the finite element method. This is a technique which simplifies complex problems. It involves breaking a structure into a finite number of pieces called elements. For a specific analysis, a simplified equation is developed for each element. For example, if an axial displacement for a given force is desired, then a simplified equation is derived for that type of analysis. If all the elements are similar, then the same type of equation can be used. Once all the elements are mathematically described and boundary conditions are prescribed, then all the equations for each element are simultaneously solved with a linear algebraic approach.

The finite element method can incorporate multiple geometric and material properties. Nonlinear functions can also be incorporated through iteration methods. However, since a simplified equation describes the element, the results are only approximate. In addition, a complex structure requires large computational resources. The computer requirements include a fast central processing unit (CPU), a large amount of random access memory (RAM), a large storage disk, and a lot of time. The method also requires that the user have training and knowledge of how to input the data as well as interpret the results.

The degree of approximation depends upon many factors. In wave propagation problems, a limitation of this approximation method is evident. A string of pipe has a continuous distribution of mass, but the finite element method requires that the mass be lumped at the ends (called nodes) of the elements. This is similar to a series of springs connected to points of mass. If the analysis was done at the atomic level, this approach would work well; however, it is virtually impossible to model every atom in a section of pipe.

A rule of thumb in finite element method solution techniques is to use 20 elements over a wavelength (ANSYS, Inc. 1992). A 1,000 Hertz wave (not uncommon is jarring analysis) would have a wavelength in steel of 16.84 feet. This means that an element should not have a length greater than 0.84 feet.

A popular finite element method for wave propagation problems is as follows. The structure to be analyzed is built with various multiple elements. Initial conditions at a given time point are then imposed. The equations making up the structure are solved. This solution becomes the initial values for the next step in time, which is solved and so on. Time marches on.

The size of the step in time is critical to the solution of the wave propagation problem. The step size (time duration) must be small enough for the finite element method wave propagation algorithm to be stable. If the time step is too large, the algorithm will not be stable and will not converge to an answer.

In addition, the time step must be small for wave tracking. This means that for a given element length, if the time step is larger than the time it takes for a wave to propagate across the element, then the wave literally passes through the element without being seen! Another rule of thumb in finite element method solution techniques is to use a time step of aproximately 1.5 times the amount of time for a wave to propagate through an element (ANSYS, Inc. 1992). A time step for wave propagation in a one foot steel element would be 84 microseconds at the longest. This is 11,909 steps per second. A longer element would have a larger time step. A 20 foot element would have a maximum time step of 1,680 microseconds or 595 steps per second.

As previously noted, longer elements do not model the continuous mass of the string very well. An increasing number of elements are needed to accu-

rately model the wave propagation. This means that each element must be smaller which, in turn, requires the time step be smaller. More time steps are required. More elements need to be solved simultaneously over many time steps. The more accuracy needed, the more elements and time steps required. This can rapidly get out of hand.

For example, a wave in steel travels 3,450 feet in 0.2048 seconds. If the 1,000 Hertz example is used, then at 0.84 feet per element, 4,107 elements would be required. A 0.84 foot element requires a time step of 74.8 microseconds. For 0.2048 seconds, 2,738 time steps are needed. That means that 4,107 equations must be simultaneously solved 2,738 times. This is 11,244,966 calculations! This takes time and out on the drilling rig, no one will be waiting for the answer. There must be a better method. There is, but some preliminary work must be done first.

This is not to say that all time based finite element methods will not work. There are some implicit methods of time domain based finite element methods that can treat mass as a continium. In those situations, element length may not need to be as critical as in the time domain explicit methods. In addition, time step sizing may not be a critical issue. This is an area that needs more investigation.

Wave Theory

After an external force is impressed on a body, a real world elastic body does not instantly react over its entire length. The point immediately under the external force reacts first, then the section just under that point reacts to the previous section’s reaction, and so on. This transfer of reactions travels at a

specific velocity. The reactions propagate through the body over a period of time. This series of reactions is called wave propagation. If the rate of change of the external force is slow enough, static equilibrium analysis can model the reactions adequately for most engineering applications. However, if the external force rapidly changes, wave propagation analysis is necessary to effectively model the reactions. For this reason, wave propagation theory must be used in jarring.

Types of Waves

There are five types of elastic waves: longitudinal, lateral, Rayleigh, Stonley, and bending (Meyers 1994). (See Figure 3-1.)

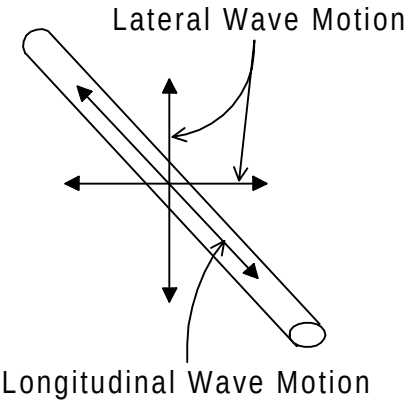

Figure 3-1: Wave Types

A longitudinal wave (other descriptions include compression/tension wave, axial wave, dilatational wave, or irrotational wave) is a wave in which the particles that make up the elastic media are forced directly into and away from each other. The motion of the particles is parallel to the direction of the wave motion. The speed at which these waves travel in most steels is approximately 16,842 feet per second.

A lateral wave (other descriptions include shear wave, transverse wave, equivolumal wave, or distortional wave) is a wave in which the particles slip against each other. The motion of the particles is perpendicular to the direction

of the wave motion. Because slipping uses more energy, lateral waves are slower. The speed at which these waves travel in steel is approximately 10,428 feet per second. A rapidly changing torsional force on a section of pipe will cause a lateral wave to propagate from the point of application to all other parts of the pipe. All other waves are made up of either longitudinal or lateral waves.

A Rayleigh wave is a surface wave that travels along the surface of a solid elastic media. The particle motion is elliptical and is analogous to a buoy reacting to an ocean wave. It is a special form of a wave. These waves are slower than lateral waves and move approximately 9,656 feet per second in steel.

A Stoneley wave is a wave that travels along an interface. With two different types of solids joined together, any wave crossing that boundary will induce a wave traveling along the interfacial boundary. With many layers of media, a Love wave occurs (as in wave propagation through the Earth).

A bending wave is also called a flexural wave. It is a wave that travels as a bend in a bar or plate. Both longitudinal and lateral components are present in this type of wave. Rotary shears and moments of inertia complicate the analysis of this type of wave.

In jarring analysis in drill strings, the most logical wave to analyze is the longitudinal wave. Since the jar acts mainly in the longitudinal direction, the analysis of the jarring procedure can be one-dimensional. Although waves other than longitudinal are present to some degree, they generally do not warrant inclusion in the first pass of jarring analysis. It should be noted, however, that in curved boreholes, a bending wave is induced by the motion of the string during jarring. Since the bending wave is a mixture of the longitudinal and lateral

waves, the analysis required is considerably more complex and is not a part of this dissertation. The authors of the six papers discussed in Chapter 2 have not included waves of types other than longitudinal. Furthermore, the surface type of waves in drill strings are not significant. Surface waves are more important in semi-infinite media than in long narrow rods like pipe.

Natural Frequencies

Everything has a frequency at which it would vibrate if it was given the energy to vibrate and was left alone. This is called a natural frequency. For instance, the human body has a natural frequency of around five cycles per second. All drill strings have a natural frequency. This frequency depends on the drill string material and the geometry of the drill string. The material determines the speed of a wave in the material. The geometry determines how waves are reflected and refracted.

During wave propagation, the wave will eventually reach an end of the material. Some of the wave will reflect back to the source of the wave. If the reflection reaches the source at the same time a new wave is generated, the two waves will add together and be synchronized in phase. Later, those two waves' reflections will return to the source at the same time the next new wave is generated. All three waves will add. This continues for as long as waves are generated. The wave will increase in amplitude, theoretically to infinity. This is called resonance. The frequency at which resonance occurs is the natural frequency or an integer multiple of that frequency (called a harmonic). If this wave reinforcement is allowed to continue, eventually the system will either self destruct or fatigue to failure.

There are an infinite number of natural frequencies in a continuous system. A system made up of a point mass on a massless spring, will have only one natural frequency. If two point masses are connected using two springs, then there will be two natural frequencies. A section of pipe divided into elements and the mass lumped at the nodes is essentially converting the pipe into a the system into a series of point masses and massless springs. (See Figure 3-2.) This means that there will be a finite number of natural frequencies rather than the actual infinite number. In a finite element analysis, the model becomes increasingly accurate with an increasing number of elements (which results in an increasing number of natural frequencies). The need for such a large number of elements is a major limitation of the finite element method of wave propagation in the time domain.

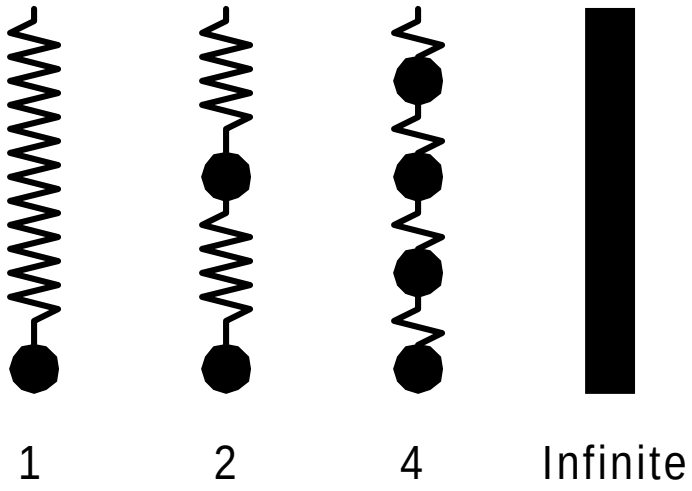

Figure 3-2: Number of Natural Frequencies

Resonance energy does not reach an infinite value because of damping. A wave propagating in a system adds energy to a system. Damping takes energy out of a system. However, if damping does not take enough energy out of a system, the system could have an energy overload and self destruct. The amount of energy in a drill string at a given time is reflected in its stress level. The more stress in the drill string, the higher the energy level. After the stress

reaches a value greater than the yield strength of the drill string, failure is imminent. If the stress is greater than the ultimate strength of the drill string, failure is immediate.

Wave Relationships

There are some basic wave relationships that must be defined. These will be referred to in the coming chapters.

The amplitude of a wave is the difference between the maximum and minimum values of a sinusoidally varying quantity. The crest of a wave is its maximum amplitude. The trough of a wave is its minimum amplitude. The wave period (T) is the length of time is takes a wave to travel as measured from crest to crest. The wave length (λ) is the distance covered by one wave period (Harris 1988).

The wave frequency (f) is the inverse of the wave period. It is the number of crests that occur in a given time unit. This is also called a cyclic frequency. An angular (sometimes called circular) frequency (ω) is a frequency measured in radians per unit time. The angular frequency is cyclic frequency times 2π (Harris 1988).

The phase angle (abbreviated to “phase”) of a wave (ϕ) is the fraction of the distance the wave has traveled relative to an arbitrary reference. The point at which the various waves cross the average amplitude line do not coincide unless the phase is zero. The phase is negative if the crossing occurs before the reference wave crossing. The phase is positive if the crossing occurs after the reference wave crossing.

The velocity of a given point on a sinusoidal wave is defined by the phase angle from the average amplitude crossing to that given point. This is called the phase velocity (c).

The wave number (k) is the ratio of the wave length to 2π (Achenbach 1993). If this ratio is a real number, the wave will have a constant phase velocity for all of its components and will retain its shape. This is called a non-dispersing wave. If the wave number is complex, then the wave components will have differing phase velocities. The wave will not retain its shape and will disperse over time. This is called a dispersing wave. All waves encountered in macroscopic reality are dispersing to some extent.

The group speed (c_g) is different than the phase velocity. Since any wave is comprised of a group of sinusoidal components, the response of the group is important. The interaction of all the wave components in terms of wave number, amplitude, and frequency results in the appearance of a carrier wave of some wave number, amplitude, and frequency. This carrier wave is modulated by group waves that propagate at group speeds. In a non-dispersing wave, the group speeds are the same as the phase velocity of the wave components.

In a dispersing wave, these group speeds can be different. If the group speeds are greater than the phase velocities, it will appear that a carrier wave will originate at the back of the wave and propagate forward until it reaches the front of the wave. At that point, it vanishes and reappears at the back of the wave again. If the group speeds are less than the phase velocities, it will appear that a carrier wave will originate at the front of the wave and propagate backwards until it reaches the back of the wave. At that point, it vanishes and reappears at the front of the wave again. This can be visualized by using a caterpil-

lar. The ripples of the caterpillar appear to move backwards yet the caterpillar moves forward (Doyle 1989). This is the reason dispersing waves can be very complicated.

The mathematical relationships and their units are shown below.

Period (time) $$T = \frac{1}{f} = \frac{2\pi}{\omega} \quad (3.1)$$

Wavelength (length) $$\lambda = 2\pi\frac{c}{\omega} = \frac{2\pi}{k} \quad (3.2)$$

Cyclic Frequency $\left(\text{Hertz}, \frac{1}{\text{time}}\right)$ $$f = \frac{\omega}{2\pi} \quad (3.3)$$

Angular Frequency $\left(\frac{\text{radians}}{\text{time}}\right)$ $$\omega = 2\pi f \quad (3.4)$$

Phase of Wave (radians) $$\phi = kx - \omega t = \frac{\omega}{c}(x - ct) = \frac{2\pi}{\lambda}(x - ct) \quad (3.5)$$

Phase Velocity $\left(\frac{\text{length}}{\text{time}}\right)$ $$c = \frac{\omega}{k} = 2\pi\omega\lambda \quad (3.6)$$

Wavenumber $\left(\frac{1}{\text{length}}\right)$ $$k = \frac{2\pi}{\lambda} = \frac{\omega}{c} \quad (3.7)$$

Group Speed $\left(\frac{\text{length}}{\text{time}}\right)$ $$c_g = \frac{d\omega}{dk} \quad (3.8)$$

Time Domain versus Frequency Domain

In the time domain, time is an independent variable. In the frequency domain, frequency is an independent variable. Any function, including a wave function, which has time as an independent variable is in the time domain. As a result, the time history of a function is its values at specific times. Any function, including a wave function, which has frequency as an independent variable is in the frequency domain. Since humanity lives in a four dimensional universe (at least to human perception), three dimensions of space and one of time, this is the "natural" way of looking at things. But there are other ways of looking at the universe.

In Figure 3-3, a time function is shown. This particular time function, labeled Function 1+2, is made up of the summation of two other time functions,

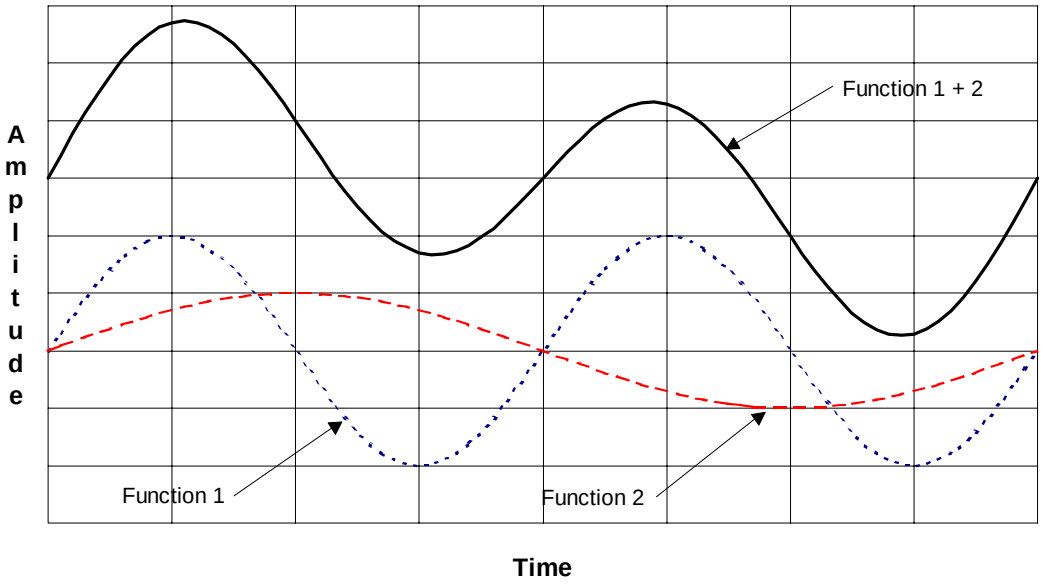

Figure 3-3: The Time Domain

labeled Function 1 and Function 2. The amplitudes of the two time functions at any given point in time are additive. A famous theorem invented by J. B. Fourier proves that this is true (given the Dirichlet conditions). The summation of the amplitudes of the two time functions will be recorded as only one total amplitude at any given time. Only Function 1+2 will be recorded. This is true for any number of time functions. Only the **single** value, called the combined function, comprised of the linearly combined values of the various components, will be recorded. This single value can appear very complex. Trying to describe this single wave in the time domain would require an infinite number of points.

In this example, since these two time functions are sinusoidally varying, they can be approached from a different viewpoint. Figure 3-4 shows a three-dimensional graph of the individual components in Figure 3-3. These two components in the time domain can be seen on the three-dimensional graph if one looks from the left perpendicular to the amplitude-time plane. To visualize the frequency domain, it is only necessary to look at the three-dimensional graph perpendicular to the amplitude-frequency plane, that is along and down the time axis; i.e., view the plot from the right. Each of the sinusoidally varying components has an amplitude, phase, and frequency value associated with it.

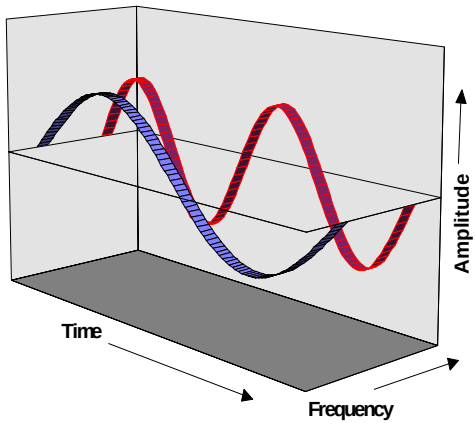

Figure 3-4: Time and Frequency Domains

An example of the frequency domain for Function 1 and Function 2 is shown in Figure 3-5. There is a steady state amplitude, which is the average value of all of the waves' component amplitudes. It has a zero frequency and zero phase. The other two values show an amplitude at a frequency. There also is a phase associated with each component. The combined function can be described by only seven numbers: the steady state amplitude; Function 1's amplitude, frequency, and phase; and Function 2's amplitude, frequency, and phase.

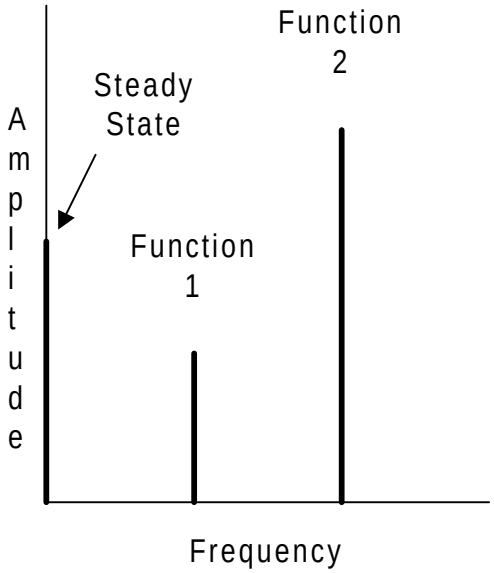

Figure 3-5: Frequency Domain

The combined Function 1+2 does not appear in the frequency domain because it is a wave composed of Function 1 and Function 2. Only the component functions appear in the frequency domain. In contrast, only the combined function shows up in the time domain. The goal of frequency analysis is to determine the values of Function 1 and Function 2.

Converting from Time Domains to Frequency Domains

The Fourier Transform

Time functions can be converted to the frequency domain with an accuracy sufficient for engineering operations using an approximation called the

discrete Fourier transform. This method assumes the Dirichlet conditions are met for a given time function. Since all time domain functions are continuous in time (that is, they are analog in nature), the time domain function must be sampled at given increment of time. This leads to problems that will be discussed later. Since the advent of computers, the processing of time domain functions to the frequency domain has been made much easier. A method that is quick and especially suited for computers is the fast Fourier transform (FFT). The FFT is the base of most computer based methods to transform time domain data to the frequency domain. The transformation of frequency domain functions to time domain functions are also possible through an inverse FFT.

The Continuous Fourier Transform

Jean B. Fourier proved in 1822 that most functions can be described as consisting of an infinite series of sinusoidal waves. The process involves using a Fourier integral (Doyle 1989). This is called the continuous Fourier transform (CFT).

The conditions for using a Fourier integral are referred to as Dirichlet conditions. The time function must be integrable in any given period, have a finite number of discontinuities (if any), and contain a finite number of maxima and minima during any period. Also, the function must have started at minus infinite time and end at plus infinite time. All functions that occur in reality meet these conditions.

The equations that describe the transform are

$$C(\omega) = \int_{-\infty}^{\infty} F(t) e^{-i\omega t} dt \qquad (3.9)$$

and its inverse is

$$F(t) = \frac{1}{2\pi}\int_{-\infty}^{\infty} C(\omega)e^{i\omega t}d\omega \tag{3.10}$$

where

F(t) = time domain function

t = time

C(ω) = frequency domain function

Using the Fourier integral allows the user to transform a time domain function into a frequency domain function. This is the method used to find the amplitude, frequency, and phase of the components of a given wave. The plot of C(ω) versus ω (the angular frequency) is called a frequency spectrum. In general, the values of C(ω) are complex.

$$C(\omega) = a + ib = Re^{i\phi} \tag{3.11}$$

The amplitude, R, is found by taking the absolute value of C(ω)

$$R = \sqrt{a^2 + b^2} \tag{3.12}$$

And the phase, ϕ, is found

$$\phi = a\tan\left(\frac{a}{b}\right) \tag{3.13}$$

The solution of a Fourier integral for any given function of time can be difficult to determine. The Fourier series is a method that can be applied to any given function, provided it meets the Dirichlet conditions.

In a Fourier series, an arbitrary function can be described as an infinite summation of coefficients multiplied by a sinusoidal value. The summation of all the sinusoids is the original function. This is shown is Equation 3-14

$$F(t) = \frac{1}{2}a_0 + \sum_{n=1}^{\infty}\left[a_n \cos\left(2\pi n \frac{t}{T}\right) + b_n \sin\left(2\pi n \frac{t}{T}\right)\right] \tag{3.14}$$

where

$$a_n = \frac{2}{\pi}\int_0^T F(t)\cos\left(2\pi n \frac{t}{T}\right)dt \tag{3.15}$$

and

$$b_n = \frac{2}{\pi}\int_0^T F(t)\sin\left(2\pi n \frac{t}{T}\right)dt \tag{3.16}$$

A more compact method of showing the Fourier series using complex notation is

$$F(t) = \frac{1}{T}\sum_{n=-\infty}^{\infty} C(\omega_n)e^{i\omega_n t} \tag{3.17}$$

where

$$\omega_n = 2\pi\frac{n}{T} \tag{3.18}$$

The Discrete Fourier Transform

The Fourier integral may be discretized so that a given function can be sampled over time. A time function is discretized into N equal segments. Each segment is ΔT wide, where ΔT is the time step. It is the time duration of interest, often called the period (T), divided by the number of segments (N) of that time duration. This implies that the function is periodic with a period of T. The amplitude of the segment is $F(t_m)$, which is the average of the amplitude over ΔT for a given point in time, t_m, where m is an incremental counter.

The equations for the discrete Fourier transform (DFT) are

$$C(\omega_n) = \Delta T \sum_{n=0}^{N-1} F(t_m) e^{\frac{-i2\pi nm}{N}} \tag{3.19}$$

And its inverse

$$F(t_m) = \frac{1}{T} \sum_{n=0}^{N-1} C(\omega_n) e^{\frac{i2\pi nm}{N}} \tag{3.20}$$

By discretizing the function, the section that was discretized is forced into a *periodicity.* If a greater number of points, n, are used than there are segments, N, the exponential function simply repeats itself. For example, if N is 8, then at n = 9, 11, and 17, the function is evaluated the same as at n = 1, 3, and 1 (Doyle 1989). Periodicity is enforced by the discretization process.

The CFT of a non-perioditic function can be considered to be a DFT of a periodic function with an infinite period. The DFT of a periodic function breaks the function into a finite number of frequencies. It is like a CFT of a periodic function. It is the period of the sample that determines how numerically close the DFT and CFT are.

The Fast Fourier Transform

The fast Fourier transform (FFT) is a computer algorithm for implementing the DFT. The number of calculations in the DFT involves

$$C = 2N^2 \tag{3.21}$$

where

C = number of calculations

N = number of samples

This equation normally would take a very long time to calculate. Because of the repetitive nature of the exponential equations underlying the DFT, an algorithm of the DFT, the FFT, is incredibly efficient (Cooley and Tukey 1965).

With N samples, the integral counters, n and m, which in binary form can be only 0 or 1, can be written as

$$m = m_0 + 2m_1 + 4m_2 + \cdots + 2^{M-1}m_{M-1} \tag{3.22}$$

and

$$n = n_0 + 2n_1 + 4n_2 + \cdots + 2^{M-1}n_{M-1} \tag{3.23}$$

That means that the DFT looks like

$$C(\omega_n) = \Delta T \sum_{n_0=0}^{1}\sum_{n_1=0}^{1}\cdots\sum_{n_{M-1}=0}^{1} f(t_m) e^{\frac{-i2\pi}{N}(m_0+2m_1+\cdots 2^{M-1}m_{M-1})(n_0+2n_1+\cdots 2^{N-1}n_{N-1})} \tag{3.24}$$

If, for example, M = 3, N = 8, then the CFT looks like

$$C(\omega_n) = \Delta T \sum_{n_0=0}^{1}\sum_{n_1=0}^{1}\sum_{n_2=0}^{1} f(t_m) e^{\frac{-i2\pi}{8}(m_0+2m_1+4m_2)(n_0+2n_1+4n_2)} \tag{3.25}$$

Using the exponential term, expanding it, and collecting the terms, the equation is

$$e^{\frac{-i2\pi}{8}8(m_1n_2+2m_2n_2+m_2n_1)} e^{\frac{-i2\pi}{8}(4m_0n_2)} e^{\frac{-i2\pi}{8}(2n_1(2m_1+m_0))} e^{\frac{-i2\pi}{8}(n_0(m_0+2m_1+4m_2))} \tag{3.26}$$

The first term of this equation is always equal to one. The following terms can be evaluated sequentially according to the summations in Equation 3-20.

Each sequence is used in the subsequent sequence in a bootstrap function. In addition, the first term in each sequence always is equal to one. The function also evaluates as the complex conjugates after half the number of samples have been processed (assuming a real only time function) (Clough and Penzien 1975).

In this case, the number of calculations is

$$C = \frac{3}{2} N \log_2 N \tag{3.27}$$

For N = 8, the reduction of calculations is by a factor of 3.56. At N = 1,024, the calculations are reduced by a factor of 136.5. For N = 4,096, the reduction is by a factor of 455.1 (Doyle 1989). The FFT has revolutionized the frequency analysis business. This is called digital signal processing.

For future reference, the " ^ " symbol will be used to designate anything that is in the frequency domain. The term "signal" in digital signal processing is defined as the time history of a time domain function.

Problems with Digital Signal Processing

Because the FFT, via the CFT, forces periodicity onto a function, problems can arise.

Nyquist Frequency

There is a maximum value of frequency that can be determined for a given sample rate. The sample rate is the number of samples taken over a given

time period. That maximum frequency value is called the Nyquist frequency. It is one-half of the sampling frequency. The sampling frequency is given as

$$f_{SAMPLE} = \frac{1}{\Delta T} \tag{3.28}$$

The Nyquist frequency is

$$f_{NYQUIST} = \frac{1}{2\Delta T} \tag{3.29}$$

In an FFT analysis, the signal evaluates as the complex conjugates after half the number of samples have been processed (assuming a real only time signal). Therefore, frequencies which are one-half or less of the sampling frequency can be identified.

The Nyquist sampling theory states that the sampling rate must be at least twice the frequency of the highest identifiable frequency component in the sampled signal. If the sampling rate is 60 samples per second, then the highest frequency component that can be identified is 30 cycles per second (cps). If there are frequency components above the Nyquist frequency, then aliasing occurs.

Aliasing

Aliasing is a high frequency wave masquerading as a low frequency wave. In western movies, the wagon wheels often appear to be running back-wards. This is aliasing. A movie is a sequence of pictures run at 24 frames per second. Since all the spokes look alike, the sampling process, “filming,” is catching the spokes in a frame just prior to their reaching the position of the spokes in the previous frame. Thus, the wheel appears to be running backward.

Figure 3-6 shows aliasing. The same high frequency time signal is shown in both figures. In Figure 3-6a, the time signal is being sampled at a frequency which is slightly less than the signal's frequency. This is shown by the equally spaced boxes. If, as shown in Figure 3-6b, the amplitudes at each sampled location are connected, a low frequency wave appears.

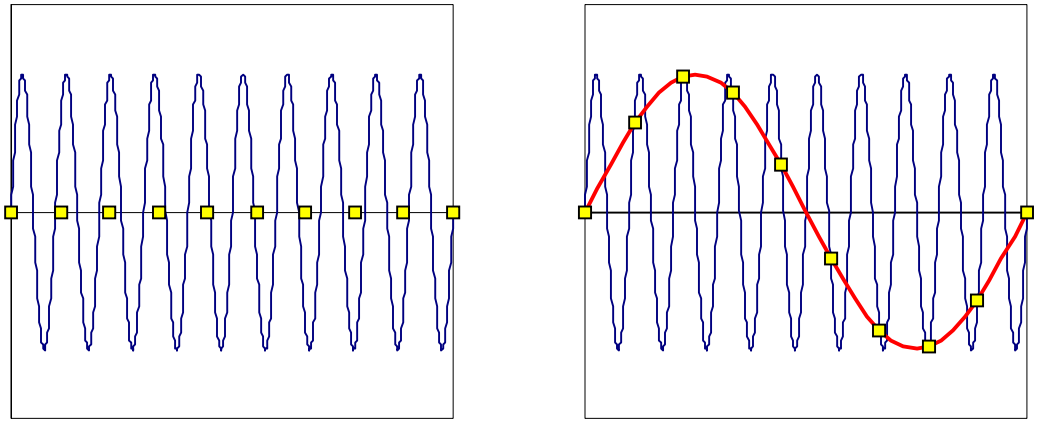

a **b**

Figure 3-6: Aliasing

If there are frequency components above the Nyquist frequency, because of the mathematics of the CFT, the amplitudes of the frequencies above the Nyquist frequency are "folded back" onto the lower frequency components. Aliasing appears as frequency components that add amplitude to frequencies that are below the Nyquist frequency. There is no method to separate an actual amplitude from an aliased amplitude, therefore, it is impossible to differentiate an actual frequency component from an aliased high frequency component.

The best way to minimize aliasing is to sample at a higher rate. Aliasing also may be reduced by filtering out nonessential high frequency components (anti-aliasing filters). If it is important to keep the high frequency components, a higher sampling rate is the only way to reduce aliasing.

Windowing

The assumption of the Dirichlet conditions and the sampling process can give problems. One of the Dirichlet conditions is the assumption that the time the signal exists is from minus to plus infinity . All time signals that are based in reality have a beginning and an end. They are not infinite in time, therefore a window is used to simulate infinite time.

This is accomplished by looking at a signal through a “window” in time. One cannot see beyond the sides of the windows. Instead, the assumption is that the signal simply repeats in window sized time chunks to plus and minus infinity. In Figure 3-7a, the actual time signal is shown. The signal is non-zero only once. However, in Figure 3-7b, the DFT mathematically sees the actual time signal as an infinite series of the windowed part of the signal. All the other windowed signals, except for the one real signal, are virtual signals. Since the math requires an infinitely repeating sample, a signal is sampled and then assumed it repeats over and over based on the size of the window. Window size is based on the time step and the number of samples.

Leakage

If the endpoints at the edge of the windowed signal do not match, then a discontinuity is introduced. A jump appears to occur, which in reality, does not

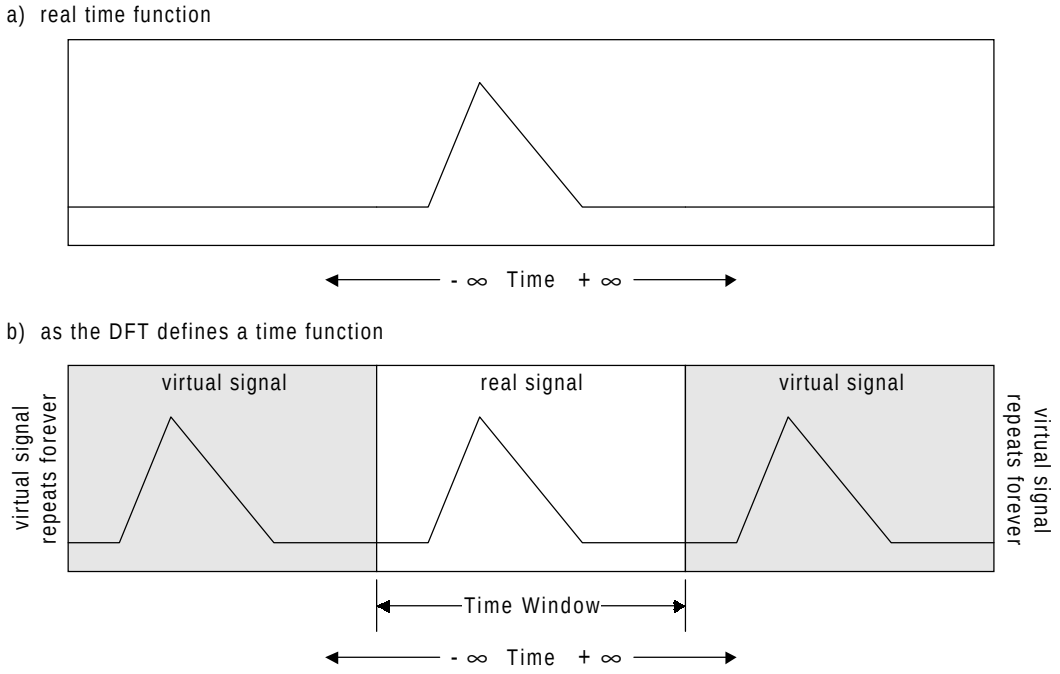

Figure 3-7: Windows

exist. In Figure 3-8a, the signal within the time window has the same amplitude endpoints at the window edges. In Figure 3-8b, the signal has a discontinuity at the window edges. The signal appears to “jump” to get into the next time window. This leads to problems such as leakage.

The discontinuities introduced at the endpoints of the signal from window to window cause false frequencies. It will appear as if the amplitudes of an actual frequency component have leaked and generated the other frequency components adjacent to the actual frequency components. This is called leakage.

If the time signal is harmonically related to the window size (i.e. the signal “fits” perfectly in the window), the discrete frequencies in the original signal will

a) Endpoints in each time window match. Leakage will not occur.

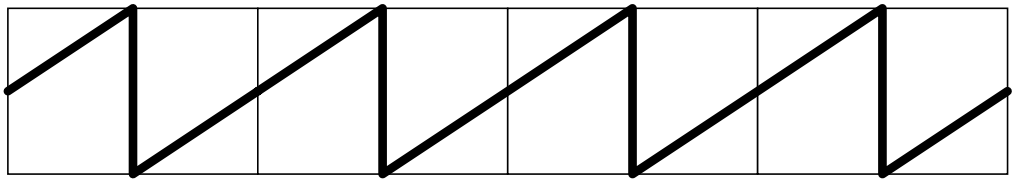

b) Endpoints in each time window do not match. Leakage will occur.

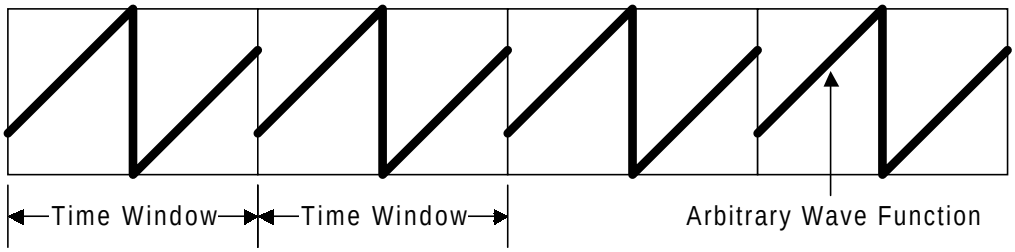

Figure 3-8: Leakage

be “sharp.” This is shown in Figure 3-9a. The actual frequency components are shown in Table 3-1. If the time signal is not harmonically related to the window size, the amplitudes tend to get leaked over a range of adjacent frequencies. The amplitudes of the actual component frequencies have been decreased, too. This is shown in Figure 3-9b. Since real time signals can have various frequencies, not all harmonics of each other, leakage is inevitable.

Frequency (Hz)	Amplitude
4	1
8	2
12	3
24	4

Table 3-1: Actual Frequency Components

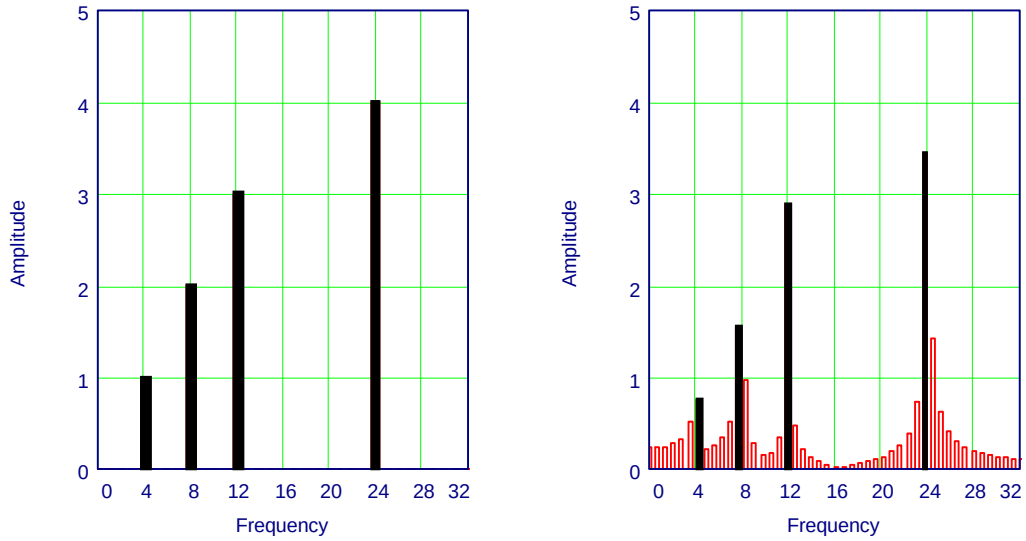

a) no leakage b) leakage

Figure 3-9: Example of Leakage

There are so-called window functions that try to minimize the jump at the endpoints of the time signal within the time window. This is usually accomplished by setting the endpoints of the time signal to zero. The time signal is multiplied in the time domain by various window functions. For example, a Hamming or a Hanning window function can be used. However, the time signal is shaped differently while using any window function other than the rectangular window function. This affects the amplitude of the frequency components.

The shape of the time signal between the endpoints after multiplication by a window function determines the amount of leakage. This has the property of minimizing the leakage, but it also affects the amplitude of the frequency components. By taking this into account, the true amplitudes can be determined.

Noise

During actual data collection for digital signal processing, noise—small inexplicable signals generated by the data gathering process—will occur. Noise in the time domain transforms into noise in the frequency domain. Noise, which is attendant in all data, is reduced with the filtering process. The filtering process assumes small amplitudes of frequency are noise and excludes them from the presentation of the data. Filtering improves the appearance of the plotted data but detail is lost.

Noise due to the data gathering process can occur because of time jitter or quantizing error. Time amplitude variation occurs with improper triggering of the acquisition gate by the signal processing equipment. The signal must reach some predefined amplitude before measuring starts. If this gate is triggered at slightly different levels, then the signal appears to have a jitter to it. Signal averaging helps reduce this problem.

Quantizing error occurs because of the sampling process. If the signal amplitude happens to be in between two digital values, the processor must pick one of the digital values. If the signal continues to run between two digital values, the processor might pick one, then the other value. This is because of the rounding process and is part of the processing. This can show as a high frequency component that does not really exist.

Digitizing (Picket Fence Effect)

Another problem in data gathering has to do with taking analog data and converting it to digital data. In the Figure 3-10, two identical analog functions are shown sampled at the same interval step. Only the starting points are differ-

ent. However, Figure 3-10a on the left has a step that samples at the maximum point of the signal. Figure 3-10b on the right shows a step that misses the maximum. All the user can see of the time signal is the data points shown by the dots. Thus, in the right digital signal, the maximum appears less than it really is. The energy of the signal has been “smeared” into the adjacent digital points. It is as if the user was looking at the time signal through a picket fence.

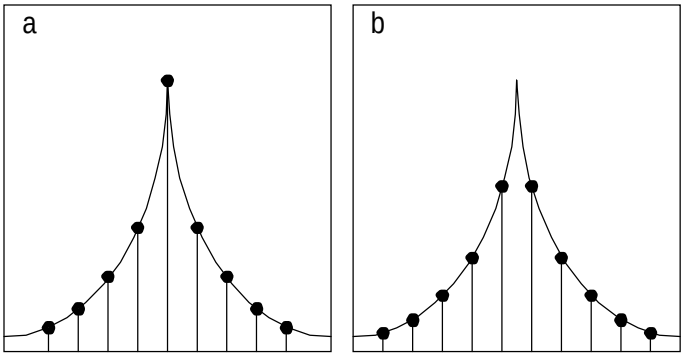

Figure 3-10: Digitizing Effect

CHAPTER 4

DERIVING THE SPECTRAL ELEMENT

This chapter sets forth the details of spectral analysis. It starts with a general description of spectral analysis. Then the static and dynamic forces on a drill string during jarring are shown. Using the dynamic forces, an axial equation of motion for a drill string under jarring conditions is derived and solved. From there, the spectral solution is derived using a finite element model composed of an axial two-noded spectral element and an axial one-noded semi-infinite spectral element. The elements are then globally assembled into one structure, the drill string. A linear algebraic solution for the globally assembled structure is made and post-processing is shown. The general procedure and the limitations of spectral analysis are described.

Stress wave tracking and finite element analysis are the two current jarring models. Both methods, rooted in the time domain, have limitations.

Wave tracking analysis is a closed form partial differential model. It has the advantage of being exact and can be solved at any location and time without regard to any previous solutions. The disadvantage, on the other hand, is that these types of solutions can be difficult (if not impossible) to solve. The analysis is also restricted to linear conditions (i.e., constant geometric and material properties).

Using iteration methods, the finite element method incorporates multiple geometric and material properties and nonlinear functions. This method requires large computational resources not generally available in the field. More importantly, the results only approximate the mass distribution of a drill string and there are algorithm stability problems with the time step choices.

The semi-analytic finite element method, set forth in this dissertation, combines wave tracking analysis with the finite element method. The semi-analytic finite element method uses the actual equations of motion rather than an approximation of the equations between nodes of motion. The equations of motion in the frequency domain are derived from the sinusoidally varying components of the equations of motion in the time domain.

This is accomplished by using the FFT. Then, a series of forced frequency responses based on the results of the decomposed force values can be analyzed. After the analysis, the resulting displacement functions can be inverted back into their calculated time displacement functions. This process also can work in reverse; i.e., starting with a time displacement function and returning with the time force function.

A sinusoidal input will cause a sinusoidal output. (Another way of looking at this is that a harmonic excitation generates a harmonic response.) The output or response will have the same frequency, but not necessarily the same amplitude or phase. This is called a forced frequency response. Equation 4-1 shows a sinusoidally varying force, P. This, with the appropriate calculations dependent on the type of analysis, gives a sinusoidally varying displacement, U.

$$P = pe^{i\omega t} \Rightarrow ue^{i\omega t} = U \tag{4.1}$$

where

ω = angular frequency

t = time

p = sinusoidal force amplitude

u = sinusoidal displacement amplitude

Remember that Euler's formula is

$$Re^{j\theta} = R\left(\cos(\theta) + i\sin(\theta)\right) \tag{4.2}$$

where

θ = angular frequency

R = amplitude

The p and u in equation 4.1 are the amplitudes of the sinusoidal waves and correspond to the R in equation 4.2. The forced frequency response can apply to any number of frequencies and they can be added together through linear algebra. This is shown in equation 4.3

$$\begin{Bmatrix} P_1 \\ P_2 \\ \vdots \\ P_n \end{Bmatrix} = \begin{Bmatrix} p_1 \\ p_2 \\ \vdots \\ p_n \end{Bmatrix} e^{i\omega t} \Rightarrow \begin{Bmatrix} u_1 \\ u_2 \\ \vdots \\ u_n \end{Bmatrix} e^{i\omega t} = \begin{Bmatrix} U_1 \\ U_2 \\ \vdots \\ U_n \end{Bmatrix} \tag{4.3}$$

This is where the frequency domain gets involved. The conversion from the time domain to the frequency domain involves the exponential function

$$e^{i\omega t} \tag{4.4}$$

The values in equation 4.3 are a set of linear equations multiplied by this same exponential function. The Fourier transform turns time based data into fre-

quency based data. The inverse Fourier transform reverses the process. It transforms frequency based data into time based data. In the frequency domain, equation 4.3 would looks like equation 4.5

$$P_n = \hat{p}_n e^{i\omega_n t} \Rightarrow \hat{u}_n e^{i\omega_n t} = U_n \tag{4.5}$$

At first, this process may not appear to be much of an advantage over any strictly time domain processes. If anything, more steps appear to be needed. However, the process of determining the frequency equations for the forced function response analysis involves taking a second order partial differential equation (PDE) and converting it to a second order ordinary differential equation (ODE). ODE's are easier to solve than PDE's. In addition, the shape function used to determine the finite element equations continuously describes the mass distribution. There is no need to determine a maximum element size. It can be as large as geometry or material permits. Finally, the FFT process that determines the frequency spectrum is computationally very efficient.

In this dissertation, assumptions have been made. One such assumption is that there are no transverse waves. All of the waves generated by the jarring impact are assumed to be planar longitudinal stress waves traveling in the axial direction. It is also assumed that there is no reduction or enlargement in the area affected by the wave from the Poisson's effect.

These assumptions are reasonable because of the fact that the majority of the jarring waves are generated in the axial direction for most straight hole situations. Torsional and bending waves are not significant because, in straight holes, the method used to generate the forces is an impact in the axial direction.

There are a number of forces acting on the drill string. They can be broken into static and dynamic forces.

Static Forces

Static forces are those that do not significantly change within the time frame of the jarring process. This includes such forces as gravity and overpull. In the context of jarring analysis, both the static and dynamic forces can be analyzed separately. The stresses from the static forces can be linearly added to the dynamic forces. For example, even though there might be two equal dynamic force stress waves propagating outward from a jar, the actual stresses in the drill string will reflect the stress from the dynamic forces plus the stress from the static forces.

Axial stress is real tension divided by the cross-sectional area of the drill string (Mitchell 1995). Tension causes two marks on a drill string to separate. Compression causes two marks on a drill string to converge. To analyze static stress, it is important to ascertain all of static forces acting on a section of the drill string. Since this dissertation is limited to the one dimensional axial case, only those stresses that directly affect axial stress will be considered. This is a uniaxial load case.

Static axial stress is calculated by dividing the tension or compression by the cross-sectional area of the drill string.

Gravity

Part of the axial stress at a given point in the drill string is based on gravity and the fluids in which it is immersed. The fluids have a density which determines the hydrostatic pressure and possibly an additional pressure from the

surface. The force from the fluids must have a pressure area to act over. Because this is a one dimensional case, only areas perpendicular to the axial direction need be considered. The drill string also has weight.

Overpull Force

The overpull force is the force necessary to trigger the jars. It is a force at the trigger mechanism in the jars. As such, this force is the determining factor for all of the static stresses in the drill string at the time the jar triggers. Since this force vanishes as the jar is triggered, it acts as a negative stress wave after the jar triggers and before the jar impact. The force at the top of the stuck point is determined by taking the overpull force and subtracting the weight of the drill string below the jars and above the top of the stuck point.

Dynamic Forces

Dynamic forces are those that significantly change within the time frame of the jarring process. That includes such forces which arise from strain changes and damping.

Strain

Changes in strain occur because a wave of stress is being propagated. An assumption is made that the wave propagation stress remains in the linear portion of the stress-strain curve. This allows for the use of Hooke's Law which is

$$\sigma = E\frac{\partial u}{\partial x} \tag{4.6}$$

where

E = modulus of elasticity

σ = stress

u = displacement

x = location

Since stress is a force acting over a cross-sectional area, then the forces from strain can be determined as

$$F = AE\frac{\partial u}{\partial x} \tag{4.7}$$

where

A = cross-sectional area

F = force

This is a very important equation to remember for jarring analysis.

Damping

Damping is the dissipation of energy over time or distance (Harris 88). If damping, or friction, did not occur, vibrations could race out of control, leading to structural failure. Energy from vibrations would simply build until there is too much energy for the structure to sustain. Most of the time, the dissipated energy from the vibration is converted into heat. In the borehole, three distinctive types of damping occur. They are hysteretic, viscous, and Coulomb damping.

Hysteretic Damping

Another name for hysteretic damping is structural damping. This is the type of damping that arises from internal friction within a structure. A wave moves through a material because the atomic structure is reacting to an applied

force. As the atoms of the structure move, energy is lost from the interaction of these atoms with their neighboring atoms. Hysteretic damping is the energy wasted as atoms move relative to each other.

If a material had a perfectly linear stress-strain relationship, hysteretic damping would not occur. But in reality, there is no such thing as a perfectly linear stress-strain curve. As a material is stressed and relieved, two curves on the stress-strain diagram will develop. The center area between the two curves represents the energy lost to internal friction. This hysteresis loop is the source

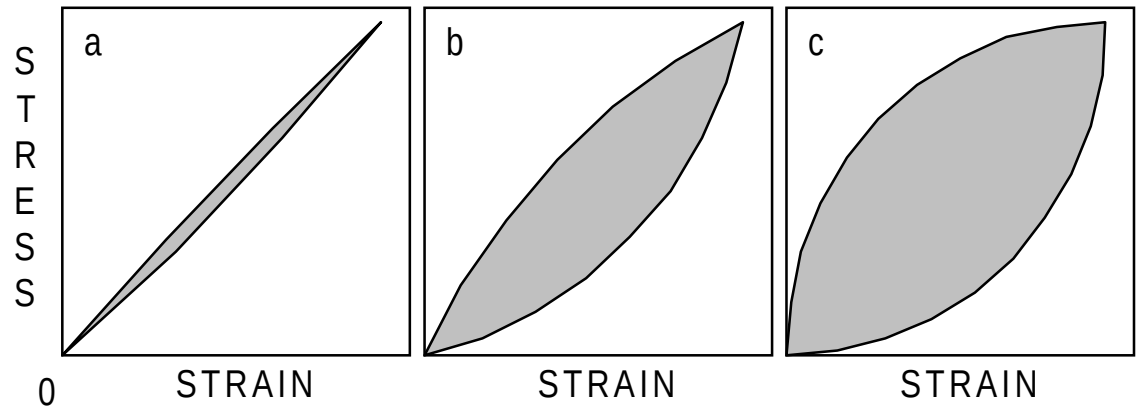

Figure 4-1: Examples of Hysteretic Damping

of the name for this type of damping. The gray shaded areas in Figure 4-1 show various values for hysteretic damping. Note that in Figure 4-1a, the loop is very small. However, because high frequency vibrations can cause this loop to be repeated many, many times over a given time period, the actual energy dissipated can be large (Kolski 1963).

The value of hysteretic damping is highly dependent on a number of factors. One factor is the condition of the material (i.e., chemical composition,

inhomogeneities, and property changes due to thermal and stress histories). Another factor is the state of internal stress from initial and subsequent thermal and stress histories. Also, the type and variation of stress—axial, torsional, shear, and/or bending— will affect the hysteretic damping value.

A way of looking at hysteretic damping force is to set it proportional to the particle velocity divided by the wave frequency. This is shown in equation 4.8 (Doyle 1991)

$$F_H = \frac{h}{\omega}\frac{\partial u}{\partial t} \tag{4.8}$$

where

h = hysteretic damping factor

F_H = hysteretic damping force

If this is converted into the frequency domain, the hysteretic damping is proportional to the spectral displacement but is in the imaginary plane. This is shown in equation 4.9 (Doyle 1991)

$$\hat{F}_H = ih\hat{u} \tag{4.9}$$

In this manner, a form of hysteretic damping can be included in the jarring model. Unfortunately, h is difficult to determine.

Viscous Damping

Any time the damping force is proportional to the velocity of the particles, it is called viscous damping. This is shown as follows

$$F_D = \gamma\frac{\partial u}{\partial t} \tag{4.10}$$

where

γ = damping coefficient

F_D = viscous damping force

One way viscous damping arises in jarring analysis is from the interaction of a solid and liquid at their interface. This occurs along the sides of the drill string where the steel contacts the liquid mud.

A method of determining the viscous damping involves noting the decrement of acceleration over one vibration cycle (Dareing and Livesay 1968). An impulse is impressed on the drill string producing a wave. While the wave is decaying, the acceleration is measured and recorded over multiple times at one location on the string. It is necessary that the two recordings to be compared are at the same phase (i.e. crest to crest). The time (T) between the two recordings is also noted. These values are used in equation 4.11 to compute the value of the damping coefficient γ. Unfortunately, this method gives the total damping and does not distinguish between viscous and Coulomb damping

$$\gamma = \frac{2AE}{c_A^2 T} \ln \frac{A_1}{A_2} \tag{4.11}$$

where

c_A = axial wave propagation speed

Coulomb Damping

Coulomb damping is the friction that occurs from two dry surfaces sliding over each other. The Coulomb damping force is a constant value that is independent of particle velocity and displacement, but dependent on the friction factor, μ, and the force normal to the friction surface. This value is shown as follows

$$F_F = \mu F_N \tag{4.12}$$

where

μ = friction factor

F_N = normal force

F_F = Coulomb friction force

This force is always of the opposite sign from the particle velocity. This means that as the particle velocity changes signs, there is a complete reversal of the damping force. It is this discontinuity that makes this a nonlinear damping force. This is shown in as follows

$$F_F = \text{sgn}\left(\frac{\partial u}{\partial t}\right)\mu F_N \tag{4.13}$$

where

sgn = sign of term in parenthesis

This nonlinearity makes a closed form solution to an equation of motion virtually impossible.

Equivalent Viscous Damping

One potential way to include Coulomb damping in a linear manner, is to determine an equivalent viscous damping system such that the energy dissipated over a given cycle is the same as for a given Coulomb damping system (Jacobson 1930). For a constant friction force, the equivalent viscous damping coefficient is

$$C_{EQ} = \frac{4}{\pi}\frac{F_F}{X\omega} \tag{4.14}$$

where

C_{EQ} = equivalent viscous damping coefficient

X is the maximum displacement for a given frequency and is

$$X = \frac{\left[\hat{P}^2\left\{c^2\omega^2 + \left(k - m\omega^2\right)^2\right\} - \frac{16}{\pi^2}F_F^2\left(k - m\omega^2\right)^2\right]^{\frac{1}{2}} - \frac{4}{\pi}c^2F_F\omega}{c^2\omega^2 + \left(k - m\omega^2\right)^2} \tag{4.15}$$

where

k = spring constant

m = mass

c = viscous damping coefficient

According to Jacobson, equation 4.14 does not tend to be accurate if the ω value is not near a resonant value. Unfortunately, too many variables are unknown to make this work very well.

General Derivation of the Axial Equation of Motion

The axial equation of motion starts with Newton's Second Law of Motion and a freebody analysis. A typical segment of the drill string is selected. It can be inclined as long as it is straight. The various dynamic forces acting on a differential element are shown in Figure 4.2.

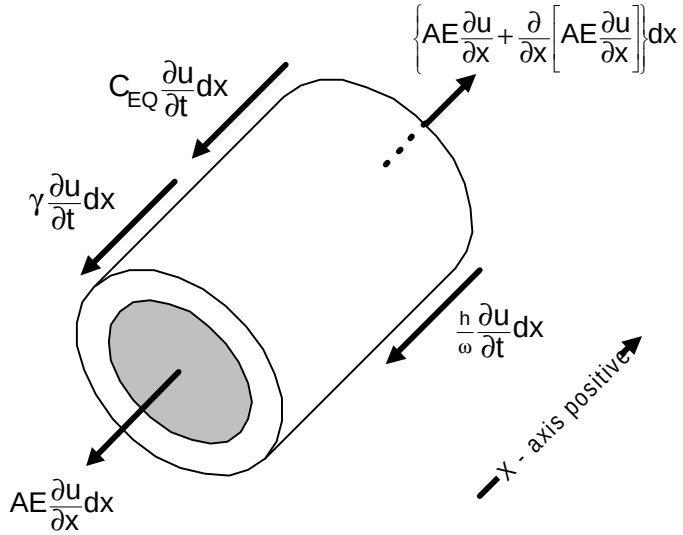

Figure 4-2: Axial Freebody Diagram

The forces include viscous damping, hysteretic damping, equivalent viscous damping (for Coulomb damping), and strain forces. Using Newton's Second Law of Motion, the forces are summed and set equal to the mass multiplied by acceleration. This is shown in equation 4.16

$$pdx\frac{\partial^2 u}{\partial t^2}=\left\{AE\frac{\partial u}{\partial x}+\frac{\partial}{\partial x}\left[AE\frac{\partial u}{\partial x}\right]\right\}dx-AE\frac{\partial u}{\partial x}dx$$
$$-\gamma\frac{\partial u}{\partial t}dx-C_{EQ}\frac{\partial u}{\partial t}dx-\frac{h}{\omega}\frac{\partial u}{\partial t}dx \qquad (4.16)$$

where

p = mass per unit length

t = time

x = location on the string

Simplifying this equation and assuming a constant area and modulus of elasticity yields

$$p dx \frac{\partial^2 u}{\partial t^2} = AE \frac{\partial^2 u}{\partial x^2} dx - \gamma \frac{\partial u}{\partial t} dx - C_{EQ} \frac{\partial u}{\partial t} dx - \frac{h}{\omega} \frac{\partial u}{\partial t} dx \quad (4.17)$$

Canceling the differential distance dx and collecting like terms gives

$$p \frac{\partial^2 u}{\partial t^2} = AE \frac{\partial^2 u}{\partial x^2} - \left(\gamma + C_{EQ} + \frac{h}{\omega} \right) \frac{\partial u}{\partial t} \quad (4.18)$$

This is the axial equation of motion for the differential element. The next step is to find a solution for it.

General Solution for the Axial Equation of Motion

This equation is amenable to solution by way of the separation of variables method. This is shown as

$$U(x,t) = X(x)T(t) \quad (4.19)$$

where

U(x,t) = solution in time and space

X(x) = function of space only

T(t) = function of time only

If the following assumption is made concerning the time function

$$T(t) = e^{i\omega t} \quad (4.20)$$

Then the solution looks like

$$U_D(x,t) = X(x)e^{i\omega t} \tag{4.21}$$

This equation can be differentiated as follows

$$\frac{\partial U_D(x,t)}{\partial t} = i\omega X(x)e^{i\omega t} \tag{4.22}$$

$$\frac{\partial U_D^2(x,t)}{\partial t^2} = -\omega^2 X(x)e^{i\omega t} \tag{4.23}$$

$$\frac{\partial U_D(x,t)}{\partial x} = \frac{\partial X(x)}{\partial x}e^{i\omega t} \tag{4.24}$$

$$\frac{\partial U_D^2(x,t)}{\partial x^2} = \frac{\partial^2 X(x)}{\partial x^2}e^{i\omega t} \tag{4.25}$$

These four equations can be substituted back into the original equation of motion

$$-p\omega^2 X(x)e^{i\omega t} = AE\frac{\partial^2 X(x)}{\partial x^2}e^{i\omega t} - \left(\gamma + C_{EQ} + \frac{h}{\omega}\right)i\omega X(x)e^{i\omega t} \tag{4.26}$$

Collecting terms and dividing out the exponential term gives

$$0 = \frac{\partial^2 X(x)}{\partial x^2} + \left[\frac{p\omega^2 - \left(\gamma + C_{EQ} + \frac{h}{\omega}\right)i\omega}{AE}\right]X(x) \tag{4.27}$$

Equation 4.27 is of the form

$$y'' + a^2 y = 0 \tag{4.28}$$

The standard solution of this equation is

$$X(x) = \mathcal{A}e^{-ikx} + \mathcal{B}e^{ikx} \tag{4.29}$$

where

$\mathcal{A}$ and $\mathcal{B}$ = constants of integration

The constants of integration are determined by the boundary conditions.

k is a collection of the constants and is equal to

$$k = \sqrt{\frac{p\omega^2 - \left(\gamma + C_{EQ} + \frac{h}{\omega}\right)i\omega}{AE}} \tag{4.30}$$

Therefore, the total dynamic solution is

$$U_D(x,t) = \left[\mathcal{A}e^{-ikx} + \mathcal{B}e^{ikx}\right]e^{i\omega t} \tag{4.31}$$

The Spectral Solution

The next step is to convert the previous solution into the frequency domain. In Chapter 3, the Fourier analysis of a time function was discussed. In equation 3.17, it was shown that a Fourier solution in complex terms was

$$F(t) = \frac{1}{T}\sum_{n=-\infty}^{\infty} C(\omega_n)e^{i\omega_n t} \tag{3.17}$$

Looking at equation 4.31, similarities between the two equations can be seen. One can say that for a given location in space that the Fourier coefficients are

$$\frac{1}{T}\sum_{n=-\infty}^{\infty} C(\omega_n) = \mathcal{A}e^{-ikx} + \mathcal{B}e^{ikx} \tag{4.32}$$

Therefore, the equation to determine the frequency domain solution at a given point on the drill string is

$$\hat{u}(x) = \mathcal{A}e^{-ikx} + \mathcal{B}e^{ikx} \tag{4.33}$$

where

$\hat{u}(x)$ = displacement spectrum

Finite Element Method

The previous discussion centered on a closed form solution to the dynamic axial equation of motion for a finite element. Now that will be applied to the finite element method.

The basic procedure for applying the finite element method is as follows.

1) The structure is divided into logical elements. How this is accomplished is dependent upon the method used to formulate the element properties. Current time-based domain methods require a large number of elements to model the mass distribution in a lumped manner for wave propagation problems. In the frequency domain, this is not needed. The mathematics model the mass continuously rather than in a lumped manner. The only element division needed is for differences in geometric and material properties (i.e. changing from drill collars to drill pipe).

2) Formulate the element properties. This formulation involves using a shape function. This function is the “simplified” equation discussed earlier. In the frequency domain, this equation need not be simplified; it is exact. This is why this method is often called a semi-analytical finite element method. It is also why the mass distribution is modeled continuously.

3) Each of the elements is then assembled into a global system. The elements are added together at their endpoints

(called nodes) using linear algebra. This is accomplished in the model developed in this dissertation because this is a one-dimensional model. Although adding more dimensions complicates the procedure, it is primarily a bookkeeping problem (assuming the stiffness matrices are derived correctly).

4) The external boundary conditions are added to the global system. This is addressed in the next chapter.

5) Solve the system of element equations. This is a simultaneous solution using linear algebraic techniques. This gives the displacement values at the nodes.

6) Back substitute the displacement nodal values into the shape function equations to return displacement values to the element level.

7) Assess the results.

After dividing the structure into elements, the shape function for a spectral finite element is

$$\hat{u}(x) = \mathcal{A}e^{-ikx} + \mathcal{B}e^{ik(x-L)} \tag{4.34}$$

where

L = element length

Note that the second term has the element length built into it. The $\hat{u}(x)$ is called the spectral displacement.

A General Axial Two-Noded Spectral Element

A general axial two-noded spectral element is shown in Figure 4-3.

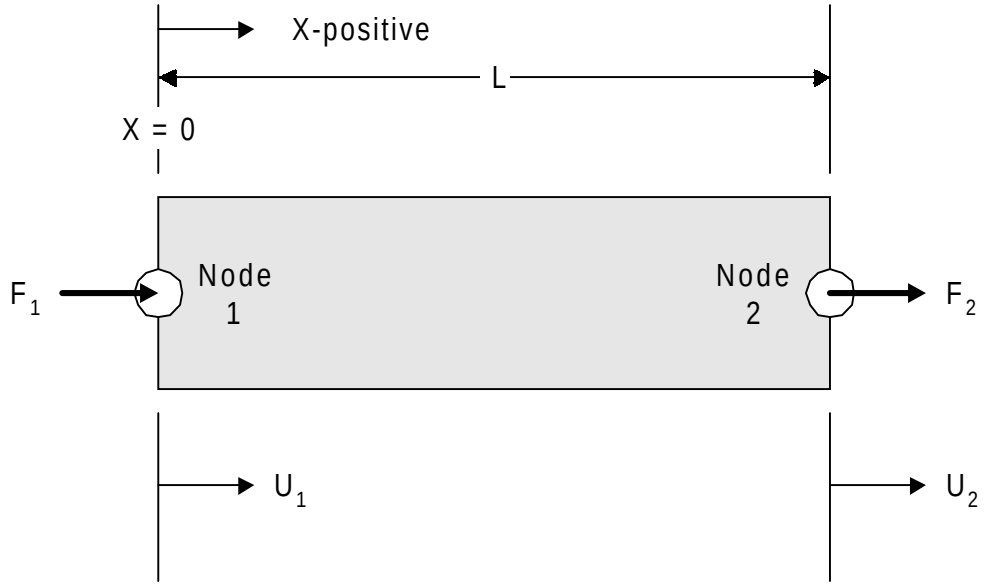

Figure 4-3: Two Noded Axial Finite Element

At node 1, the x value is 0 and at node 2, the x value is L. Using equation 4.33, the spectral displacement, $\hat{u}_1$, at node 1 is

$$\hat{u}_1 = \hat{u}(0) = \mathcal{A} + \mathcal{B}e^{-ikL} \tag{4.35}$$

and $\hat{u}_2$ at node 2

$$\hat{u}_2 = \hat{u}(L) = \mathcal{A}e^{-ikL} + \mathcal{B} \tag{4.36}$$

Combining the previous two equations into a linear algebraic form gives

$$\begin{bmatrix} \hat{u}_1 \\ \hat{u}_2 \end{bmatrix} = \begin{bmatrix} 1 & e^{-ikL} \\ e^{-ikL} & 1 \end{bmatrix} \begin{bmatrix} \mathcal{A} \\ \mathcal{B} \end{bmatrix} \tag{4.37}$$

Solving for $\mathcal{A}$ and $\mathcal{B}$ gives

$$\begin{bmatrix} \mathcal{A} \\ \mathcal{B} \end{bmatrix} = \frac{1}{1-e^{-i2kL}} \begin{bmatrix} 1 & -e^{-ikL} \\ -e^{-ikL} & 1 \end{bmatrix} \begin{bmatrix} \hat{u}_1 \\ \hat{u}_2 \end{bmatrix} \tag{4.38}$$

Now, remembering equation 4.7, the shape function is differentiated with respect to x

$$\frac{\partial \hat{u}(x)}{\partial x} = ik\left(-\mathcal{A}e^{-ikx} + \mathcal{B}e^{ik(x-L)}\right) \tag{4.39}$$

and multiplied by cross-sectional area, A, and modulus of elasticity, E, to get the force equation

$$\hat{F}(x) = ikAE\left(\mathcal{A}e^{-ikx} + \mathcal{B}e^{ik(x-L)}\right) \tag{4.40}$$

Using this equation, the nodal forces are determined

$$\hat{F}_1 = \hat{F}(0) = -ikAE\left(-\mathcal{A} + \mathcal{B}e^{-ikL}\right) \tag{4.41}$$

and

$$\hat{F}_2 = \hat{F}(L) = ikAE\left(-\mathcal{A}e^{-ikL} + \mathcal{B}\right) \tag{4.42}$$

to get

$$\begin{bmatrix} \hat{F}_1 \\ \hat{F}_2 \end{bmatrix} = ikAE \begin{bmatrix} 1 & -e^{-ikL} \\ -e^{-ikL} & 1 \end{bmatrix} \begin{bmatrix} \mathcal{A} \\ \mathcal{B} \end{bmatrix} \tag{4.43}$$

Substituting back into equation 4-43 with 4-38 gives

$$\begin{bmatrix}\hat{F}_1\\ \hat{F}_2\end{bmatrix} = ikAE\begin{bmatrix}1 & -e^{-ikL}\\ -e^{-ikL} & 1\end{bmatrix}\frac{1}{1-e^{-2ikL}}\begin{bmatrix}1 & -e^{-ikL}\\ -e^{-ikL} & 1\end{bmatrix}\begin{bmatrix}\hat{u}_1\\ \hat{u}_2\end{bmatrix} \tag{4.44}$$

after algebraic manipulation, the finite element equation is

$$\begin{bmatrix}\hat{F}_1\\ \hat{F}_2\end{bmatrix} = \frac{ikAE}{1-e^{-2ikL}}\begin{bmatrix}1+e^{-2ikL} & -2e^{-ikL}\\ -2e^{-ikL} & 1+e^{-2ikL}\end{bmatrix}\begin{bmatrix}\hat{u}_1\\ \hat{u}_2\end{bmatrix} \tag{4.45}$$

This equation is in the form of

$$F = Ku \tag{4.46}$$

The K in the above equation is called the stiffness matrix. It is

$$K = \frac{ikAE}{1-e^{-2ikL}}\begin{bmatrix}1+e^{-2ikL} & -2e^{-ikL}\\ -2e^{-ikL} & 1+e^{-2ikL}\end{bmatrix} \tag{4.47}$$

Some items of note concerning the above equation. First, the k in the equation is based on the damping factors, mass distribution, and most importantly, the frequency. (See equation 4.30.) This means that this finite element equation works for one frequency at a time. This is not a problem as the FFT of a force gives a frequency and an associated force for that frequency.

Also to be noted is that the modulus of elasticity and the cross-sectional area for the elements are constant. The structure must be divided wherever a change in geometry or material occur. Note that the division is not for the purpose of lumping the mass.

Derivation of the Axial One-Noded Semi-Infinite Spectral Element

Because these equations are written in the frequency domain, a semi-infinite element is now possible. This element is unusual in that it has only one active node. The other end which is at an infinite distance has no effect on the model. This has the advantage of conducting and dissipating all of the energy away from the area of interest with no returning energy.

A semi-infinite element is placed where a reflection of a wave from the far end can not take an active role within the time frame of analysis. For example, if a wave reflection takes 2 seconds to return to the original location and the time of interest is 0.5 seconds, it does not really matter if the reflection shows up in 2 seconds or 2,000,000 seconds. It has no effect on the analysis. In essence, the element is infinitely long.

To derive this element, a value of infinity is used for L

$$\begin{bmatrix} \hat{F}_1 \\ \hat{F}_2 \end{bmatrix} = \frac{ikAE}{1-e^{-2ik\infty}} \begin{bmatrix} 1+e^{-2ik\infty} & -2e^{-ik\infty} \\ -2e^{-ik\infty} & 1+e^{-2ik\infty} \end{bmatrix} \begin{bmatrix} \hat{u}_1 \\ \hat{u}_2 \end{bmatrix} \tag{4.48}$$

This reduces the equation to

$$\begin{bmatrix} \hat{F}_1 \\ \hat{F}_2 \end{bmatrix} = ikAE \begin{bmatrix} 1 & 0 \\ 0 & 1 \end{bmatrix} \begin{bmatrix} \hat{u}_1 \\ \hat{u}_2 \end{bmatrix} \tag{4.49}$$

The individual values for the spectral displacements and forces become detached. The value for $\hat{u}_2$ has no effect on the value of $\hat{u}_1$. This element has the advantage of reducing the number of equations to be solved by one. The element equation is

$$\hat{F}_1 = ikAE\hat{u}_1 \tag{4.50}$$

Globally Assembling the Spectral Elements

The next step is to assemble the elements into a global assembly. Since this is a one dimensional problem, each element is connected to its neighbor at only one place, the nodes. This is shown in Figure 4-4. The nodes and elements are numbered from the bottom up. The user is cautioned not to mix the order of the elements. This will have severe consequences upon the solution.

The global assembly procedure involves adding the stiffness matrix values for each connected node. For example, global node 1 on the global system is the same as local node 2 for element 1 and local node 1 for element 2. The stiffness values that correspond to these two local nodes are summed. In addition, the local nodal displacement on connected elements must be equal, otherwise, the elements have separated.

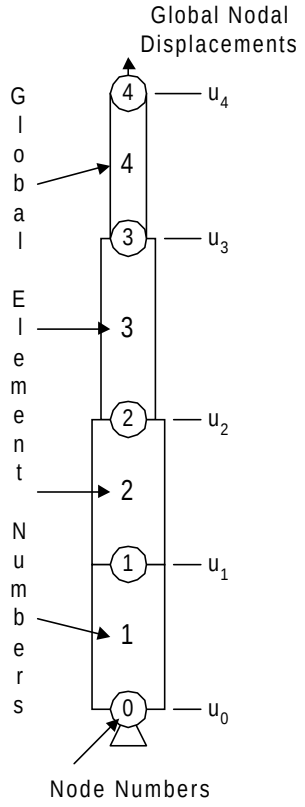

Figure 4-4: Example of Global Assembly

Also, for nodal equilibrium, the sum of the internal forces at a node must be equal to zero. In the following equation, the spectral forces are shown in local nodal form and the spectral displacements are shown in global form

$$\begin{bmatrix} \hat{F}_1^1 \\ \hat{F}_2^1 - \hat{F}_1^2 \\ \hat{F}_2^2 \end{bmatrix} = [K] \begin{bmatrix} \hat{u}_0 \\ \hat{u}_1 \\ \hat{u}_2 \end{bmatrix} \tag{4.51}$$

where

$$[K] = \begin{bmatrix} ik_1A_1E_1\left(1+e^{-2ik_1L_1}\right) & -ik_1A_1E_1\left(2e^{-ik_1L_1}\right) & 0 \\ -ik_1A_1E_1\left(2e^{-ik_1L_1}\right) & ik_1A_1E_1\left(1+e^{-2ik_1L_1}\right)+ik_2A_2E_2\left(1+e^{-2ik_2L_2}\right) & -ik_2A_2E_2\left(2e^{-ik_2L_2}\right) \\ 0 & -ik_2A_2E_2\left(2e^{-ik_2L_2}\right) & ik_2A_2E_2\left(1+e^{-2ik_2L_2}\right) \end{bmatrix} \tag{4.52}$$

The rest of the global assembly is along the same lines.

Applying the Boundary Conditions

The next step is to apply the external boundary conditions. In the example, node 0 is shown as fixed and node 4 is shown with an external force. Therefore, for node 0, $\hat{u}_0$ is equal to zero. The rest of the nodal spectral displacements are unknown.

For node 4, the sum of the forces would be equal to the external spectral force. The other forces sum to zero except for the reaction external force at node 0, which is unknown. Therefore, all of the unknown spectral displacements have known spectral forces acting upon them. And all of the unknown spectral

forces have known spectral displacements. This is a necessity. The equations cannot be solved if an unknown spectral displacement and an unknown spectral force coincide!

Other external boundary conditions can be applied at any node. These can include a point mass, viscous damper, spring, or other force. Other forces will include the force from the jar impact. There can be as many forces as there are nodes. And there can be as many nodes as needed.

Solving the Assembled System

In a system of equations where all the forces are prescribed, the solution involves inverting the stiffness matrix (the inverted form of the stiffness matrix is called the transfer matrix) and multiplying by the spectral force vector. This may or may not be trivial. One of the advantages of the spectral method is that very few elements are needed to describe the system. That means that the stiffness matrix will be small and banded. There are many solvers available for the inversion of a matrix.

More than likely, the spectral force and displacement vectors will have a mixture of known and unknown values. The matrix system must be partitioned in that situation. In partitioning, the matrix and vectors are rearranged to get the known values together and the unknown values together. There are partitioning schemes available in finite element method or linear algebraic texts (Reddy 1984, Zienkiewicz and Taylor 1989, Doyle 1989).

Post-Processing

The solution of the linear equations give the nodal spectral displacements and forces. From these values, other information can be derived. For example, the strain can be determined by differentiating the shape function with respect to space. This value can be multiplied by the modulus of elasticity to get stress. Multiply this value by cross-sectional area to get the force. Note that all of this must be accomplished while still in the frequency domain.

Between the Nodes

Once the solution for the nodal values is available, the shape functions allow for the resolution of displacements and forces between the nodes. The post-processing shape function, derived specifically to separate the nodal values, is

$$\hat{u}(x) = \frac{1}{e^{-2ikL} - 1}\left(\left[e^{-ik(2L-x)} - e^{-ikx}\right]\hat{u}_1 + \left[e^{-ik(L+x)} - e^{-ik(L-x)}\right]\hat{u}_2\right) \tag{4.53}$$

The force values can be derived from this equation by differentiating with respect to x and multiplying by A and E.

$$\hat{F}(x) = \frac{ikAE}{e^{-2ikL} - 1}\left(\left[e^{-ik(2L-x)} + e^{-ikx}\right]\hat{u}_1 - \left[e^{-ik(L+x)} + e^{-ik(L-x)}\right]\hat{u}_2\right) \tag{4.54}$$

In any case, all of these values are still in the frequency domain. It is a simple matter of reinverting the values back into the time domain using an inverse FFT. This should be the last step. Once again, note that none of the variables may be recovered in the time domain. It must be accomplished in the frequency domain prior to inverting back into the time domain.

Spectral Analysis Procedure

The procedure used for spectral analysis as follows.

1) Determine a known time domain force or displacement function.
2) Run a fast Fourier transform on that function.
3) The spectral force or displacement spectrum is determined.
4) Apply the finite element method previously discussed.
5) The spectral displacement or force spectrum is determined.
6) The inverse fast Fourier transform is applied to the spectral displacement or force spectrum.
7) The time domain displacement or force values are determined.

This is graphically shown in Figure 4-5. Note that the procedure can run in either direction.

Limitations of the Method

As in all good methods and procedures, there are limitations and caveats.

Knowledge of the Input

This method is one for wave propagation analysis only. It determines all of the reflections and refractions of the originating wave(s) (which generates

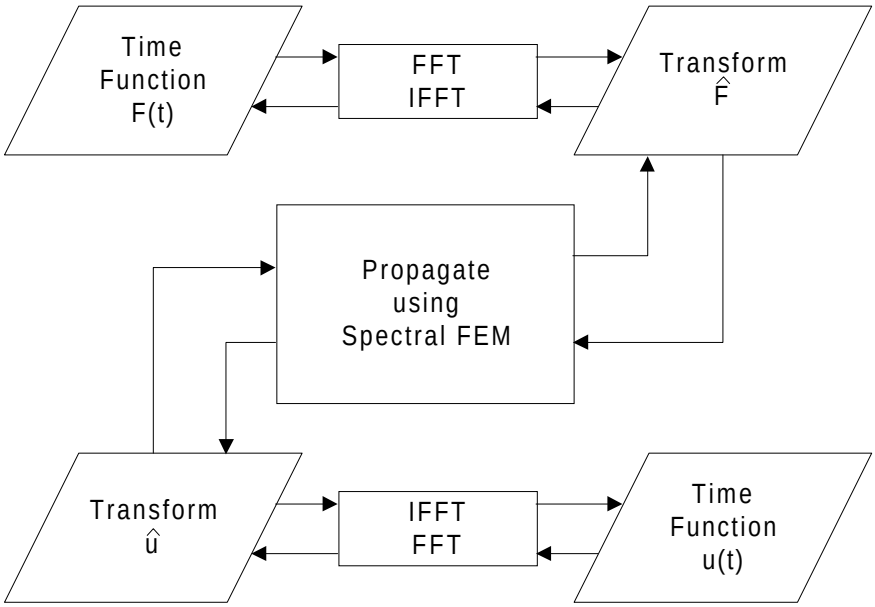

Figure 4-5: Spectral Analysis Procedure

more reflected and refracted waves). It does **not** generate the originating wave(s). Therefore, there must be an entire time history of the originating wave(s). It is this time history of the originating wave(s) that is transformed into the frequency domain.

Windows and Wave Migration

Because this method uses the DFT, it can have the problems inherent in all frequency analysis including aliasing, leakage, noise, and digitizing error. These errors can be minimized by padding (adding zeroes) and windowing. However, there is one problem that limits this method to wave propagation only, not vibration.

The frequency methods all assume a periodic function, even if the function is not periodic. Since infinity is a very long time, this limitation has been built into the mathematics of frequency analysis. The problem arises after a wave has completely propagated across a time window. Since this wave is assumed periodic, a virtual wave will appear on the other side of the time window. This virtual wave is from the neighboring window. It will ride on top of the original time function.

Figure 4-6 shows an example of this phenomena. Since the spectral analysis is location specific, a time window represents what happened in time at a specific location. The wave is not being followed. Rather, it is as if one was sitting watching traffic go by. In the figure, this is a triangular wave going by a specific location. It is being reflected back and forth while it is decaying.

In Figure 4-6a, the wave is decaying before the window is traversed. In Figure 4-6b, the time window is of shorter duration. Since this is the same wave as in Figure 4-6a, the wave is not decaying before it migrates through the shorter time window. Part of the wave is appearing in the next window. This wave is labeled as the “wrap-around wave” and is the virtual wave. The reconstructed time window looks quite different than the actual conditions. Extreme care must be taken to insure this migration does not occur. It will significantly affect the results of an analysis!

Therefore, it is **critical** to have the wave decay to practically zero before the time window closes. This is accomplished by either dumping the energy using damping or a semi-infinite element (remember it conducts energy out of a system) or by using a very long window.

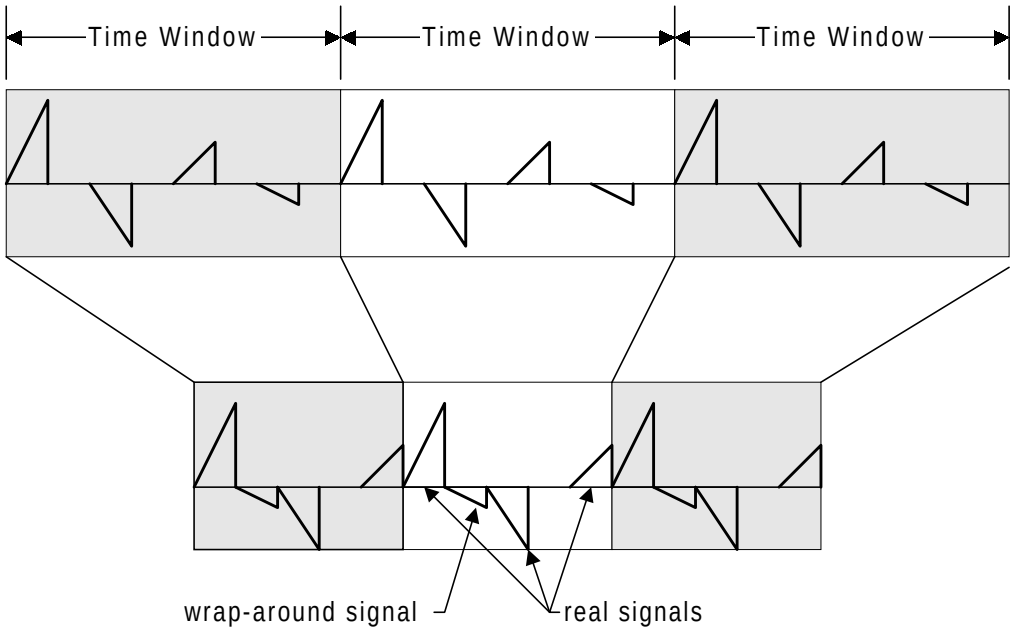

Figure 4-6: Wave Propagation into Windows

Nonlinearity

Finally, since the time signal is built into the frequency analysis, there can be no control of time once inside the frequency domain. This means that nonlinear effects, such as free contraction to impact conditions, cannot not be directly analyzed. As will be seen in the next chapter, this analysis can be made, but it must be separated. In addition, Coulomb damping cannot be directly addressed.

CHAPTER 5

THE USE OF SPECTRAL ANALYSIS IN WAVE PROPAGATION

This chapter presents five models that validate the spectral analysis method. The first example will show the effect of a wave interacting with a fixed end point (a wall). The second example will show the effect of a wave interacting with a free end point. The third and fourth examples will show how changes in cross-sectional areas affect the wave propagation through the interface. The last example will show how multiple cross-sectional areas affect wave propagation.

Wave Reflections from Various Geometric Boundaries

For future developments and confidence in the model presented in this dissertation, it is required that a corollary model be developed which contains wave propagation and wave interaction with geometric discontinuities. What happens as a wave meets a fixed or free boundary condition? Also, what happens to a wave as it encounters a cross-sectional area change?

A fixed end is one in which there can be no displacement. According to wave theory, during a wave encounter with a fixed end, the stress at that end will double during the passage of the wave. This effect can be looked at as if the incident stress wave encounters an identical stress wave coming out of the fixed

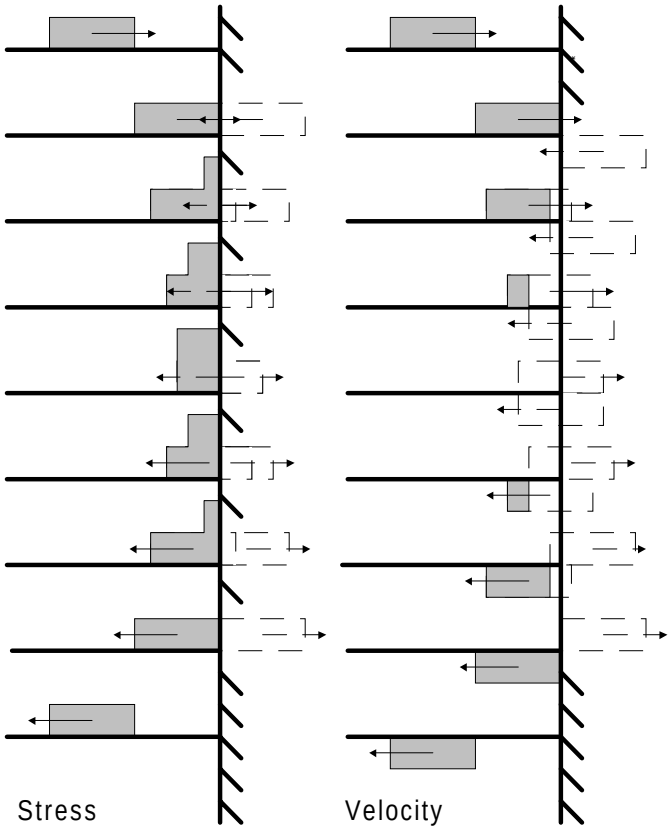

Figure 5-1: Fixed End Boundary Conditions

end. The two waves, one incident and one virtual, will interact and exchange places. This is shown in Figure 5-1. The boxes in the figure represent the amplitude of either stress or velocity. Above the line is positive and below the line is negative. A reflection of a stress wave will simply bounce back with the same sign. A compression wave will reflect as a compression wave and a tension wave will reflect as a tension wave.

At a fixed end, because the displacement is equal to zero, the particle velocity will be zero. It is as if the wave encounters a virtual wave with velocity of the opposite sign. The waves will interact and cancel each other during the encounter. The wave particle velocity amplitude will be inverted during a reflection from a fixed end.

A free end is defined as a traction free end. The stress at the free end is always equal to zero. A free end will cause the opposite effects on stress and particle velocity as the effects on a fixed end. This is shown in Figure 5-2.

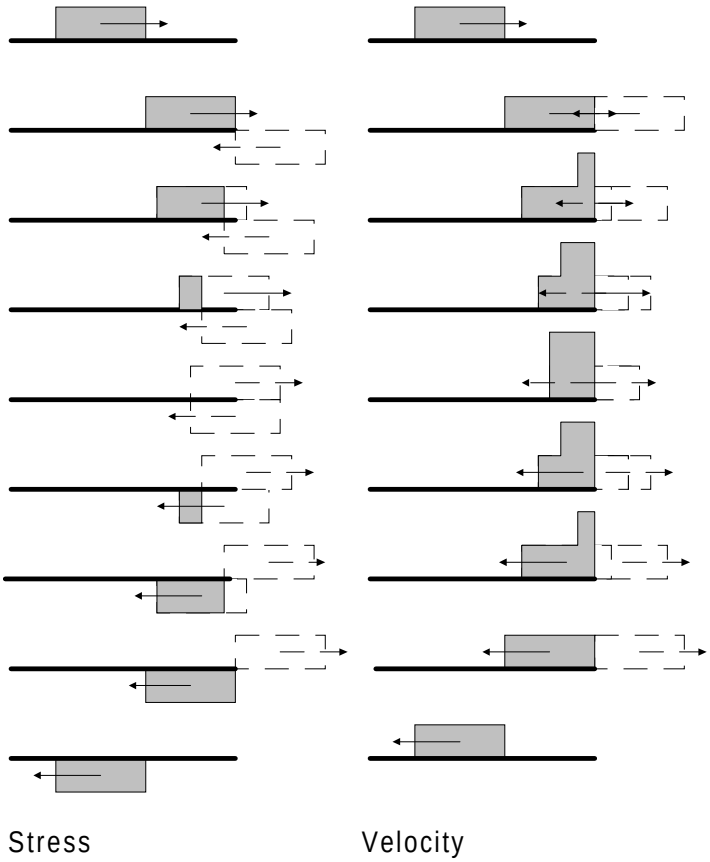

Figure 5-2: Free End Boundary Conditions

In this case, the incident stress wave encounters a virtual wave with stress with the opposite sign. The incident and virtual waves interact and exchange places. They cancel each other during the encounter and the virtual wave exchanges places with the incident wave to become the outgoing wave. A compression wave encountering a free end will reflect as a tension wave. A tension wave will reflect as a compression wave.

At a free end, because a displacement must occur, the virtual wave will have particle velocities of the same sign. The incident and virtual waves will interact and reinforce each other during the encounter. The wave particle velocity values will double during an encounter with a free end and will reflect with the same sign.

As an incident wave encounters a change in cross-sectional area, some of the wave is reflected and some of the wave is transmitted (refracted). The amplitudes and sign of the waves are dependent upon the relative change in cross-sectional area.

The equations that describe the effect of either a cross-sectional area, density, or modulus of elasticity change for the transmitted wave is

$$F_T = 2\frac{\sqrt{\frac{E_2\rho_2}{E_1\rho_1}}}{\sqrt{\frac{E_2\rho_2}{E_1\rho_1}}\frac{A_2}{A_1}+1}F_I \tag{5.1}$$

and for the reflected wave is

$$F_R = \frac{\sqrt{\frac{E_2\rho_2}{E_1\rho_1}}\frac{A_2}{A_1}-1}{\sqrt{\frac{E_2\rho_2}{E_1\rho_1}}\frac{A_2}{A_1}+1}F_I \tag{5.2}$$

If an incident wave encounters a junction where the relative change in cross-sectional area is greater than one (a smaller to a larger area), most of the wave will transmit through the junction. Some of the wave will reflect from the junction and will keep the same sign. For example, a compression wave will transmit through the junction and keep going as a somewhat diminished compression wave. The part of the wave that is reflected is still a compression wave. It will have an amplitude less than the wave that transmitted though the junction.

On the other hand, if an incident wave encounters a junction where the relative change in cross-sectional area is less than one (a larger to a smaller area), most of the wave will reflect off of the junction. Some of the wave will

transmit through the junction and will keep the same sign. For example, a compression wave will transmit through the junction and keep going as a diminished compression wave. The reflected part of the wave is a tension wave. The absolute amplitude of the tension wave will be greater than the compression wave that is transmitted through the junction.

Spectral Analysis Example Set-Up

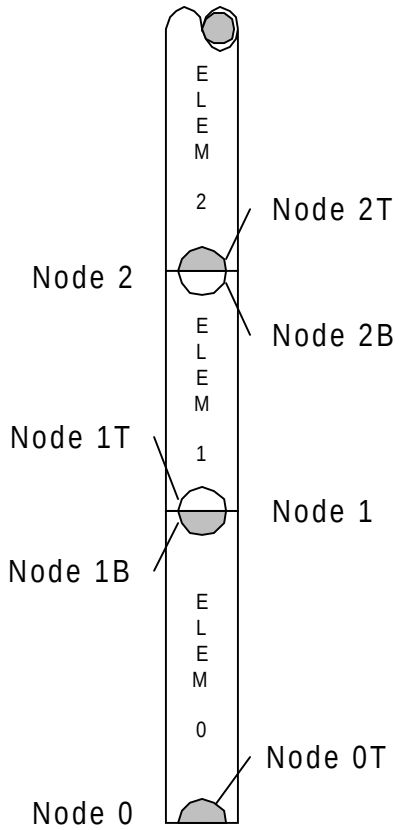

Figure 5-3: Example Node and Element Numbering

It is important to keep the node numbering in order. The scheme for the examples is shown in Figure 5-3. There are four nodes: 0, 1, 2, and 3. Node 3 is not shown because it is an infinite distance away. The nodes are broken into two halves. This is done because the forces on one side of a node are not always equal to the forces on the other side of the node, although the overall nodal forces balance. This occurs because there could be an external force at that node or changes in material or geometric properties.

The nodes' halves have been labeled with the node number and the side of the node on which it is located. For example, a force at the top side of node 1 would be labeled $Force_{1T}$.

In each example, the changes involve different cross-sectional areas and the node 0 boundary condition. In all five examples, the force input on node 1 is always the same and the lengths and material properties of the elements are always the same.

The length of element 0 is 1,684.2 feet and of element 1 is 14,210.5 feet. This is a travel time distance of 100 milliseconds and 250 milliseconds, respectively. The length of element 2 is infinite. Since the longitudinal wave propagation speed is the same for the same material, a time multiplied by 16,842 feet per second will give a distance. However, it is easier to interpret the following figures by considering the distance as an equivalent time.

The figures may be confusing at first glance. It is important to remember that the figures of force, displacement, velocity, and acceleration are at a specific location. It is as if one was sitting on a street corner watching traffic go by. (See Figure 5-4.) For example, an observer is sitting on a street corner with a dead end street. A car goes past the observer at time 100. The car is traveling down the dead end street, but the observer can only see the corner. At time equals 200, the car finds the dead end and turns

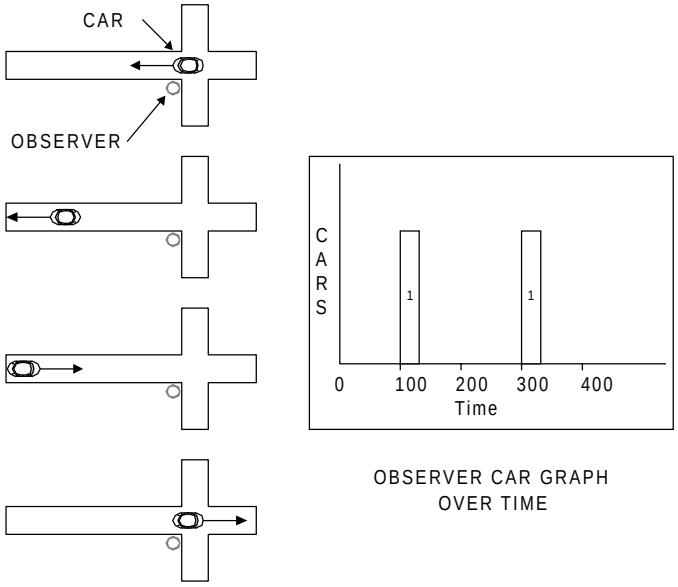

Figure 5-4: Traffic Example

around. Then at time 300, the observer notes that a car has come out of the dead end street. As far as the observer has seen, a car went by at time 100 and time 300. The appearance of the figures for spectral analysis are very similar to this example.

The propagating wave is identical in all five examples. It is a rectangular pulse that starts at 100 milliseconds and lasts for 50 milliseconds. The wave has an amplitude of 100,000 lbf. It is imposed at node 1. The time domain appearance of this wave is plotted in Figure 5-5.

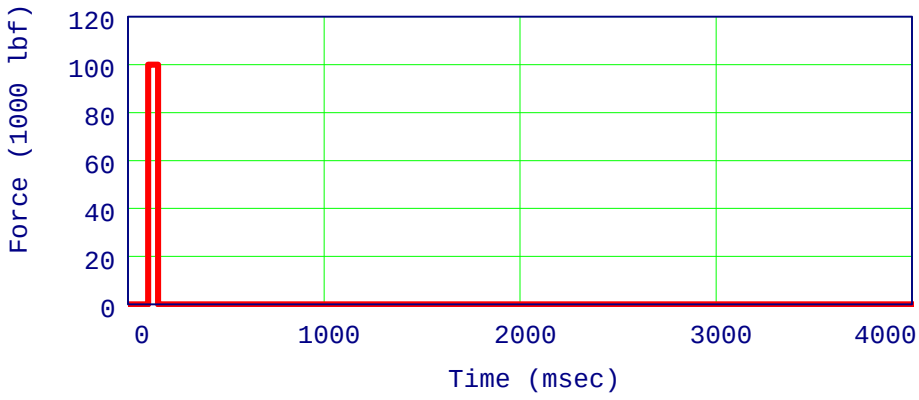

Figure 5-5: Wave in the Time Domain

The wave is sampled at 1,000 Hz, the sampling frequency. This gives a Nyquist frequency of 500 Hz. Therefore, if any frequencies which are present in the signal are higher than the Nyquist frequency, then aliasing may occur. The sampling time step, ΔT, is 0.001 seconds. In the first four examples, 4,096 samples are taken. This is 2^{12} samples. In the last example, 8,192 samples are taken. This is 2^{13} samples. A frequency graph, often called a frequency spectrum plot is shown in Figure 5-6. It is the amplitudes of the sinusoidal compo-

nents (individual points) plotted versus the frequency. Note that the amplitudes of the high frequency components are very low. Aliasing will not be a problem. Also, since the wave starts in the window at zero and ends at zero, leakage will not be a problem. This type of function is called a self-windowed function because the endpoints match without resorting to windowing shape functions.

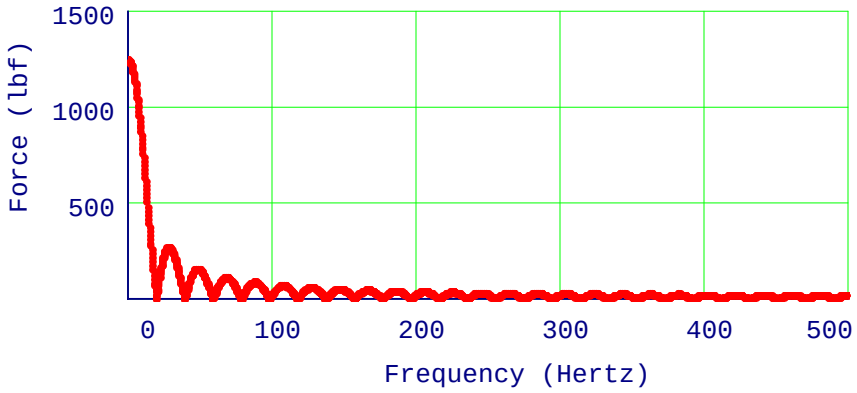

Figure 5-6: Wave in the Frequency Domain

In each example, the element modulus of elasticity is 30×10^6 psi. The element density is 490 lbm/ft^3. Damping is set to zero in order to not distort the wave as it propagates.

Calculations for the Examples

The spectral analysis procedure starts with the conversion of the time domain wave to the frequency domain wave. The first step is to determine the wavenumbers for each frequency, which is

$$\hat{k} = \sqrt{\frac{\omega^2}{c^2} + \frac{i\omega\gamma}{AE}} \tag{5.3}$$

With these values, the stiffness matrix elements can be determined for each element. For the on diagonal values

$$\hat{K}_D = \frac{i\hat{k}AE}{1 - e^{-2i\hat{k}L}}\left(1 + e^{-2i\hat{k}L}\right) \tag{5.4}$$

For the off diagonal values

$$\hat{K}_{OD} = \frac{i\hat{k}AE}{1 - e^{-2i\hat{k}L}}\left(-2e^{-i\hat{k}L}\right) \tag{5.5}$$

These values are true for the non-infinite elements. For the semi-infinite element, the stiffness matrix values for the on diagonal value is

$$\hat{K}_{DSI} = i\hat{k}AE \tag{5.6}$$

and for the off diagonal value

$$\hat{K}_{ODSI} = 0 \tag{5.7}$$

The entire stiffness matrix is assembled for the global solution. In the fixed boundary examples, since the U_0 value is known to be zero for all time and frequencies, a reduced stiffness matrix can be used. In addition, because the off-diagonal values of the semi-infinite element are zero, the stiffness matrix can be reduced further. The solution for the spectral displacements are

$$\begin{bmatrix} \hat{u}_1 \\ \hat{u}_2 \end{bmatrix} = \begin{bmatrix} \hat{K}_{D0} + \hat{K}_{D1} & \hat{K}_{OD1} \\ \hat{K}_{OD1} & \hat{K}_{D1} + \hat{K}_{DSI} \end{bmatrix}^{-1} \begin{bmatrix} \hat{F} \\ 0 \end{bmatrix} \tag{5.8}$$

The numbers in the stiffness matrix subscripts represent the element numbers and the numbers on the spectral displacements represent the node numbers.

For the free boundary example, the reduced stiffness matrix cannot be used. The solution for the spectral displacements are

$$\begin{bmatrix} \hat{u}_0 \\ \hat{u}_1 \\ \hat{u}_2 \end{bmatrix} = \begin{bmatrix} \hat{K}_{D0} & \hat{K}_{OD0} & 0 \\ \hat{K}_{OD0} & \hat{K}_{D0} + \hat{K}_{D1} & \hat{K}_{OD1} \\ 0 & \hat{K}_{OD1} & \hat{K}_{D1} + \hat{K}_{DSI} \end{bmatrix}^{-1} \begin{bmatrix} 0 \\ \hat{F} \\ 0 \end{bmatrix} \tag{5.9}$$

Once the spectral displacements are known, the spectral forces at the nodes can be reconstructed. For the top side of the node (local x value of zero) the following equation is used

$$\hat{F}_T = i\hat{k}AE\left[\frac{e^{ikL} + e^{-1kL}}{e^{ikL} - e^{-1kL}}\hat{u}_T - \frac{2}{e^{ikL} - e^{-1kL}}\hat{u}_B\right] \tag{5.10}$$

For the bottom side of the node (local x value of L) the following equation is used

$$\hat{F}_B = i\hat{k}AE\left[\frac{2}{e^{ikL} - e^{-1kL}}\hat{u}_T - \frac{e^{ikL} + e^{-1kL}}{e^{ikL} - e^{-1kL}}\hat{u}_B\right] \tag{5.11}$$

The spectral velocities are calculated as follows

$$\hat{v} = i\omega\hat{u} \tag{5.12}$$

and the spectral accelerations are calculated as follows

$$\hat{a} = -\omega^2\hat{u} \tag{5.13}$$

In the previous equations, note that the wavenumber is in every equation. If the wavenumber is zero, corresponding to a frequency of zero, these equations are zero also. However, the amplitude of the zeroth frequency equals the average amplitude of the entire wave form over the entire time span. Unless the average value of the wave is zero, it is important to include this zeroth frequency value. If it is not included, the inverted time domain values are shifted by the value of the missing amplitude.

The values to add depend upon the location of the input wave. These values can be calculated using standard static analysis procedures. For example, in the fixed boundary examples, the $\hat{u}_1$ and $\hat{u}_2$ values at the zeroth frequency are equal to

$$\hat{u}_1 = \hat{u}_2 = \frac{\hat{F}L_0}{A_0E_0} \tag{5.14}$$

Note that only the zero frequency values are calculated with this equation. All the other frequency values use the previous equations.

The free end boundary condition is very important in the jarring model. Between the triggering of the jar and impact, the hammer and anvil are free ends. Sometimes, after impact, the hammer and anvil are free ends again.

In the free end boundary condition with a semi-infinite element case, a problem occurs. One end of the system is free and the other end is an infinite distance away. This leads to an unconstrained condition. The zeroth values of the forces, displacements, velocities, and accelerations have an offset induced the unconstrained condition. The offset occurs because the mathematics dictate that the entire system undergo a rigid body motion, even though in reality, it does not. The motion is related to the free contraction speeds of the various

elements, the time span being investigated, and the zeroth frequency values. Offsets to the zeroth frequency values have been included in the free end example to cancel the non-existant rigid body motion effects.

After the spectral values are calculated, it is a matter of using the inverse FFT to return to the time domain.

Example One—A Wave Interacting with a Fixed Boundary

This example shows how a wave interacts with a fixed boundary. A force function, labeled F(t) in Figure 5-7 and shown in Figure 5-5 (time domain) and 5-6 (frequency domain), is an 100,000 lbf force applied upwards on node 1. Because the cross-sectional areas on both sides of node 1 are equal, a compressive wave (shown as a positive value) equal to one half of the overall force is propagated from the top of node 1 upwards the semi-infinite element 2. A tension wave (shown as a negative value) equal to one half of the overall force is propagated from the bottom of node 1. This tension wave will travel to the fixed end at node 0, reflect, and propagate to the top. The compression force is 50,000 lbf on element 1 at node 1 and the tensile force is 50,000 lbf on element 0 at node 1. Both forces sum to 100,000 lbf. There is no damping in any of these examples.

At 100 milliseconds (ms), the wave input starts (force is applied at node 1). At 150 ms, the wave input stops (force is removed from node 1). It takes 100 ms to traverse element 0 and 250 ms to traverse element 1.

At node 0, a tension wave with double the amplitude of the force that started in element 0 at node 1, 100,000 lbf, should be seen from 200 to 250 ms.

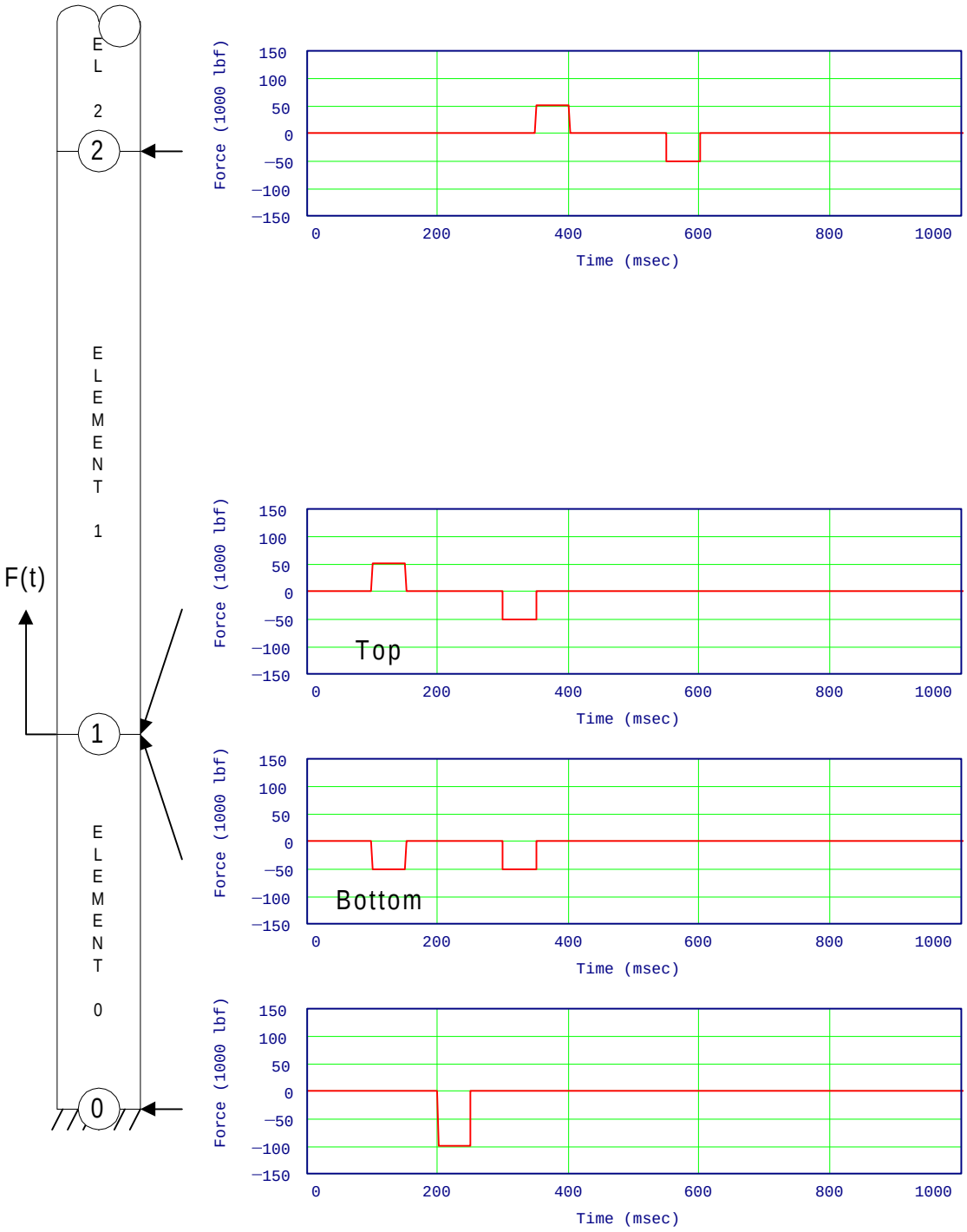

Figure 5-7: Example 1

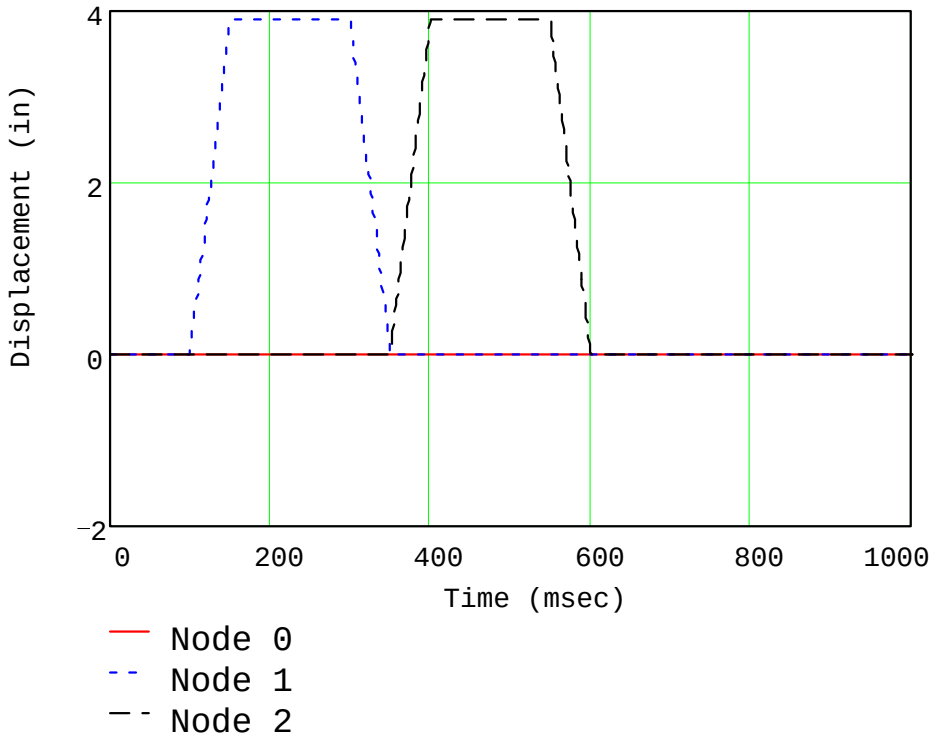

Figure 5-8: Example 1—Displacements

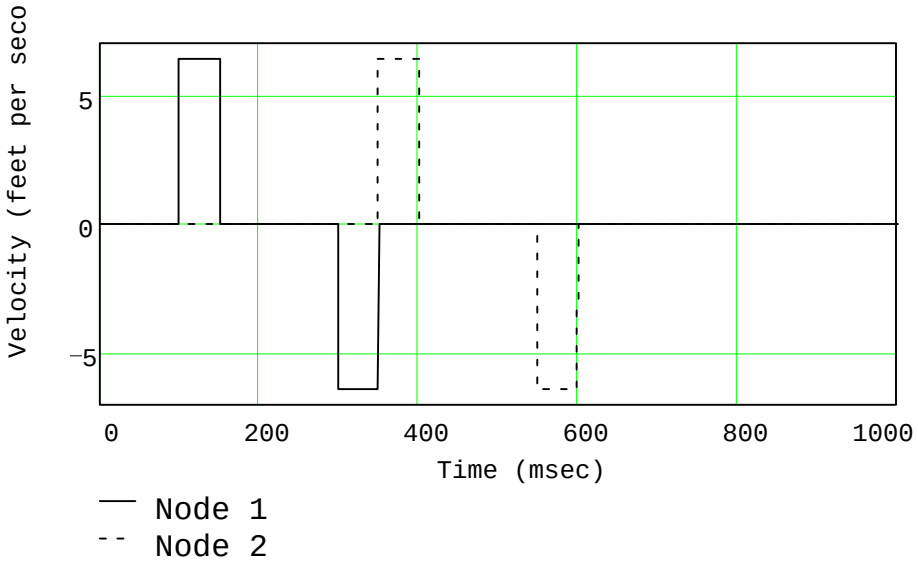

Figure 5-9: Example 1—Velocities

This is the initial wave starting at 100 ms plus the transit time of 100 ms. Because there are no reflections from anywhere else in the string, there should be no more waves appearing at node 0.

At node 1, the initial wave should be seen at 100 to 150 ms. On the top side of node 1, a compression wave of 50,000 lbf should be seen. On the bottom side of node 1, there should be a tension wave of one-half the overall amplitude of the wave, 50,000 lbf. On both sides of the node, at 300 ms (the start at 100 ms plus a round trip to the fixed end of 200 ms), another 50 ms wave of 50,000 lbf should be seen. This is the reflected wave from the fixed end (node 0).

The same waves travel through the bottom and top sides of Node 2. Both sides should be identical because there is no original wave input at this node. The waves traveling through this node are the same waves that traveled through the top side of node 1, 250 ms earlier. There should be a 50,000 lbf compressive wave at 350 ms and a 50,000 lbf tension wave at 550 ms (100 ms plus 200 ms plus 250 ms).

The displacement and velocity histories of nodes 0, 1, and 2 are shown in Figure 5-8 and Figure 5-9. The displacement and velocity at node 0 are zero for all time. This is the fixed boundary and is modelled correctly. The displacement is nonzero until both the compressive and tension wave passes through the node. Nodes 1 and 2 show the displacements as the wave passes through. The velocities are nonzero only while the wave is traveling through the node.

Example Two—A Wave Interacting with a Free Boundary

This example shows how a wave interacts with a free boundary. All of the conditions in Example 2 are the same as in Example 1 except that the boundary

at node 0 is a free boundary. (See Figure 5-10.) The same 100,000 lbf 50 ms wave starts at node 1 at 100 ms. A 50,000 lbf compressive wave is propagated from the top of node 1 and a 50,000 lbf tension wave is propagated from the bottom of node 1. This tension wave will travel to the free end, reflect and invert into a compressive wave, and propagate to the top. The timing on all the waves are the same as in Example 1. The force from the wave at node 0 should be zero for all times. This is the definition of a traction free end.

The wave at 100 ms is the same as in Example 1, the wave at 300 ms is inverted from Example 1. This is the expected inverted tension wave reflected as a compression wave from the free end.

As in all of these examples, the bottom and top sides of node 2 react to the same waves.

The displacements shown in Figure 5-11 and velocities shown in Figure 5-12 have the previously mentioned rigid body motion removed. The displacements show a permanent change of location. There were two compressive waves rather than a tensile and compressive wave. In Example 1, the compressive wave traveled through first and then the tensile wave traveled through canceling the displacements. In this example, the two compression waves doubled the displacement.

The rigid body motion is removed because it is an artificial construct of the wave theory where semi-infinite elements are involved. This rigid body motion is the free contraction speed of the particular element. This gives a zero velocity to the nodes except while the wave is travelling through the nodes. The velocity at node 0 is double the velocities at the other two nodes. This is a free end effect and is modelled correctly.

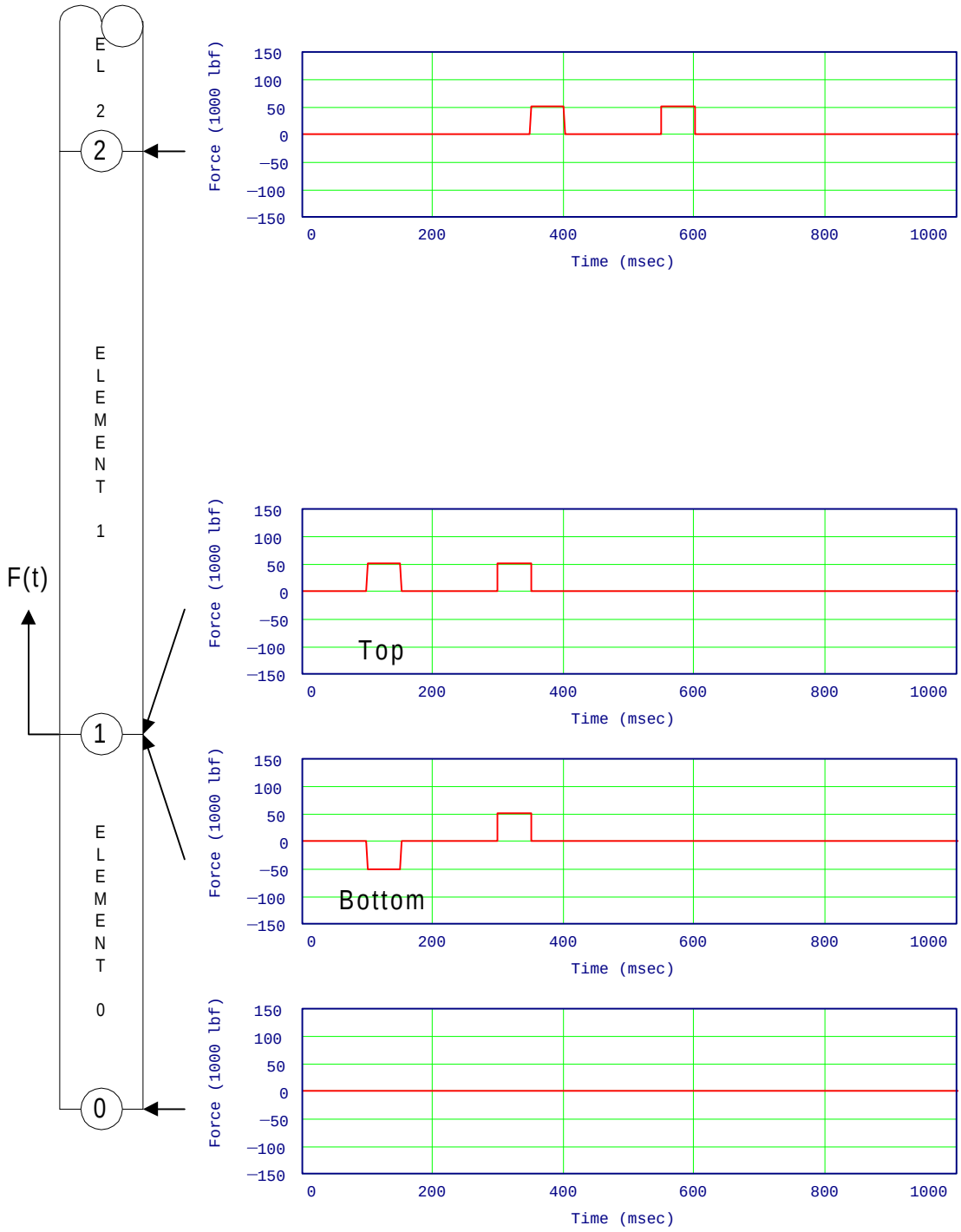

Figure 5-10: Example 2

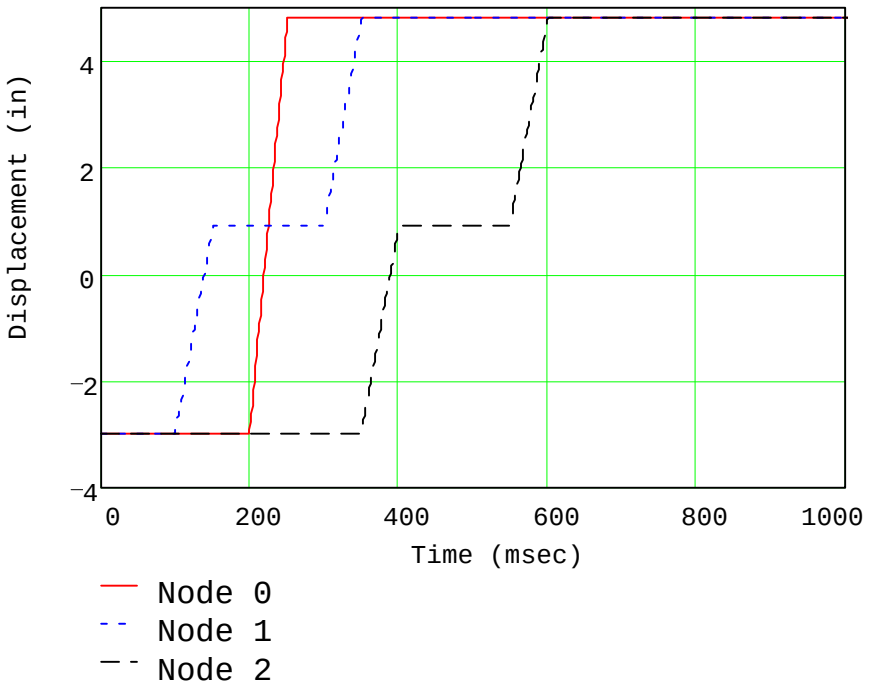

Figure 5-11: Example 2—Displacements

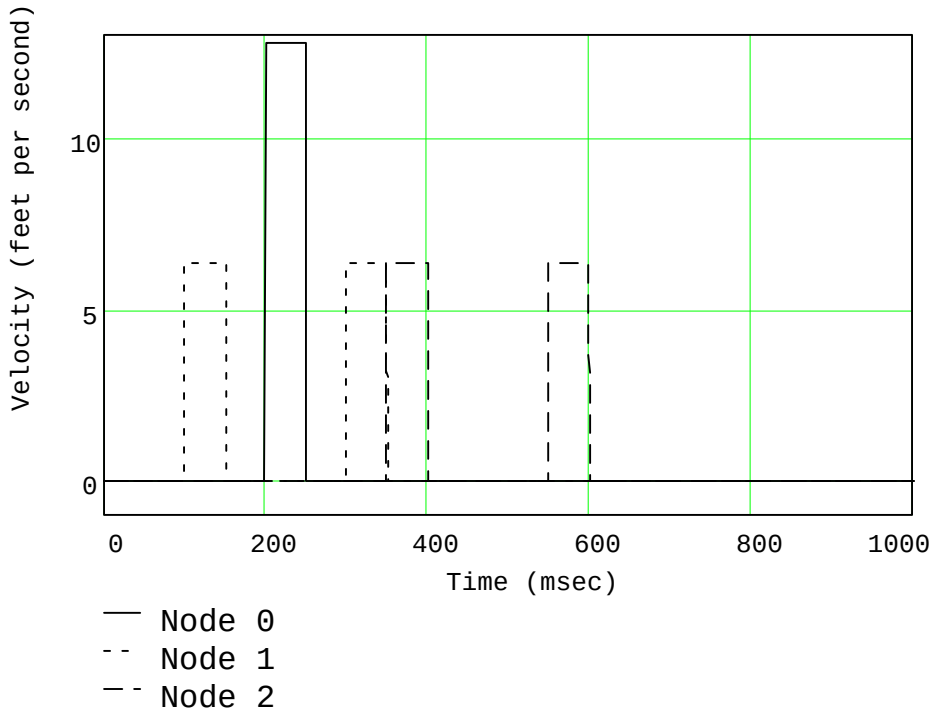

Figure 5-12: Example 2—Velocities

Example Three —A Wave Propagating from a Small to a Large Area

This example shows how a wave propagates from a small cross-sectional area to a large cross-sectional area. The boundary condition at node 0 is returned to the fixed end condition. Elements 1 and 2 have the same cross-sectional areas. The cross-sectional area of element 0 is one-half the cross-sectional areas of elements 1 and 2. A drawing of this is shown in Figure 5-13.

This difference in areas has a profound effect on the distribution of forces propagating from the original wave. The original wave is identical to the previous two examples; however, the waves propagating from the input wave are different. In this example, the wave propagating from the bottom of node 1 is a 33,300 lbf tensile wave and the wave propagating from the top is a 66,700 lbf compressive wave. The equation that describes the force propagating from the bottom is

$$\hat{F}_B = -\frac{A_B}{A_B + A_T}\hat{F} \tag{5.15}$$

and the equation that describes the force propagating from the top is

$$\hat{F}_R = \frac{A_T}{A_T + A_B}\hat{F} \tag{5.16}$$

where

A_B = cross-sectional area of bottom section

A_T = cross sectional areas of top section

$\hat{F}$ = incident force

$\hat{F}_R$ = reflected force

$\hat{F}_T$ = transmitted force

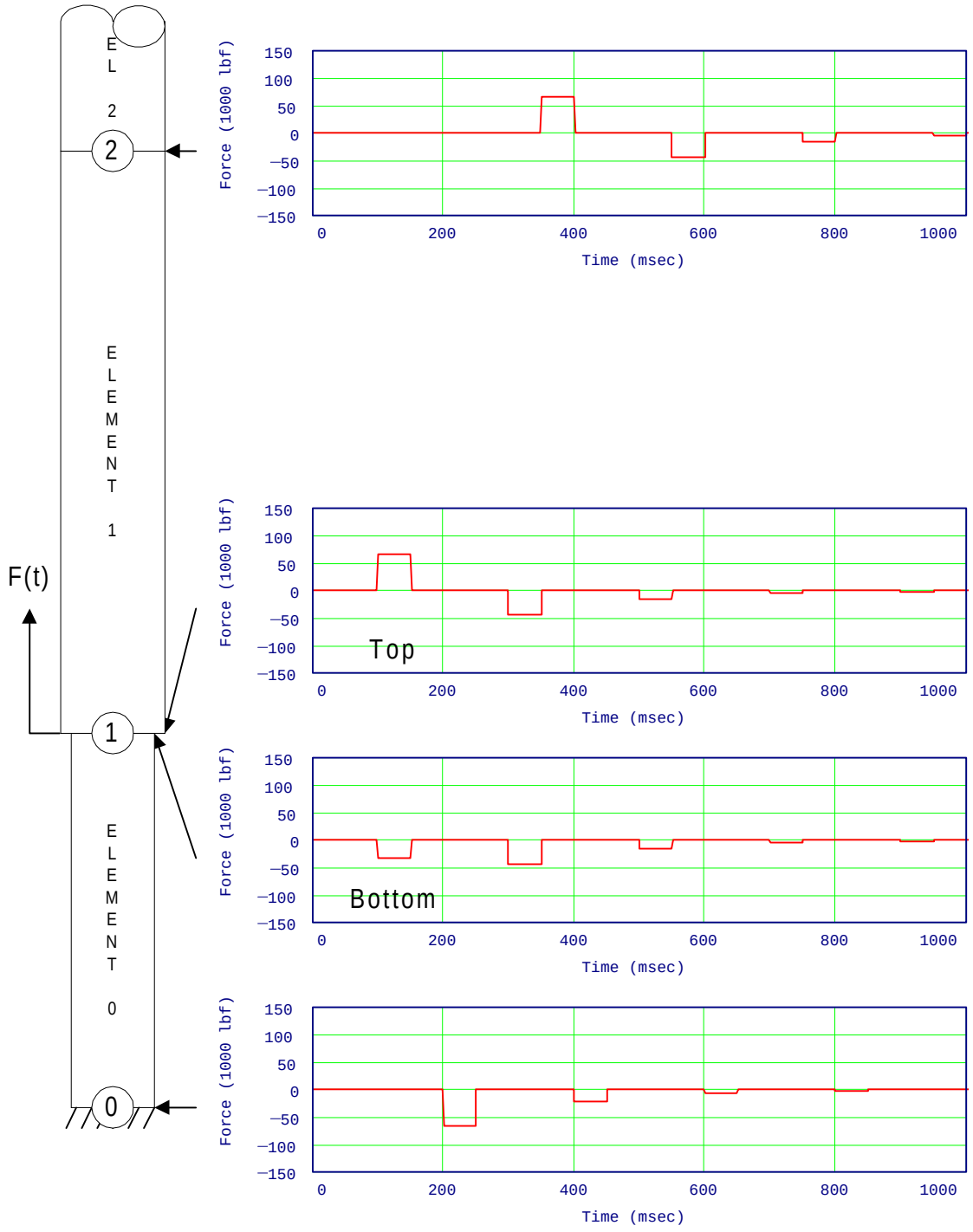

Figure 5-13: Example 3

The force time history for node 0 will show a doubling of the 33,300 lbf tensile wave at time 200 ms. The wave will reflect off of the fixed end with the same sign, therefore, a 33,300 lbf tensile wave will propagate to the top after reflection. In this example, unlike the previous two, there will be more reflections from the change in geometric properties at node 1. Some of the wave will transmit through the junction, and some will reflect off of the junction. These calculations are shown in equations 5.1 and 5.2.

For each reflection at the junction, a smaller amplitude tensile wave will propagate back to the fixed end, reflect off of the fixed end, and return to the junction as the diminished tensile wave. The wave eventually decays with every reflection at the junction. This is the advantage of the semi-infinite element. The waves will not return to set up a resonance or other complications.

At node 0, the reflection from the junction is always in the same sign. A tensile wave reflects as a tensile wave and a compressive wave reflects as a compression wave. As a wave travels from a smaller to a larger cross-sectional area, the junction acts as a fixed end, as far as the sign of the wave is concerned.

Node 1 shows a difference in the bottom and top sides only for the originating wave. There is a 66,700 lbf compressive wave propagating to the top and a 33,300 lbf tensile wave propagating to the bottom. The tensile wave reflects off of the fixed end and returns to the junction. The wave then reflects back and forth between the fixed end and the junction, slowly diminishing.

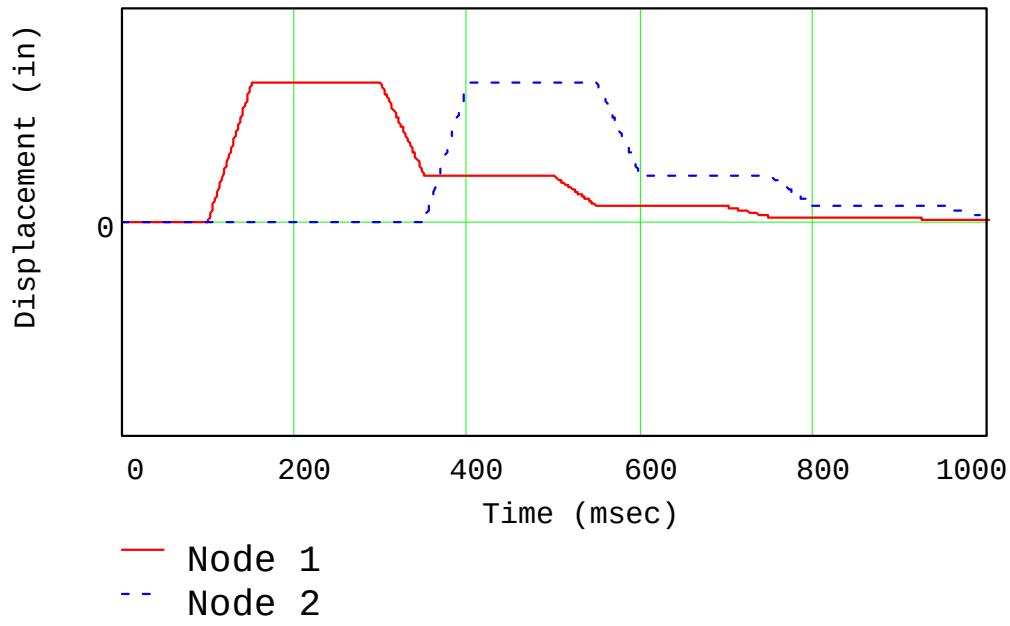

Figure 5-14: Example 3—Displacements

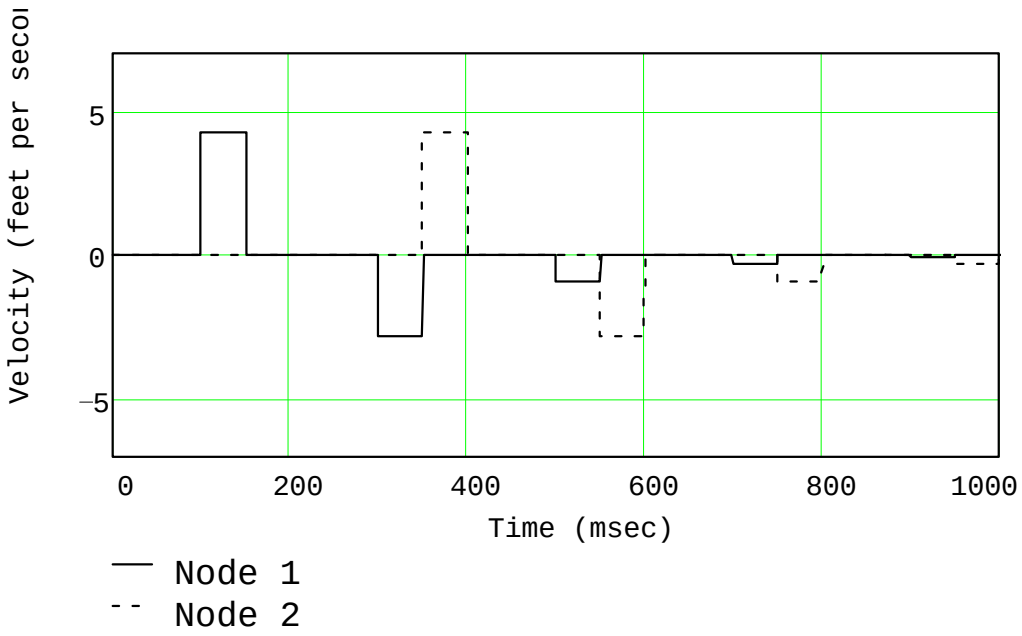

Figure 5-15: Example 3—Velocities

At the bottom side of node 1, after the originating wave, the wave force values are the same, 44,400 lbf tensile, on both sides of the node. Yet at node 0, a 22,200 lbf tensile is seen as the second wave. It would seem that a 22,200 lbf tensile wave should appear on the bottom side of the node. There is a interesting effect occurring during a wave transmittal through a junction. The wave at the node acts the same on both sides of the junction. This is correct as the forces on both sides of the node were summed to zero. However, since this junction is acting like a fixed end, the incident force amplitude plus the reflected force amplitude is the force on the bottom side of the node. This is equal to the force amplitude on the top side of the node. This has a duration of exactly one-half the length of the wave. Afterwards, the wave propagating from the bottom is the expected 22,200 lbf tensile wave. The wave propagating from the top is the 44,400 lbf tensile wave.

Node 2 shows the waves from node 1 shifted in time by the value necessary to traverse element 1, which is 250 ms.

The displacements, shown in Figure 5-14, show the effect of the waves' reflections. Because this example has a fixed end boundary condition, the displacements will return to zero. The velocities in Figure 5-15 are nonzero during wave transit through the node. This is the same as in all the fixed end boundary condition examples.

Example Four—A Wave Propagating from a Large to a Small Area

This example shows how a wave propagates from a large cross-sectional area to a small cross-sectional area. This example (shown in Figure 5-16), the

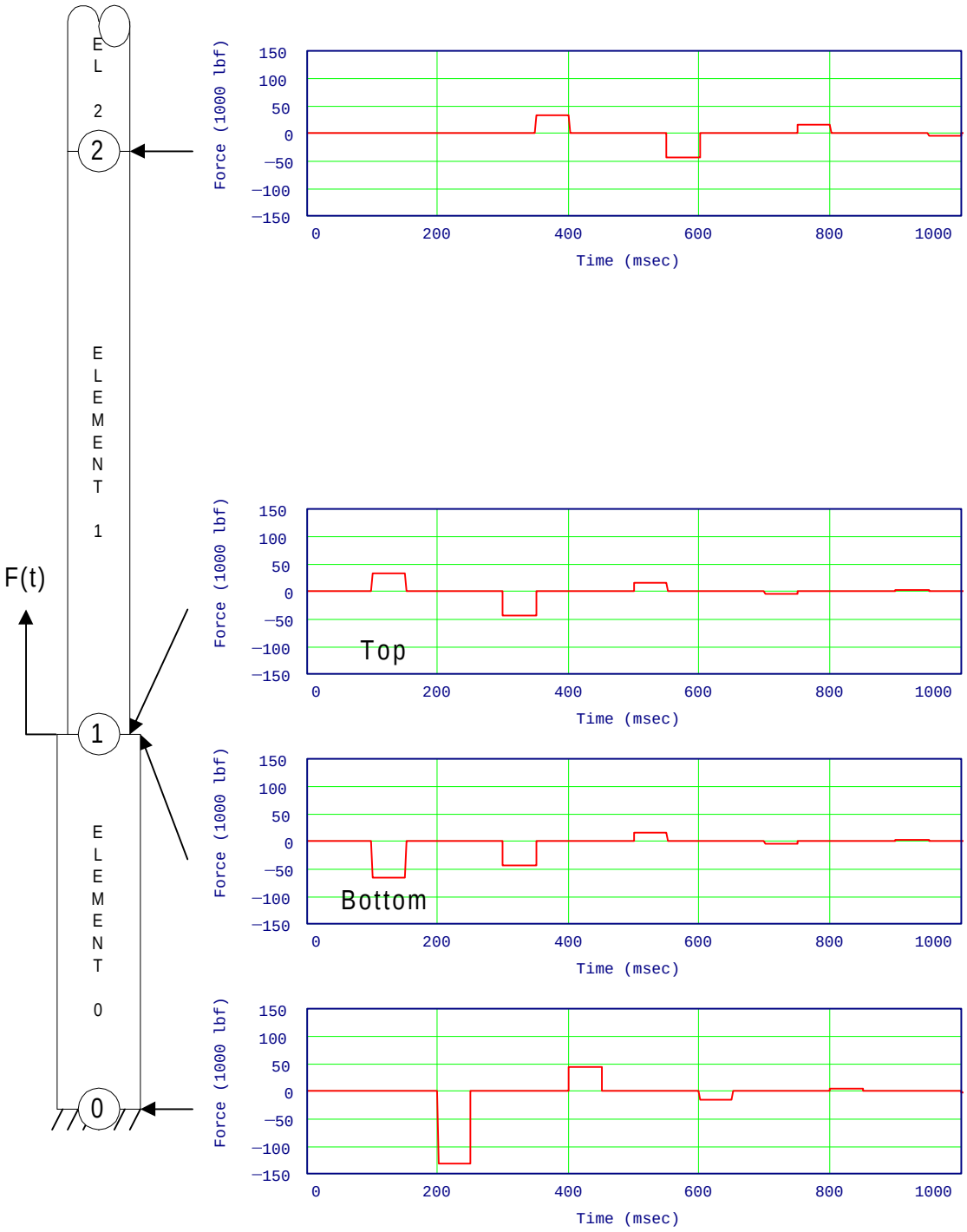

Figure 5-16: Example 4

cross-sectional areas have been reversed. Element 0 now has the larger cross-sectional area and elements 1 and 2 have the same smaller cross-sectional area of one-half the cross-sectional area of element 0. All the equations from the previous examples still hold.

The force time history for node 0 will show a doubling of the 66,700 lbf tensile wave at time 200 ms. The wave will reflect off of the fixed end with the same sign, therefore, a 66,700 lbf tensile wave will propagate to the top after reflection. In this example, like the last example, there will be more reflections from the change in geometric properties at node 1.

For the first reflection at the junction, the tensile wave will reflect as a compressive wave. The junction is acting like a free end, as far as the sign of the wave is concerned. The compressive wave propagates back to the fixed end, reflects off of the fixed end, and returns to the junction. The compressive then reflects as a tensile wave. This reversal occurs every time the wave reflects off of the junction at node 1. These reversals are clearly seen at node 0.

The bottom and top sides of node 1 show the alternating compressive and tensile waves, too. The amplitudes on both sides of the node are the same as in example 3. Node 2 shows the time shifted waves seen at node 1.

The displacements (Figure 5-17) show an alternating effect; however, over time, the displacements are approaching zero. The velocities (Figure 5-18) also show the alternating amplitudes.

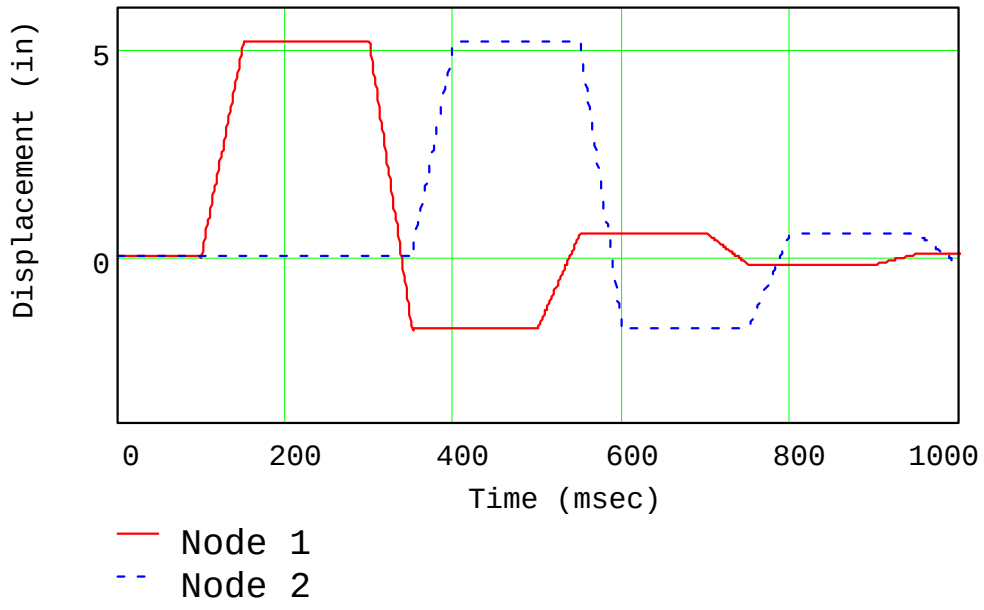

Figure 5-17: Example 4—Displacements

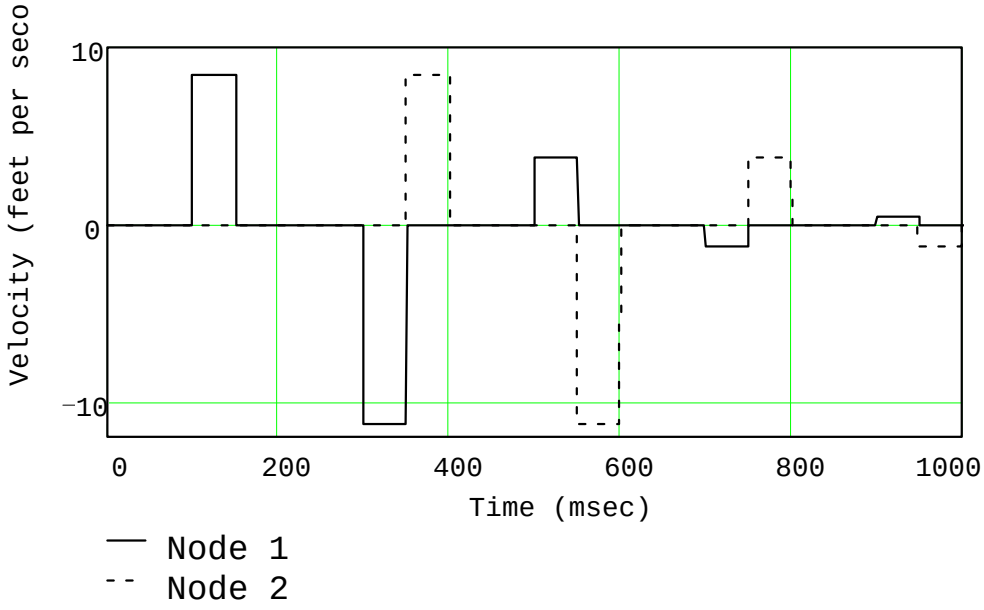

Figure 5-18: Example 4—Velocities

Example Five—A Wave Propagating in Various Areas

Example 5 shows how a wave propagates across various cross-sectional areas. Three different cross-sectional areas are shown (see Figure 5-19). Here, element 0 has a cross-sectional area one-half that of element 1 and twice that of element 2. These geometric changes lead to a complex wave propagation pattern.

There are numerous reflections. In each node, there appears to be a very small amplitude wave propagating before the originating wave. This is an example of a window that is not long enough. The small amplitude wave is the wrap-around from the end of the waves. However, in this case, the amplitudes are small and can be ignored.

The originating wave has a 66,700 lbf compressive wave propagating from the top of node 1 and a 33,300 lbf tensile wave propagating from the bottom of node 1. In this example, reflections occur at the fixed end boundary and the junction at node 1. Reflections and transmissions also occur from the junction at node 2.

These examples show the level of complexity of wave propagation problems. The spectral analysis method has no trouble keeping up with the reflections and transmissions and can do it very quickly. In the next chapter, this method will be applied to drill string jarring analysis.

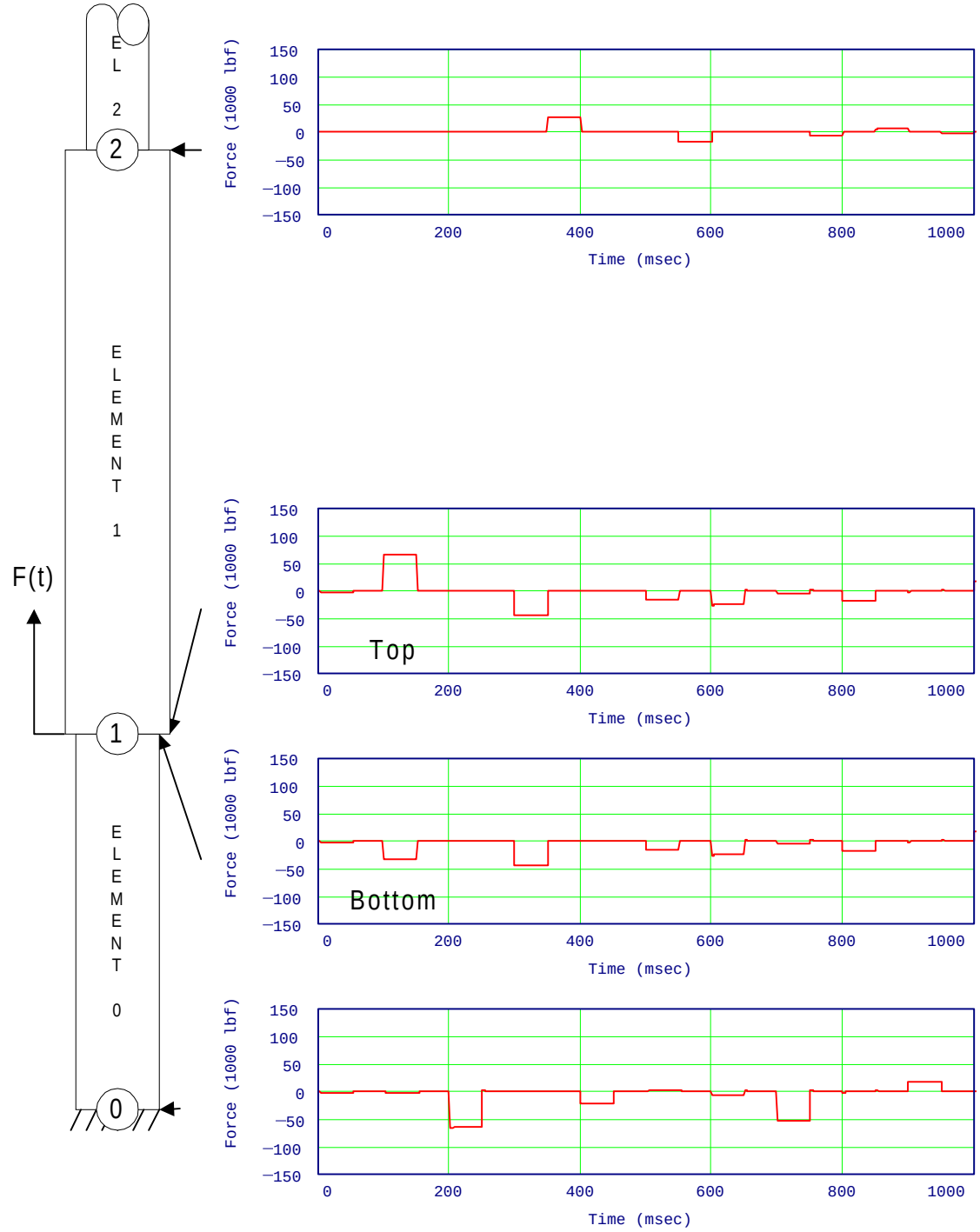

Figure 5-19: Example 5

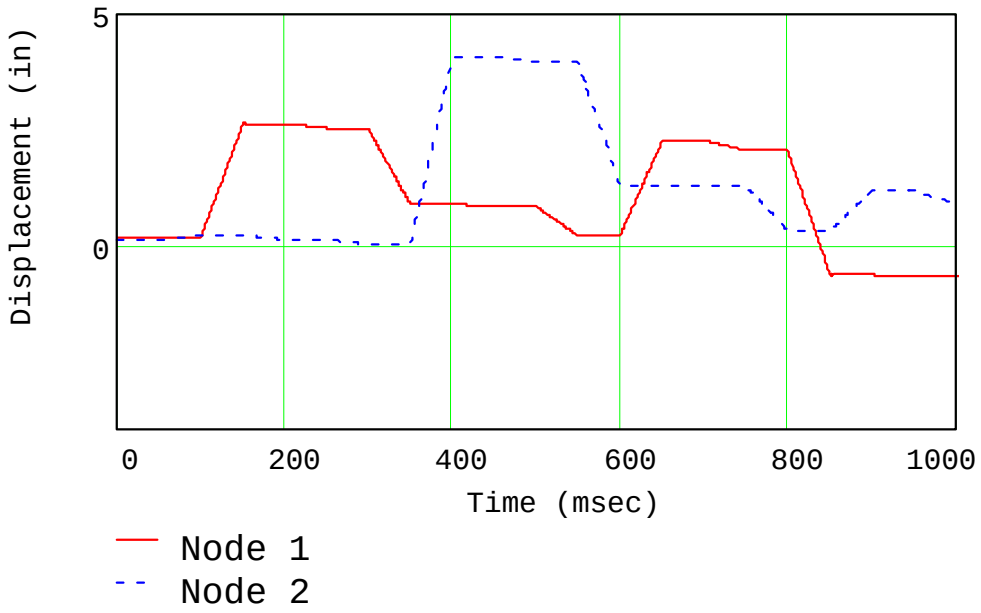

Figure 5-20: Example 5—Displacements

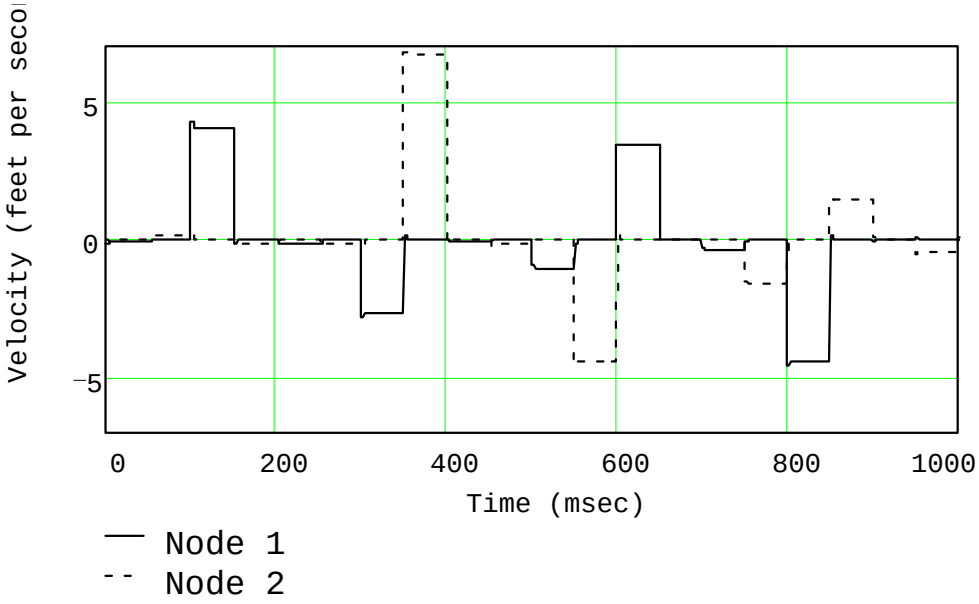

Figure 5-21: Example 5—Velocities

CHAPTER 6

THE NEW JARRING MODEL

This chapter presents the spectral analysis-based model of jarring. A generic drill string model is described and each phase of the jarring process is presented. Spectral analysis remedies the lack of accuracy and the need for inordinate computational resources and time that are inherent in current jarring models.

With the spectral analysis-based jarring model, a generic drill string can be customized to include various sections of pipe and equipment as conditions dictate. For example, a stuck section of pipe, drill collars, heavy weight drill pipe, drill pipe, and an accelerator can be input into the model.

The Spectral Analysis Jarring Model

A generic jarring model using the spectral analysis method is shown in Figure 6-1. The nodes define the various elements of the model. In each element, friction forces and the geometric and material properties of the string can be varied.

Starting from the bottom up, the nodes consist of

Node 8 - the ground

Node 7 - the bottom of the stuck pipe

Node 6 - the top of the stuck pipe

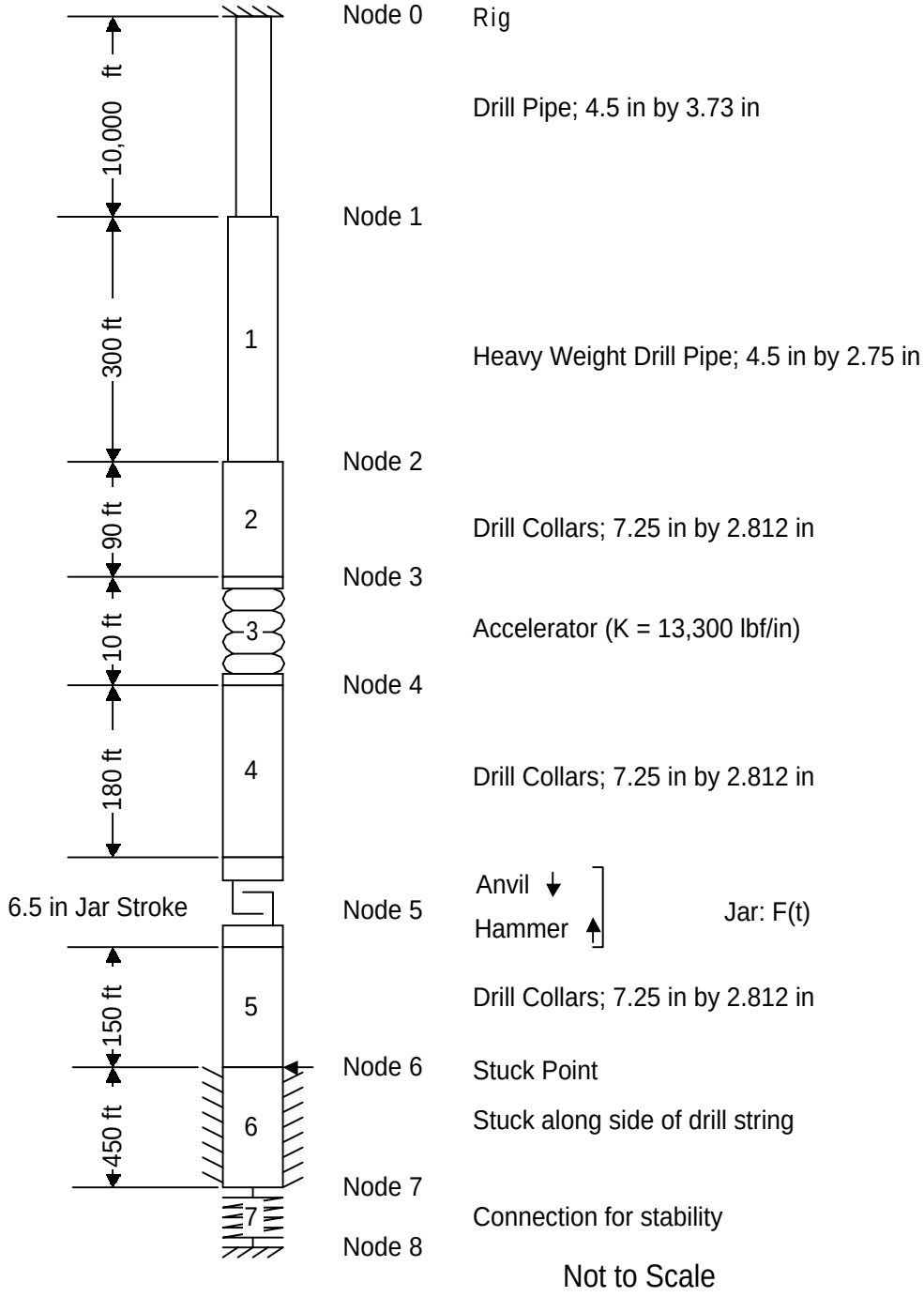

Figure 6-1: Typical Drill String

Node 5 - the jar

Node 4 - the bottom of an accelerator (if present)

Node 3 - the top of an accelerator (if present)

Node 2 - the bottom of heavy weight drill pipe

Node 1 - the bottom of drill pipe

Node 0 - the top of the drill pipe (the rig)

The elements represent the areas from which mathematical modeling equations are formulated. The elements are

Element 7 - the connection of the model to the Earth

(This may be a very light spring or simply more of the string.)

Element 6 - the section of the string that is stuck.

(The friction factors in this section can be set to various values depending upon the manner of sticking. In differential sticking, high values would be used; in mechanical sticking, ultra high values. By setting the cross-sectional area of either element 6 or 7 to a very large number, the user can simulate a fixed end at either node 6 or node 7, respectively.)

Element 5 - the free part of the drill string below the jars.

Element 4 - the drill collars above the jar

Element 3 - an accelerator

Element 2 - drill collar above the accelerator

Element 1 - heavy weight drill pipe or drill pipe

Element 0 - drill pipe

Any section of this model can be built into any part of the drill string. The geometric properties (with units) that can be varied include

Outside diameter (OD - length)

Inside diameter (ID - length)

Length (L - length)

The material properties (with units) that can be varied include

Modulus of elasticity (E - force/length^2)

Density (ρ - mass/length^3)

Viscous Damping (γ - mass/time length)

The Jarring Process

The jarring process can be broken into four phases. They are the pre-stretch, free contraction, impact, and post-impact. This is shown in Figure 6-2.

Pre-Stretch

Pre-stretch is defined as the activities that take place prior to the jar triggering. This includes the pulling (or pushing) on the jar in order to trigger the jar. The forces are applied slowly; therefore, they are defined as static. Usually, the rig cannot move within the defined time frame for dynamic conditions (at least not intentionally). It is assumed that the drill string is in static equilibrium just prior to triggering. That implies that the stresses from the static conditions do not change over the time frame of the jarring action. These stresses can be simply added to the drill string dynamic stresses.

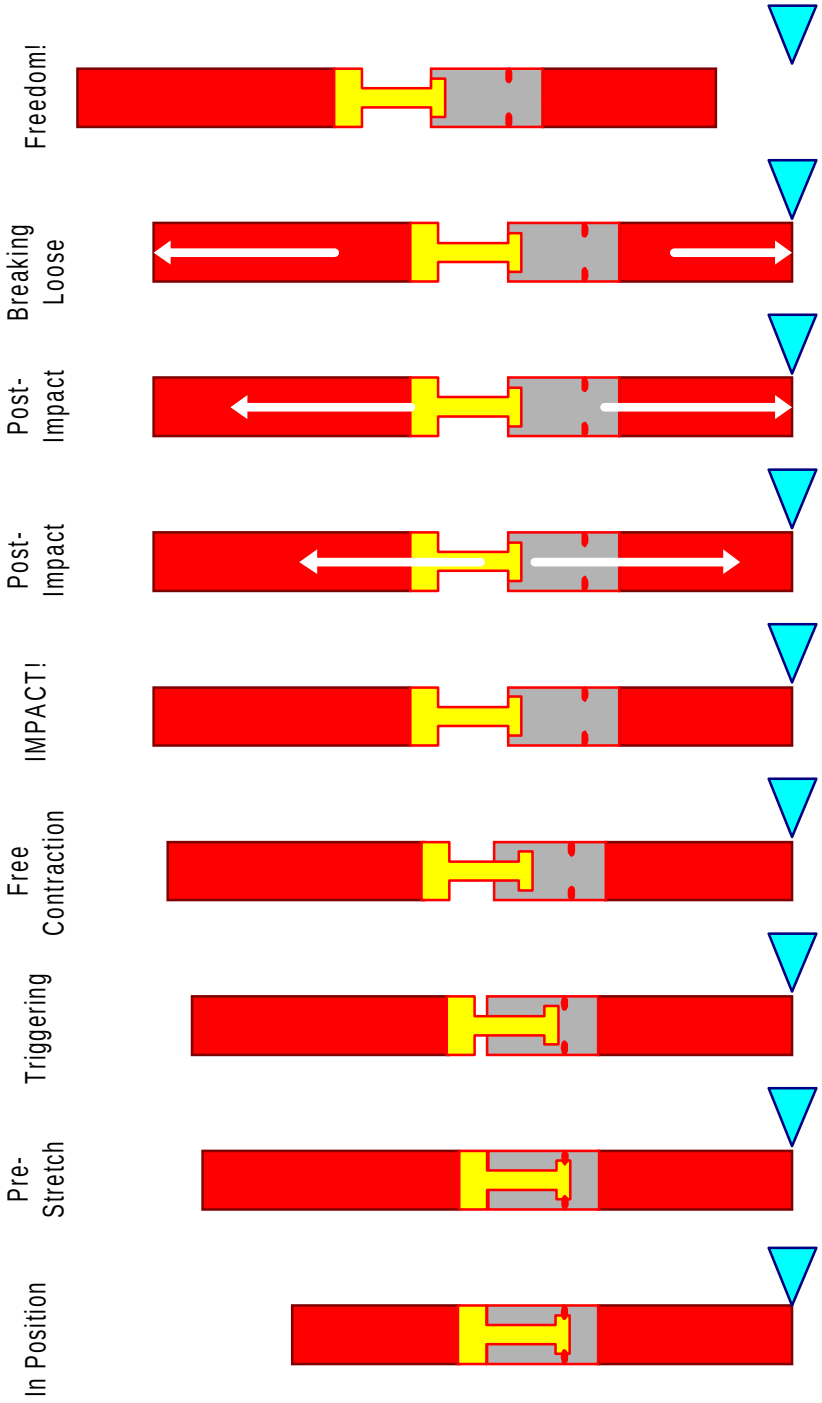

Figure 6-2: The Jarring Process

The values of the static stresses are derived using free body diagrams (Mitchell 1995). In addition, it is assumed that the stresses will be from the overpull load at the jar trigger mechanism. That is, the force at the jar trigger mechanism is known and is the overpull necessary for the jar to trigger. All other loads are derived from this condition.

The real axial stress loads are determined with a free body diagram showing the weight of the drill string below the point of interest and the loads from the stuck point and the overpull force. The effective axial stress takes into account the fluid pressure area loads.

Bending loads from curved bore holes and doglegs are not addressed in this particular model.

Free Contraction

After the jar triggers, the jar converts the strain energy from the static loading in the drill string to kinetic energy. The bottom part of the jar, called the hammer, disconnects from the top of the jar, called the anvil. The hammer travels up with the top of the drill string. The anvil travels down with the bottom of the drill string. Both parts freely contract until the combined distance the anvil and hammer travels is equal to the stroke length. The hammer traveling upward strikes the anvil traveling downwards. The stroke length is adjustable in most jars (at the surface only).

Before the jar triggers, there is a force on the hammer and anvil equal to the overpull force. After the jar triggers, the force on the hammer and anvil drops

to zero. In effect, a negative force wave has been formed (Aarrestad and Kyllingstad 1994). This negative wave will continue until the hammer and anvil impact.

The important variables to determine are the velocities of the hammer and anvil and the distance traveled by both. The velocities are used to determine the impact force. The distance traveled by both and the wave reflection characteristics determine how fast the hammer and anvil are traveling at impact.

The velocities of the hammer and anvil are dependent upon the overpull force and the number of wave reflections from the various parts of the drill string. For every reflection from below the jar, the anvil increases or decreases in velocity, depending upon the type of reflection. The wave reflected can either be a compressive or tension wave. A compressive wave will increase the velocity of the anvil; a tension wave will slow the anvil and can even reverse the direction of the anvil.

The same conditions occur in the drill string above the jar. The hammer velocity will increase or decrease. In most cases, however, the drill string decreases in cross-sectional area as one follows the drill string to the surface. Therefore, the wave reflections continually increase the velocity of the hammer.

An accelerator will act as a free end, reflecting most of a wave back to the jar. The jar will accelerate with each reflection of the wave from the accelerator (hence the tool name). The faster the hammer is traveling at impact, the more force is generated. However, since the waves have a shorter round trip time, the duration of the impact pulse will be shorter.

The spring constant (K) of an accelerator determines the effect of the accelerator. A spring constant can be thought of as a cross-sectional area. Assuming a length (L) and modulus of elasticity (E), one can derive a cross-sectional area (A)

$$A = \frac{KL}{E} \tag{6.1}$$

A small spring constant is equivalent to a small cross-sectional area. The smaller the cross-sectional area, the more the propagating wave will reflect back to the jar. An accelerator acts very much like a free boundary. Very little of the wave will get through the accelerator. This causes the wave reflections to return to the hammer. This will cause the hammer to accelerate to a faster velocity. If an accelerator is not used, then the properties can be set to drill collar values making this section a drill collar.

The time until impact is an unknown. This means that the length of the negative force wave is an unknown. This can be remedied by insuring that the negative wave lasts longer than the time to impact, but is not so excessively long that it propagates into neighboring windows.

The hammer and anvil free contraction are modeled by disconnecting the model at the jar (node 5), creating, in effect, two sub-models.

After the combined distances which the hammer and anvil traveled are equal to the stroke length, this phase of the jarring process is finished. The velocities of the hammer and anvil are then determined. These two values are used to determine the impact force.

Impact

After the hammer and anvil finally impact, the kinetic energy of the hammer and anvil is converted back to strain energy. An impact force is generated. The impact force in this model is determined using the standard Hopkinson bar approach, the same method used in all other jarring papers to determine the impact force.

The Hopkinson bar experiment consisted of two bars. One bar is static and the other is in motion. The bar in motion is constrained to impact the static bar at a known velocity. The force generated is directly related to the velocity of the bar in motion. The force is calculated using conservation of momentum.

The length of the impact pulse is determined by the time required from initial impact for the stress wave to propagate back and forth across the shortest bar. It is assumed that there is no loss in transmission from damping and that the bars are both made of the same material. Therefore, the wave “cancels” itself out upon returning to the impact point. The time duration of the wave is the round trip length in the shortest bar divided by the speed of sound in the bar.

$$t = 2\frac{L}{c} \tag{6.2}$$

where

L = length of shortest bar

c = wave propagation speed in bar

t = time of travel

The velocity of the impact face will be the same as the particle velocity. It is the average of the hammer and anvil velocities at impact.

The shape of the impact pulse is assumed to be rectangular. Actual tests have shown that the impact wave has a quick, but not instantaneous, rise time and oscillations along the maximum value of stress. This is explained by the fact that the assumed impact case is for a one dimensional model. Reality is three dimensional. Poisson effects and wave interaction with the side boundaries of the bar will cause the observed fluctuations (Meyers 1994). However, for simplicity, other jarring papers assume the ideal case. That is assumed in this dissertation, too.

Another implicit assumption is that a “perfect” impact occurs. This is an impact in that the hammer and anvil impact with perfectly flat faces that are perpendicular to the direction of travel. Damping and refraction are not considered.

Post-Impact

The impact force is applied as two waves propagating outward from the jar (at node 5) up and down the drill string. After impact, there is a very brief finite time in which the hammer and anvil are in contact. After that time, the hammer and anvil are assumed to disconnect. In effect, they “bounce” off of each other. This is the rationale for creating separate sub-models for the hammer and anvil. (See “Free Contraction” in this section.)

In reality, after the first impact, the hammer and anvil may or may not come back into contact. If the hammer and anvil come back into contact, the impact junction becomes a nonlinear element. If the junction is closed, a wave can propagate across the junction or this wave can cause the junction to open, thus preventing the wave from crossing the junction. Also, if the junction opens,

the junction becomes two free ends. Depending upon the wave form and amplitude, the wave may alternately open or close the junction allowing the wave to propagate through it. This can occur repeatedly, resulting in chatter. The junction may stay open or closed for the duration of the period of interest, or the junction may open and close intermittently. As pointed out in Chapter 4, the spectral analysis method, at this time, is not amenable to the inclusion of nonlinear elements. This means that the junction either needs to stay open or stay closed for the duration of interest. Technology in this area is deficient at the time of the writing of this dissertation and is an area for future work.

In deriving the spectral element, the assumption was made that the sum of the forces at a node were in equilibrium. This means that if a force is applied at a node, an equal and opposite force is generated on the other side of the node. This is clearly shown in the examples in Chapter 5. However, in an impact junction, the forces are not necessarily in equilibrium. In the case of a hammer and anvil in a jar, two tension waves are generated at the junction. In this model, a tension wave can be input on one side of a node. This tension wave is offset by an equal compression wave (assuming equal cross-sectional areas) on the other side of the node because of equilibrium conditions. As an equal tension wave is impressed on the other side of the node, as it occurs in a jar, the compression wave from the previous tension wave cancels this tension wave. In addition, the other tension wave is offset by another compression wave on the side of the first tension wave. It too is canceled, leaving no waves to be propagated. This does not model reality.

As for the open junction condition, this is easily modeled by using two separate sub-models (in fact the same sub-models as in the free contraction

phase) for the hammer and anvil sides of the drill string. The primary impact force is applied as tension waves at the jar node on each sub-model, just as in the free contraction model. This wave propagates up and down the drill string on the side it was applied. The hammer or anvil acts as a free end.

This model is accurate during the time of the primary impact regardless of what happens to the junction. After the primary impact, the model may or may not reflect reality. If the hammer and anvil bounce off of each other, resulting in a open junction, the model will continue to reflect reality. In other cases, if the hammer and anvil stay closed or chatter, there may be reflections of waves that get through the junction and have a minor effect on the forces at the stuck point. Although these reflections may appear in reality, research in this area suggests that they are not significant to the "unsticking" of the drill string and can be ignored. It appears that the primary impact force is the largest force and determines the outcome of the jarring process.

Example Calculations

The spectral analysis model is broken into the same four phases as the jarring process: pre-stretch, free contraction, impact, and post-impact. In every phase, the outside diameters, inside diameters, lengths, modulus of elasticity, density, and damping coefficients of each necessary element are required. The outside, inside, and cross-sectional areas are calculated. In addition, the wave propagation speed and weight per unit length are calculated.

Pre-Stretch

In addition to the above input values, the trigger force and inside and outside mud weights are needed. The pipe is assumed to be stuck at the top of element 6. Therefore, no pressure-area forces and loads from below this point are transmitted to the sections above node 6. A requirement is that the load at node 5, the jar, is equal to the trigger force.

The pressure-area forces are determined at each node. These forces are added or subtracted (depending on the direction of the force) at the bottom of each element. The weight of the element below each node is added at the top of each element. The equation for the bottom of an element is

$$F_B = F_{TP} + P_O + P_I \tag{6.3}$$

and for the top of an element

$$F_T = F_B + W_N L_N \tag{6.4}$$

where

F_{TP} = force at top of element below current element

P_O = pressure-area force on outside of drill string

P_I= pressure-area force on inside of drill string

F_B = force at the bottom of the element

N = element number

W_N = weight of element N per unit length

L_N = length of element N

F_T = force at the top of the element

The exceptions to this are at and below the jar. The force at the jar is equal to the trigger force. Below the jar, the forces are calculated at the top of the stuck point by taking the trigger force and subtracting the weight of the element below the jar and above the top of the stuck point.

Free Contraction

In the free contraction phase, in addition to all of the previous data, the jar stroke is input. The next step is to take the free contraction wave and convert it to the frequency domain.

The wave time is chosen long enough to insure the displacements of the hammer and anvil are greater than the stroke length. In addition, the time of investigation must be long enough to minimize wave migration from side windows. This time length is dependent upon the geometry and damping coefficients and is set by the number of samples and the sampling rate.

Once the wave is converted to the frequency domain, the wave numbers are calculated. The equation is

$$k_{m,j} = \sqrt{\frac{\omega_m^2}{c_j^2} - \frac{i\omega_m \gamma_j}{A_j E_j}} \qquad (6.5)$$

where

ω_m = circular frequency (radians/time)

c_j = the j^{th} element wave propagation speed (length/time)

i = imaginary

γ_j = the j^{th} element damping coefficient (mass/length time)

A_j = the j^{th} element cross-sectional area (length^2)

E_j = the j^{th} element modulus of elasticity (force/length^2)

$k_{m,j}$ = the m^{th} frequency and j^{th} element wavenumber

The element values for the stiffness matrix are determined. For the on diagonal values

$$D_{m,j} = \frac{ik_{m,j}A_jE_j}{1-e^{-2ik_{m,j}L_j}}\left(1+e^{-2ik_{m,j}L_j}\right) \tag{6.6}$$

and for the off diagonal values

$$OFD_{m,j} = \frac{ik_{m,j}A_jE_j}{1-e^{-2ik_{m,j}L_j}}\left(-2e^{-ik_{m,j}L_j}\right) \tag{6.7}$$

where

L_j = length of the j^{th} element (length)

$D_{m,j}$ = the m^{th} frequency and j^{th} element on diagonal stiffness matrix value

$OFD_{m,j}$ = the m^{th} frequency and j^{th} element off diagonal stiffness matrix value

The hammer spectral displacements are

$$\begin{bmatrix}\hat{u}_{m,1}\\ \hat{u}_{m,2}\\ \hat{u}_{m,3}\\ \hat{u}_{m,4}\\ \hat{u}_{m,5}\end{bmatrix} = \begin{bmatrix} D_{m,0}+D_{m,1} & OFD_{m,1} & 0 & 0 & 0\\ OFD_{m,1} & D_{m,1}+D_{m,2} & OFD_{m,2} & 0 & 0\\ 0 & OFD_{m,2} & D_{m,2}+D_{m,3} & OFD_{m,3} & 0\\ 0 & 0 & OFD_{m,3} & D_{m,3}+D_{m,4} & OFD_{m,4}\\ 0 & 0 & 0 & OFD_{m,4} & D_{m,5}\end{bmatrix}^{-1}\begin{bmatrix}0\\0\\0\\0\\\hat{F}\end{bmatrix} \tag{6.8}$$

and the anvil spectral displacements

$$\begin{bmatrix} \hat{u}_{m,5} \\ \hat{u}_{m,6} \\ \hat{u}_{m,7} \end{bmatrix} = \begin{bmatrix} D_{m,5} & OFD_{m,5} & 0 \\ OFD_{m,5} & D_{m,5} + D_{m,6} & OFD_{m,6} \\ 0 & OFD_{m,6} & D_{m,6} + D_{m,7} \end{bmatrix}^{-1} \begin{bmatrix} \hat{F} \\ 0 \\ 0 \end{bmatrix} \tag{6.9}$$

where

$\hat{u}_{m,j}$ = spectral displacement (length)

$\hat{F}$ = spectral force (force)

The spectral velocities are found using

$$\hat{v}_m = i\omega_m \hat{u}_{m,j} \tag{6.10}$$

where

$\hat{v}_m$ = spectral velocity (length/time)

Note that $\hat{u}_8$ and $\hat{u}_0$ are equal to 0. They are fixed boundary conditions.

The spectral displacements are used to determine the spectral forces. These are then re-inverted back into the time domain using the inverse FFT. The spectral displacements and velocities are also re-inverted back into the time domain. After the displacement of u_5 from the hammer and u_5 from the anvil is equal to the stroke length, the hammer and anvil have impacted. The time of this occurrence can be noted and the corresponding velocities found.

Impact

The third phase of analysis is the impact phase. The impact velocity is the average velocity of the hammer and anvil velocities at just prior to impact.

The velocities of the hammer and anvil must be equal during the impact or otherwise, there would not be any contact at the impact junction. The velocity after the impact is calculated using an equation from Donnell in 1930

$$V_I = \frac{V_{HB} + V_{AB}}{2} \tag{6.11}$$

$$V_{HA} = V_{HB} - V_I \tag{6.12}$$

$$V_{AA} = V_I - V_{AB} \tag{6.13}$$

where

V_{HB} = hammer velocity prior to impact (length/time)

V_{AB} = anvil velocity prior to impact (length/time)

V_I = impact velocity (length/time)

V_{HA} = hammer velocity after impact (length/time)

V_{AA} = anvil velocity after impact (length/time)

The force, according to the same source (Donnell, 1930) is

$$F_I = V_I A_H \sqrt{\rho_H E_H} \tag{6.14}$$

where

A_H = hammer cross-sectional area (length^2)

ρ_H = hammer density (mass/length^3)

E_H = hammer modulus of elasticity (force/length^2)

F_I = impact force (force)

An implicit assumption with the use of equation 6.14 is that the anvil has identical geometric and material properties.

The duration of time that the force is in effect is assumed to be the time it takes a wave to make a round trip through the element on either side of the jar. The duration of the impact and the impact wave will be determined by which of the two waves returns to the junction first. After the wave returns to the impact junction, the force will drop to the pre-stretch conditions.

The wave for the final phase will be a square wave with an amplitude of the impact force.

Post-Impact

The post-impact phase also uses the spectral analysis procedure. It is almost identical to the free contraction phase. The inputs are the same except impact force and its duration replaces trigger force and its duration. The re-inverting of the forces, displacements, and velocities are the same as in the free contraction phase.

CHAPTER 7

JARRING ANALYSIS CASES

This chapter presents cases of jarring under various conditions. Cases include the use of drill collars and drill pipe with and without heavy weight drill pipe and with and without an accelerator. Finally, a comparison of the frequency-domain model with a time-domain finite element model demonstrates the superior results of the spectral analysis method derived in this dissertation.

Mathcad

The jarring models shown in this chapter were constructed using Mathcad 6.0 Plus®. This is a powerful mathematical programming tool. The program allows the user to input equations in typical handwritten mathematical style. Using the equations input by the user, calculations are made. The results can then be plotted. One example of the Mathcad documents used for this analysis can be found in Appendix A.

The procedure has been split into two different Mathcad documents. The first phase of the jarring procedure, pre-stretch, has its own document. Since in every case in this chapter, this section is practically the same, this was done to simplify this part of the jarring calculations. The next three phases, free contraction, impact, and post-impact, are included in a single document. Future imple-

mentations of these procedures will combine the documents into one stand-alone program.

Jarring Examples

For the purpose of demonstrating the capability of this jarring model, five typical jarring cases are presented. The drill string used in these models is similar to the drill string used in the paper, **Transient Dynamic Analysis of the Drillstring Under Jarring Operations by the FEM** (Kalsi, Wang, and Chandra 1987). The first case is a drill string consisting only of drill collars and drill pipe. The second case adds an accelerator to the first case. The third case is a drill string consisting of drill collars, heavy weight drill pipe, and drill pipe. The fourth case adds an accelerator to the third case. The fifth case is the same as the fourth case except the drill string is “fixed” at the top of the stuck element during the free contraction phase. This corresponds to the conditions shown in the Kalsi paper and will allow for a direct comparison.

In each case, the top of the stuck point is 150 feet below the jar with 450 feet of stuck drill collars below that point. There is a 10 foot connecting element at the bottom of the drill string.

The sticking is accomplished by setting a very high damping coefficient over the stuck drill collar element (between node 6 and 7). The sticking type, as defined in Chapter 1, has a strong bearing upon the nature of the stuck element. For example, in the first four cases, the element is stuck over a long distance, modeling pressure differential sticking. The fifth case shows the string stuck at a point, thus modeling mechanical sticking.

In all cases, the damping factors are 100 lbm per foot per second over every element except in the stuck section and the connecting element. In the stuck section (element 6), the damping factor is increased by a factor of fifty to 5,000 lbm per foot per second. The connecting element (7) has zero damping.

This model can be segmented into elements that correspond to different parts of the hole (i.e., deviated sections and doglegs), rather than the typical correspondence to changes in the drill string. Varying damping factors can then input for the varying elements that correspond to the hole changes. This can model the effects of deviated hole conditions.

The material properties are based solely on steel and are identical in every element. The modulus of elasticity is 30,000,000 psi. The density is 490 lbm per cubic foot.

The jar stroke is 6.5 inches. The triggering force is set to 165,000 lbf. The trigger is set to start 10 ms from the start of the jar analysis simulation. This insures that the wave is self-windowing.

Case One: Drill Collars and Drill Pipe

In Case One, a drill string made up of only drill collars and drill pipe is used. A diagram of this string is shown in Figure 7-1.

The first step is to calculate the static forces from the pre-stretch phase. The is accomplished in the Mathcad document set forth in “Appendix A, Mathcad Examples” under the heading “Pre-Stretch Phase.” The results, which are practically the same for every case (and therefore will not be shown for the next four cases), are shown in Figure 7-2. The figure shows the static forces in pounds

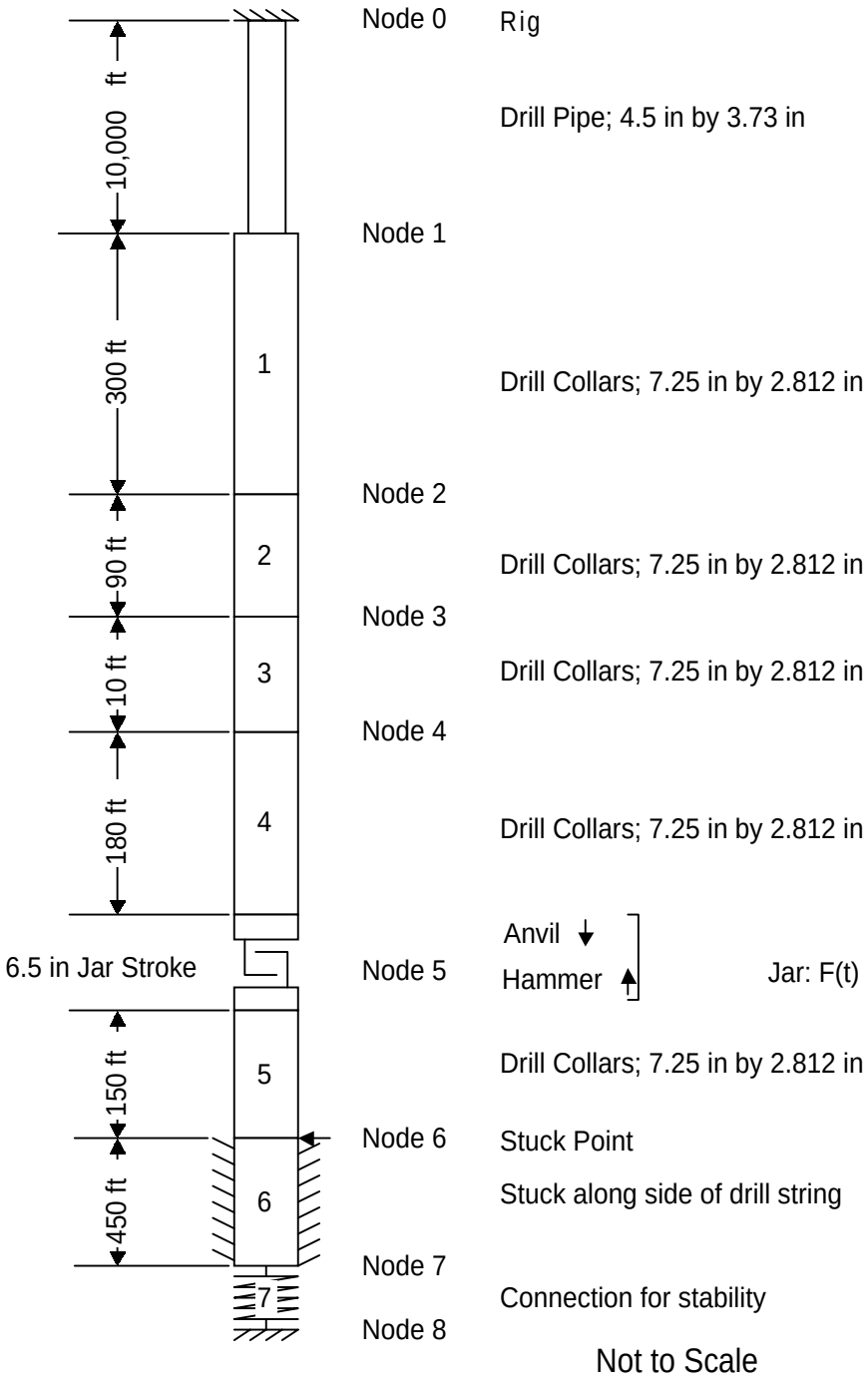

Figure 7-1: Case 1—Drill String Schematic

force versus the depth in feet. Note that the depth axis increases downward. The diamond on the chart is the jar location with the trigger force. Since linear superposition is assumed to be in effect, the static and dynamic forces can be added to determine the total force acting at a location on the drill string.

The next phase is the free contraction phase. All of the calculations in this phase are used to find the velocities of the hammer and anvil at impact. Impact is determined by adding the displacements of the hammer and anvil. After the total displacement equals the stoke of the jar, the velocities are then determined at that point in time. In this model, it is important to note that, in this phase, the calculations are still made beyond the point of impact even though, in reality, the jar has impacted and no further motion from free contraction is possible. Because the actual time of impact cannot be determined prior to the calculations, the calculations must be run beyond the impact time in order to find

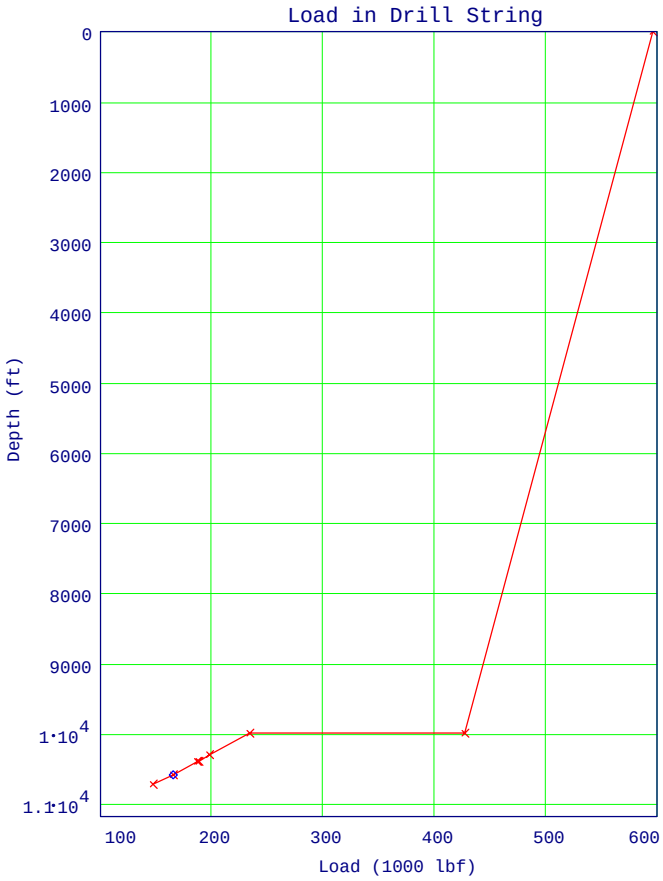

Figure 7-2: All Cases—Pre-Stretch

the impact time. This has an advantage: if the stroke can be varied, the velocities can immediately be determined without re-running the free contraction phase of the model. In addition, because of the neighboring windows' wave propagation migration problem, the model must have a window long enough in time to insure the waves have decayed prior to propagating out of the window.

Figure 7-3 shows the displacement history of the hammer and anvil versus the time. The starting points of the hammer and anvil displacements are offset by the stroke length. As the stroke line crosses the stroke length line, the jar has impacted. In this case, the jar impacts 94.682 ms from jar triggering The time on the chart is 104.682 ms which includes the 10 ms lead prior to the trigger. The displacements in the free contraction phase beyond the initial impact are not plotted on this figure. Instead, the displacements of the hammer and anvil from the post-impact calculations are plotted from initial impact forward. This plotting strategy is true for all of the figures.

The velocities of the hammer and anvil can be observed in Figures 7-4 and 7-5, respectively. The charts show the velocities of the hammer and anvil versus time. At 104.682 ms (94.682 ms from triggering), the velocity of the hammer is 75.444 inches per second (ips). For the anvil, the velocity is -27.588 ips. Note that both the hammer and anvil have opposite velocities. The hammer is traveling upwards and the anvil is traveling downwards. This increases the impact **significantly**.

A curious phenomenon is shown in the anvil velocity in Figure 7-5. At 27.8 ms, the velocity starts to slow in a nonlinear manner. The phenomena, to be called the damping reflection effect, is from the wave reflecting off of the

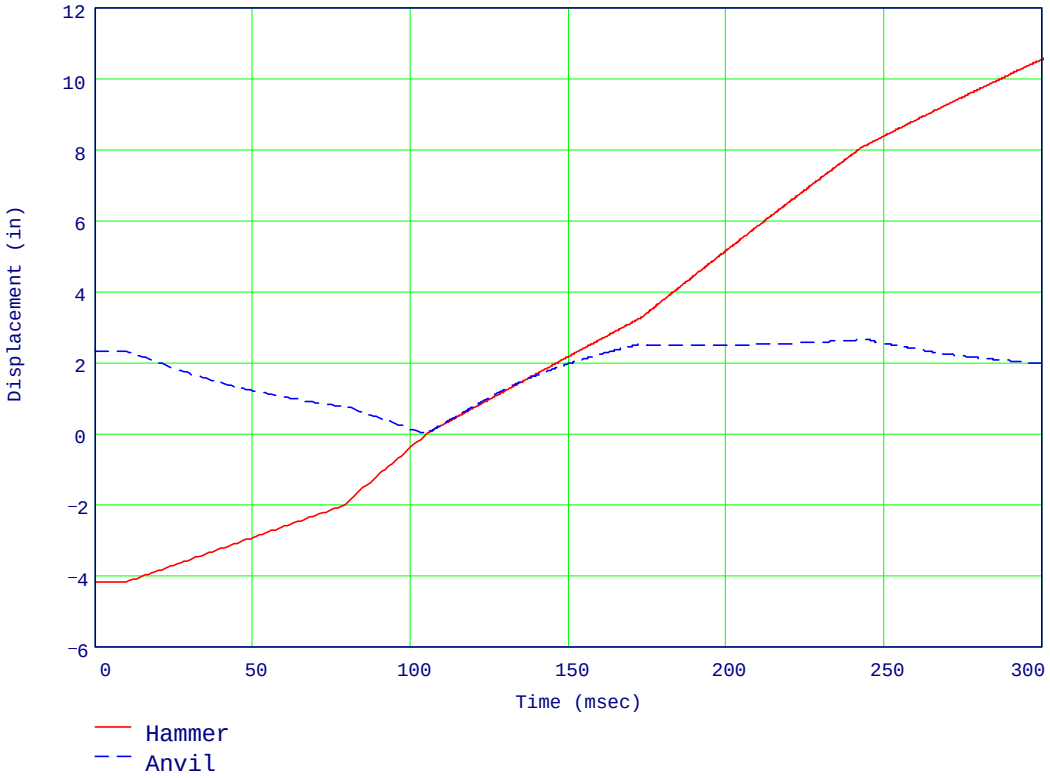

Figure 7-3: Case 1—Displacement of Hammer and Anvil

damping starting at the top of the stuck point. The damping ratio between the free and stuck parts of the drill string is 50. This figure shows that even though the geometric and material properties of the free and stuck sections are identical, waves can still reflect from just the change in damping. This is something new that has not been noted in any publications and is not taken into account in any other state-of-the-art jarring program.

This effect can be seen to reduce the velocity of the anvil from -31.5 ips to about -12.8 ips. This is over half of the initial velocity. This would reduce the

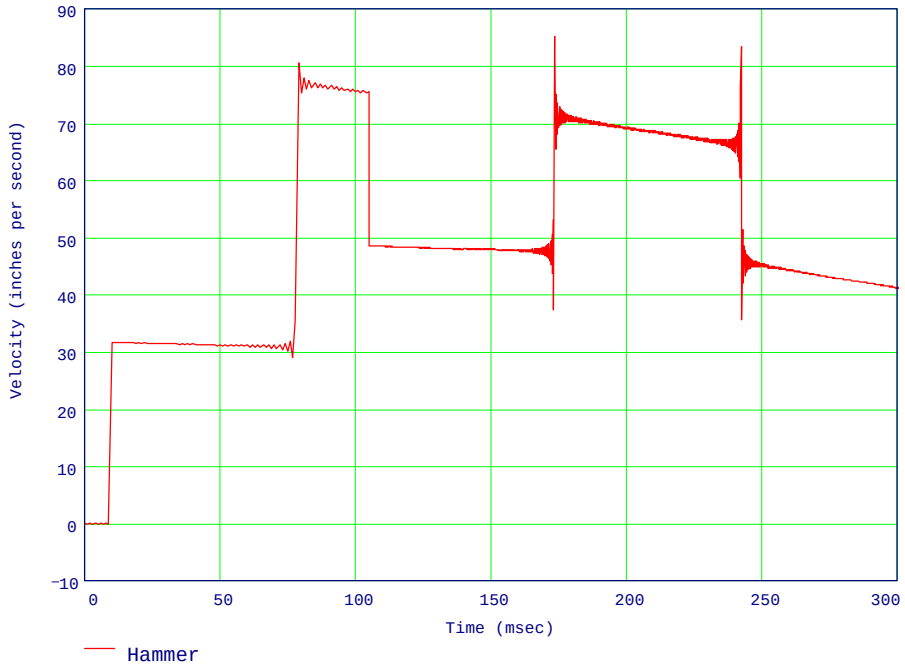

Figure 7-4: Case 1—Hammer Velocity

Figure 7-5: Case 1—Anvil Velocity

impact by about 38,497 lbf if impact occurred assuming the same hammer velocity. However, at 81.25 ms, a reflection of the initial free contraction wave off of the connection element hits the anvil causing it to accelerate prior to impact.

In Figure 7-3, it can be seen from the displacement values that the anvil oscillates. If the stroke or trigger force were such that the anvil was traveling upwards at impact, the impact force would be far less. Assuming the same velocity for the anvil to be upwards, the impact force would be 289,574 lbf (which includes the static trigger force), a decrease of 143,627 lbf.

The next phase is the impact phase. The calculation of the impact force is made. The impact force in this case is 433,201 lbf. A tension wave of this impact force propagates outward through the hammer and anvil. This is shown in Figure 7-6. Initially, the trigger force is applied. Then the jar is triggered, freeing both the jar and anvil. Because the hammer and anvil are free ends, the force should be zero. At impact, a 433,201 lbf square tension wave in the anvil is generated. This is the force that will propagate to the stuck point. As noted in Chapter 4, the spectral analysis procedure cannot generate the original wave. In these cases, a wave shape and duration is assumed. This is shown in the figure by the symmetric square waves about trigger force. The waves in the hammer and anvil propagate outwards from the jar.

In this case, the displacements of the hammer and anvil, as shown in Figure 7-3, show that the hammer and anvil travel together for the duration of the impact. After that, the displacements indicate that the hammer continues to travel upwards and the anvil continues to travel downwards. However, in reality, the hammer and anvil are prevented from traveling past each other by the design

of the jar. Because of this, the model is indicating a condition that cannot physically occur. The calculation values shown beyond the end of the impact at the jar are suspect. Because of the finite wave propagation velocities, the calculations for the drill string (such as at the stuck point) remain valid up to the time that a reflected wave could have propagated from the jar.

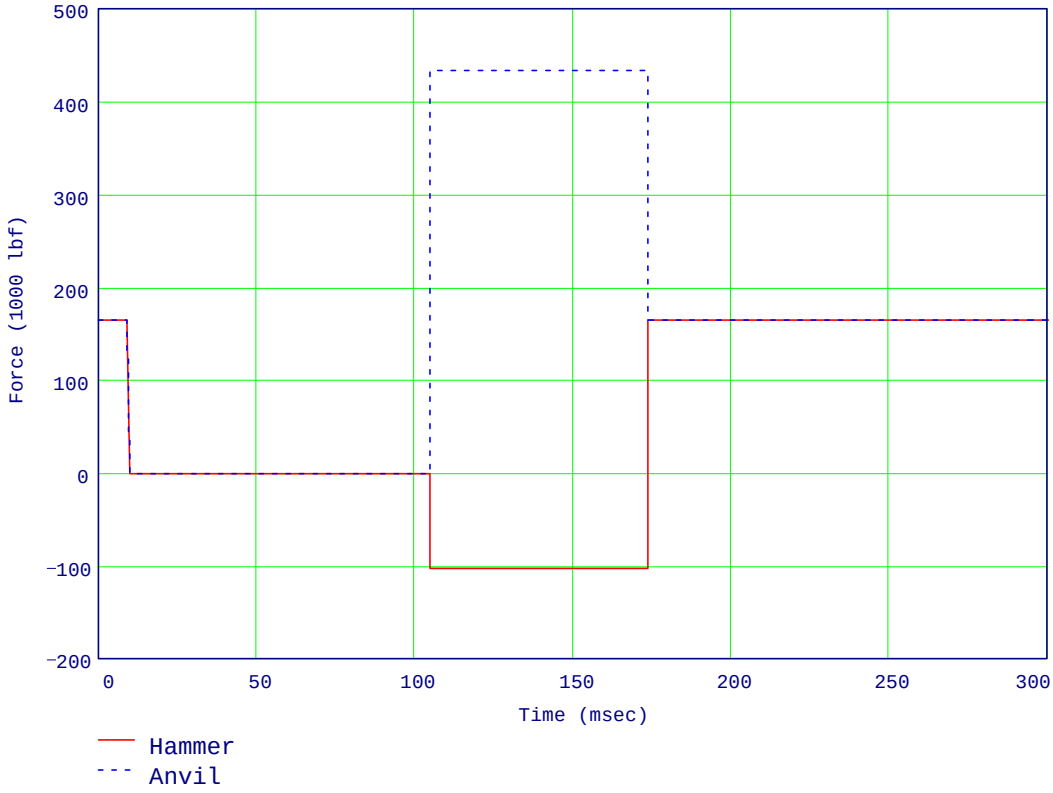

Figure 7-6: Case 1—Forces at the Jar

The duration of the impact force is the time for the wave to make a round trip from the nearest interface. For this case, it is the time it takes for the wave to propagate up to the drill pipe/drill collar interface and reflect back to the impact junction. This is the quickest round trip time. This time is 68.875 ms.

The final phase is the post-impact phase. This is another spectral analysis procedure. Figure 7-7 shows the force at the top of the stuck point. Initially, the top of the stuck point has a force on it equal to the trigger force minus the weight of the drill string above it to the jar. The jar triggers at 10 ms. The wave from the free contraction of the anvil hits the top of the stuck point 8.9 ms later.

Figure 7-7: Case 1—Forces at the Top of the Stuck Point

This force also shows the damping reflection effect noted in the anvil displacement curve. At 72.3 ms, the reflection of the free contraction wave off of the bottom of the drill string is seen. It is much smaller because of the significant damping encountered in the stuck section. At 113.588 ms, the primary impact wave is felt at the top of the stuck point. It hits a peak of 456,000 lbf at 131 ms and ends at 182.457 ms. A reflection of the leading edge of this wave from bouncing off of the bottom of the drill string is seen at 167.037 ms. The primary impact wave is still traveling downwards, thus there is some wave interference until 182.457 ms. After that point, the waves are false reflections from the free anvil end. As noted earlier, in this case, since the hammer and anvil are locked together, the waves should not have reflected but instead have traveled on through the jar. Still, the primary impact wave is accurate.

Case Two: Drill Collars and Drill Pipe with an Accelerator

In Case Two, the same drill string as in the first case is used with the addition of an accelerator 180 feet above the jar. As noted in Chapter 1, an accelerator is used to intensify the impact forces. This is accomplished by causing more reflections to reflect to the hammer during the free contraction phase. A diagram of this string is shown in Figure 7-8.

The accelerator has a equivalent spring constant of 13,300 lbf per inch. This is the equivalent of having a cross-sectional area, for a 10 foot length, of 0.0532 in^2. This is in contrast to the cross-sectional area of the drill collars of 35.072 in^2. Using equations 5.1 and 5.2 and setting the input force to 1 shows that 0.3 percent of the force transmits through the accelerator and 99.7 percent reflects off of the accelerator. It is doubtful that the wave would be felt at the

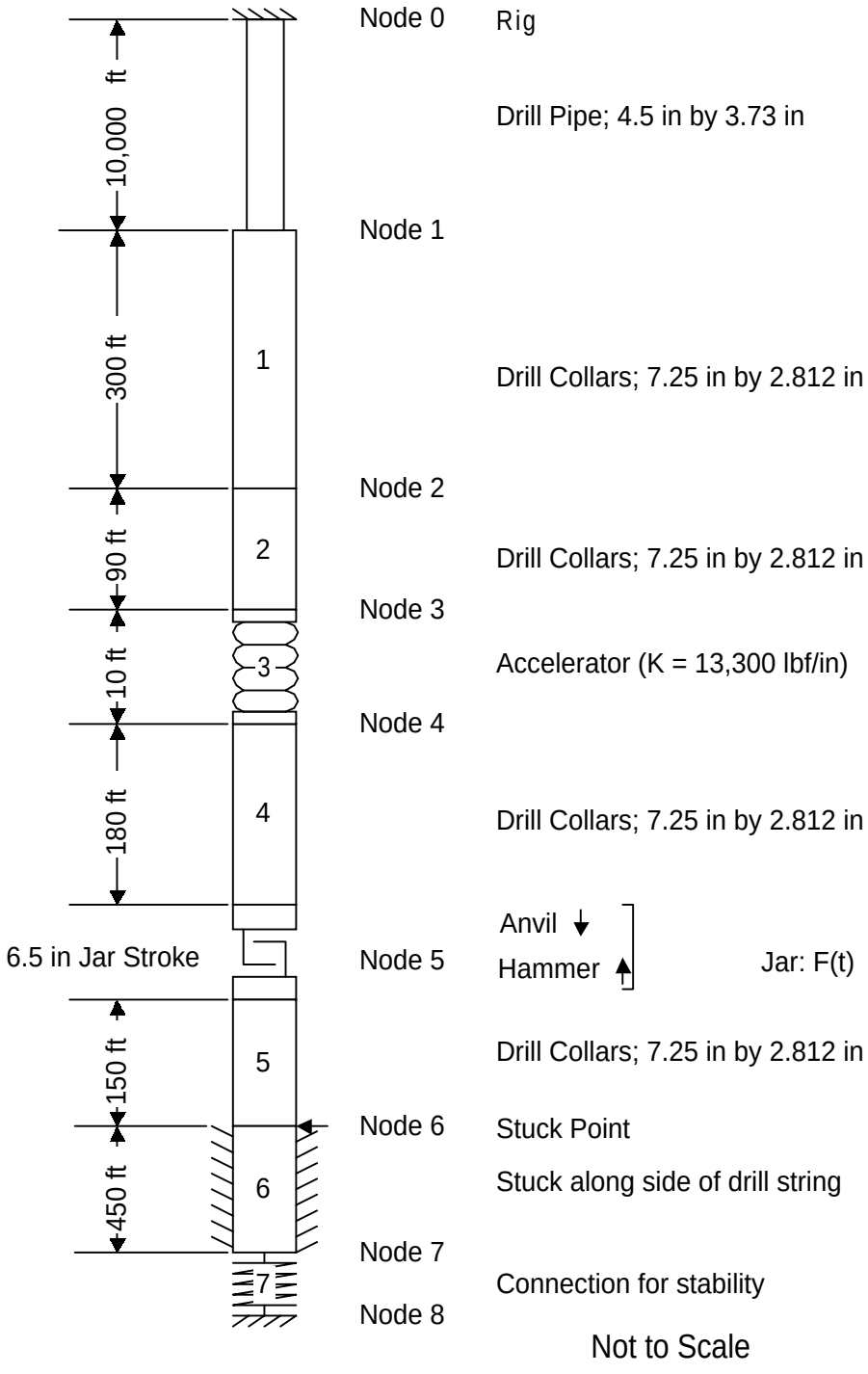

Figure 7-8: Case 2—Drill String Schematic

surface. Accelerators with larger spring constants would allow more wave transmission. This is also assuming the accelerator does not overextend itself and hit the stops in the tool.

The pre-stretch calculations are the same as before. (See Figure 7-2.) The free contraction phase shows some differences. Figure 7-9 shows the hammer and anvil displacements. In this case, there are approximately three hammer reflections for every anvil reflection. The round trip time for wave propagation from the jar to the accelerator is 21.4 ms versus the 71.3 ms round trip time to the bottom of the stuck drill string. This is a 3.33 ratio and explains the reflection ratio.

The velocity charts show these reflections much more clearly. Figure 7-10 is the hammer velocity and Figure 7-11 is the anvil velocity. The hammer

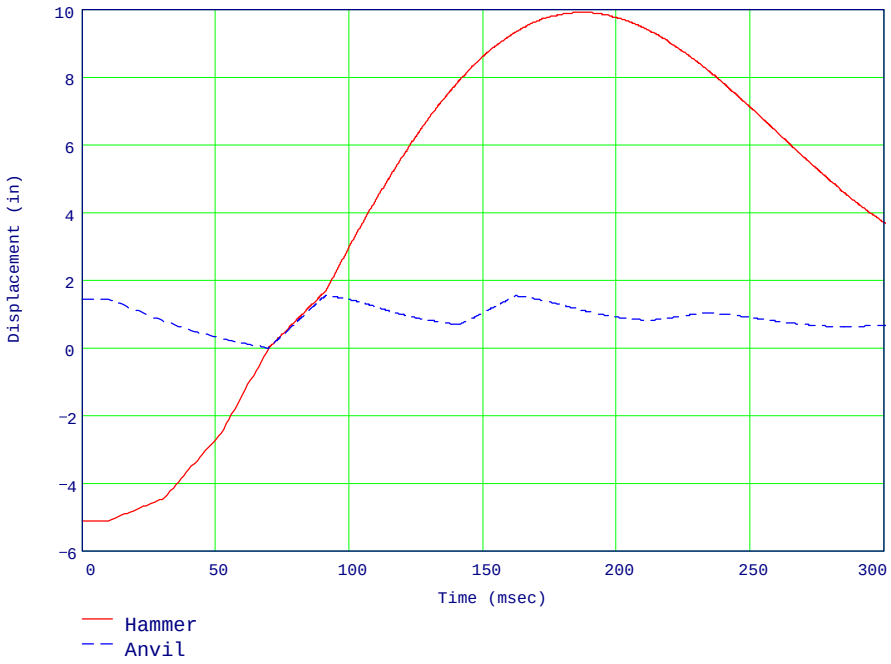

Figure 7-9: Case 2—Displacement of Hammer and Anvil

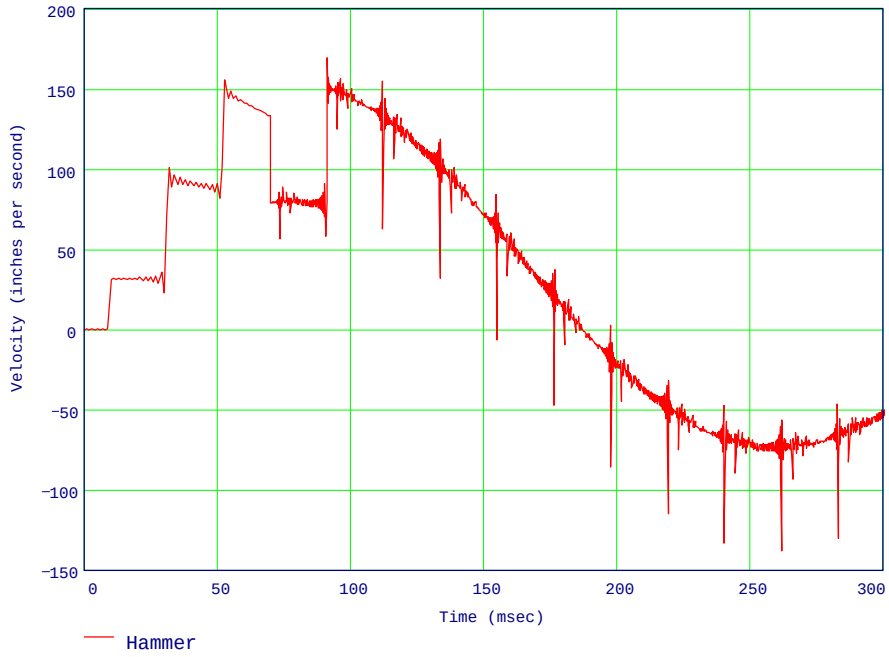

Figure 7-10: Case 2—Hammer Velocity

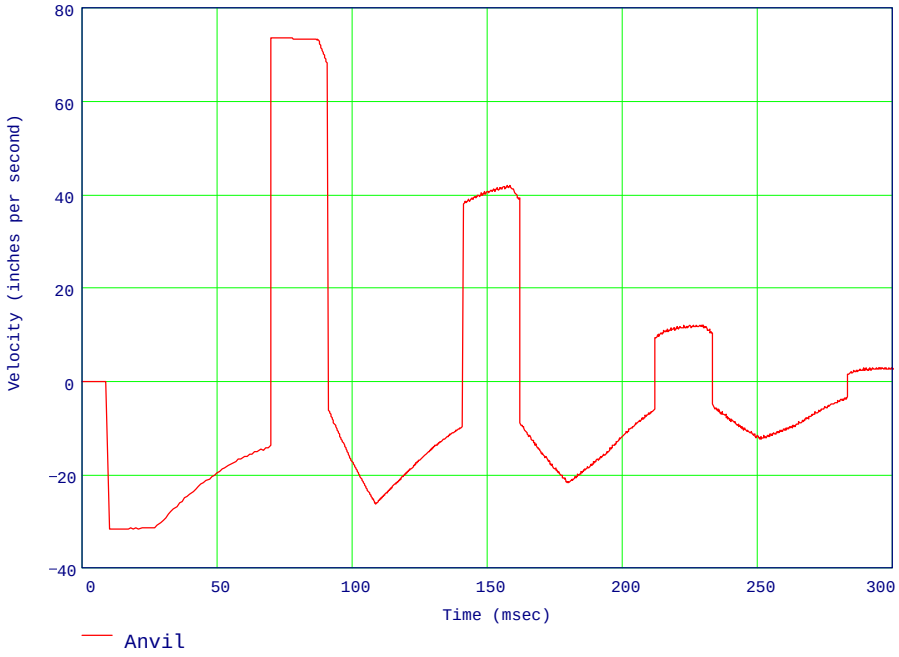

Figure 7-11: Case 2—Anvil Velocity

velocity shows the reflections from the accelerator rapidly increased the velocity of the hammer prior to impact. The hammer impact velocity is 133.333 ips.

For the anvil, the time for a reflection off of the bottom of the drill string is longer than the time until impact. Consequently, the anvil does not receive any reflections prior to impact; therefore, the free contraction velocity of the anvil does not increase over the initial value. The anvil velocity is -14.059 ips. The free contraction velocity of the anvil is -31.6 ips. The damping reflection effect has reduced the velocity of the anvil prior to impact by 17.541 ips. This is over half of the free contraction speed. This effect has reduced the impact force by 45,659 lbf.

Since the hammer is moving faster, the impact time is sooner, occurring at 59.538 ms from trigger . (Actual time is 69.538 ms.) In Case One, impact occurred at 94.682 ms, 35.144 ms later than this case. The jar also has a higher impact force of 548,664 lbf as compared to the 433,201 lbf impact in the first case. This is an increase in force over the first case by 27 percent.

The duration of the impact is much less, however. Because of the proximity of the accelerator, the primary impact wave bounces off of it and returns to the jar first. Therefore, the wave is 21.375 ms long.

Examination of the displacement chart (Figure 7-9) shows that the hammer “passes” by the anvil. Since this is physically impossible, the same caveats concerning the forces beyond the primary impact apply to this case. The jar forces are shown in Figure 7-12.

The primary impact force is 548,664 lbf and occurs at 69.538 ms and lasts until 90.913 ms. However, as shown in Figure 7-13, the force at the top of the

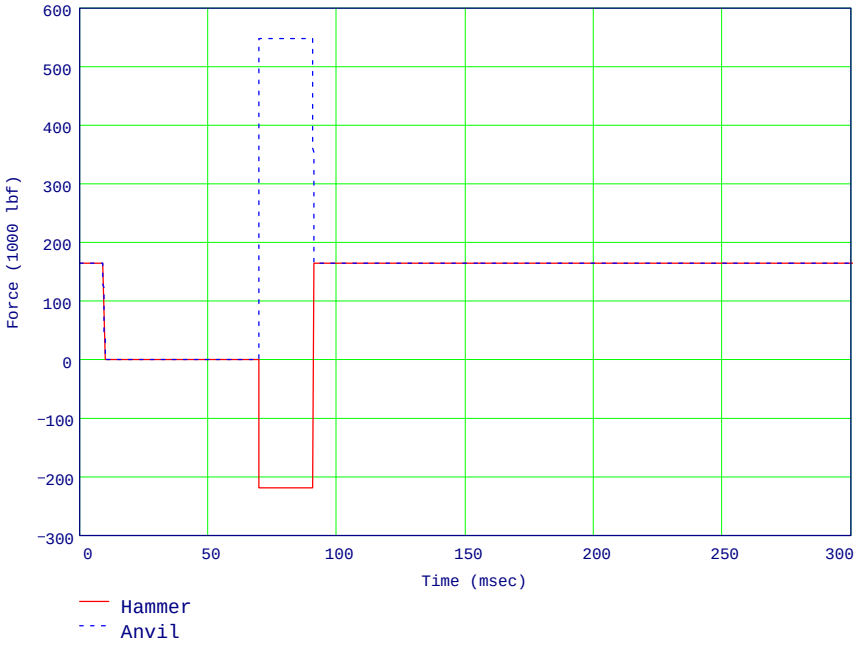

Figure 7-12: Case 2—Forces at the Jar

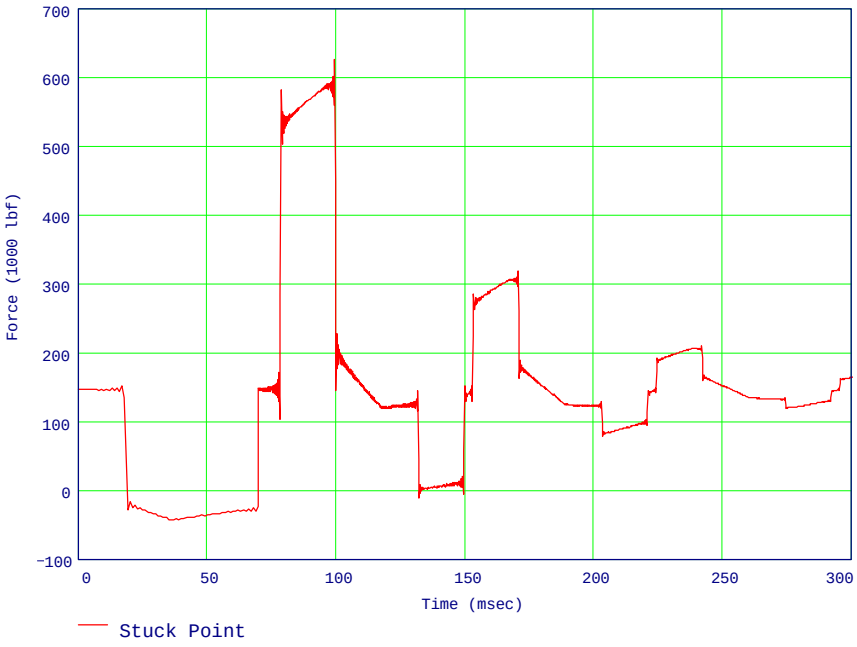

Figure 7-13: Case 2—Forces at the Top of the Stuck Point

stuck point increase to a value of 591,000 lbf. This is also the damping reflection effect. Some of the wave is reflecting back a little at a time, adding its small value to the overall force. Although it is not as prevalent in this figure as it was in Figure 7-7, the primary impact force shows a decrease after 17.8 ms. This is the round trip time from the top of the stuck point to the jar. The waves from the damping reflection effect are reflecting off of the jar thus decreasing the primary impact force. The ramp from 99.819 ms to 117.632 ms is caused by waves from the damping reflection effect continuing beyond the primary impact. The other waves are the reflections of the primary wave between the anvil and the bottom of the drill string.

Case Three: Drill Collars, Heavy Weight Drill Pipe, and Drill Pipe

In Case Three, 300 feet of heavy weight drill pipe is added between the drill pipe and drill collars cited in Case One. The heavy weight drill pipe replaces 300 feet of the drill collars. A diagram of this string is shown in Figure 7-14.

In this case, instead of an accelerator, the heavy weight drill pipe acts to partially accelerate the hammer. The heavy weight drill pipe is further away from the jar, therefore the round trip time is longer; and, the heavy weight drill pipe has a much larger cross-sectional area than the equivalent cross-sectional area of the accelerator. More of the wave passes through the drill collar/heavy weight drill pipe interface than did the wave through the accelerator.

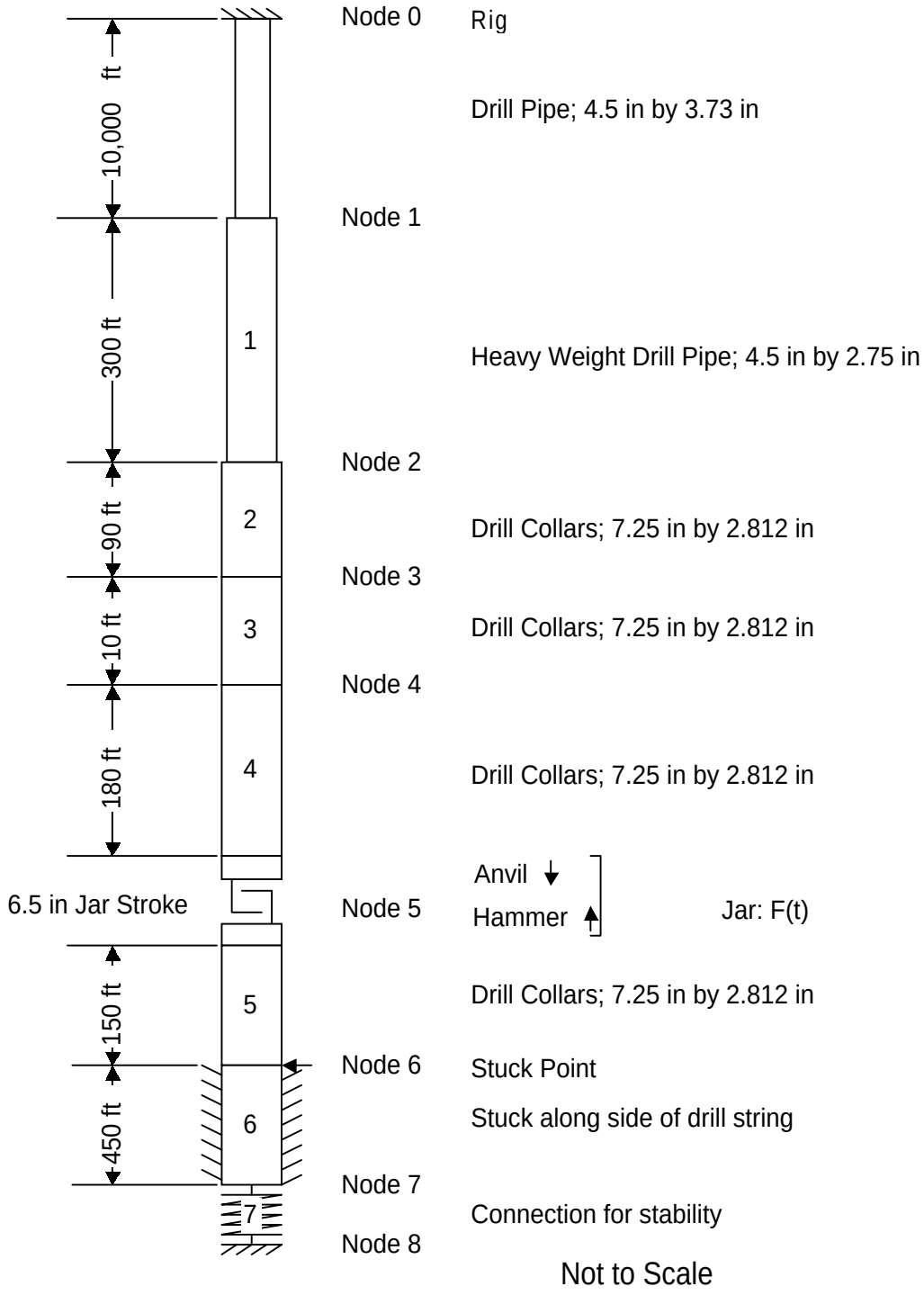

Figure 7-14: Case 3—Drill String Schematic

Using equations 5.1 and 5.2, about 44.3 percent of the incident wave is transmitted and 55.7 percent of the wave is reflected. Consequently, some of the wave bounces off of the heavy weight drill pipe/drill pipe interface. About 66.6 percent of the remaining wave is transmitted and 33.4 percent of the remaining wave is reflected. This reflected wave encounters the drill collar/heavy weight drill pipe and undergoes a transmission ratio of 155.7 percent (because the wave is going from a smaller to a larger cross-sectional area). Multiplying all of the wave transmission percentages gives a value of 23 percent of the primary incident wave. This is a significant value and will cause some additional acceleration of the hammer. These extra wave reflections are modeled in this program; they have not been modelled in other state-of-the-art jarring programs.

The hammer and anvil displacements are shown in Figure 7-15. Once again, as in all these cases, the hammer is shown traveling past the anvil.

The hammer velocity is shown in Figure 7-16. There are four reflections prior to impact. The first two are at 31.694 ips and 67.032 ips. The third reflection barely appears. It is the small mark at 86.732 ips on the side of the fourth reflection. The first three reflections are from the drill collar/heavy weight drill pipe interface. The fourth reflection is from the heavy weight drill pipe/drill pipe nterface and is 97.715 ips. This additional reflection adds 10.983 ips. This increases the impact force by 23,665 lbf.

The anvil velocity is shown in Figure 7-17. It shows the same damping reflection effect (decrease in the velocity) as in the first and second cases.

The impact force is 496,676 lbf. The duration of the impact is the round trip time from the drill collar/heavy weight drill pipe interface. This is 33.25 ms. Figure 7-18 shows the forces at the jar.

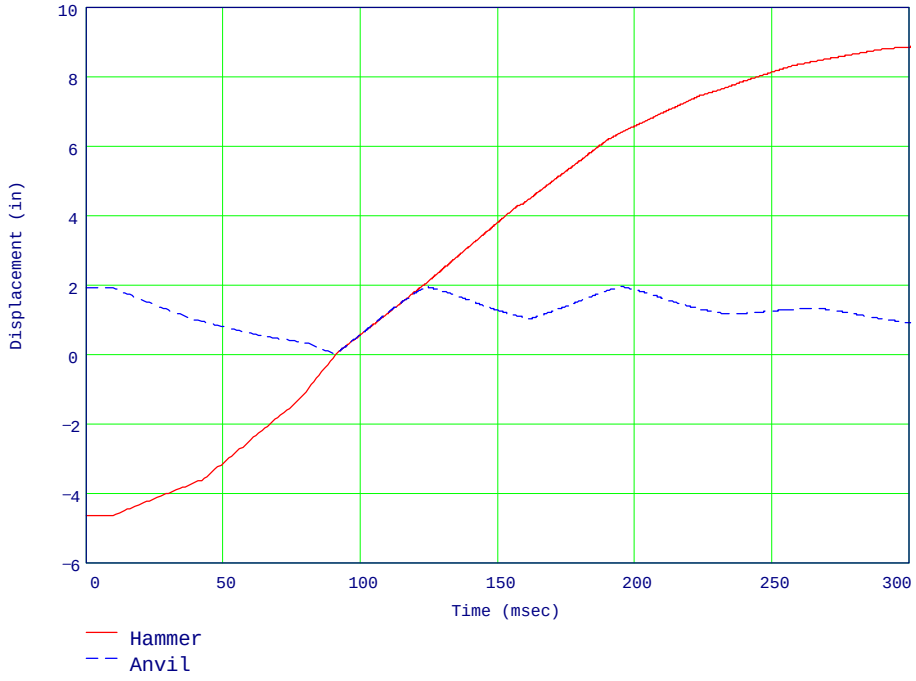

Figure 7-15: Case 3—Displacement of Hammer and Anvil

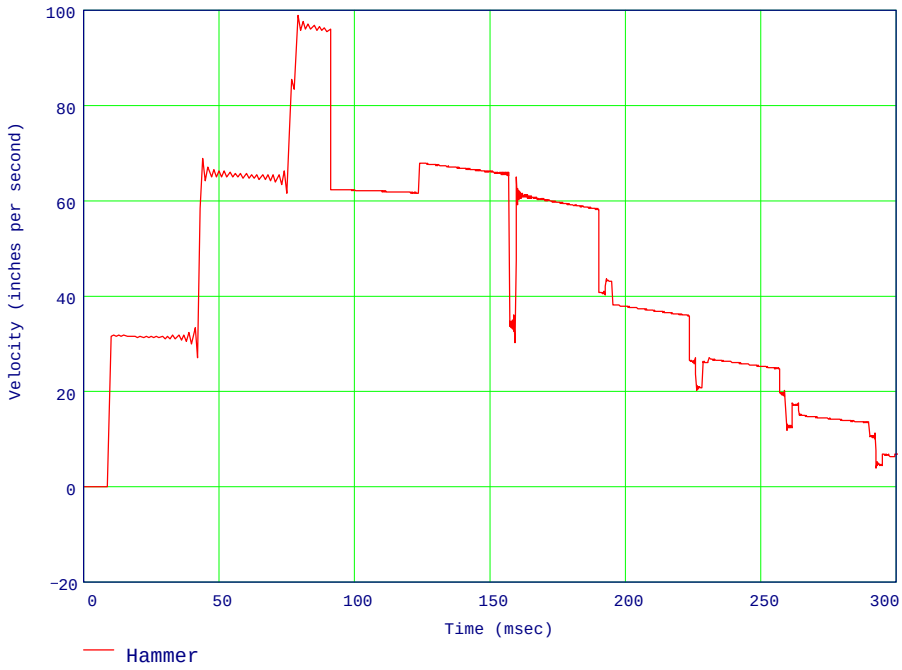

Figure 7-16: Case 3—Hammer Velocity

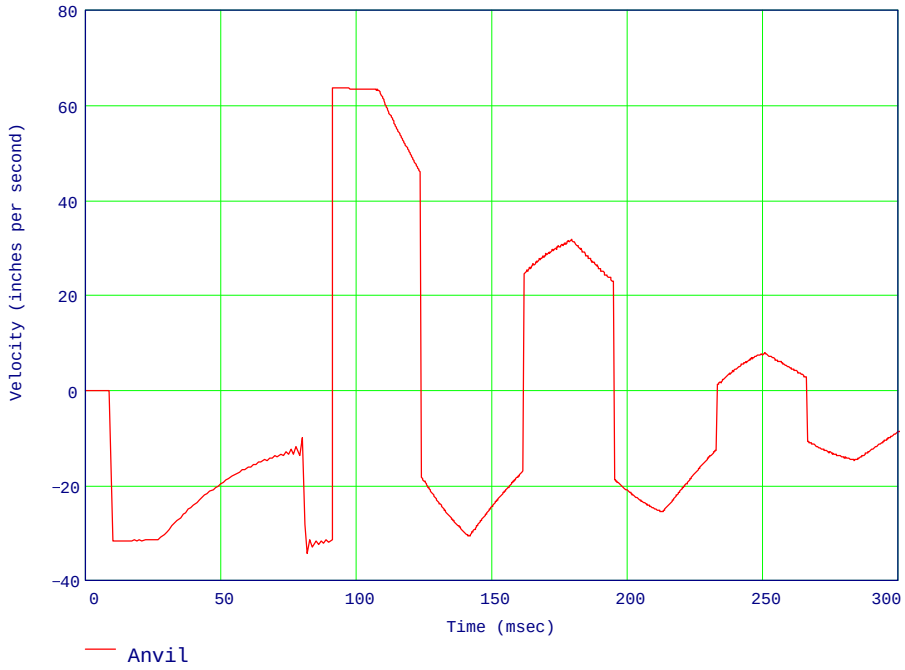

Figure 7-17: Case 3—Anvil Velocity

The force at the top of the stuck point is shown in Figure 7-19. The force is 496,676 lbf at 100.51 ms. It climbs to 528,000 lbf by 118.32 ms because of the damping reflection effect. The force starts falling after this because of reflections off of the anvil. The primary impact wave is complete at 133.76 ms.

Case Four: Drill Collars, Heavy Weight Drill Pipe, Drill Pipe, and an Accelerator

Case Four is the same as Case Three except that an accelerator is added 180 feet above the jar. The drill string schematic is shown in Figure 7-20.

Case Four is also similar to the second case. Because of the closeness of the accelerator to the jar, the waves bounce off the accelerator first. Also, since only 0.3 percent of the wave transmits through the accelerator, any reflec-

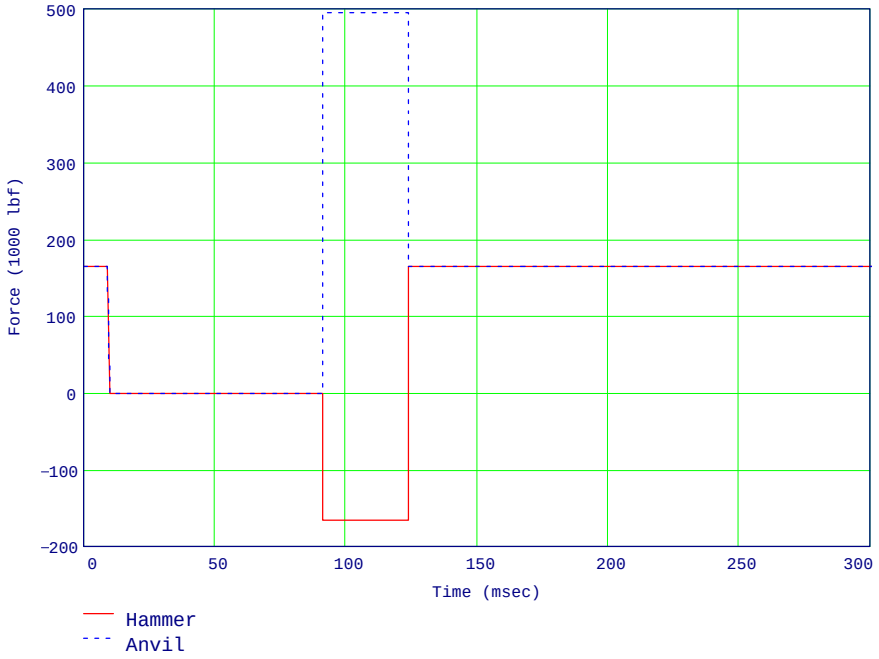

Figure 7-18: Case 3—Forces at the Jar

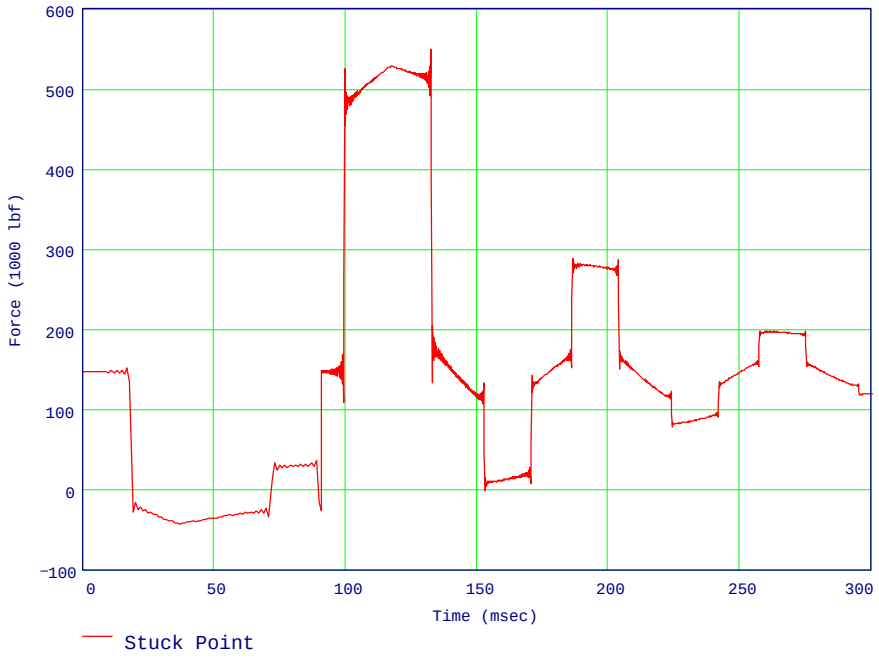

Figure 7-19: Case 3—Forces at the Top of the Stuck Point

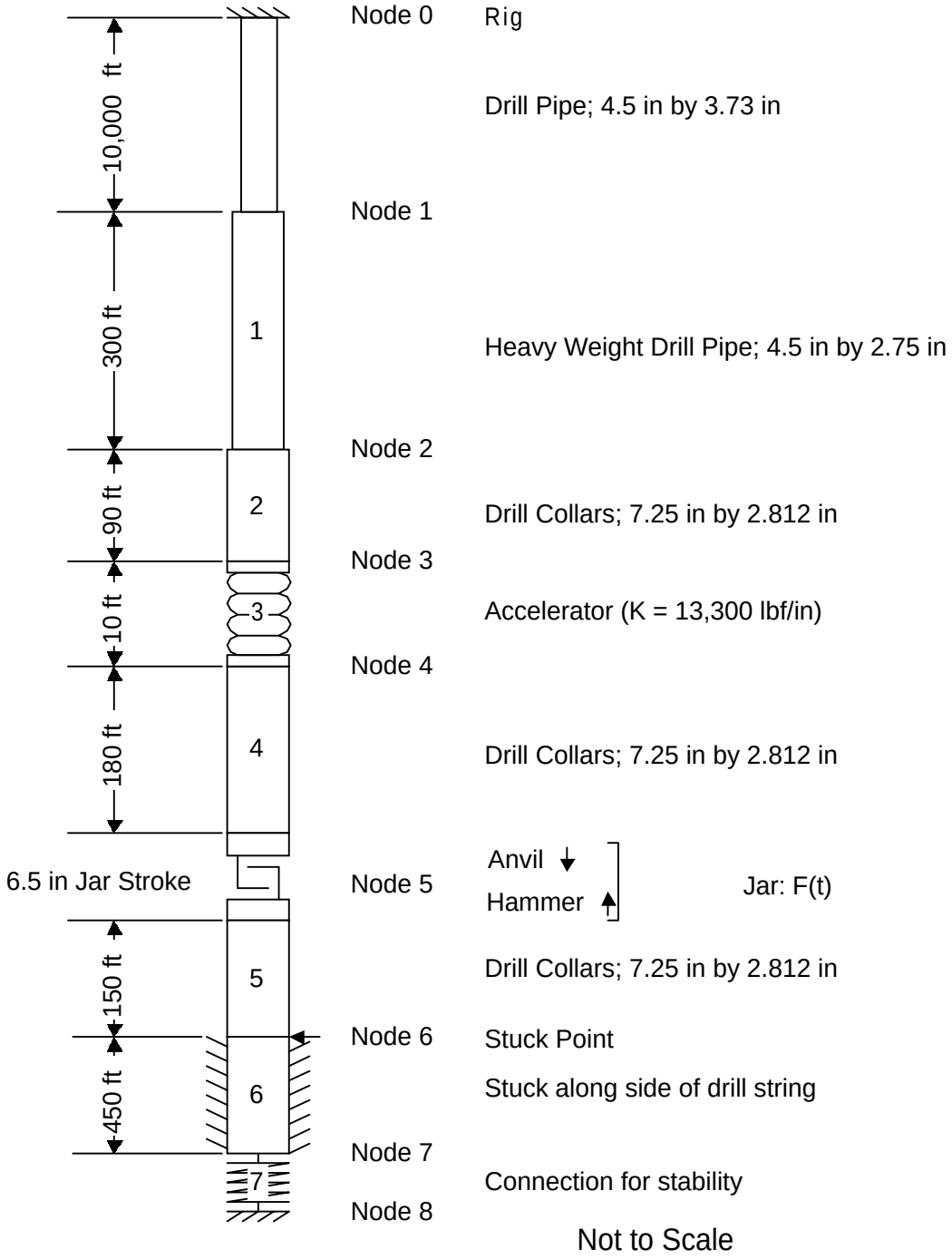

Figure 7-20: Case 4—Drill String Schematic

tions from the drill collar/heavy weight drill pipe or heavy weight drill pipe/drill pipe interface are minuscule. The accelerator dominates the wave propagation characteristics.

This can be seen by comparing the displacements of the hammer and anvil in the second case (Figure 7-9) to the displacements of the hammer and anvil in this case (Figure 7-21). The two charts can practically be overlain.

This is true for the hammer velocities (Figure 7-22) and the anvil velocities (Figure 7-23). As seen in Figure 7-24, the jar forces are also equal (since the velocities are equal). In addition, because the anvil side of the drill string was not changed in any manner, the top of the stuck point forces are identical as seen in Figure 7-25.

This case shows that even though the drill strings are different, one can get the same wave propagation response with the proper tools. An accelerator "disconnects" whatever is above it from whatever is below it (as long as it does not hit the stops). It does not matter what is above the accelerator, whether it be multiple drill string geometries, a dogleg, or another jar. The accelerator isolates the drill string below it.

Case Five: Drill Collars, Heavy Weight Drill Pipe, Drill Pipe, and an Accelerator with a Rigid Stuck Point

Case Five is a direct comparison to the drill string response as seen in the *Transient Dynamic Analysis of the Drillstring Under Jarring Operations by the FEM* paper (Kalsi, Wang, and Chandra 1987). This paper shows the analysis of a jarring wave propagation problem using a time based finite element program. See Chapter 2 for a discussion of this paper.

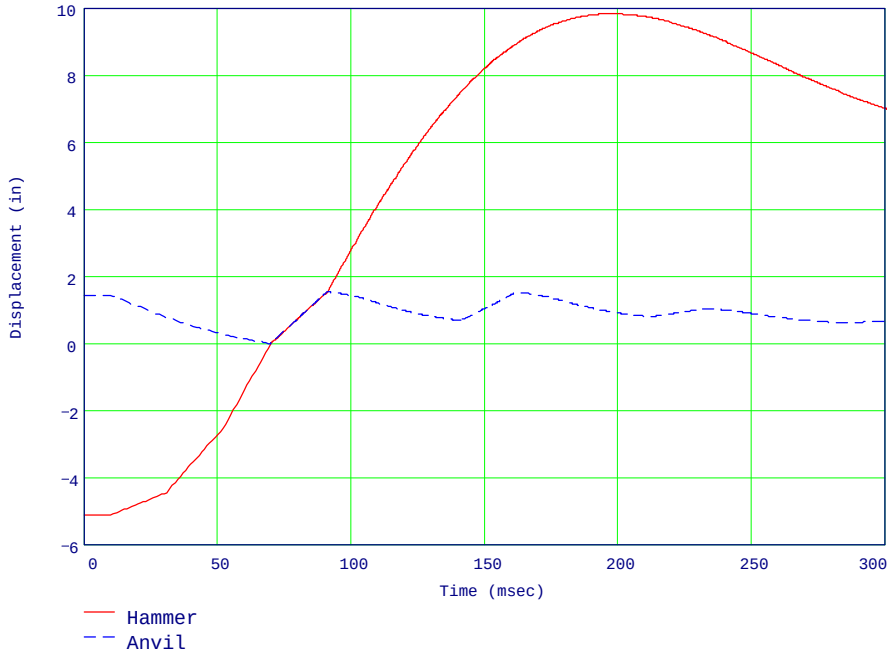

Figure 7-21: Case 4—Displacement of Hammer and Anvil

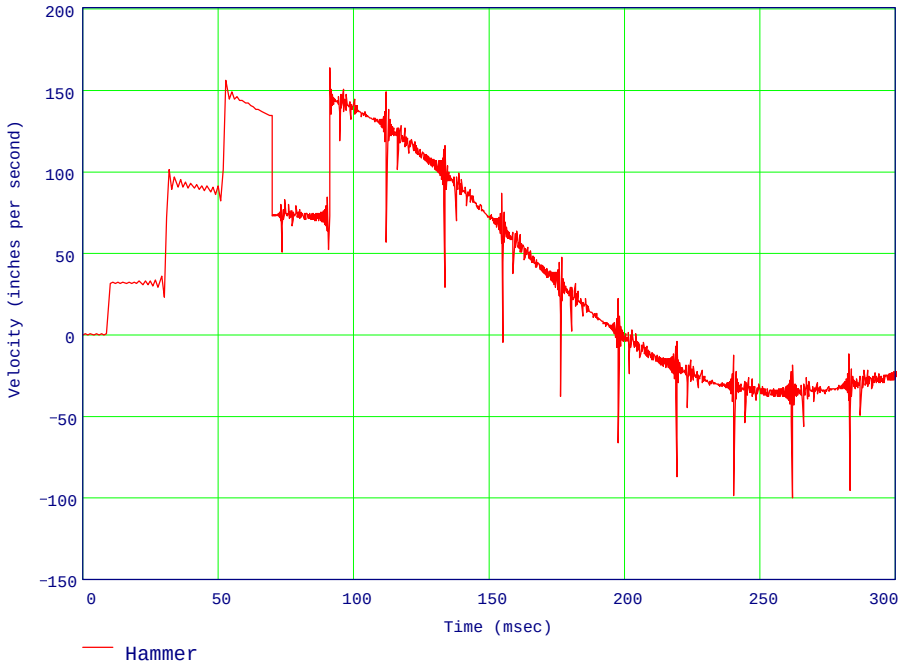

Figure 7-22: Case 4—Hammer Velocity

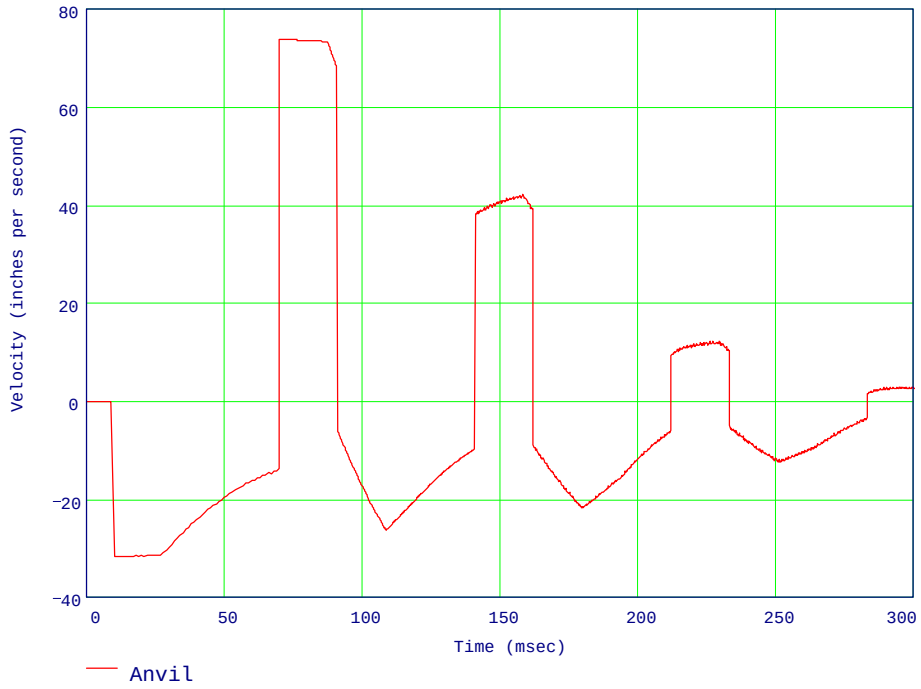

Figure 7-23: Case 4—Anvil Velocity

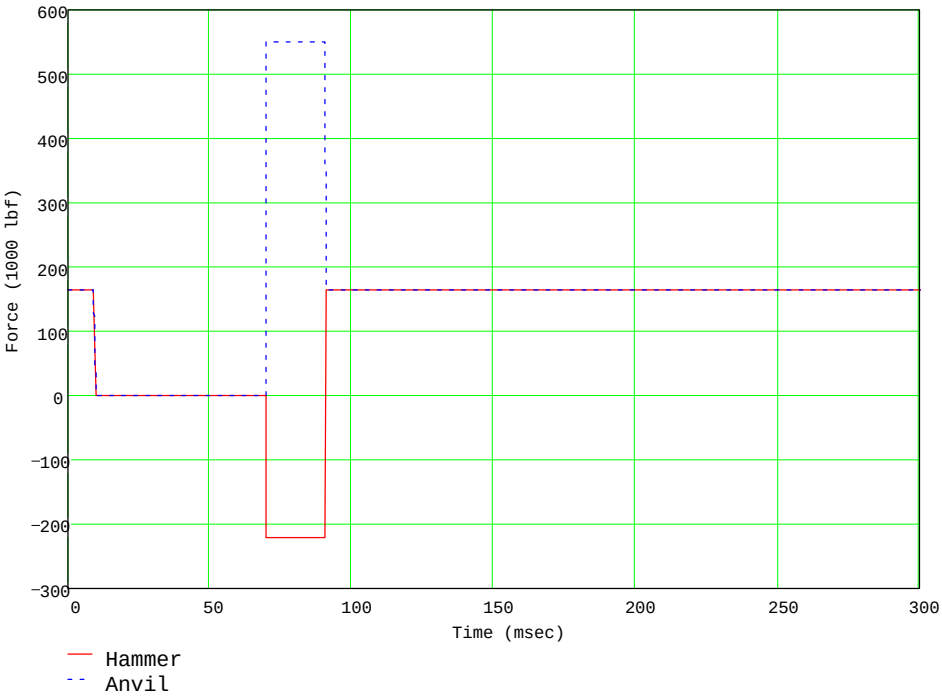

Figure 7-24: Case 4—Forces at the Jar

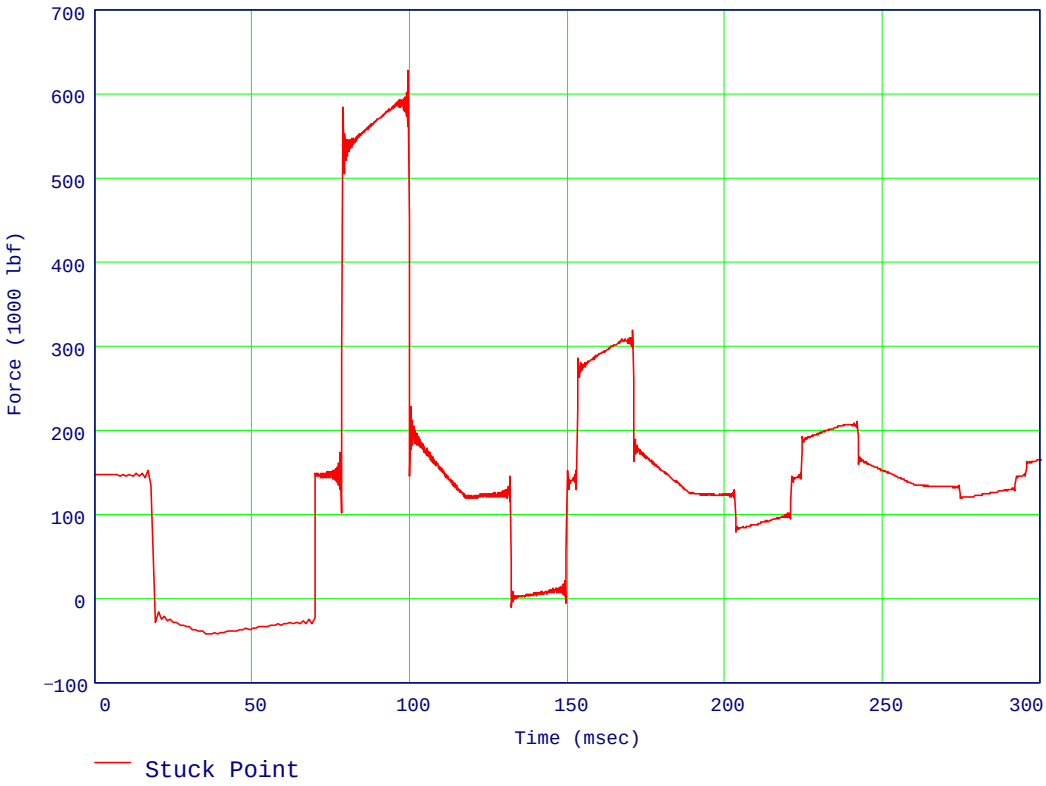

Figure 7-25: Case 4—Forces at the Top of the Stuck Point

The drill string is the same as in the fourth case and is shown in Figure 7-26. The only difference is that in Case Five, the top of the stuck point was considered a rigid connection during the free contraction phase and was free to move during the post-impact phase. This is shown in Figure 7-26 as the two triangles at the top of the stuck point.

In the spectral analysis model demonstrated here, the rigid connection at the top of the stuck point is simulated rather than mathematically re-built. The cross-sectional area of the stuck element (element 6) can be increased by a very large factor. This is similar to connecting the free part of the drill string to a wall. This is

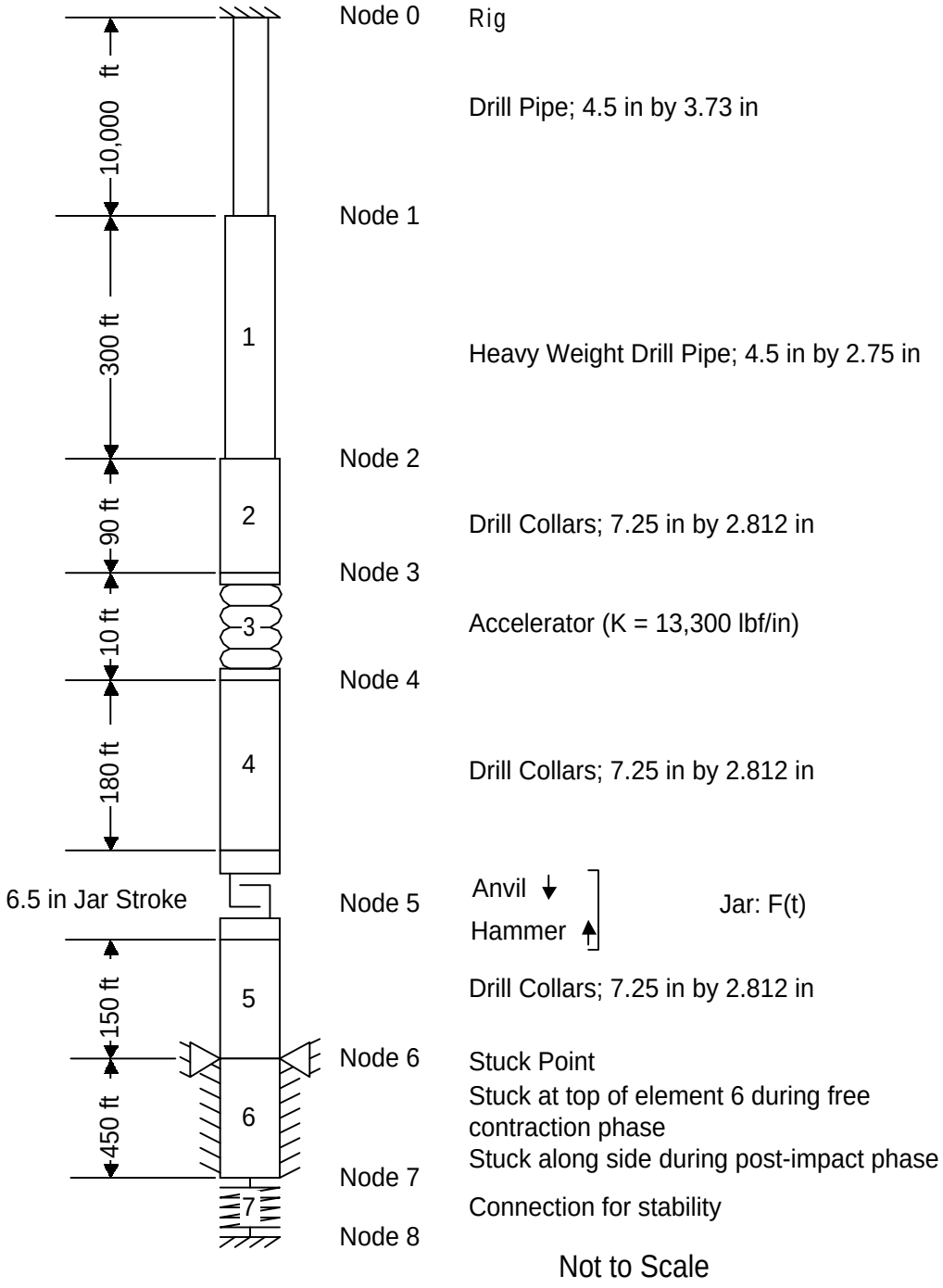

Figure 7-26: Case 5—Drill String Schematic

accomplished by changing the outside diameter of the drill collars in element 6 to a very large number. In this example, the outside diameter was multiplied by 1,000. The cross-sectional area has been increased by a factor of 1,177,078. It is the same as hitting a wall that is 6.581 acres in area. The wave response is the same as hitting a fixed end.

At impact, this “fixed end” at the top of the stuck point must be freed. This is accomplished by re-setting the cross-sectional area of the stuck element back to its original value prior to running the calculations for the post-impact phase. It returns to being a movable element.

Because these changes affect only the anvil portion of the jar, and then only during the free contraction phase, it can be expected that the hammer displacement (Figure 7-27) and velocity (Figure 7-28) should be the same as in Case Four’s displacement and velocity. (See Figures 7-21 and 7-22, respectively.) The charts look similar except that the impact occurs at 77.975 ms in Case Five case rather than at 69.514 ms in Case Four. The change in the impact time can be attributed to the anvil’s reaction.

The anvil displacement and velocity is considerably different in Case Five than Case Four. The anvil displacement is shown in Figure 7-27 and the anvil velocity is shown in Figure 7-29. In Case Four, the anvil shows no reflection effects and simply drives downward until impact. In Case Five, the anvil oscillates twice before impact. This is attributable to the waves bouncing off of the top of the stuck point, rather than having to travel to the bottom of the drill string. The round trip time from the jar to the top of the stuck point is 17.813 ms. There

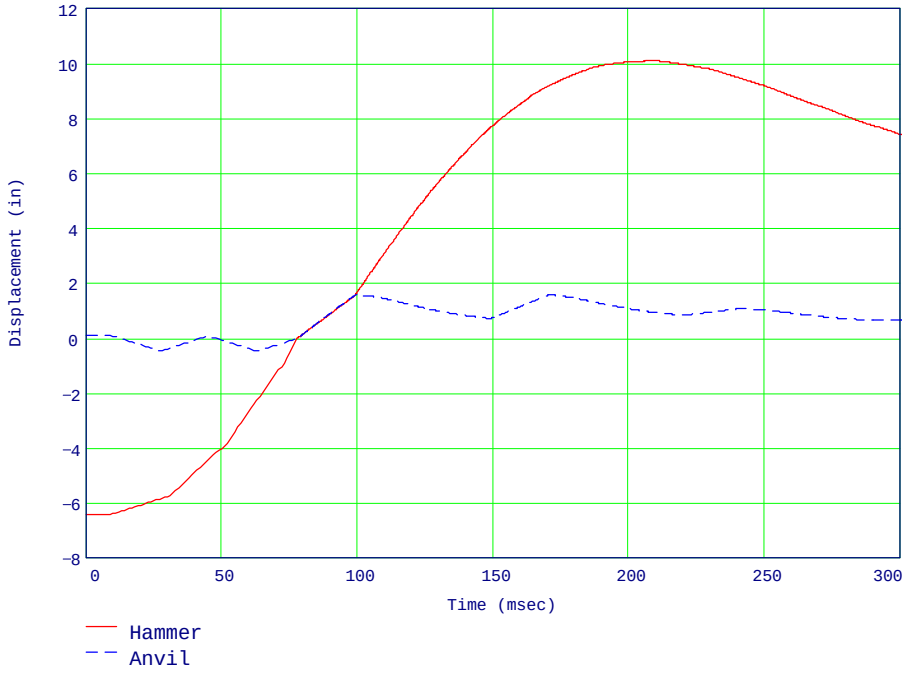

Figure 7-27: Case 5—Displacement of Hammer and Anvil

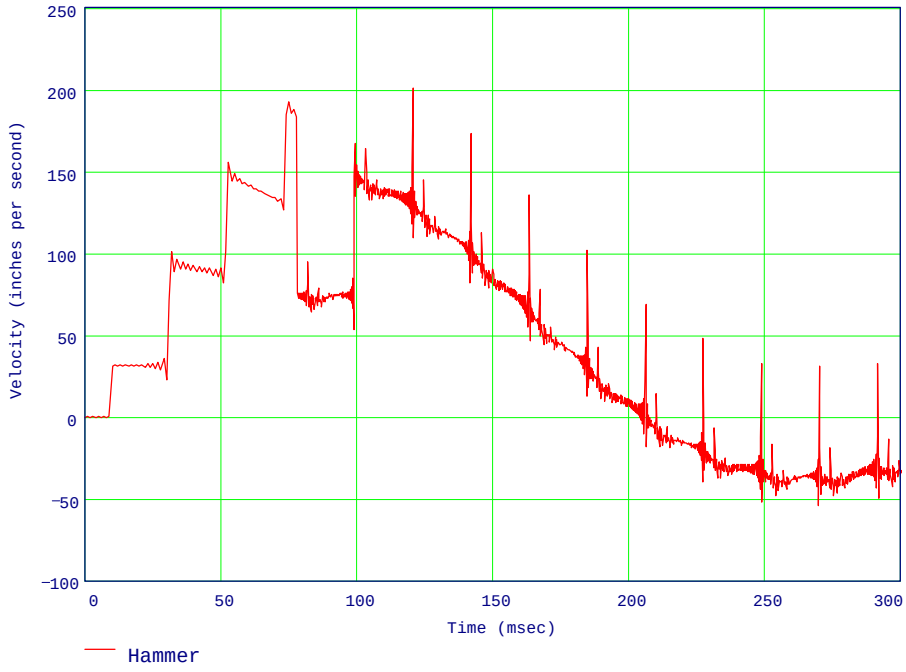

Figure 7-28: Case 5—Hammer Velocity

is time for over four round trips before impact. In the fourth case, the round trip time is 71.250 ms. The wave does not return to the jar before impact at 69.514 ms.

The effect of these rapid oscillations of the anvil in Case Five is to slow down the anvil. It is oscillating between 31.6 ips and -31.6 ips. In the fourth case, the velocity jumps to 31.6 ips and stays there until the damping reflection effect starts to decay the velocity. The damping reflection effect has no effect in the free contraction phase in Case Five because the waves bounce off of the top of the stuck point rather than traveling through the stuck element.

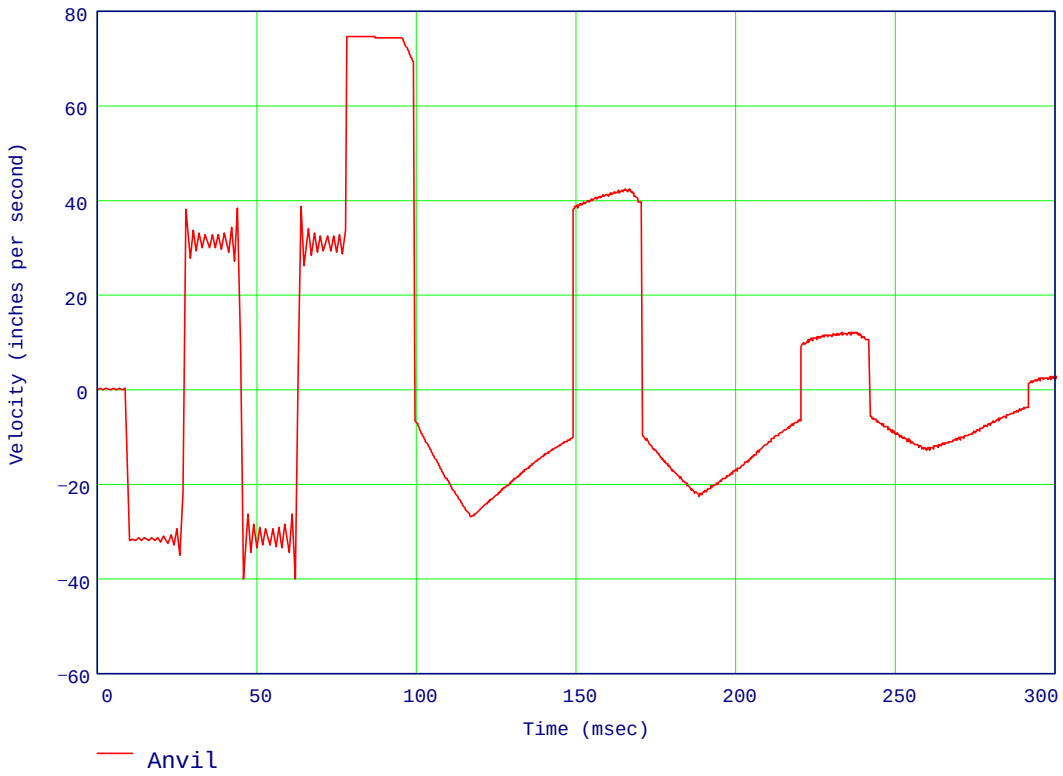

Figure 7-29: Case 5—Anvil Velocity

This oscillation can mean that the anvil is “caught” traveling upwards at impact. That occurs in this case. The anvil velocity is 33.529 ips upwards as opposed to -14.073 ips downwards in the fourth case, a difference of 47.602 ips. However, because the impact required a longer free contraction time, the hammer had time to accelerate to a higher velocity. Its velocity at impact is 183.176 ips as opposed to 133.763 ips in the fourth case, a difference of 49.413 ips. Since the impact force is related to the difference in velocities, the anvil’s lost velocity is made up by the hammer’s gain in velocity. This is a coincidence! It does not always happen this way.

The impact force is 554,531 lbf in Case Five versus 549,820 lbf in Case Four. This is not a significant difference. In fact, from the impact time onwards, there is no difference in the primary impact waves in the jar as shown in Figure 7-30 or at the top of the stuck point as shown in Figure 7-31 except for the 4,711 lbf difference and the different impact time. The duration of the impact pulse is still determined by the round trip time from the jar to the accelerator and is 21.375 ms. If the top of the stuck point was still regarded as a fixed end, then it would determine the impact pulse duration as it is closer to the jar. Because it was changed back to a regular drill collar, the round trip time would be the time for the wave to travel from the jar to the bottom of the drill string.

The charts of the displacements, velocities and forces shown in the Kalsi paper compare favorably to the spectral analysis method figures of the sam

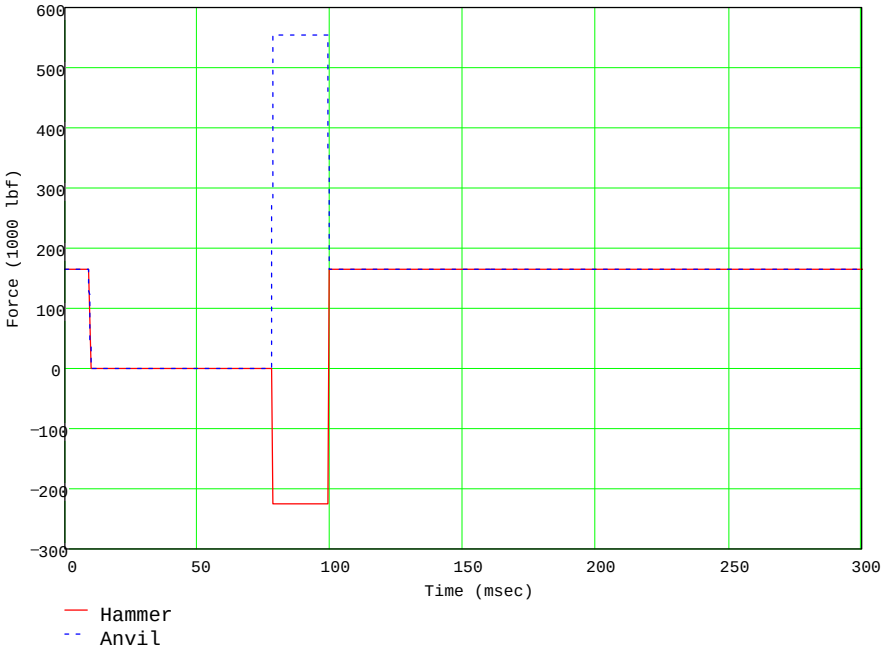

Figure 7-30: Case 5—Forces at the Jar

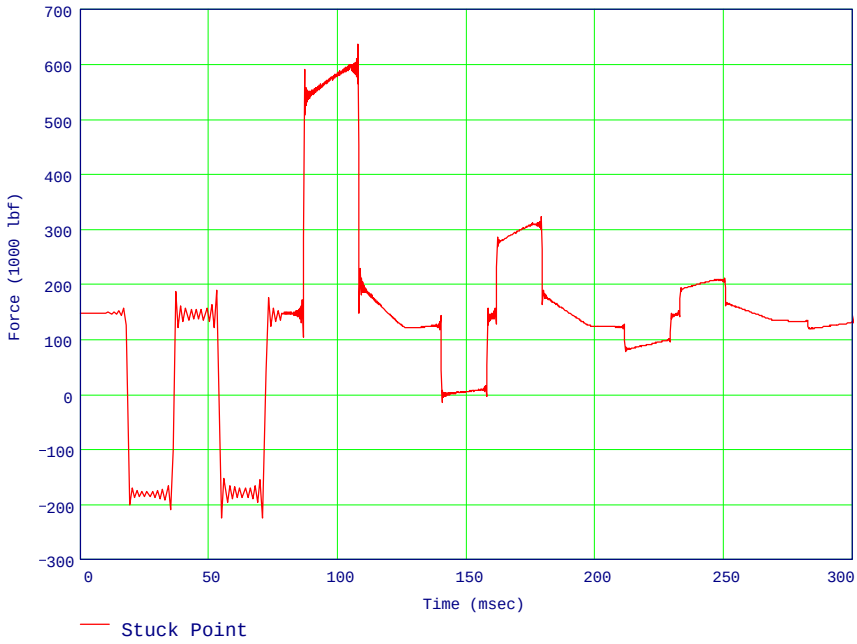

Figure 7-31: Case 5—Forces at the Top of the Stuck Point

CONCLUSIONS AND RECOMMENDATIONS

In this dissertation, it has been shown that the frequency domain approach to drill string jarring analysis is a superior method to earlier jarring models. Accuracy has been improved to the degree that even wave reflections from damping can be observed (the damping reflection effect). Unlimited reflection points can be incorporated into the spectral analysis model and each reflection will be modeled faithfully. The anvil motion is included and has been shown to have a major effect on the impact force.

The spectral analysis method has eliminated the need for small elements necessary in time-based methods for accurate wave tracking. The time step problem noted in the time-based methods has been improved. The time step selection in spectral analysis is based on window length and frequency resolution, not on algorithm stability and wave capture. The time steps can be larger and longer without the penalty of excess computational time.

Although it is difficult to compare the time needed to calculate the jarring conditions using the finite element method versus the spectral analysis approach, it appears that the spectral analysis approach is much faster. For the cases in Chapter 7, it takes aproximately eight minutes per run using a 120 MHz Pentium laptop computer. Although no direct comparison has been run, the experiences of this author have been that the finite element method can take up

to half an hour or more. Some of the papers reviewed in Chapter 2 allude to the time of FEM analysis, too. These Mathcad documents are by no means optimized for speed. A future stand-alone program optimized for speed and accuracy could improve the time requirements of spectral analysis significantly.

The spectral analysis method is easier to use than the finite element method. The ANSYS finite element program, while a very powerful engineering application, can be intimidating. The spectral analysis method also can be adapted for a driller to use in the field.

This model is not a panacea for all the jarring analysis problems. For example, waves cannot be generated; they can only be propagated, transmitted, and reflected. Other methods are needed to generate the actual impact wave. However, one advantage of the spectral analysis method is that any wave form can be used. If actual wave forms from jarring operations can be recorded, these wave forms can be used as the input. This adds a higher level of realism to this model not found in any other model.

Currently, nonlinear effects such as Coulomb damping cannot be incorporated. This is the subject of future research.

Other Areas of Research

The spectral analysis procedure is not limited to jarring problems. Any transient vibration problem can be analyzed using this technique. Problems such as bit catching (called slip-stick) and bit bounce can be analyzed. Shock

loading from hitting ledges or dropping tools can be determined. Even thermal shocks can be modeled, albeit with thermal spectral equations rather than the motion equations used in this dissertation.

Vibration Analysis

Using the stiffness matrix, the resonant frequencies of a system can be determined. For example, in the API standards (RP 7-G), a very simplistic approach was taken for the determination of the critical rotary speeds, where rough drilling occurs because of resonance. Basically, the API threw up their hands and said this is too complex to calculate. However, the spectral analysis procedure can be applied to find the critical rotary speeds for very complex drill strings. The model can be built and then run through a series of frequencies with a unit amplitude. The frequencies with the largest amplitude response are the resonant frequencies. The relative amplitudes give an indication of the severity of the vibration.

Impact Study

The spectral analysis procedure can be used for reverse transient wave propagation problems. For example, the Baker Hughes Inteq ADAMS system measures vibrations at the kelly on a drilling rig. It is theoretically possible to take the vibrations measured at that point and back propagate the waves to determine their origin. It might also be possible, given full knowledge of the drill string and bit vibration behavior, to determine the lithology of the formations being drilled by back propagating the vibrations measured at the surface.

More Work to Do

There is considerable research that can be done based upon the work presented in this dissertation. The areas that need the most research are jarring impact and damping. Today's knowledge is not strong in these areas. The output of this model is sensitive to the impact magnitude and duration and to the amount of damping. The model is excellent for determining the impact forces anywhere on the string; but, its accuracy is only as good as the data input. A better understanding of impact and damping areas is the first area of continued research.

Jarring Impact

The reverse transient wave propagation technique would be very valuable for jar impact analysis in a laboratory. Currently, the jar impact wave is assumed to be similar to the Hopkinson bar experiments. But jars have a considerably more complex internal arrangement than a simple bar. How does an off-center, nonparallel hammer and anvil impact? What bending and torsional waves arise from such an event? How much of an impact wave actually damps out before leaving the jar?

These are questions that can be answered using the reverse transient wave propagation techniques. A jar could be instrumented with strain gages and accelerometers. Then the jar could be triggered and impacted. Using a spectral analysis structure of the jar mechanisms, the waves measured by the instruments could be back propagated to the source, the hammer and anvil faces. This could help find energy losses within the jar. It would also help improve the

efficiency of the jar for getting energy out to the drill string. Finally, it would give real data to input into the model in this dissertation rather than the assumed rectangular shape impact pulse.

Coulomb Damping

In Chapter 4, the nature of Coulomb damping was discussed. One of the problems of the spectral analysis method is its inability to incorporate nonlinear effects. Once in the frequency domain, it is difficult to determine the occurrence of time-based events that are determined by the condition of the model. For example, there was no method available to “turn off the jarring model” after the stroke length was reached. Since this is unknown prior to running the model, it is unknown where to stop the model until after the model has completely run its course. It cannot be stopped in the middle of a run.

This limitation might be mitigated by using what this author calls a flying FFT approach. While analyzing vibrations using a spectrum analyzer, such as the ADAMS system, the instrument collects data in packets. It then runs an FFT on the data it just gathered. If the FFT computational time is less than the time used to collect the data, then the system can continue to show the frequency spectrum in real time. It is taking an FFT of the data “on the fly”.

The flying FFT approach could possibly be used in reverse. The procedure would be to analyze a time domain situation in the frequency domain and determine the FFT response. Then, back in the time domain, that FFT response would be used to modify the conditions for the next block of time in the next FFT analysis. This technique would run repeatedly at a very high speed, maybe at 100,000 Hertz, using small time jumps. This would have the advantage of an

unlimited time span with the ease of structure assembly found in spectral analysis. It would allow for the incorporation of vibrations and transient analysis in the same model. The difficulty will be overcoming the wave migration problem. Some of the other frequency analysis problems could limit this technique as well. But this author believes this is worth pursuing.

Torsional Waves

Using the torsional equations of motion for waves, torsional waves can be added to the stiffness matrix. This would allow for the study of the bit slip-stick phenomenon and its effect on a drill string.

Lateral Waves

Although far more complex, the bending equations of motion also can be incorporated into the stiffness matrix. The effect of bending waves can be included by incorporating the same techniques used to derive the stiffness matrix for axial motion in this dissertation. Adding the bending wave to the axial and torsional wave stiffness matrix will make this a full three-dimensional model. In addition, based on discussions with others in this field, there may be a connection between lateral frequencies and buckling.

Tool Joints

Tool joints in the drill pipe and heavy weight drill pipe have an effect on the wave propagation characteristics. Most of the time, this effect is thought to be small; however, given the right frequency, the joints occasionally become

excited through resonance. The taper of the tool joints can also change the transmission and reflection characteristics of wave propagation through a tool joint. This can be modeled with a tapered spectral element.

Stabilizers

Stabilizers and other bottom hole assembly tools do not have the same geometries and material properties as drill collars. This will have some effect on the wave propagation characteristics of the drill string. The magnitude of this effect is unknown.

A stabilizer could be assembled into a spectral analysis sub-structure. A sub-structure is a complicated structure that uses simpler models as building blocks. These building blocks are assembled into a single stiffness matrix model. This single stiffness matrix model, the sub-structure, can then be incorporated into an even more complex structure wherever needed.

Curved Boreholes

In the model presented in this dissertation, only straight holes were considered. Curved boreholes are important in today's drilling. However, in wave propagation, curved drill strings lead to coupled axial and bending waves. An axial wave can cause a bending wave to self-generate; a bending wave can cause an axial wave to self-generate. These effects are very complex. However, the frequency domain approach may make the solution to these problems more easily accomplished. A curved borehole element could be assembled and added to the existing straight hole elements' library and used wherever needed.

REFERENCES CITED

Aarrestad, Thor V., and Åge Kyllingstad. 1994. Loads on drillpipe during jarring operations. *SPE Drilling and Completion* (December): 271-275. Originally presented at 1992 European Petroleum Conference at Cannes, France.

Achenbach, J.D. 1993. *Wave propagation in elastic solids*. 7th ed. Amsterdam, The Netherlands: Elsevier Science Publishers B.V.

Anderson, L.B., and P. Lembourn. 1994. Analysis of interruption and lost rig time due to equipment failure in offshore drilling operations. IADC/SPE 27511 paper presented at 1994 IADC/SPE Drilling Conference, 15-18 February, at Dallas, Texas.

ANSYS, Inc. 1992. *ANSYS theoretical reference manual*. Houston, Pennsylvania: ANSYS, Inc.

Askew, W.E. 1986. Computerized drilling jar placement. IADC/SPE 14746 paper presented at 1986 IADC/SPE Drilling Conference, 10-12 February, at Dallas, Texas.

Clough, Ray W., and Joseph Penzien. 1975. *Dynamics of structures*. New York, New York: McGraw-Hill, Inc.

Cooley, J.W., and J.S. Tukey. 1965. An algorithm for the machine calculation of complex Fourier series. *Math. Comput.* 19: 297-301.

Dareing, D[on], and B. Livesay. 1968. Longitudinal and angular drillstring vibrations with damping. *Journal of Engineering for Industry*, Trans. ASME, (November): 671-679.

Doyle, James F. 1989. *Wave propagation in structures: an FFT-based spectral analysis methodology*. New York, New York: Springer-Verlag New York, Inc.

Doyle, James F. 1991. *Static and dynamic analysis of structures with an emphasis on mechanics and computer matrix methods*. AA Dordrecht, The Netherlands: Kluwer Academic Publishers.

Fershter, A., B. Bleikh, and S. Sheinbaum. 1972. Vybor optimal' nykh uslovi raboty yasa, *Neft Khoz* 2 (February), 17-19,

Harris, Cyril M., ed. 1988. *Shock vibration handbook*. 3rd ed. New York, New York: McGraw Hill Book Company.

Jacobsen, Lydik S. 1930. Steady forced vibration as influenced by damping. APM-52-15 paper presented at Semi-Annual Meeting of The American Society of Mechanical Engineers, 9-12 June, at Detroit, Michigan.

Kadaster, Ali G., C. Wilton Townsend, and E. Kurt Albaugh. 1993. Drilling time analysis—a TQM tool for drilling in the 90s. *Petroleum Engineer International* (February): 31-38.

Kalsi, M.S., J.K. Wang, and U. Chandra. 1987. Transient dynamic analysis of the drillstring under jarring operations by the FEM. *SPE Drilling Engineering*, (March): 47-55. Originally SPE paper 13466 presented at 1985 SPE/IADC Drilling Conference, 6-8 March, at New Orleans, Louisiana.

Kolsky, H. 1963. *Stress waves in solids*. New York, New York: Dover Publications, Inc. Originally published in 1953: Oxford, United Kingdom: Clarendon Press.

Kemp, Gore. 1990. *Oilwell fishing operations: tools and techniques*. 2d ed. Houston, Texas: Gulf Publishing.

Lerma, M.K. 1985. A study of how heavy-weight drillpipe affects jarring operations. SPE 14326 paper presented at 60th Annual Technical Conference and Exhibition of the SPE, 22-25 September, at Las Vegas, Nevada.

Meyers, Marc A. 1994. *Dynamic behavior of materials*. New York, New York: John Wiley & Sons, Inc.

Mitchell, Bill. 1995. *Advanced oil well drilling engineering handbook & computer programs*. 10th ed. Golden, Colorado: Mitchell Engineering.

NL McCullough. 1978. *Pipe recovery manual*. Houston, Texas: NL McCullough.

Reddy, J.N. 1984. *An introduction to the finite element method*. New York, New York: McGraw-Hill, Inc.

Skeem, Marcus R., Morton B. Friedman and Bruce H. Walker. 1979. Drill string dynamics during jar operation. *JPT* (November): 1381-1386. Originally SPE 7521 paper presented at 53rd Annual Fall Technical Conference and Exhibition of the SPE of AIME, 1-3 October, at Houston, Texas.

Tri-State Oil Tool Industries, Inc. n.d. *Basics of fishing*. Bossier City, Louisiana: Oil Industries, Inc.

Wang, Jaw-Kuang, Manmohan S. Kalsi, René A. Chapelle, and Thomas R. Beasley. 1990. A practical approach to jarring analysis. *SPE Drilling Engineering* (March): 86-92. Originally SPE paper 16155 presented at the 1987 IADC/SPE Conference, 15-18 March, at New Orleans, Louisiana.

Watson, Bruce, and Randy Smith. 1994. Training reduces stuck pipe costs and incidents. *Oil & Gas Journal* (September 19): 44-47.

Zienkiewicz, O.C., and R.L. Taylor. 1989. *The finite element method*. 4th ed. Vol 1. London, United Kingdom: McGraw-Hill Book Company Europe.

SELECTED BIBLIOGRAPHY

Aadnoy, Brent S. 1986. Transversal vibrations in stabilized drilling assemblies. *Energy Sources* 8, no. 4: 305-329.

Aarrestad, T[hor] V., and Å[ge] Kyllingstad. 1986. An experimental and theoretical study of coupled boundary conditions for vibrations in drillstrings. SPE 15563 paper presented at 61st Annual Technical Conference and Exhibition of the SPE, 5-8 October, at New Orleans, Louisiana.

Aarrestad, T[hor] V., and Å[ge] Kyllingstad. 1989. Measurements and theoretical models on rig suspension and the effect on drillstring vibrations. SPE 19553 paper presented at 64th Annual Technical Conference and Exhibition of the SPE, 8-11 October, at San Antonio, Texas.

Aarrestad, T[hor] V., and Åge Kyllingstad. 1993. Rig suspension measurements and theoretical models and the effect on drillstring vibrations. *SPE Drilling & Completion* (September): 201-206.

Aarrestad, T[hor] V., H.A. Tonnesen, and Å[ge] Kyllingstad. 1986. Drillstring vibrations: comparison between theory and experiments on a full-scale research drilling rig. IADC/SPE 14760 paper presented at 1986 IADC/SPE Drilling Conference, 10-12 February, at Dallas, Texas.

Aarrestad, Thor V., and Åge Kyllingstad. 1988. An experimental and theoretical study of a coupling mechanism between longitudinal and torsional drillstring vibrations at the bit. *SPE Drilling Engineering* (March): 12-18.

Adelung, Denny, Warren Askew, Jaime Bernardini, A.T. (Buck) Campbell, Mike Chaffin, Guy Congras, Rodney Hensley, Bill Kirson, Randy Reese, and Don Sparling. 1991. Stuck pipe: techniques for breaking free. *Schlumberger Oilfield Review* 3, no. 4 (October) 27-35.

Adelung, Denny, Warren Askew, Jaime Bernardini, A.T. Campbell, Jr., Mike Chaffin, Rodney Hensley, Bill Kirton, Randy Reese, and Don Sparling. 1991. Jars, jarring and jar placement. *Schlumberger Oilfield Review* (October): 52-61.

Aldred, W.D., and M.C. Sheppard. 1992. Drillstring vibrations: a new generation mechanism and control strategies. SPE 24582 paper presented at 67th Annual Technical Conference and Exhibition of the SPE, 4-7 October, at Washington, D.C.

Allemang, R.J., and D.L. Brown. 1986. Multiple-input experimental modal analysis—a survey. *IJMA* (January): 37-44.

Anstey, N.A. 1982. *Simple seismics*. Boston, Massachusettes: International Human Resources Development Corporation.

Apostal, M.C., G.A. Haduch, and J.B. Williams. 1990. A study to determine the effect of damping on finite-element-based, forced-frequency-response models for bottomhole assembly vibration analysis. SPE 20458 paper presented at 65th Annual Technical Conference and Exhibition of the SPE, 23-26 September, at New Orleans, Louisiana.

Bailey, J.J., and I. Finnie. 1960. An analytical study of drill-string vibration. *Journal of Engineering for Industry,* Trans. ASME (May): 122-128.

Bailey, Louis, Tim Jones, Jim Belaskie, Jacques Orban, Mike Sheppard, Otto Houwen, Stuart Jardine, and Dominic McCann. 1991. Stuck pipe: causes, detection and prevention. *Schlumberger Oilfield Review* 3, no. 4 (October) 13-26.

Baker Hughes INTEQ. 1993. Vibration signature of roller cone and PDC bits. *Baker Hughes INTEQ Drilling Dynamics Technical Note* DDTN 9305-001 (May).

Barez, F., W. Goldsmith, and J.L. Sackman. 1980. Longitudinal wave propagation in axisymmetric structures with material and/or aereal discontinuity. *Experimental Mechanics* (October): 325-333.

Baruh, H., and J.B. Boka. 1993. Modeling and identification of boundary conditions in flexible structures. *Modal Analysis: the International Journal of Analytical and Experimental Modal Analysis* 8, no. 2 (April): 107-117.

Beer, Ferdinand P., and E. Russell Johnston, Jr. 1962. *Mechanics for engineers: statics*. 2d ed. New York, New York: McGraw-Hill, Inc.

Beer, Ferdinand P., and E. Russell Johnston, Jr. 1976. *Mechanics for engineers: dynamics*. 3rd ed. New York, New York: McGraw-Hill, Inc.

Behr, S[uzanne] M., T.M. Warren, L.A. Sinor, and J.F. Brett. 1991. Three-dimensional modeling of PDC bits. SPE/IADC paper 21928 presented at SPC/IADC Drilling Conference, 11-14 March, at Amsterdam, The Netherlands.

Bergeron, L. 1961. *Water hammer in hydraulics and wave surges in electricity.* Paris, France: Dunod. Authorized translation by The American Society of Mechanical Engineers.

Besaisow, A.A., and M.L. Payne. 1986. A study of excitation mechanisms and resonances inducing BHA vibrations. SPE 15560 paper presented at 61st Annual Technical Conference and Exhibition of the SPE, 5-8 October, at New Orleans, Louisiana.

Booer, A.K., and R.J. Meehan. 1993. Drillstring imaging—an interpretation of surface drilling vibrations. *SPE Drilling & Completion* (June): 93-98.

Boresi, Arthur P., and Omar M. Sidebottom. 1985. *Advanced mechanics of materials*. 4th ed. New York, New York: John Wiley & Sons.

Bradbury Jr., R.E., and J.C. Wilhoit, Jr. 1963. Effect of tool joints on passages of plane longitudinal and torsional waves along a drill pipe. *Journal of Engineering for Industry,* Trans. ASME. (May): 156-162. Originally paper 62 presented at the Petroleum Mechanical Engineering Conference, 23-26 September 1962, at Dallas, Texas.

Bradley, William, B. 1991. The human factor in the stuck pipe equation. *Schlumberger Oilfield Review* 3, no. 4 (October) 1.

Brett, [J.] Ford, Thomas M. Warren, and Suzanne M. Behr. 1990. Bit whirl—a new theory of PDC bit failure. *SPE Drilling Engineering* (December): 275-281.

Brett, J. Ford. 1992. The genesis of torsional drillstring vibrations. *SPE Drilling Engineering* (September): 168-174.

Brillouin, L. 1953. *Wave propagation in periodic structures; electric filters and crystal lattices*. 2d ed. New York, New York: Dover Publications, Inc.

Broch, Jens Trampe. 1984. *Mechanical vibration and shock measurements*. 2d ed. Nærum, Denmark: Brüel & Kjær.

Brüel & Kjær. 1982. *Measuring vibration*. Nærum, Denmark: Brüel & Kjær.

Chin, Wilson C. 1994. *Wave propagation in petroleum engineering*. Houston, Texas: Gulf Publishing Company.

Clayer, F., Elf Aquitaine, J.K. Vandiver, and H.Y. Lee. 1990. The effect of surface and downhole boundary conditions on the vibration of drillstrings. SPE 20447 paper presented at 65th Annual Technical Conference and Exhibition of the SPE, 23-26 September, at New Orleans, Louisiana.

Clegg, J.M. 1992. An analysis of the field performance of antiwhirl PDC bits. IADC/SPE paper 23868 presented at IADC/SPE Drilling Conference, 18-21 February, at New Orleans, Louisiana.

Cline, Marc, Gene Granger, Jean, Michel Hache, and Jack Lands. 1991. Stuck pipe: backoff basics. *Schlumberger Oilfield Review* 3, no. 4 (October): 48-51.

Cochin, Ira. 1980. Modeling of lumped elements. Chapter 2 in *Analysis and design of dynamic systems*. New York, New York: Harper & Row.

Conway, H.D., and M. Jakubowski. 1969. Axial impact of short cylindrical bars. *Journal of Applied Mechanics* (December): 809-813.

Cook, Robert D., David S. Malkus, and Michael E. Plesha. 1990. *Concepts and applications of finite element analysis*, 3rd ed. New York, New York: John Wiley & Sons.

Cooley, C.H., P.E. Pastusek, and L.A. Sinor. 1992. The design and testing of anti-whirl bits. SPE paper 24586 presented at 67th Annual Technical Conference and Exhibition of the SPE, 4-7 October, at Washington, DC.

Cornelius, C.S., and W.K. Kubitza. 1970. Experimental investigation of longitudinal wave propogation in an elastic rod with coulomb friction. *Experimental Mechanics* (April): 137-144.

Cunningham, R.A. 1968. Analysis of downhole measurements of drill string forces and motions. *Journal of Engineering for Industry,* Trans. ASME (May): 208-216.

Dailey Petroleum Services Corp. 1991. *Hydraulic drilling jar*. Conroe, Texas: Dailey Petroleum Services Corp.

Dailey Petroleum Services Corp. n.d. *Dailey fishing jar*. Conroe, Texas: Dailey Petroleum Services Corp.

Dale, B.A. 1988. An experimental investigation of fatigue-crack growth in drillstring tubulars. *SPE Drilling Engineering* (December): 356-362.

Dally, James W. 1989. Statistical analysis of experimental data. Chapter 2 of *Manual on experimental stress analysis*. 5th ed. Edited by James F. Doyle and James W. Phillips. Bethel, Connecticut: Society for Experimental Mechanics.

Dareing, Don W. 1984. Drill collar length is a major factor in vibration control. *JPT* (April): reprint. Originally SPE paper 11228 presented at 57th (1982) SPE Annual Technical Conference and Exhibition of the SPE, 26-29 September, at New Orleans, Louisiana.

Dareing, Don W. 1984. Vibrations increase power at bit. *Oil & Gas Journal* (March 5): 91-98.

DeGrande G., and G. De Roeck. 1992. A spectral element method for two-dimensional wave propagation in horizontally layered saturated porous

media. *Computers and Structures* 44, no. 4: 717-728.

Deily, F.H., D[on] W. Dareing, G.H. Paff, J.E. Ortloff, and R.D. Lynn. 1968. Downhole measurements of drill string forces and motions. *Journal of Engineering for Industry,* Trans. ASME (May): 217-225.

Den Hartog, J.P., 1961. *Mechanics*. New York, New York: Dover Publications, Inc.

Den Hartog, J.P., 1985, *Mechanical vibrations*. New York, New York: Dover Publications, Inc.

Donnell, L.H. 1930. Longitudinal wave transmission and impact. APM-52-14 paper presented at Semi-Annual Meeting of The ASME, 9-12 June, at Detroit, Michigan.

Doyle, J[ames] F., and S. Kamie. 1985. An experimental study of the reflection and transmission of flexural waves at discontinuities. *Journal of Applied Mechanics* 52 (September): 669-673.

Doyle, J[ames] F., and S. Kamie. 1987. An experimental study of the reflection and transmission of flexural waves at an arbitrary T-joint. *Transactions of the ASME* 54 (March): 136-140.

Doyle, J[ames] F., and T.N. Farris. 1990. A spectrally formulated finite element for flexural wave propogation in beams. *The International Journal of Analytical and Experimental Mode Analysis* 5, no. 2 (April): 99-107.

Doyle, J[ames]. F., and T.N. Farris. 1990. A spectrally formulated element for wave propagation in 3-D frame structures. *The International Journal of Analytical and Experimental Modal Analysis* 5, no. 4 (October): 223-237.

Doyle, James F. 1984. An experimental method for determining the dynamic contact law. *Experimental Mechanics* (March): 10-16.

Doyle, James F. 1984. Further developments in determining the dynamic contact law. *Experimental Mechanics* (December): 265-270.

Doyle, James F. 1986. Application of the fast-fourier transform (FFT) to wave-propagation problems. *IJMA* (October): 18-25.

Doyle, James F. 1987. An experimental method for determining the location and time of initiation of an unknown dispersing pulse. *Experimental Mechanics* (September): 229-233.

Doyle, James F. 1988. A spectrally formulated finite element for longitudinal wave propagation. *The International Journal of Analytical and Experimental Modal Analysis* 3, no. 1 (January): 1-5.

Doyle, James F. 1993. Force identification from dynamic responses of a bimaterial beam. *Experimental Mechanics* (March): 64-69.

Dubinsky, V[ladimir] S.H., H[enry] P. Henneuse, Elf Aquitaine, and M[atthew] A. Kirkman. 1982. Surface monitoring of downhole vibrations: Russian, European, and American approaches. SPE 24969 paper presented at European Petroleum Conference, 16-18 November, at Cannes, France.

Dunayevsky, V.A., A[rnis] Judzis, and W.H. Mills. 1984. Onset of drillstring precession in a directional borehole. SPE 13027 paper presented at 59th Annual Technical Conference and Exhibition of the SPE, 16-19 September, at Houston, Texas.

Dunayevsky, V.A., A[rnis] Judzis, W.H. Mills, and G. Griffin. 1985. Dynamic stability of drillstrings under fluctuating weights-on-bit. SPE 14329 paper

presented at 60th Annual Technical Conference and Exhbition of the SPE, 22-25 September, at Las Vegas, Nevada.

Dunayevsky, V.A., Fereldoun Abbassian, and Arnis Judzis. 1993. Dynamic stability of drillstrings under fluctuating weight on bit. *SPE Drilling & Completion* (June): 84-92.

Dutta, P.K. 1968. The determination of stress waveforms produced by percussive drill pistons of various geometrical designs. *Rock Mech. Min. Sci*. 5: 501-518.

Elmore, William C. and Mark A. Heald. 1985. *Physics of waves*. New York, New York: Dover Publications, Inc.

Erickson, J.L. 1965. On the propagation of waves in isotropic incompressible perfectly elastic materials. Reprint. In Vol. 8, Part 3 of *International Science Review Series*. New York, New York: Gordon and Breach Science Publishers, Inc. Originally published in *Journal of Rational Mechanics and Analysis* 2, no. 2 (April 1953).

Evans, R.W., and T.R. Beasley. 1990. *Improved drilling jar combines hydraulic time delay with mechanical triggering*. Paper presented at Offshore and Arctic Operations Symposium, Book No. G00510, vol. 29. Reprinted by American SPE.

Exlog, Inc. (a Baker Hughes Company). 1991. Drilling Dynamics. *Exlog, Inc. Marketing Bulletin Number 1.*

Exlog, Inc. (a Baker Hughes Company). 1992. DynaByte[SM]. *Exlog, Inc. Marketing Bulletin Number 2.*

Farris, T.N., and J[ames] F. Doyle. 1989. Wave propagation in a split timoshenko beam. *Journal of Sound and Vibration* 130, no. 1: 137-147.

Fay, Hubert. 1993. Practical evaluation of rock-bit wear during drilling. *SPE Drilling & Completion* (June): 99-104.

Fertis, Demeter G. 1993. *Nonlinear mechanics*. Boca Raton, Florida: CRC Press, Inc.

Finnie, I., and J.J. Bailey. 1960. An experimental study of drill-string vibration. *Journal of Engineering for Industry,* Trans. ASME (May): 129-135.

Fontenot, E.P. 1986. Drilling a 26-in. diameter hole to 12,550 ft: a case history. SPE paper 15365 presented at 61st Annual Technical Conference and Exhibition of the SPE, 5-8 October, at New Orleans, Louisiana.

Fox, Chris, ed. 1991. Stuck pipe: oil company perspectives: *Schlumberger Oilfied Review* 3, no. 4 (October) 36-47. Excerpted from a roundtable at Offshore Technology Conference, 7 May, at Houston, Texas.

French, A. n.d. Horizontal coring using air as the circulating fluid: some prototype studies conducted in G tunnel at the Nevada Test Site for the Yucca Mountain Project. Las Vegas, Nevada: Reynolds Electrical and Engineering Company.

Gade, S[vend], N. Thrane, H. Konstantin-Hansen, and J. Wismer. n.d. Time windows. *Brüel & Kjær Application Note BO 0436-11*.

Gade, Svend, and Henrik Herlufsen. 1994. Digital filter tehniques vs. FFT techniques for damping measurements. *Brüel & Kjær Technical Review No. 1*: 1-35.

Gade, Svend, and Henrik Herlufsen. 1994. The use of impulse response function for modal parameter estimation. *Brüel & Kjær Technical Review No. 2*: 1-44.

Gatzwiller, Kevin, and Henrik Herlufsen. n.d. Mobility measurements. *. Brüel & Kjær Application Notes BO 0419-11*.

Gaught, T.M., and B.J. Dobson. 1986. The transient analysis of a structure using a modal model. *IJMA* (January): 11-17.

Gopalakrishnan, S., and J[ames] F. Doyle. 1995. Spectral super-elements for wave propagation in structures with local non-uniformities*. Computer Methods in Applied Mechanics and Engineering* 121: 77-90.

Gopalakrishnan, S., M. Martin, and J[ames] F. Doyle. 1992. A matrix methodology for spectral analysis of wave propagation in multiple connected timoshenko beams. *Journal of Sound and Vibration* 188, no. 1: 11-24.

Graff, Karl F. 1975. *Wave motion in elastic solids*. New York, New York: Dover Publications, Inc. Originally published: London, United Kingdom: Oxford University Press.

Gupta, R.B. 1979. Propagation of elastic waves in rods with variable cross section. *Journal of Applied Mechanics* 46 (December): 951.

Halsey, G.W., Å[ge] Kyllingstad, T[hor] V. Aarrestad, and D. Lysne. 1986. Drillstring torsional vibrations: comparison between theory and experiment on a full-scale research drilling rig. SPE 15564 paper presented at 61st Annual Technical Conference and Exhibition of the SPE, 5-8 October, at New Orleans, Louisiana.

Henneuse, Henry. 1992. Surface detection of vibrations and drilling optimization: field experience. IADC/SPE 23888 paper presented at 1992 IADC/SPE Drilling Conference, 18-21 February, at New Orleans, Louisiana.

Holden, Arun V. 1986. *Chaos*. Princeton, New Jersey: Princeton University Press.

Hood, James, Edward Robnett, Michael Taylor, and Ercill Hunt. 1992. Lithology and formation fracture identification from measurement of drillstring vibration. Paper presented at the AAPG International Conference and Exhibition, 2-5 August, at Sydney, Australia.

Huang, F., and S. Gu. 1993. A new approach for frequency response function estimation by bispectrum. *Modal Analysis: the International Journal of Analytical and Experimental Modal Analysis* 8, no. 4 (October): 301-312.

Huang, Tseng, and D[on] W. Dareing. 1968. Buckling and lateral vibration of drill pipe. *Journal of Engineering for Industry,* Trans. ASME (November): 613-619.

Jacobsen, Lydik S., and Robert S. Ayre. 1958. Vibratory systems influenced by friction. In *Engineering Vibrations with Applications to Structures and Machinery*. New York: McGraw-Hill.

Jansen, J[an] D. 1992. Whirl and chaotic motion of stabilized drill collars. *SPE Drilling Engineering* (June): 107-114.

Jones, Alfred T. 1970. Vibration of beams immersed in a liquid. *Experimental Mechanics* (February): 84-88.

Jordan, R.W., and G.S. Whitson. 1984. Remote impact analysis by use of propagated acceleration signals, II: comparison between theory and

experiment. *Journal of Sound and Vibration* 97, no. 1: 53-63.

Journal of Sound and Vibration. 1981. Letter to the Editor, 75, no. 3: 453-457. The determination of propagation path lengths of dispersive flexural waves through structures.

Karl, John H. 1989. *An introduction to digital signal processing*. San Diego, California: Academic Press, Inc.

Kaul, R.K., and J.J. McCoy. 1964. Propagation of axisymmetric waves in a circular semiinfinite elastic rod. *The Journal of the Acoustical Society of America* 36, no. 4 (April): 653-660.

Kawata, K., and S. Hashimoto. 1967. On some differences between dynamic- and static-stress distributions. *Experimental Mechanics*, (February): 91-96.

Kennedy, L.W., and O. E. Jones. 1969. Longitudinal wave propogation in a circular bar loaded suddenly by a radially distributed end stress. *Journal of Applied Mechanics*, (September): 470-479.

Kenner, Vernal H. 1982. Discussion: Elastic-pulse propagation in thin hollow cones. *Experimental Mechanics* (May): 192-193.

Kraniauskas, Peter. 1992. *Transforms in signals and systems*. Workingham, England: Addison-Wesley Publishing Company.

Kreisle, Leonardt F., and John M. Vance. 1970. Mathematical analysis of the effect of a shock sub on the longitudinal vibrations of an oilwell drill string. SPE Journal (December): 349-356).

Lai, Michael W., David Rubin, and Erhard Krempl. 1978. *Continuum mechanics*. Elmsford, New York: Pergamon Press Inc.

Langeveld, C.J. 1992. PDC bit dynamics. IADC/SPE paper 23867 presented at IADC/SPE Drilling Conference, 18-21 February, at New Orleans, Louisiana.

Lifschitz, J.M., and G. Mor. 1982. Elastic-pulse propagation in thin hollow cones. *Experimental Mechanics* (May): 166-170.

Love, A.E.H. 1944. *A treatise on the mathematical theory of elasticity*. 4th ed. New York, New York: Dover Publications. Originally published in 1927: London, United Kingdom: Cambridge University Press.

Lubinski, Arthur. 1988. Dynamic loading of drillpipe during tripping. *JPT* (August): Originally SPE paper 17211 presented at 1988 IADC/SPE Drilling Conference, 28 February - 2 March, at Dallas, Texas.

Mace, B.R. 1984. Wave reflection and transmission in beams. *Journal of Sound and Vibration* 97, no. 2: 237-246.

Mal, Ajit K., and Jit Sarva Singh. 1991. *Deformation of elastic solids.* Englewood Cliffs, New Jersey: Prentice-Hall Inc.

Martin, George H. 1969. *Kinematics and dynamics of machines*. New York, New York: McGraw-Hill, Inc.

Martin, M., S. Gopalakrishnan, and J[ames] F. Doyle. 1994. Wave propagation in multiply connected deep waveguides. *Journal of Sound and Vibration* 174, no. 4: 521-538.

McQuillin, R., M. Bacon, M., and W. Barclay. 1984. *An introduction to seismic interpretation: reflection seismics in petroleum exploration*. Houston, Texas: Gulf Publishing Company.

Mead, D.J. 1986. A new method of analyzing wave propagation in periodic structures; application to periodic timoshenko beams and stiffened plates. *Journal of Sound and Vibration* 104, no. 1: 9-27.

Meirovitch, Leonard. 1986. *Elements of Vibration Analysis*. 2d ed. New York, New York: McGraw-Hill Book Company.

Miklowitz, Julius. n.d. Traveling compressional waves in an elastic rod according to the more exact one-dimensional theory. Paper presented to Office of Naval Research.

Mindlin, R.D., and G. Herrmann. 1952. A one-dimensional theory of compressional waves in an elastic rod. *Transactions of the American Society of Mechanical Engineers* (June) 187-191. Paper originally presented in 1951 to the Office of Naval Research.

Mitchell, Bill J., Alfred W. Eustes III, Mark G. Miller and Michael S. Stoner. 1993. *Vibratory core rod simulator*, version 2.2. Manual produced for Yucca Mountain Project and presented to Science Applications International Corporation, Las Vegas, Nevada.

Mitchell, Bill J., Alfred W. Eustes III, Mark G. Miller and Michael S. Stoner. 1993. *ResonantSonic Drilling Simulator*^{SM}*,* version 1.0. Manual produced for Westinghouse Hanford, Richmond, Washington.

Mitchell, Larry D. 1986. Signal processing and the fast-fourier-transform (FFT) analyzer—a survey. *IJMA* (January): 24-36.

Moon, Francis C. 1987. *Chaotic vibrations: an introduction for applied scientists and engineers*. New York, New York: John Wiley & Sons, Inc.

Mortimer, R.W., J.L. Rose, and P.C. Chou. 1972. Longitudinal impact of cylindrical shells. *Experimental Mechanics* (January): 25-31.

Naganawa, Shigemi, Shoichi Tanaka and Naoki Sugaya. 1995. Experimental and theoretical analysis of roller cone bit vibrations. Paper presented at ASME/ETCE Energy & Environmental Expo 94, Drilling Symposium, 29 January - 1 February, at Houston, Texas.

Olsen, Gerner A. 1974. *Elements of mechanics of materials*. 3rd ed. Englewood Cliffs, New Jersey: Prentice-Hall, Inc.

Oppenheim, Alan V., and Alan S. Willsky. 1983. *Signals and systems*. Englewood Cliffs, New Jersey: Prentice-Hall, Inc.

Paslay, P[aul] R., Yih-Min Jan, J[ohn] E.E. Kingman, and J[ohn] D. Macpherson. 1992. Detection of BHA lateral resonances while drilling with surface longitudinal and torsional sensors. SPE 24583 paper presented at 67th Annual Technical Conference and Exhibition of the SPE, 4-7 October, at Washington, D.C.

Pastusek, P.E., C.H. Cooley, L.A. Sinor, and Mark Anderson. 1992. Directional and stability characteristics of anti-whirl bits with non-axisymmetric loading. SPE Paper 24614 presented at 67th Annual Technical Conference and Exhibition of the SPE, 4-7 October, at Washington, D.C.

Pestel, Eduard C., and Frederick A. Leckie. 1963. *Matrix methods in elasto mechanics*. New York, New York: McGraw-Hill Book Company.

Plunkett, Robert. 1992. Damping analysis: an historical perspective. In *M³D: Mechanics and Mechanisms of Material Damping, ASTM STP 1169*. Philadelphia: American Society for Testing and Materials.

Rader, D., and M. Mao. 1972. Amplification of longitudinal stress pulses in elastic bars with an intermediate tapered region. *Experimental Mechanics* (February): 90-94.

Ramirez, Robert W. 1985. *The FFT: fundamentals and concepts*. Englewood Cliffs, New Jersey: Prentice-Hall, Inc.

Randall, R.B., and B.Tech. 1987. *Frequency analysis*. 3rd ed. Nærum, Denmark: Brüel & Kjær.

Rappold, Keith. 1993. Drilling optimized with surface measurement of downhole vibrations. *Oil & Gas Journal* (February 15): 58-62.

Rappold, Keith. 1993. Drillstring vibration measurements detect bit stick-slip. *Oil & Gas Journal* (March 1): 66-70.

Ripperger, E.A., and L.M. Yeakley. 1963. Measurement of particle velocities associated with waves propagating in bars. *Experimental Mechanics*, (February): 47-56.

Rizzi, S.A., and J[ames] F. Doyle. 1992. A spectral element approach to wave motion in layered solids. *Journal of Vibration and Accoustics* 114 (October): 569-577.

Rizzi, S.A., and J[ames] F. Doyle. 1992. Spectral analysis of wave motion in plane solids with boundaries. *Journal of Vibration and Accoustics* 114 (April): 133-140.

Rizzo, Anthony R. 1991. FEA gap elements: choosing the right stiffness. *Mechanical Engineering* (June): 57-59.

Rose, J.L., R.W. Mortimer, and A. Blum. 1973. Elastic-wave propagation in a joined cylindrical-conical-cylindrical shell. *Experimental Mechanics* (April): 150-156.

Rowley, John. 1991. Recent polycrystalline diamond cutter developments . . . potential for geothermal drilling? *Geothermal Resources Council Bulletin*, 20, no. 8: 221-227.

Roy, A.K., and R. Plunkett. 1985. Dispersive bending waves in uniform bars. *Experimental Mechanics* (September): 308-311.

Salvini, P., and Sestieri, A. 1993. Predicting the frequency response function of a structure when adding constraints. *Modal Analysis: the International Journal of Analytical and Experimental Modal Analysis* 8, no. 1 (January): 55-62.

Schwieger, Horst. 1970. Central deflection of a transversely stuck beam. *Experimental Mechanics* (April): 166-169.

Scipio, L[ouis] Albert. 1967. *Principles of continua with applications*. New York, New York: John Wiley & Sons, Inc.

Seto, William W. 1964. *Schaum's outline series: theory and problems of mechanical vibrations*. New York, New York: McGraw-Hill Book Company.

Shabana, A.A. 1991. *Theory of vibration*. 2 vols. New York, New York: Springer-Verlag.

Sheppard, M.C., C. Wick, and T. Burgess. 1986. Designing well paths to reduce drag and torque. Paper presented at 61st Annual Technical Conference and Exhibition of the SPE, 5-8 October, at New Orleans, Louisiana.

Shigley, Joseph E. 1977. *Mechanical engineering design*. 3rd ed. New York, New York: McGraw-Hill, Inc.

Sinor, L.A., S[uzanne] M. Behr, and M.R. Wells. 1992. Development of an anti-whirl core bit. SPE 24587 paper presented at 67th Annual Technical Conference and Exhibition of the SPE, 4-7 October, at Washington, DC.

Skaugen, E. and Å[ge] Kyllingstad. 1986. Performance testing of shock absorbers. SPE 15561 paper presented at 61st Annual Technical Conference and Exhibition of the SPE, 5-8 October, at New Orleans, Louisiana.

Skudrzyk, Eugene. 1968. *Simple and complex vibratory systems*. University Park, Pennsylvania: The Pennsylvania State University Press.

Snowdon, J.C. 1968. Longitudinal vibration of internally damped rods. Chapter 6 in *Vibration and shock in damped mechanical systems*. New York, New York: John Wiley & Sons, Inc.

Snyder, Virgil W. 1986. Structural modification and modal analysis—a survey. *IJMA* (January): 45-52.

Sperry-Sun Drilling Services, Inc. 1994. *The sledgehammer™ HMD hydromechanical drilling jar*. Houston, Texas: Sperry-Sun Drilling Services, Inc.

Strang, Gilbert. 1986. *Introduction to applied mathematics*. Wellesley, Massachusetts: Wellesley-Cambridge Press.

Thompson, William T. 1965. *Vibration theory and applications*. Englewood Cliffs, New Jersey: Prentice-Hall, Inc.

Thompson, William T. 1968. *Theory of vibration with applications*. 3rd ed. Englewood Cliffs, New Jersey: Prentice-Hall, Inc.

Vandiver, J. Kim, James W. Nicholson, and Rong-Juin Shyu. 1990. Case studies of the bending vibration and whirling motion of drill collars. *SPE Drilling Engineering* (December): 282-290.

Velichkovich, S.V. 1989. Calculation for the elastic element of the vibration damper of drilling columns. *Chemical and Petroleum Engineering* 25, nos. 3-4 (March-April): 111-115.

Walter, Patrick L. 1981. Deconvolution as a technique to improve measurement-system data integrity. *Experimental Mechanics* (August): 309-314.

White, R.M. 1958. Elastic wave scattering at a cylindrical discontinuity in a solid. *The Journal of the Acoustical Society of America* 30, no. 8 (August): 771-785.

Whitson, G.S. 1984. Remote impact analysis by use of propagated acceleration signals, I: theoretical methods. *Journal of Sound and Vibration* 97, no. 1: 35-51.

Williams, F. W., and D. Kennedy. 1994. Letters to the editor: A general method for analyzing wave propagation along longitudinally periodic structures. *Journal of Sound and Vibration* 177, no. 2: 277-281.

Wismer, N. Johan. n.d. Time domain averaging combined with order tracking. *Brüel & Kjær Application Note BO 0420-11*.

Wohlever, J.C., and R.J. Bernhard. 1992. Mechanical energy flow models of rods and beams. *Journal of Sound and Vibration* 153, no. 1: 1-19.

Wu, Jiang, and Hans C. Juvkam-Wold. 1990. Discussion of tubing and casing buckling in horizontal wells. *JPT* (August): 1062-1063.

Yang, J.C.S., and R.J. Hassett. 1972. Transient stresses in axisymmetric bodies of varying area. *Experimental Mechanics* (July): 304-309.

APPENDIX A

MATHCAD EXAMPLE

This is an example of jar analysis using spectral analysis: Pre-Stretch Phase

Outside diameter

$$OD = \begin{bmatrix} 4.5 \\ 4.5 \\ 7.25 \\ 7.25 \\ 7.25 \\ 7.25 \\ 7.25 \\ 7.25 \end{bmatrix} \cdot in$$

Inside diameter

$$ID := \begin{bmatrix} 3.73 \\ 2.75 \\ 2.812 \\ 2.812 \\ 2.812 \\ 2.812 \\ 2.812 \\ 7.24 \end{bmatrix} \cdot in$$

Length

$$L := \begin{bmatrix} 10000 \\ 300 \\ 90 \\ 10 \\ 180 \\ 150 \\ 450 \\ 10 \end{bmatrix} \cdot ft$$

Modulus of elasticity

$$E = \begin{bmatrix} 30 \\ 30 \\ 30 \\ 30 \\ 30 \\ 30 \\ 30 \\ 30 \end{bmatrix} \cdot 10^6 \cdot psi$$

Density

$$\rho = \begin{bmatrix} 490 \\ 490 \\ 490 \\ 490 \\ 490 \\ 490 \\ 490 \\ 490 \end{bmatrix} \cdot \frac{lb}{ft^3}$$

Damping coefficient

$$\gamma = \begin{bmatrix} 100 \\ 100 \\ 100 \\ 100 \\ 100 \\ 100 \\ 5000 \\ 0 \end{bmatrix} \cdot \frac{lb}{ft \cdot sec}$$

$F_{trigger} := 165000 \cdot lbf$ $MW_o := 12.0 \cdot ppg$ $MW_i := MW_o$ $K_A := 13300 \cdot \frac{lbf}{in}$

Calculated values:

Outside Area

$$A_o := \overrightarrow{\left(\frac{\pi}{4} \cdot OD^2\right)}$$

$$A_o = \begin{bmatrix} 15.904 \\ 15.904 \\ 41.282 \\ 41.282 \\ 41.282 \\ 41.282 \\ 41.282 \\ 41.282 \end{bmatrix} \cdot in^2$$

Inside Area

$$A_i := \overrightarrow{\left(\frac{\pi}{4} \cdot ID^2\right)}$$

$$A_i = \begin{bmatrix} 10.927 \\ 5.94 \\ 6.21 \\ 6.21 \\ 6.21 \\ 6.21 \\ 6.21 \\ 41.169 \end{bmatrix} \cdot in^2$$

Cross-sectional area:

$$A := \overrightarrow{\left[\frac{\pi}{4} \cdot \left(OD^2 - ID^2\right)\right]}$$

$$A = \begin{bmatrix} 4.977 \\ 9.965 \\ 35.072 \\ 35.072 \\ 35.072 \\ 35.072 \\ 35.072 \\ 0.114 \end{bmatrix} \cdot in^2$$

Weight per Length:

$$W := \overrightarrow{(\rho \cdot A \cdot g)}$$

$$W = \begin{bmatrix} 16.936124 \\ 33.907793 \\ 119.342486 \\ 119.342486 \\ 119.342486 \\ 119.342486 \\ 119.342486 \\ 0.38725 \end{bmatrix} \cdot \frac{lbf}{ft}$$

The first step is to do the static stretch calculations:

Outside mud pressures

$$P_{o_q} := \left(A_{o_q} - A_{o_{q-1}}\right) \cdot l_q \cdot MW_o$$

$$P_o = \begin{bmatrix} 0 \\ 0 \\ 164371.491 \\ 0 \\ 0 \\ 0 \\ 0 \end{bmatrix} \cdot lbf$$

Inside mud pressures

$$P_{i_q} := \left(A_{i_{q-1}} - A_{i_q}\right) \cdot l_q \cdot MW_i$$

$$P_i = \begin{bmatrix} 0 \\ 32024.23 \\ -1754.198 \\ 0 \\ 0 \\ 0 \\ 0 \end{bmatrix} \cdot lbf$$

Forces at various points in the drill string:

$F_{6T} := F_{trigger} - W_5 \cdot L_5$ $F_{6T} = 147099 \cdot lbf$

$F_{5B} := F_{6T} + P_{o_6} + P_{i_6}$ $F_{5B} = 147099 \cdot lbf$

$F_{5T} := F_{trigger}$ $F_{5T} = 165000 \cdot lbf$

$F_{4B} := F_{5T} + P_{o_5} + P_{i_5}$ $F_{4B} = 165000 \cdot lbf$

$F_{4T} := F_{4B} + W_4 \cdot L_4$ $F_{4T} = 186482 \cdot lbf$

$F_{3B} := F_{4T} + P_{o_4} + P_{i_4}$ $F_{3B} = 186482 \cdot lbf$

$F_{3T} := F_{3B} + W_3 \cdot L_3$ $F_{3T} = 187675 \cdot lbf$

$F_{2B} := F_{3T} + P_{o_3} + P_{i_3}$ $F_{2B} = 187675 \cdot lbf$

$F_{2T} := F_{2B} + W_2 \cdot L_2$ $F_{2T} = 198416 \cdot lbf$

$F_{1B} := F_{2T} + P_{o_2} + P_{i_2}$ $F_{1B} = 361033 \cdot lbf$

$F_{1T} := F_{1B} + W_1 \cdot L_1$ $F_{1T} = 371206 \cdot lbf$

$F_{0B} := F_{1T} + P_{o_1} + P_{i_1}$ $F_{0B} = 403230 \cdot lbf$

$F_{0T} := F_{0B} + W_0 \cdot L_0$ $F_{0T} = 572591 \cdot lbf$

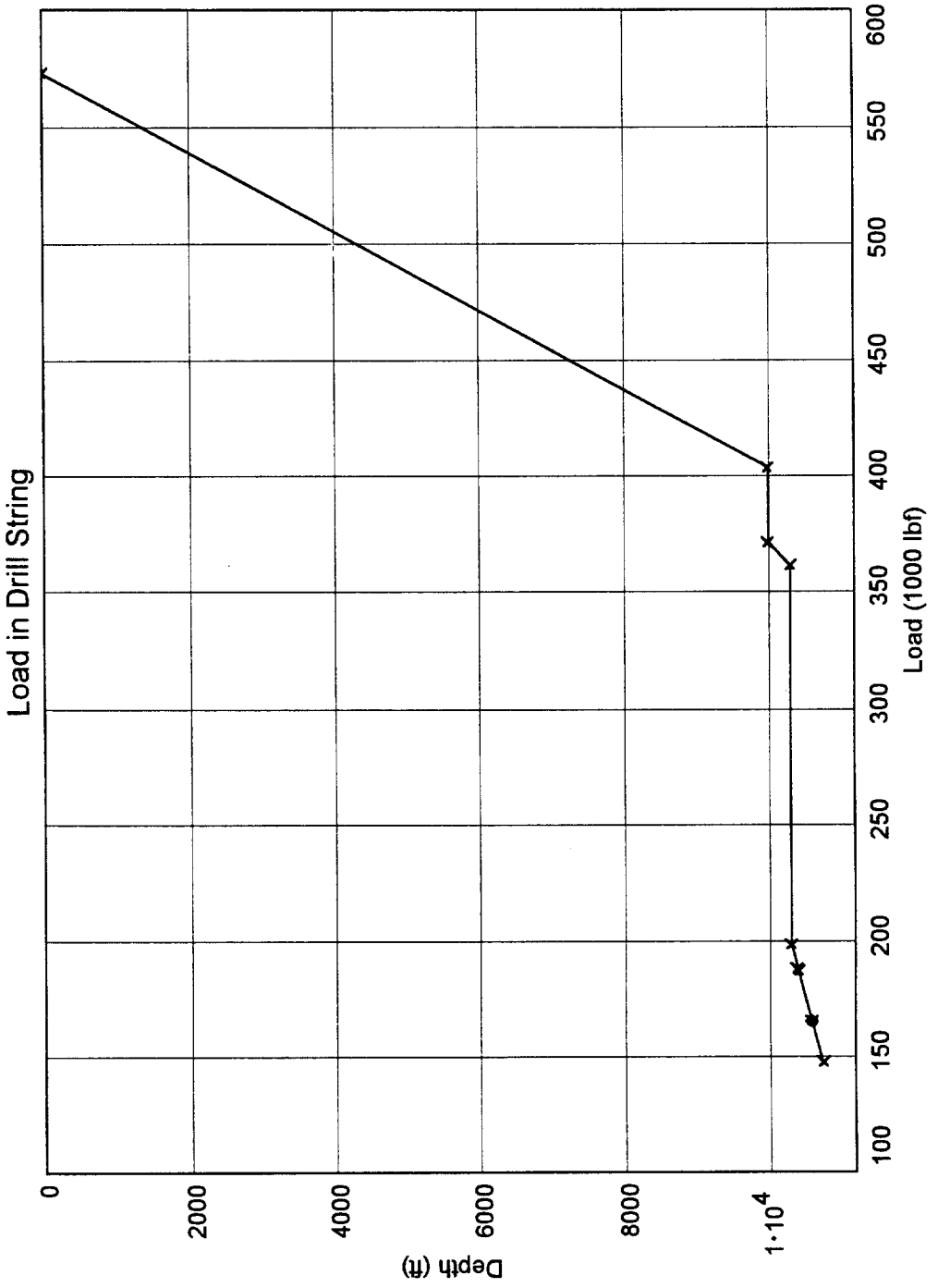
Load in Drill String
Load (1000 lbf)
100
150
200
250
300
350
400
450
500
550
600
Depth (ft)
0
2000
4000
6000
8000
1·10^4

This is an example of jar analysis using spectral analysis: INPUT DATA:

Outside diameter

$$OD := \begin{bmatrix} 4.5 \\ 4.5 \\ 7.25 \\ 7.25 \\ 7.25 \\ 7.25 \\ 7.25 \\ 7.25 \end{bmatrix} \cdot in$$

Inside diameter

$$ID := \begin{bmatrix} 3.73 \\ 2.75 \\ 2.812 \\ 2.812 \\ 2.812 \\ 2.812 \\ 2.812 \\ 7.24 \end{bmatrix} \cdot in$$

Length

$$L := \begin{bmatrix} 10000 \\ 300 \\ 90 \\ 10 \\ 180 \\ 150 \\ 450 \\ 10 \end{bmatrix} \cdot ft$$

Modulus of elasticity

$$E := \begin{bmatrix} 30 \\ 30 \\ 30 \\ 30 \\ 30 \\ 30 \\ 30 \\ 30 \end{bmatrix} \cdot 10^6 \cdot psi$$

Density

$$\rho := \begin{bmatrix} 490 \\ 490 \\ 490 \\ 490 \\ 490 \\ 490 \\ 490 \\ 490 \end{bmatrix} \cdot \frac{lb}{ft^3}$$

Damping coefficient

$$\gamma := \begin{bmatrix} 100 \\ 100 \\ 100 \\ 100 \\ 100 \\ 100 \\ 5000 \\ 0 \end{bmatrix} \cdot \frac{lb}{ft \cdot sec}$$

Calculated values:

Cross-sectional area:

$$A := \overrightarrow{\left[\frac{\pi}{4}\cdot\left(OD^2 - ID^2\right)\right]}$$

$$A = \begin{bmatrix} 4.977 \\ 9.965 \\ 35.072 \\ 35.072 \\ 35.072 \\ 35.072 \\ 35.072 \\ 0.114 \end{bmatrix} \cdot in^2$$

Wave propagation speed:

$$c := \overrightarrow{\sqrt{\frac{E}{\rho}}}$$

$$c = \begin{bmatrix} 16842 \\ 16842 \\ 16842 \\ 16842 \\ 16842 \\ 16842 \\ 16842 \\ 16842 \end{bmatrix} \cdot \frac{ft}{sec}$$

Accelerator_used := 1

0 means no
1 means yes

$$K_{Accelerator} := 13300 \cdot \frac{lbf}{in}$$

STROKE := 6.5·in

$$Force_{Trigger} := 165000 \cdot lbf$$

THE FREE CONTRACTION PHASE

Number of samples

N := 14 $2^N = 16384$

Time steps:

Time steps between samples

$\Delta T := 1 \cdot 10^{-3} \cdot sec$

$time\_fc_n := n \cdot \Delta T$

$n := 0 .. 2^N - 1$

$max(time\_fc) = 16.383 \cdot sec$

Sampling frequency: $f_s := \frac{1}{\Delta T}$ $f_s = 1000 \cdot Hz$

The wave will be a square wave. The properties of the wave are:

Start := 10·msec Duration := 200·msec

End := Start + Duration End = 210·msec

The free contraction wave is determined:

$$Timewave\_fc_n := Force_{Trigger} \cdot (Start \le time\_fc_n) \cdot (End \ge time\_fc_n)$$

A plot of the time domain free contraction wave shows:

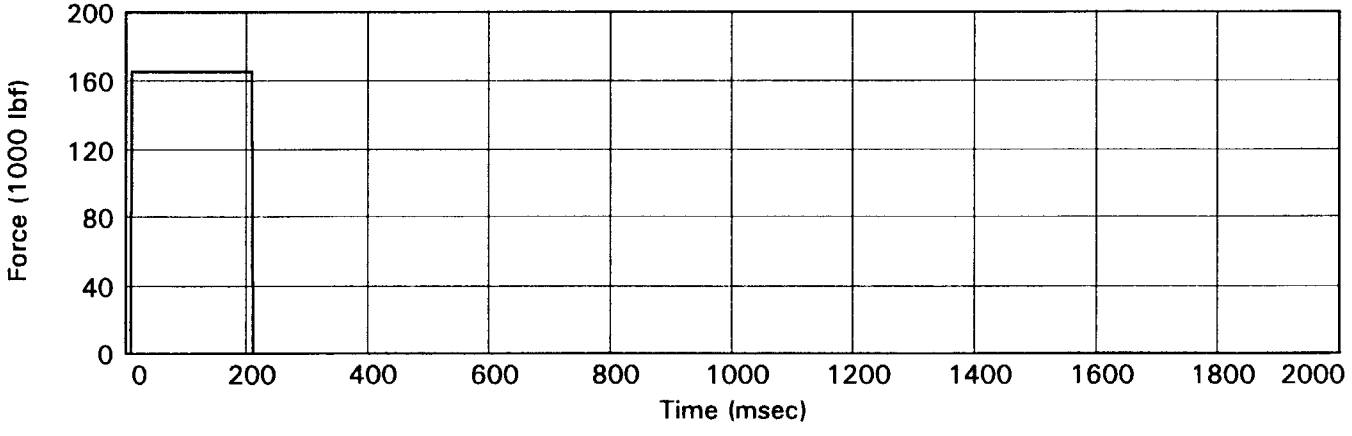

The wave is transformed from the time domain to the frequency domain:

$$\text{Freqwave} := \text{FFT}(\text{Timewave\_fc})$$

The frequencies are determined:

$$m := 0 .. 2^{N-1} \qquad \text{frequency}_m := \frac{m}{2^N} \cdot f_s \qquad \omega_m := 2 \cdot \pi \cdot \text{frequency}_m$$

A plot of the magnitude of the frequency domain free contraction wave shows:

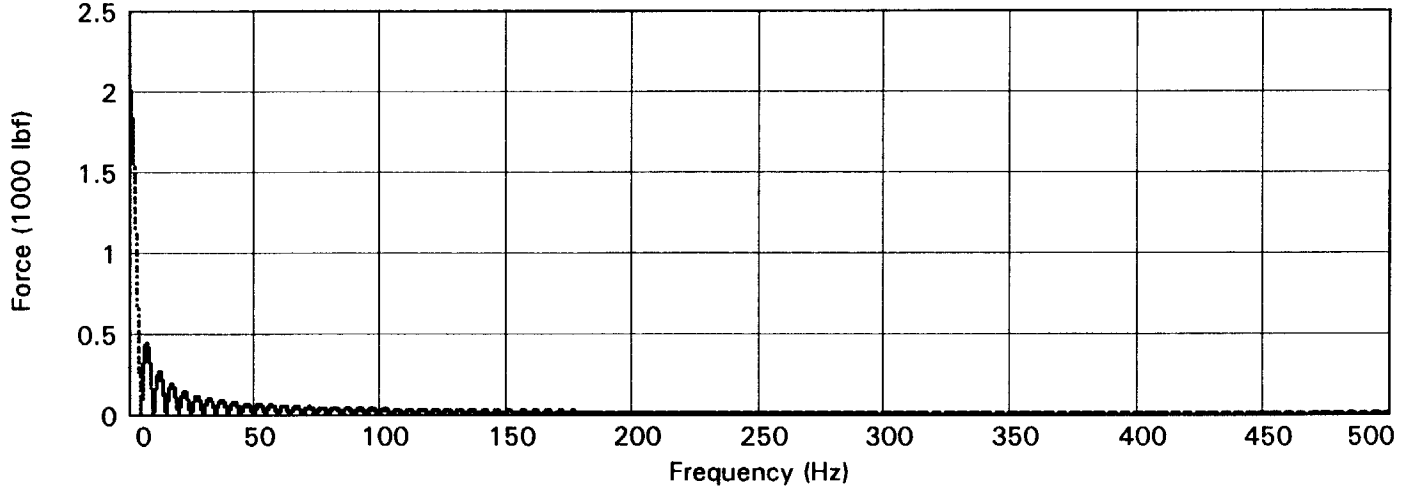

The spectral analysis starts with the determination of the wave number for each element:

$$k_{m,j} := \sqrt{\frac{(\omega_m)^2}{(c_j)^2} - \frac{i \cdot \omega_m \cdot \gamma_j}{A_j \cdot E_j}}$$

The element values are determined:

Convienent group of constants:

$$C_{m,j} := \frac{i \cdot k_{m,j} \cdot A_j \cdot E_j}{1 - e^{-2 \cdot i \cdot k_{m,j} \cdot L_j}}$$

On diagonal values:

$$D_{m,j} := C_{m,j} \cdot \left(1 + e^{-2 \cdot i \cdot k_{m,j} \cdot L_j}\right)$$

Off diagonal values:

$$OFD_{m,j} := C_{m,j} \cdot \left(-2 \cdot e^{-i \cdot k_{m,j} \cdot L_j}\right)$$

The hammer spectral finite element model is determined.

$$UH(m) := \begin{bmatrix} D_{m,0} + D_{m,1} & OFD_{m,1} & Z & Z & Z \\ OFD_{m,1} & D_{m,1} + D_{m,2} & OFD_{m,2} & Z & Z \\ Z & OFD_{m,2} & D_{m,2} + D_{m,3} & OFD_{m,3} & Z \\ Z & Z & OFD_{m,3} & D_{m,3} + D_{m,4} & OFD_{m,4} \\ Z & Z & Z & OFD_{m,4} & D_{m,4} \end{bmatrix}^{-1} \cdot \begin{bmatrix} 0 \cdot lbf \\ 0 \cdot lbf \\ 0 \cdot lbf \\ 0 \cdot lbf \\ Freqwave_m \end{bmatrix}$$

The anvil spectral finite element model is determined.

$$UA(m) := \begin{pmatrix} D_{m,5} & OFD_{m,5} & Z \\ OFD_{m,5} & D_{m,5} + D_{m,6} & OFD_{m,6} \\ Z & OFD_{m,6} & D_{m,6} + D_{m,7} \end{pmatrix}^{-1} \cdot \begin{pmatrix} -Freqwave_m \\ 0 \cdot lbf \\ 0 \cdot lbf \end{pmatrix}$$

The hammer spectral displacements are determined:

$uhfc_{m,1} := UH(m)_0$ $\quad uhfc_{m,2} := UH(m)_1$ $\quad uhfc_{m,3} := UH(m)_2$

$uhfc_{m,4} := UH(m)_3$ $\quad uhfc_{m,5} := UH(m)_4$

The anvil spectral displacements are determined:

$uafc_{m,5} := UA(m)_0$ $\quad uafc_{m,6} := UA(m)_1$ $\quad uafc_{m,7} := UA(m)_2$

$uafc_{m,8} := (0 + i \cdot 0) \cdot in$

The hammer zero frequency displacement are added in:

$$uhfc_{0,q} := -\sum_{s=0}^{q} \frac{Freqwave_0 \cdot L_s}{A_s \cdot E_s} \qquad uhfc_{0,0} := (0 + i \cdot 0) \cdot in$$

The anvil zero frequency displacement are added in:

$$uafc_{0,8} := (0 + i \cdot 0)\cdot in \qquad uafc_{0,w} := \sum_{W=7}^{w} \frac{Freqwave_0 \cdot L_W}{A_W \cdot E_W}$$

The hammer spectral forces are determined:

$$FHfc(x,m,q) := \frac{-i \cdot E_q \cdot A_q \cdot k_{m,q}}{e^{i \cdot k_{m,q} \cdot L_q} - e^{-i \cdot k_{m,q} \cdot L_q}} \cdot \left[-\left[\begin{matrix} e^{i \cdot k_{m,q} \cdot (L_q - x)} \\ + e^{-i \cdot k_{m,q} \cdot (L_q - x)} \end{matrix} \dots \right] \cdot uhfc_{m,q} \dots + \left(\begin{matrix} e^{i \cdot k_{m,q} \cdot x} \\ + e^{-i \cdot k_{m,q} \cdot x} \end{matrix} \dots \right) \cdot uhfc_{m,q+1} \right]$$

The anvil spectral forces are determined:

$$FAfc(x,m,q) := \frac{-i \cdot E_q \cdot A_q \cdot k_{m,q}}{e^{i \cdot k_{m,q} \cdot L_q} - e^{-i \cdot k_{m,q} \cdot L_q}} \cdot \left[-\left[\begin{matrix} e^{i \cdot k_{m,q} \cdot (L_q - x)} \\ + e^{-i \cdot k_{m,q} \cdot (L_q - x)} \end{matrix} \dots \right] \cdot uafc_{m,q} \dots + \left(\begin{matrix} e^{i \cdot k_{m,q} \cdot x} \\ + e^{-i \cdot k_{m,q} \cdot x} \end{matrix} \dots \right) \cdot uafc_{m,q+1} \right]$$

The spectral forces and velocities are determined:

$F0Tfc_m := FHfc(0 \cdot ft, m, 0)$ $\quad F0Tfc_0 := -Freqwave_0$

$F1Tfc_m := FHfc(0 \cdot ft, m, 1)$ $\quad F1Tfc_0 := -Freqwave_0$

$F2Tfc_m := FHfc(0 \cdot ft, m, 2)$ $\quad F2Tfc_0 := -Freqwave_0$

$F3Tfc_m := FHfc(0 \cdot ft, m, 3)$ $\quad F3Tfc_0 := -Freqwave_0$

$F4Tfc_m := FHfc(0 \cdot ft, m, 4)$ $\quad F4Tfc_0 := -Freqwave_0$

$F4Bfc_m := FHfc(L_4, m, 4)$ $\quad F4Bfc_0 := F4Tfc_0$

$F5Tfc_m := FAfc(0 \cdot ft, m, 5)$ $\quad F5Tfc_0 := -Freqwave_0$

$F6Tfc_m := FAfc(0 \cdot ft, m, 6)$ $\quad F6Tfc_0 := -Freqwave_0$

$F7Tfc_m := FAfc(0 \cdot ft, m, 7)$ $\quad F7Tfc_0 := -Freqwave_0$

$F7Bfc_m := FAfc(L_7, m, 7)$ $\quad F7Bfc_0 := F7Tfc_0$

$vhfc_{m,q} := uhfc_{m,q} \cdot i \cdot \omega_m$ $\quad vafc_{m,r} := uafc_{m,r} \cdot i \cdot \omega_m$

Now the values can be inverted into the time domain:

Forces:

$Force_{0Tfc} := IFFT(F0Tfc)$ $Force_{1Tfc} := IFFT(F1Tfc)$

$Force_{2Tfc} := IFFT(F2Tfc)$ $Force_{3Tfc} := IFFT(F3Tfc)$

$Force_{4Tfc} := IFFT(F4Tfc)$ $Force_{4Bfc} := IFFT(F4Bfc)$

$Force_{5Tfc} := IFFT(F5Tfc)$ $Force_{6Tfc} := IFFT(F6Tfc)$

$Force_{7Tfc} := IFFT(F7Tfc)$ $Force_{7Bfc} := IFFT(F7Bfc)$

Displacements:

$DHfc^{\langle q \rangle} := IFFT(uhfc^{\langle q \rangle})$ $DAfc^{\langle r \rangle} := IFFT(uafc^{\langle r \rangle})$

Velocities:

$VHfc^{\langle q \rangle} := IFFT(vhfc^{\langle q \rangle})$ $VAfc^{\langle r \rangle} := IFFT(vafc^{\langle r \rangle})$

The stroke is calculated:

$$Stroke_n := DHfc_{n,5} - DAfc_{n,5}$$

The impact time is determined:

$$\begin{pmatrix} Stroke_{ZZ-1} \\ Stroke_{ZZ} \\ Stroke_{ZZ+1} \end{pmatrix} = \begin{pmatrix} 6.352 \\ 6.504 \\ 6.66 \end{pmatrix} \cdot in \qquad \begin{pmatrix} time\_fc_{ZZ-1} \\ time\_fc_{ZZ} \\ time\_fc_{ZZ+1} \end{pmatrix} = \begin{pmatrix} 77 \\ 78 \\ 79 \end{pmatrix} \cdot msec$$

The impact velocities are determined:

$$\begin{pmatrix} VHfc_{ZZ-1,5} \\ VHfc_{ZZ,5} \\ VHfc_{ZZ+1,5} \end{pmatrix} = \begin{pmatrix} 187.738 \\ 183.061 \\ 184.06 \end{pmatrix} \cdot ips \qquad \begin{pmatrix} VAfc_{ZZ-1,5} \\ VAfc_{ZZ,5} \\ VAfc_{ZZ+1,5} \end{pmatrix} = \begin{pmatrix} 28.677 \\ 33.651 \\ 26.843 \end{pmatrix} \cdot ips$$

Linear Interpolation is used to pinpoint the exact values:

$$Impact\_time := linterp\left(\frac{vx}{in}, \frac{vy}{sec}, \frac{STROKE}{in}\right) \cdot sec \qquad Impact\_time = 77.975 \cdot msec$$

$$Velocity_{hammer\_before} := linterp\left(\frac{vx}{in}, \frac{hv}{fps}, \frac{STROKE}{in}\right) \cdot fps \qquad Velocity_{hammer\_before} = 183.176 \cdot ips$$

$$Velocity_{anvil\_before} := linterp\left(\frac{vx}{in}, \frac{av}{fps}, \frac{STROKE}{in}\right) \cdot fps \qquad Velocity_{anvil\_before} = 33.529 \cdot ips$$

THE IMPACT PHASE

Impact Velocity: $Velocity_{Impact} := \frac{Velocity_{hammer\_before} + Velocity_{anvil\_before}}{2}$

$Velocity_{Impact} = 9.029 \cdot fps$

Hammer Velocity after impact: $Velocity_{hammer\_after} := Velocity_{hammer\_before} - Velocity_{Impact}$

$Velocity_{hammer\_after} = 6.235 \cdot fps$

Anvil Velocity after impact: $Velocity_{anvil\_after} := Velocity_{Impact} - Velocity_{anvil\_before}$

$Velocity_{anvil\_after} = 6.235 \cdot fps$

Force of Impact in Hammer: $Force_{Impact\_Hammer} := Velocity_{hammer\_after} \cdot A_4 \cdot \sqrt{\rho_4 \cdot E_4}$

$Force_{Impact\_Hammer} = 389531.144 \cdot lbf$

Force of Impact in Anvil: $Force_{Impact\_Anvil} := Velocity_{anvil\_after} \cdot A_5 \cdot \sqrt{\rho_5 \cdot E_5}$

$Force_{Impact\_Anvil} = 389531.144 \cdot lbf$

Duration of Impact: $\text{Time}_{\text{Hammer}} := \sum_{n=4}^{Ha} 2 \cdot \frac{L_n}{c_n}$ $\text{Time}_{\text{Hammer}} = 21.375 \cdot \text{msec}$

$\text{Time}_{\text{Anvil}} := \sum_{n=An}^{5} 2 \cdot \frac{L_n}{c_n}$ $\text{Time}_{\text{Anvil}} = 71.25 \cdot \text{msec}$

$\text{Impact\_Duration} := \text{if}(\text{Time}_{\text{Hammer}} > \text{Time}_{\text{Anvil}}, \text{Time}_{\text{Anvil}}, \text{Time}_{\text{Hammer}})$

$\text{Impact\_Duration} = 21.375 \cdot \text{msec}$

Impact Facts:

$\text{Impact\_time} = 77.975 \cdot \text{msec}$ $\text{Impact\_Duration} = 21.375 \cdot \text{msec}$ $\text{Force}_{\text{Impact}} = 389531.144 \cdot \text{lbf}$

THE POST-IMPACT PHASE

Number of samples

$N := 13$ $2^N = 8192$

Time steps between samples

$\Delta T := 2.5 \cdot 10^{-4} \cdot \text{sec}$ $n := 0 .. 2^N - 1$

Time steps: $\text{time\_pi}_n := n \cdot \Delta T$ $\max(\text{time\_pi}) = 2.04775 \cdot \text{sec}$

Sampling frequency: $f_s := \frac{1}{\Delta T}$ $f_s = 4000 \cdot Hz$

The wave will be a square wave. The properties of the wave are:

$Impact\_End := Impact\_time + Impact\_Duration$ $Impact\_End = 99.35 \cdot msec$

The post-impact wave is determined:

$Timewave\_pi_n := Force_{Impact} \cdot (Impact\_time \le time\_pi_n) \cdot (Impact\_End \ge time\_pi_n)$

A plot of the time domain post-impact wave shows:

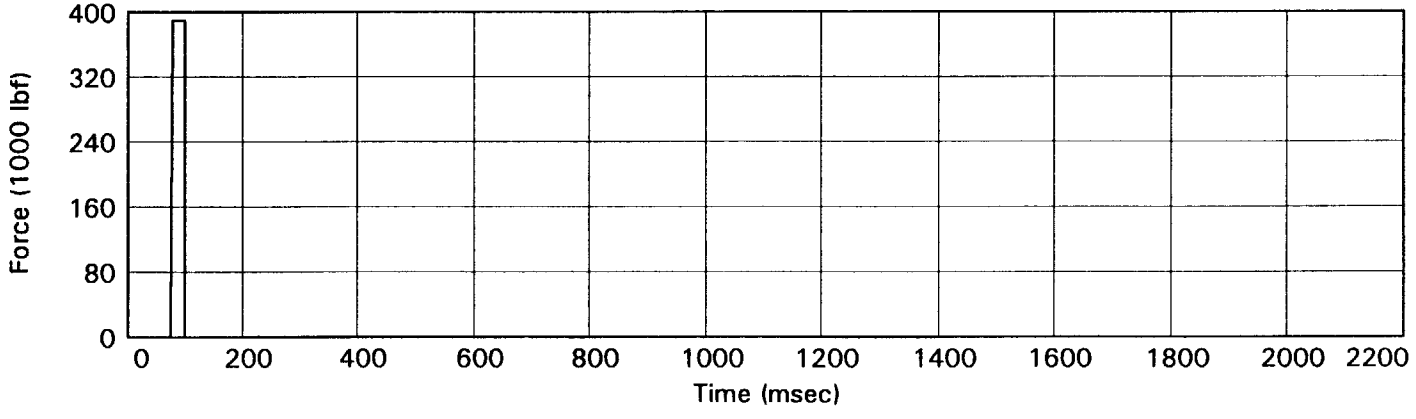

The wave is transformed from the time domain to the frequency domain:

$$\text{Freqwave} := \text{FFT}(\text{Timewave\_pi})$$

The frequencies are determined:

$$m := 0 .. 2^{N-1} \qquad \text{frequency}_m := \frac{m}{2^N} \cdot f_s \qquad \omega_m := 2 \cdot \pi \cdot \text{frequency}_m$$

A plot of the magnitude of the frequency domain post-impact wave shows:

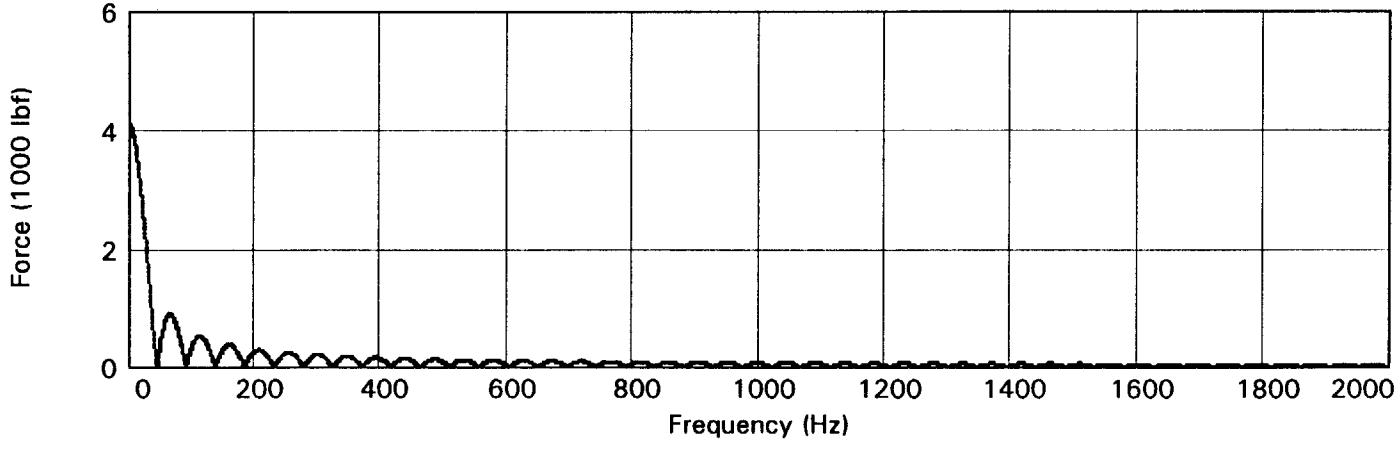

The spectral analysis starts with the determination of the wave number for each element:

$$k_{m,j} := \sqrt{\frac{(\omega_m)^2}{(c_j)^2} - \frac{i \cdot \omega_m \cdot \gamma_j}{A_j \cdot E_j}}$$

The element values are determined:

Convienent group of constants:

$$C_{m,j} := \frac{i \cdot k_{m,j} \cdot A_j \cdot E_j}{1 - e^{-2 \cdot i \cdot k_{m,j} \cdot L_j}}$$

On diagonal values:

$$D_{m,j} := C_{m,j} \cdot \left(1 + e^{-2 \cdot i \cdot k_{m,j} \cdot L_j}\right)$$

Off diagonal values:

$$OFD_{m,j} := C_{m,j} \cdot \left(-2 \cdot e^{-i \cdot k_{m,j} \cdot L_j}\right)$$

The hammer spectral finite element model is determined.

$$UH(m) := \begin{bmatrix} D_{m,0} + D_{m,1} & OFD_{m,1} & Z & Z & Z \\ OFD_{m,1} & D_{m,1} + D_{m,2} & OFD_{m,2} & Z & Z \\ Z & OFD_{m,2} & D_{m,2} + D_{m,3} & OFD_{m,3} & Z \\ Z & Z & OFD_{m,3} & D_{m,3} + D_{m,4} & OFD_{m,4} \\ Z & Z & Z & OFD_{m,4} & D_{m,4} \end{bmatrix}^{-1} \cdot \begin{bmatrix} 0 \cdot lbf \\ 0 \cdot lbf \\ 0 \cdot lbf \\ 0 \cdot lbf \\ Freqwave_m \end{bmatrix}$$

The anvil spectral finite element model is determined.

$$UA(m) := \begin{pmatrix} D_{m,5} & OFD_{m,5} & Z \\ OFD_{m,5} & D_{m,5} + D_{m,6} & OFD_{m,6} \\ Z & OFD_{m,6} & D_{m,6} + D_{m,7} \end{pmatrix}^{-1} \cdot \begin{pmatrix} Freqwave_m \\ 0 \cdot lbf \\ 0 \cdot lbf \end{pmatrix}$$

The hammer spectral displacements are determined:

$uhpi_{m,1} := UH(m)_0$ $uhpi_{m,2} := UH(m)_1$ $uhpi_{m,3} := UH(m)_2$

$uhpi_{m,4} := UH(m)_3$ $uhpi_{m,5} := UH(m)_4$

The anvil spectral displacements are determined:

$uapi_{m,5} := UA(m)_0$ $uapi_{m,6} := UA(m)_1$ $uapi_{m,7} := UA(m)_2$

$uapi_{m,8} := (0 + i \cdot 0) \cdot in$

The hammer zero frequency displacement are added in:

$$uhpi_{0,q} := -\sum_{s=0}^{q} \frac{Freqwave_0 \cdot L_s}{A_s \cdot E_s} \qquad uhpi_{0,0} := (0 + i \cdot 0) \cdot in$$

The anvil zero frequency displacement are added in:

$$uapi_{0,8} := (0 + i \cdot 0) \cdot in \qquad uapi_{0,w} := \sum_{W=7}^{w} \frac{Freqwave_0 \cdot L_W}{A_W \cdot E_W}$$

The hammer spectral forces are determined:

$$FHpi(x,m,q) := \frac{-i \cdot E_q \cdot A_q \cdot k_{m,q}}{e^{i \cdot k_{m,q} \cdot L_q} - e^{-i \cdot k_{m,q} \cdot L_q}} \cdot \left[-\begin{bmatrix} e^{i \cdot k_{m,q} \cdot (L_q - x)} & \dots \\ +e^{-i \cdot k_{m,q} \cdot (L_q - x)} & \end{bmatrix} \cdot uhpi_{m,q} \dots + \begin{pmatrix} e^{i \cdot k_{m,q} \cdot x} & \dots \\ +e^{-i \cdot k_{m,q} \cdot x} & \end{pmatrix} \cdot uhpi_{m,q+1} \right]$$

The anvil spectral forces are determined:

$$FApi(x,m,q) := \frac{-i \cdot E_q \cdot A_q \cdot k_{m,q}}{e^{i \cdot k_{m,q} \cdot L_q} - e^{-i \cdot k_{m,q} \cdot L_q}} \cdot \left[-\begin{bmatrix} e^{i \cdot k_{m,q} \cdot (L_q - x)} & \dots \\ +e^{-i \cdot k_{m,q} \cdot (L_q - x)} & \end{bmatrix} \cdot uapi_{m,q} \dots + \begin{pmatrix} e^{i \cdot k_{m,q} \cdot x} & \dots \\ +e^{-i \cdot k_{m,q} \cdot x} & \end{pmatrix} \cdot uapi_{m,q+1} \right]$$

The spectral forces and velocities are determined:

$F0Tpi_m := FHpi(0 \cdot ft, m, 0)$

$F1Tpi_m := FHpi(0 \cdot ft, m, 1)$

$F2Tpi_m := FHpi(0 \cdot ft, m, 2)$

$F3Tpi_m := FHpi(0 \cdot ft, m, 3)$

$F4Tpi_m := FHpi(0 \cdot ft, m, 4)$

$F4Bpi_m := FHpi(L_4, m, 4)$

$F5Tpi_m := FApi(0 \cdot ft, m, 5)$

$F6Tpi_m := FApi(0 \cdot ft, m, 6)$

$F7Tpi_m := FApi(0 \cdot ft, m, 7)$

$F7Bpi_m := FApi(L_7, m, 7)$

$vhpi_{m,q} := uhpi_{m,q} \cdot i \cdot \omega_m$

$F0Tpi_0 := -Freqwave_0$

$F1Tpi_0 := -Freqwave_0$

$F2Tpi_0 := -Freqwave_0$

$F3Tpi_0 := -Freqwave_0$

$F4Tpi_0 := -Freqwave_0$

$F4Bpi_0 := F4Tpi_0$

$F5Tpi_0 := Freqwave_0$

$F6Tpi_0 := Freqwave_0$

$F7Tpi_0 := Freqwave_0$

$F7Bpi_0 := F7Tpi_0$

$vapi_{m,r} := uapi_{m,r} \cdot i \cdot \omega_m$

Now the values can be inverted to the time domain:

Forces:

$$Force_{0Tpi} := IFFT(F0Tpi) \qquad Force_{1Tpi} := IFFT(F1Tpi)$$

$$Force_{2Tpi} := IFFT(F2Tpi) \qquad Force_{3Tpi} := IFFT(F3Tpi)$$

$$Force_{4Tpi} := IFFT(F4Tpi) \qquad Force_{4Bpi} := IFFT(F4Bpi)$$

$$Force_{5Tpi} := IFFT(F5Tpi) \qquad Force_{6Tpi} := IFFT(F6Tpi)$$

$$Force_{7Tpi} := IFFT(F7Tpi) \qquad Force_{7Bpi} := IFFT(F7Bpi)$$

Displacements:

$$DHpi^{\langle q \rangle} := IFFT\left(uhpi^{\langle q \rangle}\right) \qquad DApi^{\langle r \rangle} := IFFT\left(uapi^{\langle r \rangle}\right)$$

Velocities:

$$VHpi^{\langle q \rangle} := IFFT\left(vhpi^{\langle q \rangle}\right) \qquad VApi^{\langle r \rangle} := IFFT\left(vapi^{\langle r \rangle}\right)$$

$$Time_{zz} := if\left(zz \le ZZ, time\_fc_{zz}, time\_pi_{yy + zz}\right)$$

$$Displacement\ Hammer_{zz} := if\left(zz \le ZZ, DHfc_{zz,5} - DHfc_{ZZ,5}, DHpi_{zz + yy,5}\right)$$

$$Displacement\ Anvil_{zz} := if\left(zz \le ZZ, DAfc_{zz,5} - DAfc_{ZZ,5}, DApi_{zz + yy,5}\right)$$

$$Velocity\ Hammer_{zz} := if\left(zz \le ZZ, VHfc_{zz,5}, VHpi_{zz + yy,5}\right)$$

$$Velocity\ Anvil_{zz} := if\left(zz \le ZZ, VAfc_{zz,5}, VApi_{zz + yy,5}\right)$$

$$Force\ Stuckpoint_{zz} := if\left(zz \le ZZ, Force\ 6Tfc_{zz}, Force\ 6Tpi_{zz + yy}\right) + \left(Force\ Trigger - \rho_5 \cdot g \cdot A_5 \cdot L_5\right)$$

$$Force\ Anvil_{zz} := if\left(zz \le ZZ, Force\ 5Tfc_{zz}, Force\ 5Tpi_{zz + yy}\right) + Force\ Trigger$$

$$Force\ Hammer_{zz} := if\left(zz \le ZZ, Force\ 4Bfc_{zz}, Force\ 4Bpi_{zz + yy}\right) + Force\ Trigger$$

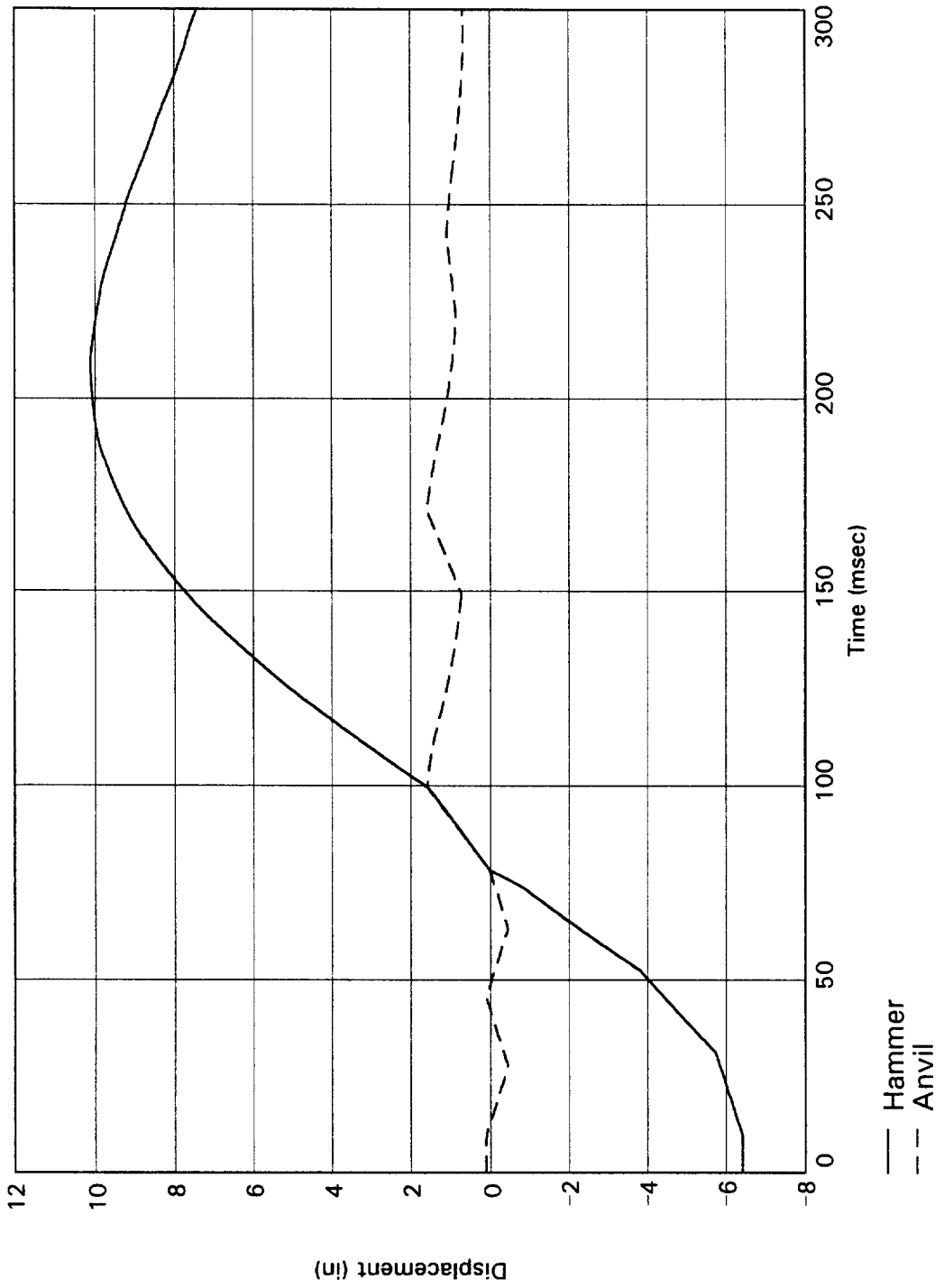
Displacement (in)
12
10
8
6
4
2
0
-2
-4
-6
-8
0
50
100
150
200
250
300
Time (msec)
Hammer
Anvil

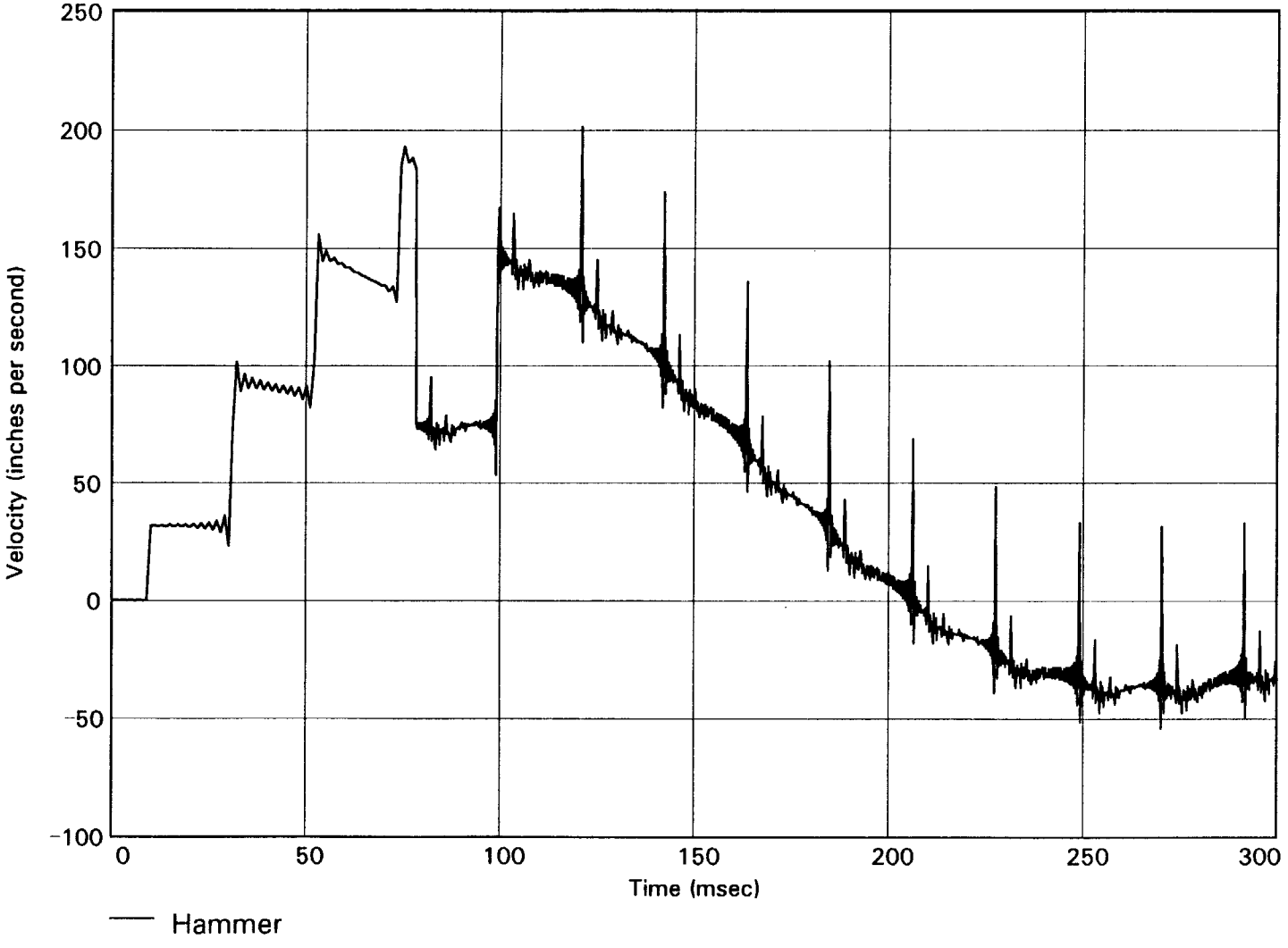
250
200
150
100
50
0
-50
-100
Velocity (inches per second)
0
50
100
150
200
250
300
Time (msec)
Hammer

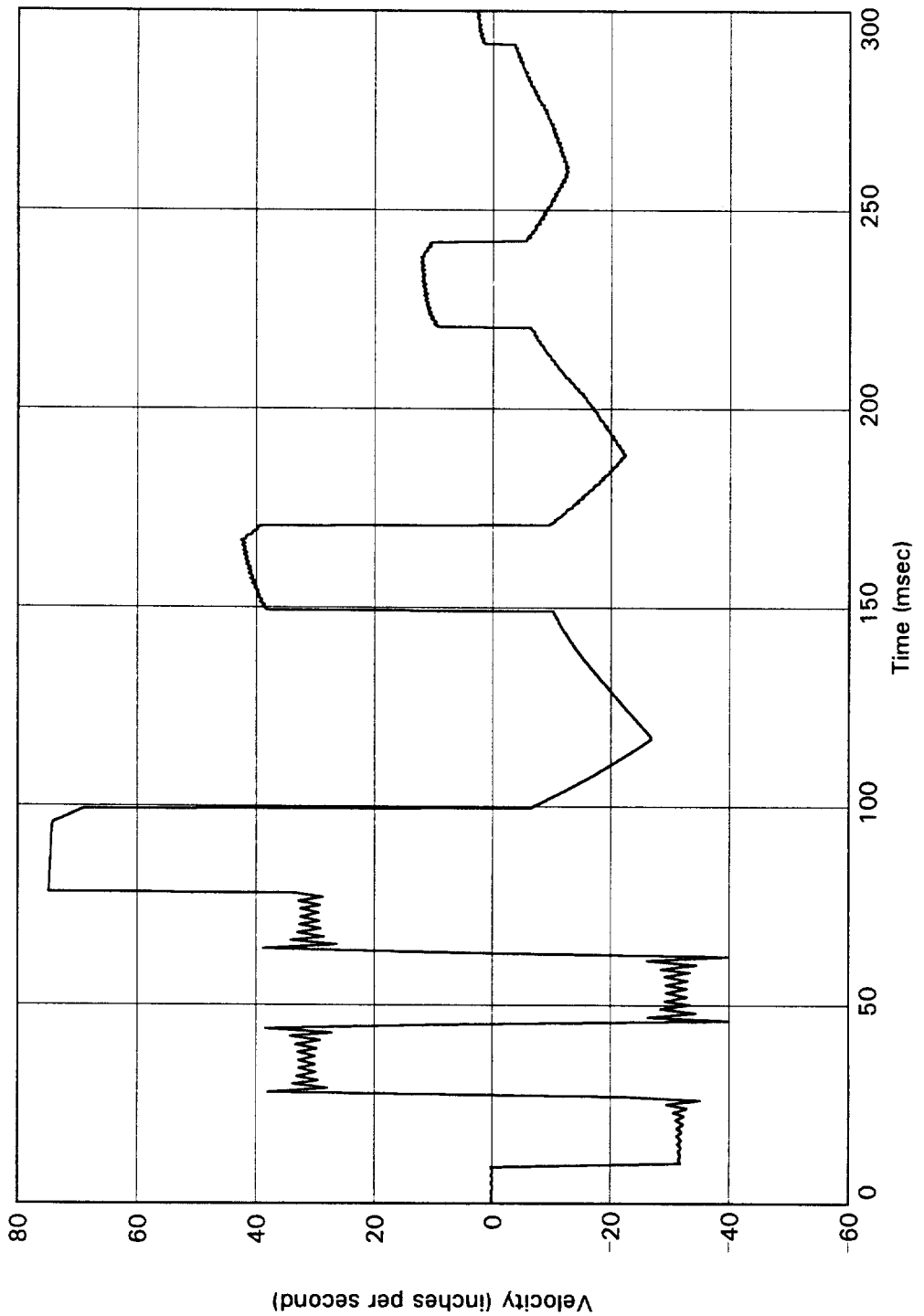
Velocity (inches per second)
80
60
40
20
0
-20
-40
-60
0
50
100
150
200
250
300
Time (msec)
Anvil

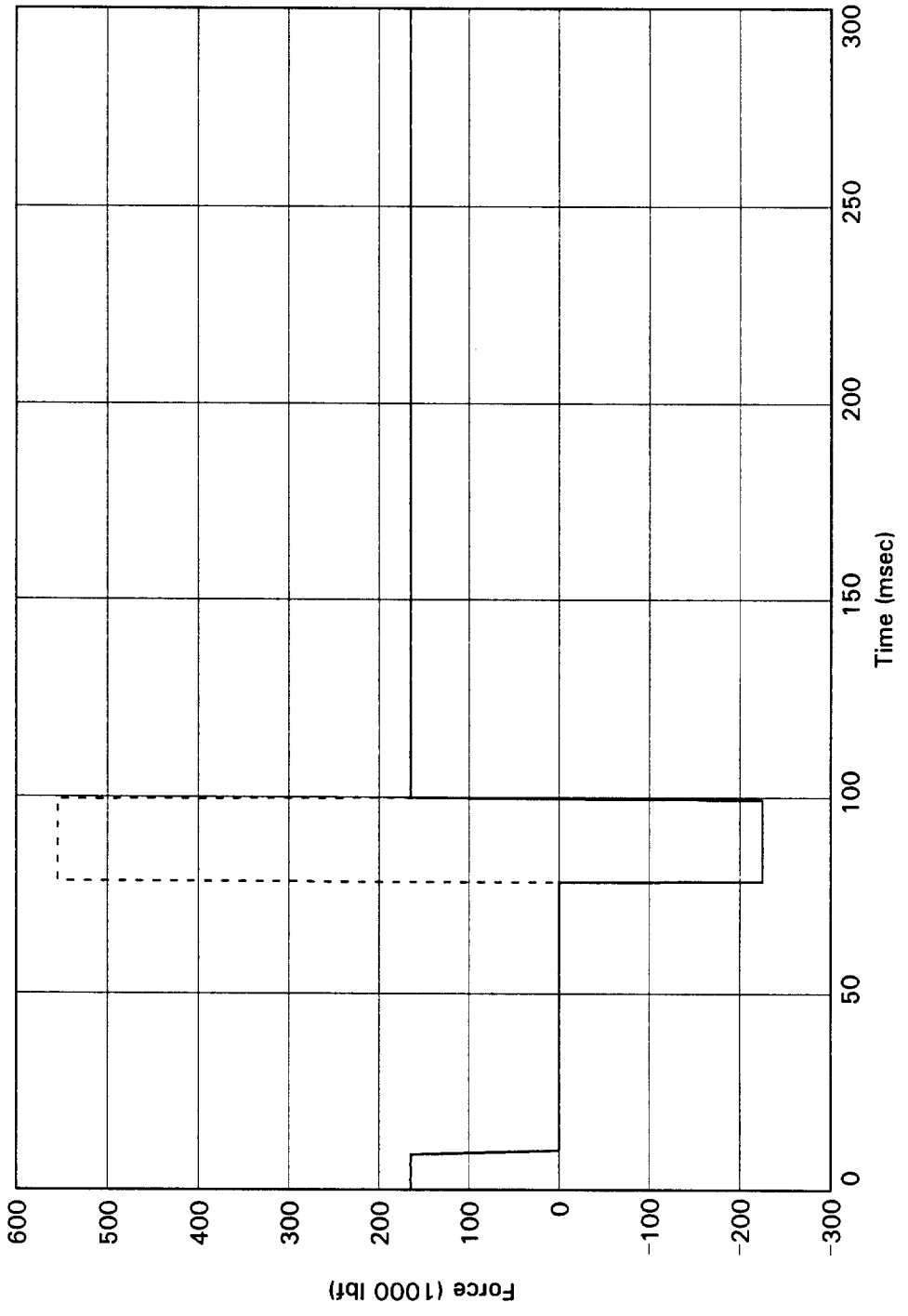
Force (1000 lbf)
600
500
400
300
200
100
0
-100
-200
-300
0
50
100
150
200
250
300
Time (msec)
Hammer
Anvil

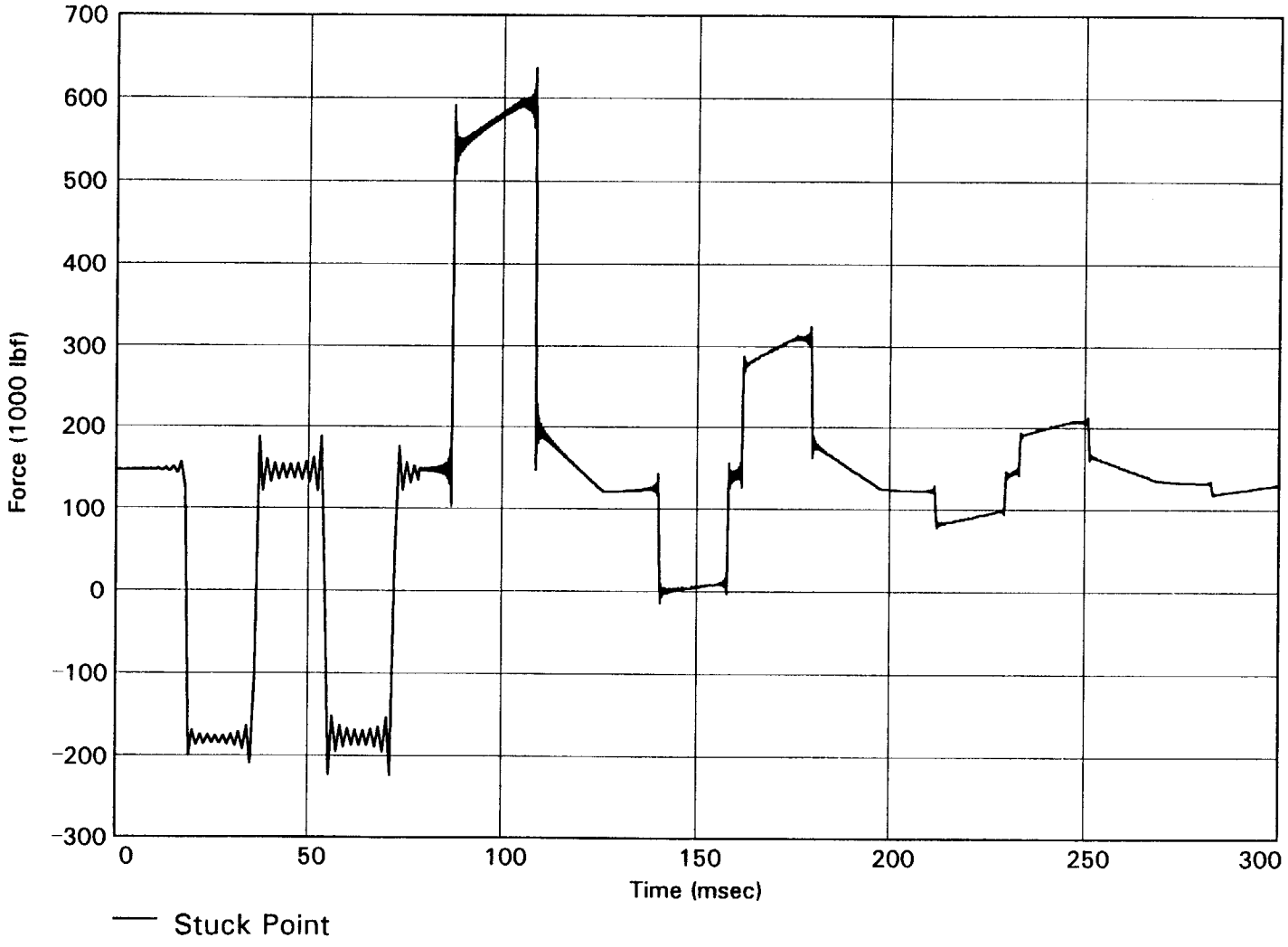
700
600
500
400
300
200
100
0
-100
-200
-300
Force (1000 lbf)
0
50
100
150
200
250
300
Time (msec)
Stuck Point